



**HAL**  
open science

## Ageing of bonded joints undershear loading

Justine Bertrand

► **To cite this version:**

Justine Bertrand. Ageing of bonded joints undershear loading. Mechanics [physics]. Université de Bordeaux, 2022. English. NNT : 2022BORD0235 . tel-03847657

**HAL Id: tel-03847657**

**<https://theses.hal.science/tel-03847657>**

Submitted on 10 Nov 2022

**HAL** is a multi-disciplinary open access archive for the deposit and dissemination of scientific research documents, whether they are published or not. The documents may come from teaching and research institutions in France or abroad, or from public or private research centers.

L'archive ouverte pluridisciplinaire **HAL**, est destinée au dépôt et à la diffusion de documents scientifiques de niveau recherche, publiés ou non, émanant des établissements d'enseignement et de recherche français ou étrangers, des laboratoires publics ou privés.

THÈSE PRÉSENTÉE  
POUR OBTENIR LE GRADE DE  
**DOCTEUR**  
**DE L'UNIVERSITÉ DE BORDEAUX**

ECOLE DOCTORALE SCIENCES PHYSIQUES ET DE  
L'INGÉNIEUR  
MÉCANIQUE

Par **Justine BERTRAND**

Durabilité des assemblages collés sous sollicitation de  
cisaillement

Sous la direction de : **Yves CHEMISKY**  
Co-directeur : **Jordi Renart**

Soutenue le 20 juillet 2022

Membres du jury :

Mme. Valérie NASSIET	Professeure des universités	ENI de Tarbes	Examinatrice
M. Éric PAROISSIEN	Enseignant-chercheur	ISAE-SUPAERO	Rapporteur
M. Rafael ESTEVEZ	Professeur des universités	Université de Grenoble Alpes	Rapporteur
M. Stéphane MOREL	Professeur des universités	Université de Bordeaux	Examineur
M. Julien JUMEL	Professeur des universités	ENSTA Bretagne	Examineur
M. Yves CHEMISKY	Professeur des universités	Université de Bordeaux	Directeur
M. Jean-Benoît KOPP	Maître de conférences	ENSAM Bordeaux	Co-encadrant
M. Simon DOUSSET	Ingénieur de Recherche	SportOptim	Invité





*La difficulté de réussir ne fait qu'ajouter à la nécessité d'entreprendre.*  
— Pierre Augustin Caron de Beaumarchais

À toutes les femmes de ma vie,



# Remerciements

Cette thèse résulte de plus de 3 ans de recherche au sein du laboratoire I2M de l'université de Bordeaux, au laboratoire AMADE de l'université de Gérone en Espagne. Puis beaucoup de télétravail un peu partout en France. Beaucoup d'expériences ont été menées, de réflexions sur leur modélisation, de questionnements sur l'intérêt de ces travaux et sur mes capacités. Mais si j'écris ces fameuses lignes de remerciements, c'est que j'y suis arrivée grâce aux personnes citées dans la suite.

Je souhaite remercier les membres de mon jury pour avoir pris le temps de lire cette thèse comme ils l'ont fait et pour la discussion scientifique que nous avons eu. C'est un moment rare dans une vie de partager avec des scientifiques ayant votre expérience et je vous en suis très reconnaissante.

Je souhaite remercier mon encadrement de thèse. Julien Jumel pour avoir monté ce projet avec Jordi Renart, pour l'excellence scientifique et l'exigence que cela a apporté à mon travail. Jordi Renart pour m'avoir accueilli en Espagne, notre travail ensemble a souffert de la pandémie mais j'ai appris beaucoup en peu de temps au sein de votre équipe. Jean-Benoît Kopp pour avoir été un co-encadrant pédagogue et d'une bienveillance sans nom, cette thèse n'aurait jamais aboutie sans ton aide.

Mes remerciements vont aussi aux membres du laboratoire, spécialement Jeremy Guillard pour son aide dans toutes mes expériences. C'était un plaisir de travailler avec vous et un manque à la fin de la thèse quand le télétravail a pris le dessus.

D'un point de vue personnel, je souhaite remercier tout les copains du labo ("les bordelais", ceux du A4, ceux de l'ENSAM), pour m'avoir toujours soutenue même loin de vous. Sarah, Julien, Arthur, Pierre, Ludo, Victor, Louise, Illan, ... cette thèse n'aurait pas été fun sans vous !

A Simon, à cause de qui mais surtout grâce à qui je me retrouve à écrire une page de remerciement ! Pour le soutien indéfectible en cette fin de thèse, merci.

A Laura, pour avoir toujours été ce diabolotin qui me sort de mes cours, merci.

A Hippolyte, arrivé sur le tard, qui arrive toujours à me surprendre, merci.

A Marie, Seb et Oscar pour m'avoir accueilli à Bordeaux et offert un cadre royal pour ma thèse, merci.

A mes soeurs, pour leur soutien incroyable même quand il y a plus de lettres que de chiffres dans mes équations, merci.

A mes parents, pour m'avoir initié aux sciences et avoir toujours cru en moi dans mes projets les plus fous dont cette thèse, merci.

Et à toi cher.e futur.e docteur.e qui ne liera peut-être que les remerciements parce qu'une thèse c'est long et qu'on l'a tous fait, tu vas y arriver ! N'oublie pas que tu es bien

entouré.e par ton encadrement, ton labo, tes amis et ta famille, le doctorat est une super expérience scientifique et de vie !

# Contents

<b>Remerciements</b>	<b>iii</b>
<b>Résumé</b>	<b>vii</b>
0.1 Motivation et problématique . . . . .	vii
0.2 État de l’art . . . . .	viii
0.3 Caractérisation mécanique des joints collés : essai Arcan et utilisation du DIC . . . . .	xi
0.4 Modèle semi-analytique de l’essai ELS et méthode d’identification de la loi cohésive . . . . .	xii
0.5 Tests de rupture : essai ELS et utilisation du DIC . . . . .	xiv
0.6 Conclusions et perspectives . . . . .	xv
<b>Introduction</b>	<b>xvii</b>
<b>Conclusions</b>	<b>xxi</b>
<b>List of Figures</b>	<b>xxvii</b>
<b>List of Tables</b>	<b>xxxv</b>
<b>1 Introduction</b>	<b>1</b>
1.1 Background . . . . .	2
1.2 Motivation . . . . .	3
1.3 Objectives . . . . .	4
1.4 Thesis description . . . . .	4
<b>2 Literature review</b>	<b>5</b>
2.1 Adhesive bonded joints description . . . . .	6
2.2 Mechanical characterisation of bonded joints . . . . .	12
2.3 Fracture tests of adhesive bonded joints . . . . .	22
2.4 Durability testing of bonded joint . . . . .	38
2.5 Conclusions . . . . .	45
<b>3 Mechanical characterisation of bonded joint under shear loading</b>	<b>47</b>
3.1 Test methods . . . . .	49
3.2 Data reduction method with Digital Image Correlation . . . . .	54

---

3.3	Experimental results . . . . .	59
3.4	Conclusions . . . . .	72
<b>4</b>	<b>Theoretical assessment of ELS test data reduction technique using virtual testing</b>	<b>73</b>
4.1	Introduction . . . . .	74
4.2	ELS test description . . . . .	75
4.3	Influence of adhesive layer compliance/nonlinear behaviour in an ELS test	78
4.4	Virtual testing results . . . . .	81
4.5	Conclusions . . . . .	91
A	Appendix . . . . .	92
<b>5</b>	<b>Use of Digital Image Correlation in mode II testing : ELS test</b>	<b>101</b>
5.1	Test method . . . . .	102
5.2	Data reduction method with Digital Image Correlation . . . . .	104
5.3	ELS test experimental results . . . . .	109
5.4	Inverse identification of the Adhesive Layer Shear Behaviour . . . . .	116
5.5	Discussion and conclusion . . . . .	117
<b>6</b>	<b>Conclusions and future work</b>	<b>119</b>
6.1	Concluding remarks . . . . .	120
6.2	Perspectives and future work . . . . .	123
<b>A</b>	<b>List of attended conferences</b>	<b>127</b>
	<b>Bibliography</b>	<b>131</b>

# Résumé

*Ceci est un résumé de la thèse en français. L'auteure recommande au lecteur de commencer la lecture du manuscrit au chapitre 1.*

## 0.1 Motivation et problématique

Cette thèse porte sur la durabilité des assemblages collés sous sollicitation de cisaillement. Les joints collés sont de plus en plus utilisés dans des domaines variés comme le génie civil, l'industrie aéronautique et marine ou le domaine médical. Cette méthode d'assemblage est en concurrence avec d'autres méthodes d'assemblages comme le rivetage, le soudage ou le pliage. L'utilisation de joints collés, au delà de l'assemblage, permet d'obtenir des liaisons étanches, d'assembler des pièces/structures aux formes compliquées et aux matériaux dissimilaires et de s'adapter à diverses conditions environnementales. De nombreuses solutions sont possibles compte tenu de la variété des adhésifs disponibles. De plus, les contraintes sont transférées sur toute la surface collée et non localement. Cependant, cette technologie n'est pas encore compétitive pour les applications qui exigent un haut niveau de fiabilité en raison du manque de techniques de contrôle de l'adhésion et de règles de conception robustes. Ces problèmes technologiques rendent difficile l'évaluation des joints collés qui doivent résister durant de longues durées (années) et qui peuvent subir des charges complexes (fatigue, stationnaire, choc, ...) combinées à un environnement physico-chimique agressif (température, humidité, ...) qui peuvent être rencontrées dans les structures pour lesquelles les joints collés sont utilisés.

Il est donc nécessaire de renforcer la robustesse des méthodes de prédiction du comportement des joints collés. Cela est possible grâce à des approches de conception où la tolérance à l'endommagement est la principale préoccupation. Cela nécessite de maîtriser les conditions d'amorçage et de propagation de fissures (aussi appelées décohésions) qui peut se produire dans un joint collé. Les joints collés sont généralement conçus pour supporter une charge de cisaillement. Les essais mécaniques généralement utilisés pour déterminer le comportement mécanique des joints collés sous sollicitation de cisaillement souffrent de nombreux artefacts comme les effets de bord et un chargement multiaxial perturbant l'analyse du comportement en cisaillement pur. Dans le cas de l'étude de la durabilité des joints collés, le problème se complexifie puisque plusieurs phénomènes sont impliqués dans le processus d'endommagement, ce qui donne lieu à des questions multiphysiques et couplées. Enfin, seules quelques procédures d'essais prennent en compte le comportement visqueux et le phénomène de zone de progrès de fissure (appelé Fracture Process Zone - FPZ - en anglais) qui se produit dans les matériaux polymères lorsqu'ils



---

sont chargés.

L'objectif principal de cette thèse est d'évaluer le comportement mécanique des joints collés sous sollicitation de cisaillement. Pour répondre à cette problématique, des procédures simplifiées sont développées dans une perspective de tolérance à l'endommagement qui aident à comprendre la propagation de fissures sous une charge de cisaillement dans les joints collés métal-métal.

## 0.2 État de l'art

L'état de l'art sur les problématiques liées aux joints collés sous sollicitation de cisaillement est divisé en plusieurs catégories : généralités, caractérisation mécanique des joints collés, tests de rupture et analyse de l'endommagement (fissure) et évaluation de la durabilité des joints collés.

### 0.2.1 Généralités sur les joints collés

Un assemblage collé consiste en deux substrats reliés ensemble par une couche adhésive en matériau polymère. Il existe deux types de tests pour évaluer le comportement mécanique des assemblages collés et leur tenue à l'endommagement : les tests de caractérisation mécanique où les propriétés telles que le module d'Young et la contrainte à rupture peuvent être déterminés et les tests de rupture où l'amorçage et la propagation de fissures sont suivis. Lorsque qu'une fissure se crée, elle peut se propager selon 3 modes différents : le mode I de pelage, le mode II de cisaillement et le mode III de torsion. La Fig. 1 présente ces trois modes. Les tests mécaniques présentés dans cette thèse consistent tous à provoquer le déplacement relatif de deux "poutres" l'une par rapport à l'autre pour provoquer du cisaillement et de fait des fissures en mode II.

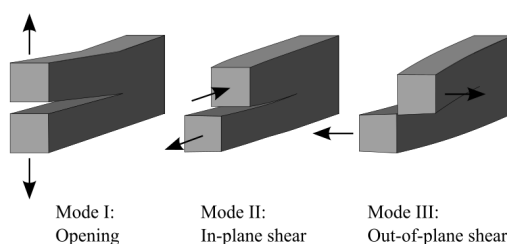


Figure 1: Modes de rupture.

Une rupture peut être adhésive (fissure se propageant le long de l'interface entre le substrat et la couche adhésive) ou cohésive (fissure se propageant dans la couche adhésive). Les adhésifs sont principalement des matériaux polymères. L'étude de leur comportement mécanique doit prendre en compte leur caractère visco-élasto-plastique. Du fait des comportements non-linéaires des polymères, le concept de zone de progrès de fissure est abordé. C'est une zone de déformation plastique qui supporte des contraintes élevées due à la singularité que représente la pointe de fissure [1, 2, 3, 4]. La rupture des joints collés

est pilotée par la qualité de l'interface entre les substrats et la couche adhésive. A l'échelle de cette thèse, seule la rupture cohésive est considérée.

### 0.2.2 Caractérisation mécanique des joints collés

Les tests de caractérisation mécanique permettent d'évaluer les principales propriétés (statiques et rhéologiques) de la couche adhésive. Plusieurs types de chargements sont possibles (quasi-statique, de fluage, de relaxation de contraintes et dynamique) durant différents temps (ou à différentes fréquences) et à différentes températures. Pour répondre à la problématique posée précédemment, seul des essais de cisaillement sont présentés. Plusieurs géométries sont proposées pour les éprouvettes des essais de caractérisation mécanique, les plus connues étant : le joint à simple et double recouvrement (Single Lap Joint - SLJ - et Double Lap Joint - DLJ) [5], le joint à substrats épais (Thick Adherend Shear Test - TAST) [5], la géométrie Arcan [6]. Cette dernière correspond à l'essai permettant de se rapprocher le plus d'un état de contrainte homogène dans la couche adhésive et sera utilisé dans le reste de cette thèse. La géométrie est présentée à la Fig. 2, elle consiste en deux parties en forme de lune dans lesquelles sont encastrés les deux substrats reliés par la couche adhésive. Les trous dans les parties en forme de lune permettent de tester les joints collés selon différentes sollicitations.

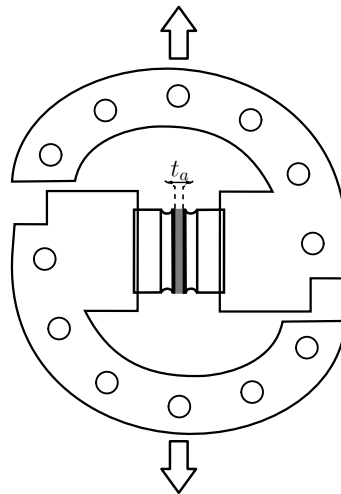


**Figure 2:** Montage Arcan.  $t_a$  est l'épaisseur d'adhésif.

Les tests de caractérisation mécanique ne permettent d'évaluer que des grandeurs participant à l'amorçage de la fissure. C'est pourquoi il est important de compléter ces essais par des tests de rupture permettant de suivre et quantifier l'endommagement dans les joints collés sous sollicitation de cisaillement.

### 0.2.3 Test de rupture et analyse de l'endommagement

Les conditions d'amorçage et de propagation de fissures dans les tests de rupture sont décrites grâce à la mécanique de la rupture linéaire et l'approche de Griffith. Ce dernier statue qu'une fissure se propage lorsque la réduction de l'énergie potentielle qui se produit

en raison de la croissance de la fissure est supérieure ou égale à l'augmentation de l'énergie de surface due à la création de nouvelles surfaces libres. On étudie alors le taux de restitution d'énergie (Strain Energy Release Rate - SERR - en anglais) libérée pendant la propagation de la fissure pour suivre et quantifier l'endommagement dans un joint collé. Le SERR peut être évalué grâce à la théorie de Griffith, or celle-ci n'est valide que pour des matériaux fragiles. Le SERR est alors noté  $G$ . Le SERR peut être évalué grâce à l'approche de Rice [7] : l'intégrale de contour  $J$  permettant de prendre en compte le comportement non-linéaire qui peut apparaître en pointe de fissure (FPZ notamment). Le SERR est alors noté  $J$ . La simulation du comportement des joints collés peut se faire grâce à des modèles analytiques s'appuyant sur la théorie des poutres et la mécanique de la rupture mais aussi avec des outils numériques de modélisation par éléments finis (Virtual Crack Closing Technique - VCCT et Cohésive Zone Model - CZM par exemple). La principale donnée d'entrée de ces modèles est la loi de comportement de l'adhésif (aussi appelée loi cohésive ou ALSB dans cette thèse). Cette loi se décrit par une courbe contrainte en fonction de la déformation et est dépendante du mode de rupture. Plusieurs formes sont possibles pour les lois ALSBs (exponentielle, bi-linéaire, trapézoïdale, ...), elles permettent de rendre compte de la propension de l'adhésif à plastifier ou s'adoucir quand la contrainte augmente à la pointe de fissure et donc de caractériser le développement de la FPZ.

Plusieurs géométries sont possibles pour les essais de rupture. De manière générale, les tests de rupture consistent à fléchir une éprouvette comportant une pré-fissure. Les essais principaux sont l'essai End Notched Flexure (ENF, flexion 3 ou 4 points) [8, 9] et l'essai End Loaded Split (ELS, flexion simple) [10, 11] présentés à la Fig. 3. Dans le cadre de cette thèse, l'essai ELS est choisi pour sa capacité à atteindre un régime de propagation de fissure stable plus facilement que l'essai ENF [12].

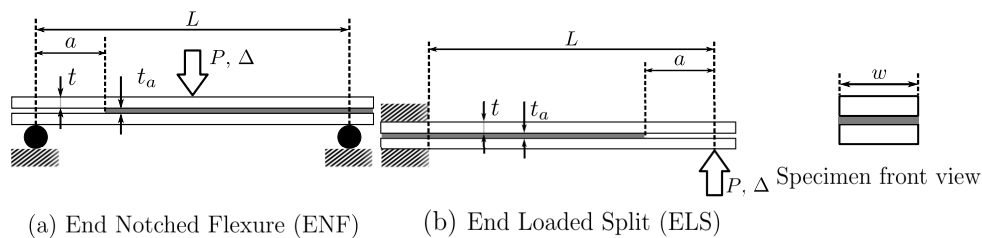


**Figure 3:** (a) Essai ENF. (b) Essai ELS.  $a$  est la longueur de fissure.  $L$  est la longueur d'éprouvette.  $t$  est l'épaisseur du substrat.  $t_a$  est l'épaisseur d'adhésif.  $w$  est la largeur de l'éprouvette.  $P$  est la charge appliquée.  $\Delta$  est le déplacement en bout d'éprouvette.

## 0.2.4 Durabilité des assemblages collés

Au vu des applications pour lesquelles les assemblages collés sont utilisés, la question de leur durabilité est à étudier. Les adhésifs, en tant que matériaux polymères, sont affaiblis par l'exposition à des charges cycliques à long terme, à l'humidité et à la température. Les conditions de vieillissement et les mécanismes d'endommagement doivent être reproduits

de manière accélérée pour valider la capacité du joint à supporter des conditions agressives à long terme en service. Dans la littérature, plusieurs études portent sur l'analyse des contraintes ou déformations résiduelles après que l'éprouvette ait été vieillie dans une chambre environnementale [13, 14]. Le suivi de l'endommagement (suivi de fissure) en temps réel commence à être abordé par les chercheurs (Wedge test par exemple [15]). Depuis trois décennies seulement, certains travaillent sur les concepts de mécanique de la rupture en fonction du temps [16]. L'essai de durabilité des joints collés est un problème complexe à résoudre. En raison des diverses conditions d'essai possibles et comme les joints collés sont constitués de matériaux différents, les essais sont difficiles à mettre en place.

### 0.3 Caractérisation mécanique des joints collés : essai Arcan et utilisation du DIC

Dans ce chapitre, une campagne d'essai a été menée sur des éprouvettes Arcan avec trois types d'adhésifs différents : deux adhésifs thermodurcissables (à base d'époxy) et un adhésif thermoplastique (à base de méthacrylate). Le montage Arcan est utilisé pour appliquer des conditions de chargement en cisaillement pur à la couche adhésive. Pour suivre l'évolution de la déformation, un système de corrélation d'images (Digital Image Correlation - DIC - en anglais) est utilisé avec une caméra à fort grossissement. Le comportement rhéologique complexe des adhésifs est testé grâce à différents types de chargement (essai quasi-statique, essai de fluage, essai cyclique de fluage-recouvrance). Pour les essais à température, un outil de régulation de la température consistant en deux thermostats encastrés sur les substrats permet de chauffer la couche adhésive et de conduire des tests à des températures allant de la température ambiante à 80 °C. Les résultats sont discutés d'un point de vue qualitatif.

La méthode de réduction des données issues de la corrélation d'images est totalement décrite. Elle consiste à étudier les mouvements des centres de gravité des deux substrats. En plus du mouvement relatif vertical associé au cisaillement de la couche adhésive, l'éprouvette tourne sur elle-même durant le test (notamment au début du chargement) et il est possible que le référentiel de l'image (de l'appareil photo) ne soit pas aligné avec le référentiel de l'éprouvette. Le programme matlab créé permet de prendre en compte les mouvements indésirables et de corriger les décalages inhérents à l'utilisation de plusieurs composants (machine de traction, montage, appareils photos, ...). La déformation en cisaillement est obtenue en divisant le déplacement relatif entre les deux substrats propre au cisaillement par l'épaisseur de l'adhésif. De plus, le champs des déplacements peut être observé tout au long de l'essai.

Des essais quasi-statiques ont été menés sur les adhésifs thermodurcissables. Ces essais montrent un comportement élastique fragile. Des ruptures cohésives mais aussi adhésives ont été observées. Ces dernières pouvant s'expliquer par une mauvaise préparation de la surface d'adhésion.

Une plus grande variété de tests a été conduite pour l'adhésif thermoplastique. La reproductibilité des tests ainsi que la procédure d'essai utilisant la corrélation d'images

---

ont été validées. De plus ces essais quasi-statiques permettent d'évaluer le module de cisaillement, la contrainte maximale admissible et l'élongation à rupture pour cet adhésif dans des conditions ambiantes. Une procédure de rajeunissement a été éprouvée et validée, elle consiste à chauffer la couche adhésive en dessous de sa température de transition vitreuse, de la laisser refroidir et de conduire un nouveau test sur la même éprouvette. Cette procédure permet de s'affranchir des défauts de fabrication. Des essais pour évaluer les conditions de stockage ont aussi été réalisés et il a été conclu qu'il n'y a pas d'impact de la durée de stockage sur l'évaluation des propriétés mécaniques.

Des essais de fluage-recouvrance de 12 h ont été réalisés à température ambiante pour détecter la transition entre le régime visco-élastique et le régime visco-plastique. Il est observé que des déformations résiduelles apparaissent après le premier cycle de chargement alors que la contrainte appliquée ne dépasse pas la limite élastique observée lors des essais quasi-statiques. Il est conclu que l'adhésif thermoplastique a un fort comportement visco-plastique.

Des essais de fluage à différentes températures ont ensuite été réalisés. Sous un chargement important (3000 N), des tests à 30 °C, 35 °C et 40 °C ont été réalisés. La rupture a été observée à 40 °C indiquant qu'une déformation irréversible est apparue pendant le fluage. Puis sous un chargement moindre (400 N), des tests à 30 °C, 35 °C, 40 °C, 45 °C, 50 °C, 55 °C, 60 °C, 65 °C et 70 °C ont été réalisés et le comportement visco-élastique a pu être observé. Enfin, des tests à différents niveaux de chargement (de 400 N à 7000 N) à température ambiante ont été réalisés. La rupture a été observée pour les charges de 5000 N et 7000 N confirmant le caractère élasto-visco-plastique de l'adhésif thermoplastique testé.

Grâce au dispositif d'essai Arcan, des campagnes d'essais sur différents types d'adhésifs peuvent être menées afin de développer des modèles rhéologiques et d'étudier l'amorçage de fissures. Les essais menés dans cette thèse conduisent à la conclusion que l'adhésif thermoplastique semble mieux approprié que les adhésifs thermodurcissables pour l'évaluation de l'endommagement en mode II dans un joint collé sous conditions environnementales sévères (temps, température) où la viscosité de la couche adhésive est prononcée. Les adhésifs thermodurcissables, quant à eux, semblent plus appropriés pour le suivi des mécanismes d'amorçage et de propagation de fissures dans les joints collés sous chargement quasi-statique. L'utilisation de la corrélation d'images comme moyen de mesure permet de suivre les déformations même dans le cas d'essais en température.

## 0.4 Modèle semi-analytique de l'essai ELS et méthode d'identification de la loi cohésive

Ce chapitre correspond à une analyse théorique des conditions d'amorçage et de propagation de fissures dans un joint collé. Plus précisément, le test ELS est décrit et un modèle semi-analytique de ce test est fourni pour prédire le comportement d'une éprouvette ELS. Une campagne d'essais virtuels est réalisée pour analyser la sensibilité des courbes "force-déplacement" et des "courbes SERR-longueur de fissure" à la forme de la loi cohésive de la couche adhésive. A partir de cette analyse, une méthode directe pour identifier le

#### 0.4. MODÈLE SEMI-ANALYTIQUE DE L'ESSAI ELS ET MÉTHODE D'IDENTIFICATION DE LA LOI COHÉSIVE

comportement en cisaillement de la couche adhésive à partir des résultats expérimentaux est décrite.

L'essai ELS est un essai de flexion simple réalisé sur une éprouvette en porte-à-faux. L'analyse est limitée aux substrats se déformant élastiquement. Le ratio  $a_0/L$  doit être supérieur à 0.55 ( $a_0$  étant la longueur de fissure initiale et  $L$  la longueur de l'éprouvette) pour avoir une propagation de fissure stable. En raison de la symétrie de l'éprouvette et des conditions de chargement, la couche adhésive subit une contrainte de cisaillement uniforme, sauf près de la pointe de fissure où des gradients de contrainte importants existent, ce qui entraîne l'apparition et la propagation de fissures. Comme la couche adhésive est sollicitée en cisaillement pur, le mode de propagation des fissures est le mode II.

Le modèle semi-analytique présenté dans ce chapitre consiste à implémenter une loi cohésive dans un modèle analytique développé à partir des formalismes classiques de la théorie des poutres et de la mécanique de la rupture. La loi cohésive est une succession de segments linéaires représentant l'évolution de la contrainte en cisaillement en fonction de la déformation en cisaillement. Les formes bi-linéaire élastique-plastique, bi-linéaire élastique-assoupli et trapézoïdale sont montrées en Fig. 4. Elles traduisent le comportement du matériau en pointe de fissure et notamment l'évolution de la FPZ.

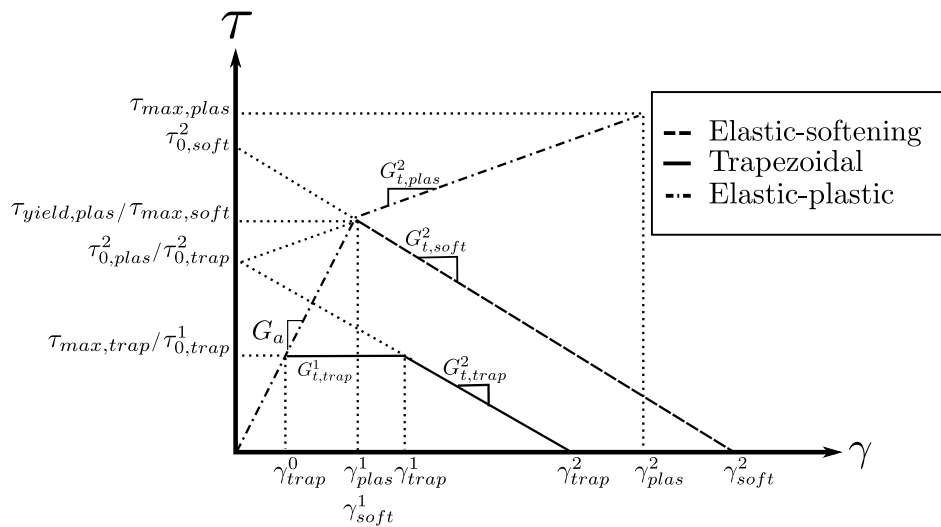


Figure 4: Différentes formes de loi cohésive (ALS).

Le comportement de l'éprouvette est simulé et décrit à travers l'évolution des efforts dans les substrats (force normale :  $N(x)$ , force de cisaillement :  $T(x)$ , moment de flexion :  $M(x)$  où  $x$  est la position le long de l'éprouvette) et l'évolution des déplacements des sections des substrats (longitudinal :  $u(x)$ , deflection :  $v(x)$ , rotation :  $\varphi(x)$ ).

Une campagne d'essais virtuels est conduite où les courbes "force-déplacement" ainsi que les évolutions des efforts et des déplacements sont produites pour 6 différentes ALSBs (rappel : lois cohésives). On observe sur les évolutions des efforts et des déplacements l'impact de la non-linéarité des ALSBs. En revanche, l'analyse des courbes "force-déplacement" ne permet pas de différencier les ALSBs implémentées. Les courbes "SERR-longueur de fissure" sont ensuite tracées. Le calcul du SERR est fait suivant la théorie

---

de Griffith  $G$  ou suivant la théorie de Rice  $J$ . Les deux approches donnent des résultats similaires. L'approche intégrale de contour  $J$  est alors préférée car elle permet de s'affranchir de la mesure de la longueur de fissure et surtout de prendre en compte la FPZ sans ajouter de coefficients correcteurs comme dans le cas de l'approche de Griffith. A l'analyse des courbes "SERR-longueur de fissure", on remarque que la partie des courbes décrivant l'évolution de la fissure avant la propagation n'a pas une large plage d'observation. En revanche, l'étude des courbes "SERR-déformation en cisaillement en pointe de fissure" permet d'avoir une plage d'observation beaucoup plus large et sensible à la forme de l'ALSB. On appellera ce type de courbe  $J(\gamma)$  par la suite. On a, d'après la théorie de Rice :

$$\tau = \frac{1}{t_a} \frac{dJ}{d\gamma} \quad (1)$$

où  $\tau$  est la contrainte en cisaillement à la pointe de fissure,  $t_a$  l'épaisseur de l'adhésif,  $J$  le SERR et  $\gamma$  la déformation en cisaillement en pointe de fissure. Ainsi, en analysant les courbes  $J(\gamma)$ , la loi cohésive (ALSB) peut être déterminée. Le modèle semi-analytique permet de prédire le comportement des éprouvettes ELS sous chargement quasi-statique. A partir de ce modèle, une nouvelle méthode directe a été évaluée pour extraire la loi cohésive à partir des résultats expérimentaux en utilisant une intégrale de contour  $J$ . Avec de nouvelles méthodes expérimentales comme la corrélation d'images, l'évolution des grandeurs nécessaires dans la formulation de l'intégrale de contour  $J$  peut être enregistrée avec précision.

## 0.5 Tests de rupture : essai ELS et utilisation du DIC

Dans ce chapitre, des essais End Loaded Split (ELS) ont été réalisés sur des éprouvettes de configurations géométriques variées (différentes tailles de longueur de fissure initiale et différentes épaisseurs des substrats et de la couche adhésive). La corrélation d'images numériques est utilisée pour obtenir la cinématique de l'éprouvette et donc le nouveau type de courbe de résistance  $J(\gamma)$  présenté dans la section 0.4. Les résultats expérimentaux et les résultats des essais virtuels du modèle semi-analytique présenté dans 0.4 sont comparés et en accord.

Deux adhésifs thermoplastiques (SAF MIB 30 de Bostik® et Araldite 2021 d'Araldite®) à base de méthacrylate sont utilisés pour les éprouvettes ELS.

Deux différents appareils de corrélation d'images ont été utilisés comme appareil de mesure des déplacements et donc des déformations. La procédure de traitement des données issues des systèmes DIC est totalement décrite. Elle consiste à découper les substrats en section dont les déplacements (longitudinal, transversal et rotation) sont ensuite extraits. La déformation en cisaillement est ensuite calculée à chaque section comme le rapport entre le déplacement entre les sections des substrats supérieur et inférieur et l'épaisseur de la couche adhésive.

Dans un premier temps des essais ELS ont été réalisés sur les éprouvettes collées avec l'adhésif SAF MIB 30. Cet adhésif testé en Arcan (voir section 0.4) a montré un comportement très souple. Des tests de reproductibilité ont été réalisés afin de valider le

montage expérimental et la méthode de réduction de données utilisant le DIC. Lors des essais réalisés, aucun amorçage de fissure n'a été observé. Ceci s'explique par l'observation d'une déformation plastique des substrats. Une perspective d'amélioration pour obtenir de meilleurs résultats est d'augmenter l'épaisseur des substrats ou de changer leur matériau.

Dans un second temps, des essais de rupture ont été réalisés avec des éprouvettes collées avec l'adhésif Araldite 2021. Cinq configurations d'éprouvette ont été testées, elles diffèrent selon la longueur d'éprouvette, la longueur de fissure initiale, l'épaisseur des substrats et de la couche adhésive. Les courbes "force-déplacements" pour les cinq éprouvettes ont été tracées ainsi que les courbes  $J(\gamma)$  correspondantes. Pour une des éprouvettes, la rupture cohésive a été observée. Pour les autres éprouvettes, pas de rupture ou des ruptures adhésives ont été observées. Ceci s'explique par des défauts de fabrication ou des configurations géométriques n'étant pas propices à l'amorçage et la propagation de fissures.

A partir de la courbe  $J(\gamma)$  de l'essai correspondant à l'éprouvette où la rupture cohésive a été observée, une loi cohésive a été extraite en suivant la méthode présentée dans la section 0.4. Cette loi a été implémentée dans le modèle semi-analytique. Les résultats expérimentaux (analyse des déplacements en bout d'éprouvette et de la déformation en cisaillement en pointe de fissure) ont été comparés avec la simulation et ils correspondent entre eux. Le modèle semi-analytique présenté dans la section 0.4 peut être utilisé comme outil de prédiction lorsque la loi cohésive est connue. Il peut également être utilisé comme un outil de vérification en vue d'extraire la loi cohésive afin de l'implémenter dans un modèle numérique de zone cohésive (CZM).

L'essai ELS est un bon candidat pour les essais de rupture en mode II des joints collés. Avec des adhésifs quasi-fragiles, l'amorçage et la propagation de fissures peuvent être observés. De plus, la méthode de réduction des données a été validée et la méthode d'identification directe de la loi cohésive aussi par comparaison des résultats expérimentaux et simulés.

## 0.6 Conclusions et perspectives

Cette thèse a pour but de définir des méthodologies d'essai fiables pour évaluer le comportement mécanique d'un joint collé sous sollicitation de cisaillement.

D'abord, deux procédures d'essai utilisant la corrélation d'images numériques ont été développées pour évaluer le comportement mécanique des joints collés : l'essai Arcan permettant d'identifier le comportement rhéologique de la couche adhésive et l'essai ELS permettant d'observer l'endommagement dans la couche adhésive.

Ensuite, une méthode expérimentale a été décrite permettant d'identifier directement le comportement en cisaillement de la couche adhésive (loi cohésive). Cette loi est la première entrée dans un outil de simulation (analytique ou numérique) qui prédit le comportement mécanique des joints collés.

Finalement, un modèle semi-analytique a été développé et est capable de prédire le comportement du joint collé (déplacements des substrats, déformation et contrainte de cisaillement dans la couche adhésive) sous une sollicitation de cisaillement dans un envi-



---

ronnement standard (température et humidité ambiantes et chargement quasi-statique).

Pour aller plus loin, une campagne expérimentale d'essai Arcan doit être conduite permettant de déterminer le comportement rhéologique complet des adhésifs. De plus, les essais de rupture conduits dans cette thèse n'ont pas tous été concluants. Une analyse plus poussée des conditions d'amorçage et de propagation pour une plus grande gamme de matériaux doit être réalisée. Ensuite, dans le modèle semi-analytique, seules trois formes de loi cohésive ont été implantées. Une plus grande variété de forme pourrait être étudiée. Pour l'étude de la durabilité, un montage spécifique consistant en un essai de rupture placé dans une chambre environnementale a été développé. Ce montage permettrait de suivre l'endommagement (amorçage et propagation de fissure) dans une éprouvette sous un chargement de fluage.

# Introduction

*Ceci est une traduction en français de l'introduction présentée au chapitre 1. L'auteure recommande au lecteur de commencer la lecture du manuscrit au chapitre 1.*

## Contexte

La technique du joint collé pour les applications structurales est développée depuis 50 ans. Une des explications de cette expansion est l'augmentation de l'utilisation de pièces structurelles en matériaux composites. En effet, leurs bonnes performances mécaniques associées à leur faible densité et donc à leur légèreté permettent d'obtenir des structures fiables. Ils présentent également un bon comportement en cas de choc et une bonne résistance à la corrosion. Mais leur prix, leur fabrication, leur recyclage et leur assemblage sont les principales problématiques à résoudre. La question de l'assemblage est le sujet principal de cette thèse. Il existe de multiples façons d'assembler des pièces structurelles : rivetage, soudage, pliage, collage. Les trois premières, dans le cas de l'assemblage de composites, impliquent des concentrations de contraintes, de l'oxydation et des problèmes de poids. La solution du collage est apparue comme la solution privilégiée pour l'assemblage de matériaux composites. Dès lors, le développement de la technique s'est étendue à de multiples domaines : industrie du transport (bateaux, voitures, avions, trains), industrie civile (panneaux solaires, ponts), domaine médical (voir Fig. 5). Un joint collé consiste en 2 substrats fait de différents type de matériaux (aluminium, composite, béton, ...) liés ensemble avec une couche adhésive (un adhésif) en matériau polymère. De même, on peut considérer les composites comme un matériau composé de plusieurs joints collés : chaque couche de résine entre les couches de fibres est considérée comme une couche adhésive.

Le collage est une technique connue et utilisée depuis l'époque égyptienne. Par exemple, une faucille a été retrouvée dont les dents étaient collées avec du goudron sur le manche en bois. Au 19<sup>ème</sup> siècle, les premiers adhésifs synthétiques sont apparus : Goodyear en 1840 a introduit le caoutchouc et Dunlop en 1888 l'a utilisé dans le premier pneu où des couches de caoutchouc étaient collées ensemble (voir Fig. 6). En 1940, les premiers collages métal-métal sont apparus et ont marqué le début de l'ère du collage structural.

Le collage, outre l'assemblage, possède des propriétés d'étanchéité, permet d'assembler des structures aux formes compliquées et réalisées à partir de matériaux dissemblables et peut s'adapter à diverses conditions environnementales. De nombreuses solutions sont possibles compte tenu de la variété des adhésifs disponibles. De plus, les contraintes sont transférées sur toute la surface collée et non localement. Cependant, cette technologie

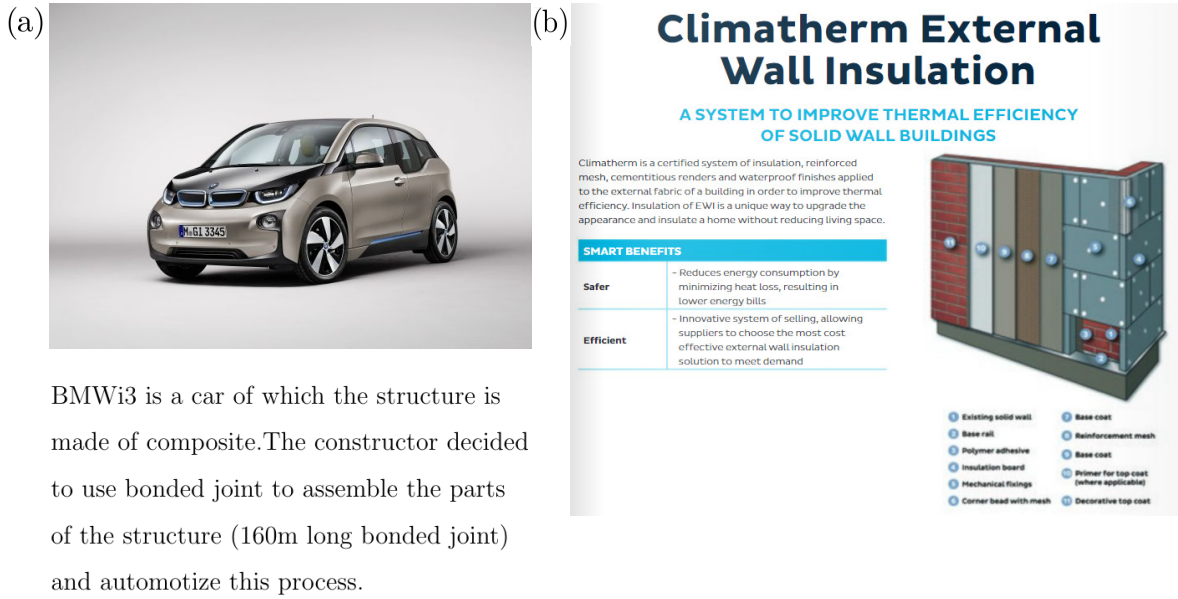


**Figure 5:** (a) Voiture BMWi3 [17]. (b) Exemple d'utilisation pour l'isolation d'un mur (Bostik <sup>®</sup>) [18].

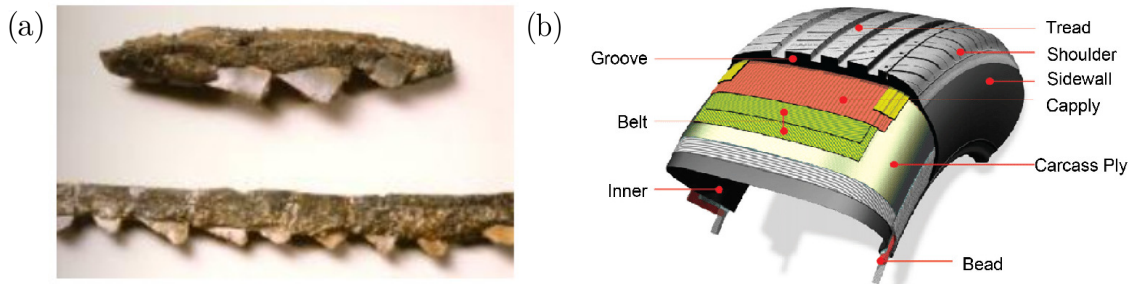


**Figure 6:** (a) Faucille égyptienne [19]. (b) Structure d'un pneu [20].

n'est pas encore compétitive pour les applications qui exigent un haut niveau de fiabilité en raison du manque de techniques de contrôle de l'adhésion et de règles de conception robustes. Ces problèmes technologiques rendent difficile l'évaluation des joints collés qui doivent résister durant de longues durées (années) et qui peuvent subir des charges complexes (fatigue, stationnaire, choc, ...) combinées à un environnement physico-chimique agressif (température, humidité, ...) qui peuvent être rencontrés dans des applications telles que les pales d'éoliennes, les turbines marémotrices et les structures aéronautiques.

Il est donc nécessaire de renforcer la robustesse des méthodes de prédiction du comportement des joints collés. Cela est possible grâce à des approches de conception où la tolérance à l'endommagement est la principale préoccupation. Cela nécessite de maîtriser les conditions d'initiation et de propagation de la décohésion (aussi appelée fissure) qui peut se produire dans un joint collé. Dans le cas de la durabilité des joints collés, ce problème est assez complexe puisque plusieurs phénomènes sont impliqués dans le processus d'endommagement, ce qui donne lieu à des questions multiphysiques et couplées.

## Motivation

De nos jours, la plupart des études se concentrent sur la ténacité des couches inter-laminaires (de la résine) dans les matériaux composites sous chargement de traction et cisaillement. Dans le cadre de l'étude du comportement mécanique de la couche adhésive dans un joint collé structural, le pelage est le mode de défaillance le plus communément évalué car c'est le mode de défaillance le plus "faible". Mais il apparaît que les joints collés sont généralement conçus pour supporter une charge de cisaillement. De plus, dans la perspective des essais de durabilité, l'essai préféré pour évaluer le comportement des joints collés sous sollicitation de cisaillement est l'essai de recouvrement Single Lap Joint (SLJ). Mais cet essai souffre de nombreux artefacts comme les effets de bord et un chargement multiaxial alors que le cisaillement est le seul chargement attendu. Enfin, seules quelques procédures d'essai prennent en compte le comportement visqueux et le phénomène de zone de progrès de fissure (appelé Fracture Process Zone - FPZ - en anglais) qui se produit dans les matériaux polymères lorsqu'ils sont chargés.

L'objectif principal de ce projet est d'évaluer le comportement mécanique des joints collés sous sollicitation de cisaillement. Le but est de développer des procédures simplifiées dans une perspective de tolérance à l'endommagement qui aident à comprendre la propagation de fissures sous une charge de cisaillement dans les joints collés métal-métal.

## Objectifs

Cette thèse vise à définir des méthodologies d'essai fiables et des méthodes de réduction des données pour évaluer le comportement mécanique des joints collés sous sollicitation de cisaillement. Plusieurs objectifs ont été définis :

- Développement de procédures afin d'obtenir le comportement mécanique d'une couche adhésive dans un joint collé métal-métal sous une sollicitation de cisaillement. Les données obtenues serviront à évaluer la durabilité du joint collé grâce à l'identification des paramètres visco-élasto-plastiques et la résistance à la propagation de fissures grâce à l'évaluation de l'énergie nécessaire pour déclencher la propagation de fissures.
- Développement d'une procédure expérimentale pour identifier la loi de comportement (également appelée loi cohésive) de la couche adhésive. Cette loi servira dans les modèles qui prédisent le comportement de la couche adhésive.
- Développement d'un modèle capable de prédire le comportement de la couche adhésive sous sollicitation de cisaillement dans un environnement "standard" (température ambiante et humidité et charges quasi-statiques).

## Organisation de la thèse

Le chapitre 2 de cette thèse présente l'état de l'art et aborde tous les concepts abordés dans cette étude.

---

Le chapitre 3 présente une procédure d'essai permettant de caractériser le comportement mécanique de la couche adhésive dans un joint collé soumis à une sollicitation de cisaillement. Cette procédure réalisée avec le banc d'essai Arcan permet d'obtenir des paramètres utiles dans une perspective d'essais de durabilité de joints collés sous sollicitation de cisaillement.

Le chapitre 4 est le texte de l'article "Theoretical assessment of ELS test data reduction technique using virtual testing" publié en 2021 [21]. Une publication sur le développement d'un modèle semi-analytique qui prédit la rupture du joint collé sous une sollicitation de cisaillement. La publication décrit également une méthode directe pour extraire la loi de comportement de la couche adhésive dans un joint collé métal-métal.

Le chapitre 5 présente une campagne expérimentale d'essais de rupture en cisaillement réalisée sur des joints collés métal-métal. Le modèle semi-analytique présenté au chapitre 4 est comparé aux résultats expérimentaux et validé.

Les conclusions et les perspectives sont mentionnées dans le chapitre 6.

Enfin, la liste des conférences suivies sont présentées en annexe.

# Conclusions

*Ceci est une traduction en français des conclusions présentées au chapitre 6. L'auteure recommande au lecteur de commencer la lecture du manuscrit au chapitre 1.*

Cette thèse porte sur l'analyse de la rupture de joints collés en mode II. L'objectif est de développer des procédures simplifiées prenant en compte la tolérance à l'endommagement afin de comprendre la propagation de fissures dans un joint collé structural métal-métal soumis à du cisaillement.

Premièrement, des essais Arcan ont été réalisés sur trois types d'adhésifs différents : deux adhésifs thermodurcissables (à base d'époxy) et un adhésif thermoplastique (à base de méthacrylate) (voir chapitre 3). Le montage Arcan a été configuré de manière à soumettre le joint collé à une charge de cisaillement. Des essais quasi-statiques et de fluage sous différents niveaux de température ont été réalisés. La température a été appliquée avec un outil de régulation thermique spécifique. Un dispositif de corrélation d'images (Digital Image Correlation - DIC - en anglais) a été utilisé pour identifier les déformations de la couche adhésive et la méthode de réduction des données a été décrite. Les comportements visqueux des trois adhésifs ont été identifiés de manière qualitative.

- La méthode DIC permet de suivre facilement les déformations dans la couche adhésive. La mesure des déformations n'a pas été perturbée par l'utilisation de l'outil de régulation thermique qui a chauffé les substrats et ainsi l'adhésif.
- La méthode DIC permet de mesurer les déformations réelles dans la couche adhésive et d'identifier où les déformations se localisent. Cela permet d'identifier le parcours de la fissure dans la couche adhésive.
- L'adhésif thermoplastique a un comportement visqueux prononcé même à température ambiante et la transition visco-élastique / visco-plastique est activée par l'augmentation de température.
- Les adhésifs thermodurcissables présentent un comportement quasi-fragile à température ambiante plutôt qu'un comportement visqueux.
- Les éprouvettes testées présentent des ruptures cohésives et adhésives. Cela met en évidence la variabilité des tests Arcan due à une mauvaise préparation de la surface d'adhésion avant collage.

Grâce au dispositif d'essai Arcan, des campagnes d'essais sur différents types d'adhésifs peuvent être menées afin de développer des modèles rhéologiques et d'étudier l'amorçage

---

de fissures dans des matériaux élastiques fragiles. Ces campagnes d'essais sont un pré-requis pour les études de rupture où le suivi de l'endommagement est la principale préoccupation. Les essais menés dans cette thèse conduisent à la conclusion suivante : les adhésifs thermoplastiques semblent mieux appropriés que les autres types d'adhésifs pour l'évaluation de l'endommagement en mode II dans un joint collé sous conditions environnementales sévères (temps, température) où la viscosité de la couche adhésive est un paramètre important à prendre en compte. Les adhésifs thermodurcissables, quant à eux, semblent plus appropriés pour le suivi des mécanismes d'amorçage et de propagation de fissures dans les joints collés sous chargement quasi-statique.

Deuxièmement, une analyse théorique des conditions d'initiation et de propagation de fissures dans un joint collé soumis à du cisaillement pur a été proposée (voir chapitre 4). Une éprouvette ELS a été testée virtuellement avec un modèle semi-analytique qui prend en compte la loi de comportement en cisaillement de la couche adhésive. Dans ce modèle semi-analytique, les substrats sont définis comme deux poutres de Timoshenko identiques. La loi de comportement de la couche adhésive, appelée aussi loi cohésive, est une succession de segments linéaires. Plusieurs configurations sont proposées : bi-linéaire élastique-plastique, bi-linéaire élastique-adoucie et trapézoïdale. Les déplacements des substrats, de leurs sections transversales ainsi que la déformation en cisaillement sont simulés avec le modèle semi-analytique et la sensibilité des déplacements aux différentes configurations de la loi de comportement de l'adhésif est évaluée. De plus, une méthode directe permettant d'extraire la loi de comportement de l'adhésif à partir de l'essai ELS est présentée. Cette méthode utilise soit la méthode de réduction des données issu de l'approche de Griffith soit l'approche intégrale de contour (J-intégral) pour l'essai ELS.

- Le comportement en cisaillement de l'adhésif est pris en compte dans le modèle semi-analytique. La loi de comportement permet de décrire l'évolution de l'endommagement à la pointe de fissure dans la couche adhésive et donc de décrire l'évolution de la zone de progrès de fissure. De plus, le module d'élasticité, la contrainte de cisaillement maximale admissible et la déformation en cisaillement à la rupture sont décrits avec la loi de comportement.
- Les principaux résultats de l'essai ELS sont les courbes force-déplacement et les "courbes R". D'après les résultats de la campagne d'essais virtuels, il a été observé que les courbes force-déplacement ne permettent pas une évaluation précise du comportement en cisaillement de la couche adhésive. En effet, il existe des artefacts expérimentaux tels que les conditions limites d'encastrement qui ne sont pas totalement respectées (degrès de liberté de rotation et de déflexion). La courbe force-déplacement est peu sensible à la forme de la loi de comportement. Les limites concernant les conditions limites ont été prises en compte grâce à des facteurs de correction déterminés analytiquement. La faible sensibilité à la forme de la loi de comportement a été corrigée en analysant le taux de restitution d'énergie (évalué à partir de  $G$  ou  $J$ ) en fonction de la déformation en cisaillement ( $\gamma$ ) plutôt que les courbes forces-déplacement ou les "courbes R".
- Pour évaluer le taux de restitution d'énergie, deux approches ont été utilisées :

l'approche utilisant la théorie de Griffith et celle utilisant l'intégrale de contour  $J$ . Les résultats montrent qu'avec l'intégrale de contour  $J$ , les artefacts expérimentaux qui perturbent les analyses avec l'approche de Griffith ne sont plus une préoccupation.

- La méthode directe pour extraire la loi cohésive de l'essai ELS consiste à "dérivée" la courbe  $J(\gamma)$ . C'est à dire d'appliquer un taux de restitution sur la courbe  $J(\gamma)$ .
- La présence d'une zone de progrès caractérisée par un comportement plastique ou d'adoucissement dans la loi cohésive a un impact visible sur la courbe  $J(\gamma)$ . Avant stabilisation du taux de restitution d'énergie : une évolution linéaire signifie que la loi cohésive a un plateau, une évolution concave signifie que la loi cohésive a une partie adoucie (linéaire à pente négative) prononcée, une évolution convexe signifie que la loi cohésive a une partie plastique prononcée.

Le modèle semi-analytique permet de prédire le comportement des éprouvettes ELS sous chargement quasi-statique. A partir de ce modèle, une nouvelle méthode directe a été évaluée pour extraire la loi cohésive à partir des résultats expérimentaux en utilisant une intégrale de contour  $J$ . Avec de nouvelles méthodes expérimentales comme la corrélation d'images, l'évolution des grandeurs nécessaires dans la formulation de l'intégrale de contour  $J$  peut être enregistrée avec précision.

Troisièmement, des essais ELS ont été réalisés sur deux adhésifs thermoplastiques : un adhésif très souple déjà testé lors de la campagne d'essais Arcan et un nouvel adhésif au comportement quasi fragile (voir chapitre 5). Ce dernier adhésif est recommandé pour observer l'évolution de l'amorçage et de la propagation de fissures dans les essais de rupture sous chargement quasi-statique. Différentes configurations géométriques (variations de la longueur de l'éprouvette  $L$ , de la longueur initiale de la fissure  $a_0$ , de l'épaisseur du substrat  $t$ ) ont été testées. La corrélation d'image est utilisée pour obtenir les grandeurs (rotations des sections des substrats à certains points repères et déformation en cisaillement) nécessaires à l'application de la méthode directe utilisant la courbe  $J(\gamma)$  présentée dans le chapitre 4. Comment utiliser la corrélation d'image dans le cas de l'évaluation de la déformation en cisaillement à la pointe de fissure est entièrement décrit. Les résultats expérimentaux et la simulation obtenue avec le modèle semi-analytique sont en accord.

- L'utilisation de la corrélation d'images permet de s'affranchir de la prise en compte de la souplesse du montage expérimental et d'accéder à toutes les grandeurs liées aux déplacements des substrats et à la déformation en cisaillement dans la couche adhésive. Avec ces données, la méthode utilisant la courbe  $J(\gamma)$  peut être appliquée pour extraire la loi de comportement de l'adhésif.
- Les résultats expérimentaux montrent que les substrats peuvent se déformer plastiquement si un adhésif souple est utilisé. Cela implique de modifier la géométrie de l'éprouvette et de prendre en compte dans la méthode de réduction des données les effets de grands déplacements.
- L'amorçage et la propagation de fissures ont été observées pour l'adhésif quasi-fragile. Des ruptures cohésives et adhésives ont été observées. Les éprouvettes avec



---

un rapport  $a_0/L$  inférieur à 0,55 ont expérimenté une propagation de fissures sur une courte distance.

- Le modèle semi-analytique ainsi que la méthode directe d'extraction de la loi cohésive en utilisant la courbe  $J(\gamma)$  ont été validés. Une loi cohésive de type trapézoïdale (segmenté) a été obtenue des essais et ensuite implémentée dans le modèle semi-analytique. Les résultats simulés et expérimentaux sont en accord.

L'essai ELS semble être un bon candidat pour les essais de rupture en mode II des joints collés. Avec des adhésifs quasi-fragiles, l'amorçage et la propagation de fissures peuvent être observées. Afin de développer des procédures d'essai de rupture de mode II, une bonne combinaison entre le test utilisé et le matériau a été trouvée. Cependant, le processus de fabrication des éprouvettes a un effet important sur leur comportement (rupture cohésive ou adhésive principalement). De plus, la méthode de réduction des données ainsi que la méthode d'identification directe de la loi cohésive ont été validées par comparaison des résultats expérimentaux et des résultats simulés. Le modèle semi-analytique peut être utilisé comme outil de prédiction pour l'essai de rupture ELS en mode II ou comme outil de vérification pour contrôler si une loi cohésive est représentative du matériau utilisé pour la couche adhésive dans un joint collé.

Cette thèse a pour but de définir des méthodologies d'essai fiables et des méthodes de réduction de données pour évaluer le comportement mécanique d'un joint collé sous sollicitation en cisaillement.

D'abord, deux procédures d'essai utilisant la corrélation d'images numériques ont été développées pour évaluer le comportement mécanique d'une couche adhésive dans un joint collé métal-métal sous sollicitation de cisaillement. Ces procédures sont :

- L'essai Arcan. Le comportement rhéologique de l'adhésif peut être déterminé avec cette méthodologie de test. L'identification du comportement élasto-viscoplastique de l'adhésif est importante surtout dans l'objectif de réaliser des tests de durabilité sur les joints collés.
- L'essai ELS. L'amorçage et la propagation de fissures peuvent être surveillées avec cette méthodologie d'essai. Suivre l'évolution de l'endommagement sous chargement quasi-statique est une première étape dans la compréhension de ce que peut supporter un joint collé au cours de son utilisation.

Ensuite, une méthode expérimentale a été décrite qui permet d'identifier directement le comportement en cisaillement de la couche adhésive. Cette loi est la première entrée dans un outil de simulation (analytique ou numérique) qui prédit le comportement mécanique des joints collés.

Finalement, un modèle semi-analytique a été développé et est capable de prédire le comportement du joint collé (déplacements des substrats, déformation et contrainte de cisaillement dans la couche adhésive) sous une sollicitation de cisaillement dans un environnement standard (température et humidité ambiantes et chargement quasi-statique).





# List of Figures

1	Modes de rupture. . . . .	viii
2	Montage Arcan. $t_a$ est l'épaisseur d'adhésif. . . . .	ix
3	(a) Essai ENF. (b) Essai ELS. $a$ est la longueur de fissure. $L$ est la longueur d'éprouvette. $t$ est l'épaisseur du substrat. $t_a$ est l'épaisseur d'adhésif. $w$ est la largeur de l'éprouvette. $P$ est la charge appliquée. $\Delta$ est le déplacement en bout d'éprouvette. . . . .	x
4	Differentes formes de loi cohésive (ALSB). . . . .	xiii
5	(a) Voiture BMWi3 [17]. (b) Exemple d'utilisation pour l'isolation d'un mur (Bostik $\text{\textcircled{R}}$ ) [18]. . . . .	xviii
6	(a) Faucille égyptienne [19]. (b) Structure d'un pneu [20]. . . . .	xviii
1.1	(a) Car BMWi3 [17]. (b) Example of use of adhesive for wall insulation from Bostik $\text{\textcircled{R}}$ [18]. . . . .	2
1.2	(a) Egyptian sickle head [19]. (b) Tyre structure view [20]. . . . .	3
2.1	Adhesive bonded joint description. Representation of adhesive and cohesive failure. . . . .	6
2.2	Failure modes. . . . .	7
2.3	Fracture Process Zone (FPZ) description [22]. (a) Under mode I loading. (b) Under mode II loading. . . . .	8
2.4	(a) Schematic representation of linear elastic spring with associated constitutive equation. (b) Schematic representation of linear dash-pot with associated constitutive equation and integrated constitutive equation. (c) Schematic representation of generalized visco-elastic models (Maxwell and Kelvin models) [23]. . . . .	13
2.5	Master curve construction from typical evolution of mechanical parameters of polymeric material [24]. . . . .	14
2.6	Shear characterisation tests for bonded joints geometries. OL is the Overlap Length. $h$ is the adherend thickness. $t_a$ is the adhesive thickness. (a) Single Lap Joint (SLJ) test. (b) Double Lap Joint (DLJ) test. (c) Thick Adherend Shear Test (TAST). (d) Arcan test. . . . .	15
2.7	Deformed state of bonded joint in SLJ test configuration under load. Shear strain $\gamma_{12} = 2\epsilon_{12}$ . $\gamma_0$ is the macroscopic imposed shear strain [5]. . . . .	16

2.8	Shear and peel stresses in the mid-plane of the adhesive layer for an average shear stress of 1 MPa for SLJ configuration with adhesive layer shape. $yy$ (black lines) corresponds to peel stresses. $xy$ (grey lines) corresponds to shear stresses. $l_2$ is the overlap length. $x$ is the position along the adhesive layer. Adherend thickness $h_1 = 6\text{mm}$ . Adhesive thickness $h_2 = 0.4\text{mm}$ . [25].	16
2.9	Effect of stiffness $E$ variation on peel (a) and shear (b) stress distributions in the adhesive layer for DLJ test configuration. Adhesive thickness $t_a = 0.2\text{mm}$ . Adherend thickness ratio $t_s/t_a = 10$ . Overlap length ratio $L_0/t_a = 200$ [26].	17
2.10	Shear stress repartition at joint mid-plane for the TAST and SLJ test configuration for two distinct joint overlap lengths: $OL = 10\text{mm}$ and $30\text{mm}$ [5].	18
2.11	Load-displacement curves of epoxy based adhesive BM1822 (a) and SP498 (b). Elastic regime followed by a large non-linear regime. Evolutions are different but great deformation of the adhesive layers are always observed under shear and tension loading [27].	18
2.12	Deformed state of bonded joint in Arcan test configuration under load. Shear strain $\gamma_{12} = 2\epsilon_{12}$ . $\gamma_0$ is the macroscopic imposed shear strain $F$ .	19
2.13	Geometry of Arcan test specimen : (A) drawing and (B) reality [28].	19
2.14	(a) Schematic representation of the combination of springs and damper elements (one Maxwell model and two Zener models in serie) used in the rheological model assumed in this study. (b) Model compliance expressed with strain as a function of time. Material constitutive parameters are the average stress $\bar{\sigma}$ , stiffnesses $E_0, E_1, E_2, E_\infty$ of the spring elements, the viscosity $\eta_1, \eta_2, \eta_3$ and characteristic time $\theta_1, \theta_2$ (defined with $E_0, E_\infty, \eta_1, \eta_2$ ). (c) Uniaxial creep test results obtained with DLJ test configuration [29].	20
2.15	Schematic representation of load-displacement curve obtained during a fracture test controlled by force with an elastic material.	23
2.16	Classical load-displacement curve for ELS test. Crack propagates when maximum of the curve is reached. $a_0$ is the initial crack length. $L$ is the specimen length. Effect of the FPZ size on stability of the test [30].	24
2.17	Schematic representation of the contour for J-integral integration for an ELS test. $\Gamma_a, \Gamma_b, \Gamma_c, \Gamma_d, \Gamma_e, \Gamma_f, \Gamma_g$ and $\Gamma_{TIP}$ are part of the integration path $\Gamma$ [31].	24
2.18	Schematic representation of classic cohesive law shapes that stands for failure of a bonded joint in mode I [32].	26
2.19	Classic beam representation of a fracture specimen for modelisation. $t$ is the adherend thickness. $a$ the crack length. $x$ the position along the specimen length. $u$ is the horizontal displacement. $v$ the vertical displacement. $\varphi$ the rotation angle.	26
2.20	Undeformed and deformed representation of material with a crack [33].	28
2.21	Comparison between VCCT and CZM (advantageous features indicated with a blue color) [34].	29
2.22	Double Cantilever Beam (DCB) test description [35].	29

2.23	Photographs of two classical mode II test set-up (End loaded Split test) from two different laboratories [36]. . . . .	30
2.24	Fracture tests for bonded joint. $L$ is the characteristic length of the specimen. $a$ the initial crack length. $t$ is the adherend thickness. $t_a$ the adhesive thickness. $P$ is the applied load. $\Delta$ is the loading tool displacement. $w$ is the specimen width. (a) End Notched Flexure (ENF) test. (b) Four-point End Notched Flexure (4ENF) test. (c) Stabilised End Notched Flexure (SENF) test. (d) End Loaded Split (ELS) test. (e) Inverse End Loaded Split (ELS). . . . .	31
2.25	Data reduction method effect on result from ENF test. CCM : Compliance Calibration Method. DBT : Direct Beam Theory. Compliance Based-Beam theory. (a) Effect on compliance estimation. (b) Effect on mode II fracture energy [37]. . . . .	33
2.26	ELS (a) and I-ELS (b) test configurations with bending moment representations along the adhesive layer [38]. I-ELS test clamping representation is different from the one presented in Fig. 2.24 but the test principal configuration is the same. . . . .	34
2.27	Classical load-displacement curve for ELS test. Crack propagates when maximum of the curve is reached. $a_0$ is the initial crack length. $L$ is the specimen length. Effect of large displacement (LD) on stability of the test [30]. . . . .	36
2.28	Gravity fixture for creep testing of adhesives [13]. . . . .	38
2.29	Effect of temperature on a bulk specimen made of PMMA under tensile loading [39]. . . . .	39
2.30	Wedge test for durability assessment of bonded joint [15]. . . . .	41
2.31	Example of environmental and alternating load coupling test device [40]. . . . .	42
3.1	Presentation of the Arcan fixture mounted in shear loading configuration. The arrow shows the loading direction. . . . .	49
3.2	Arcan adherend geometry. Dimensions are in mm. . . . .	50
3.3	Dynamic mechanical Analysis of SAF MIB 30 adhesive. Storage and loss shear modulus. Evidence of glass transition temperature. Results taken at 7.2 Hz. . . . .	51
3.4	Presentation of the Arcan specimen manufacturing set up. . . . .	52
3.5	Presentation of the test set-up : temperature regulation tool, Arcan set-up placed in the machine, camera and led lighting. . . . .	52
3.6	Presentation of the temperature regulation tool set-up. . . . .	53
3.7	Zone Of Interest (ZOI) and subsets description. . . . .	54
3.8	Picture and Arcan specimen coordinate systems. Description of the longitudinal displacement $u$ and normal displacement $v$ . . . . .	55
3.9	Description of the extracted data from the DIC software. Only half of the Arcan specimen (adherend 1) is represented. . . . .	55
3.10	Rotation angle description. Only half of the Arcan specimen (adherend 1) is represented. Dimensions are overestimated. . . . .	56

## LIST OF FIGURES

---

3.11	Relative longitudinal displacement calcul description. . . . .	57
3.12	Strain field analysis. . . . .	59
3.13	Shear stress vs shear strain for DP 490. DIC and machine data. . . . .	60
3.14	Shear stress vs shear strain for DP 760. DIC. . . . .	61
3.15	Failure surfaces of Arcan specimens bonded with DP490. Quasi-static test until failure. . . . .	62
3.16	Failure surfaces of Arcan specimens bonded with DP760. Quasi-static test until failure. . . . .	62
3.17	Failure surfaces of Arcan specimens bonded with SAF MIB 30 1. Quasi-static test until failure. Arrows designate the direction of each adherend. . . . .	63
3.18	Failure surfaces of Arcan specimens bonded with SAF MIB 30 2. Quasi-static test until failure. Arrows designate the direction of each adherend. . . . .	64
3.19	Failure surfaces of Arcan specimens bonded with SAF MIB 30 3. Quasi-static test until failure. Arrows designate the direction of each adherend. . . . .	64
3.20	Shear stress versus shear strain for Arcan specimens bonded with SAF MIB 30. Quasi static test. Speed rate was 0.2 mm/min. . . . .	65
3.21	Creep loading test at 3000 N load - 3.44 MPa on Arcan specimen bonded with SAF MIB 30 at various temperatures. Shear strain versus time. Rejuvenated Arcan specimen. Data are obtained with the DIC. . . . .	65
3.22	Creep loading test at 3000 N load on Arcan specimen bonded with SAF MIB 30. Shear strain versus time. Non-rejuvenated and rejuvenated Arcan specimen. Data are obtained with the DIC. . . . .	66
3.23	Creep loading test at 3000 N load on Arcan specimen bonded with SAF MIB 30. Shear strain versus time. Non-rejuvenated Arcan specimen. Data are obtained with the DIC. . . . .	67
3.24	Cyclic creep-recovery test on Arcan specimen bonded with SAF MIB 30 adhesive. Shear strain versus time and applied stress. Data are obtained with the DIC. . . . .	67
3.25	Cyclic creep-recovery test on Arcan specimen bonded with SAF MIB 30 adhesive. Residual shear strain at the end of each cycle versus time. Data are obtained with the DIC. . . . .	68
3.26	Creep loading test at 3000 N load - 3.44 MPa on Arcan specimen bonded with SAF MIB 30 at various temperatures. Shear strain versus time. Rejuvenated Arcan specimen. Data are obtained with the DIC. . . . .	69
3.27	Creep loading test at 400 N load - 0.41 MPa on Arcan specimen bonded with SAF MIB 30 at various temperatures. Shear strain versus time. Rejuvenated Arcan specimen. Data are obtained with the DIC. . . . .	70
3.28	Creep loading test at various load level on Arcan specimen bonded with SAF MIB 30 at room temperature. Rejuvenated Arcan specimens. Data are obtained with the DIC. . . . .	70
3.29	Creep loading test at 400 N load - 0.41 MPa on Arcan specimen bonded with SAF MIB 30 at various temperatures. (a) Shear strain at 1h, 5h, 10h, 20h, 30h, 40h versus temperature. (b) Shear strain gap versus temperature. Rejuvenated Arcan specimen. Data are obtained with the DIC. . . . .	71

4.1	End Loaded Split (ELS) test configuration description. . . . .	76
4.2	Load-displacement curve for elastic-softening (SOFT1) configuration with two different initial crack lengths. Unstability of the ELS test description. . . . .	77
4.3	Load-displacement curve for purely elastic configuration. Effect of adhesive layer compliance. . . . .	78
4.4	Kinematic and static quantities definition. . . . .	79
4.5	Different types of Adhesive Layer Shear Behaviour (ALSB). . . . .	80
4.6	Description of Fracture Process Zones and boundary conditions in a trapezoidal ALSB configuration for the ELS test. . . . .	81
4.7	Stress-strains curves of the ALSB configurations. . . . .	82
4.8	Load-displacement curves for elastic-softening (SOFT1) and trapezoidal (TRAP2) configurations. (a) Overview. (b) Close up. . . . .	83
4.9	Displacement evolutions versus position along the specimen length for elastic-softening (SOFT1) and trapezoidal (TRAP2) configurations. (a) Beam deflection. (b) Beam rotation. (c) Beam longitudinal displacement. Refer to Fig. 4.7 for ALSB identification. . . . .	84
4.10	Normal force (a) and bending moment (b) evolutions along the specimen length for elastic-softening (SOFT1) and trapezoidal (TRAP2) configurations. Refer to Fig. 4.7 for ALSB identification. . . . .	84
4.11	Shear strain (a) and stress (b) evolutions along the specimen length for elastic-softening (SOFT1) and trapezoidal (TRAP2) configurations. Refer to Fig. 4.7 for ALSB identification. . . . .	85
4.12	Crack length ratio evolutions for elastic-softening (SOFT1), trapezoidal (TRAP2) and purely elastic (ELAS) configurations. . . . .	86
4.13	Integration path, section definition of the ELS test for derivation of J-integral equation. . . . .	86
4.14	SERR normalized by the critical strain energy release rate $\mu_c$ vs effective crack length for elastic-softening (SOFT1) and trapezoidal (TRAP2) configurations according to CBTE theory (a) and J-integral theory (b). (c) and (d) are close ups of respectively (a) and (b). . . . .	87
4.15	SERR normalized by the critical strain energy release rate $\mu_c$ vs shear strain at crack tip for elastic-softening (SOFT1) and trapezoidal (TRAP2) configurations (with key-points identification). . . . .	87
4.16	First derivate of $J(\gamma)$ curve versus shear strain at crack tip for SOFT1 and TRAP2 ALSB configurations. . . . .	88
4.17	Close ups on SERR normalized by the critical strain energy release rate $\mu_c$ vs shear strain at crack tip for elastic-softening (SOFT1) and trapezoidal (TRAP2) configurations with virtual 1 % noise. . . . .	89
4.18	First derivate of $J(\gamma)$ curve versus shear strain at crack tip for SOFT1 and TRAP2 ALSB configurations with virtual noise. . . . .	89
4.19	SERR vs shear strain at crack tip for all configurations. Refer to Fig. 4.7 for ALSB identification. . . . .	90
4.20	First derivatives of SERR vs shear strain at crack tip for all configurations. Refer to Fig. 4.7 for ALSB identification. . . . .	90



LIST OF FIGURES

---

5.1	End Loaded Split (ELS) test configuration description. . . . .	102
5.2	I2M laboratory ELS test set-up. . . . .	103
5.3	AMADE laboratory ELS test set-up. . . . .	104
5.4	Description of the two zones of interest (ZOIs) on ELS test specimen. . . . .	105
5.5	Description of the two zones of interest (ZOIs) on ELS test specimen. Description of the sections and their coordinates and reference frame, displacements of the centers of the subsets, position along the adhesive layer. . . . .	105
5.6	Description of the three principal steps for the DIC data reduction method. . . . .	106
5.7	Exemple of quasi-static test on ELS specimen bonded with SAF MIB 30 adhesive. Load displacement curve (a). Shear strain versus position along the adhesive layer at maximum load (b). Rotation angle versus position along the superior adherend at maximum load (c). Picture of the specimen bent at maximum load and localisation of the adhesive layer (d). The arrow shows the crack propagation direction. . . . .	108
5.8	Experimental results for specimen bonded with SAF MIB 30 adhesive. Quasi-static tests at room temperature at 0.5 mm/min. (a) Load versus displacement curves. (b) Maximum shear strain versus position along the adhesive layer. Each curve corresponds to the load level evidenced with a cross on Fig. (a). . . . .	109
5.9	Initial geometry for the ELS test dimensioning. . . . .	110
5.10	Quasi-static tests at room temperature at 0.5 mm/min for aluminium 7075 T6 beam. Crossed red line is a linear regression. Black cross is yield onset. . . . .	111
5.11	Experimental results for specimen SAF <sub>1</sub> bonded with SAF MIB 30 adhesive. Quasi-static test at room temperature at 0.5 mm/min. (a) Load versus displacement curves. Red crossed line is a linear regression. (b) Shear strain at load level marked with a cross on (a) versus position along the adhesive layer. . . . .	111
5.12	Load-displacement curve for all Araldite specimen (a). $J(\gamma)$ curves for all Araldite Specimen (b). . . . .	112
5.13	Failure surface of specimen Araldite <sub>49</sub> . Arrow shows the crack propagation direction. . . . .	113
5.14	Failure surface of specimen Araldite <sub>52</sub> . Arrow shows the crack propagation direction. . . . .	113
5.15	Failure surface of specimen Araldite <sub>53</sub> . Arrow shows the crack propagation direction. . . . .	113
5.16	Failure surface of specimen Araldite <sub>54</sub> . Arrow shows the crack propagation direction. . . . .	114
5.17	Failure surface of specimen Araldite <sub>56</sub> . Arrow shows the crack propagation direction. . . . .	114
5.18	Shear stress versus shear strain curves and extracted ALSB for all Araldite specimens. . . . .	115
5.19	ALSB for specimens Araldite <sub>49</sub> , Araldite <sub>52</sub> , Araldite <sub>56</sub> . . . . .	115

5.20	Comparison between experimental data and simulated data of Araldite <sub>49</sub> specimen. Shear stress versus shear strain curve - ALSB (a). Load-displacement curves (b). Rotation angle versus position along the adherend (c). Deflection versus position along the adherend (d). Shear strain versus position along the adhesive layer (e). . . . .	116
5.21	$J(\gamma)$ curves obtained with the experimentation for the specimen Araldite <sub>49</sub> (full line) and with the semi-analytical model (dotted line). . . . .	117
6.1	Pure Bending Test (PBT) for bonded joint. . . . .	126
6.2	Schematic representation of the moments in PBT. . . . .	126
A.1	Aussois poster. "Comportement mécanique des joints sous sollicitation de cisaillement" . . . . .	128
A.2	JADH poster. "Modèle analytique de l'essai ELS pour l'étude des joints collés sous sollicitation de cisaillement" . . . . .	129

## LIST OF FIGURES

---

# List of Tables

3.1	DP490 properties obtained with quasi-static Arcan test in shear configuration at room temperature. DIC and machine data. . . . .	61
3.2	DP760 properties obtained with quasi-static Arcan test in shear configuration at room temperature. DIC data. . . . .	61
3.3	SAF MIB 30 properties obtained with quasi-static Arcan test in shear configuration at room temperature. DIC and machine data. . . . .	63
4.1	Adhesive layer properties for various ALSB configurations . . . . .	82
5.1	Adhesives mechanical properties. Data are extracted from the manufacturer data sheet and the study presented in chapter 3. . . . .	102
5.2	ELS Specimen bonded with SAF MIB 30 adhesive : geometrical characteristics . . . . .	109
5.3	Shear strain value at crack tip for specimen bonded with SAF MIB 30 adhesive. . . . .	110
5.4	Description of Araldite specimens geometry. $L$ is the working length. $a_0$ is the initial crack length. $a_0/L$ the ELS ratio. $t$ the adherend thickness. $t_a$ the adhesive thickness. . . . .	112
5.5	Description of extracted ALSB for specimens Araldite <sub>49</sub> , Araldite <sub>52</sub> , Araldite <sub>56</sub> . $G_a$ is the extracted adhesive shear modulus. $\tau_{max}$ is the maximum shear stress. $\gamma_2$ is the shear strain at which softening behaviour begins. $\gamma_{max}$ is the maximum shear strain. $t_a$ the adhesive thickness. . . . .	114

## LIST OF TABLES

---

# Chapter 1

## Introduction

## 1.1 Background

The bonding joint technique for structural assembly is being widely developed since 50 years. One way to explain this expansion is the increase of the use of structural parts made with composite materials. Indeed, their good mechanical performances associated to their low density allow to obtain reliable but light structures. They also have good crash behaviour and good corrosion resistance. But their price, manufacturing, recycling and assembly are their main concerns. The assembly issue is the main interest in this thesis. There are multiple ways to assemble structural parts together : riveting, welding, bolting, bonding. The first three ones, in the case of composite assembly, implies stress concentrations, oxidation and weight issues. The bonding solution has appeared to be the preferred solution for composite assembly. From that, development of the technique has spread in multiple fields : transport industry (boats, cars, planes, trains), civil industry (solar panels, bridges), medical field (see Fig. 1.1). Bonded joints consist in two adherends (also called substrats) made of various types of materials (aluminium, composite, concrete ...) linked together with an adhesive made of polymeric materials. Also, one can see composite parts as a material made of several bonded joints : each layer of resin between fibre layers being considered as an adhesive layer.

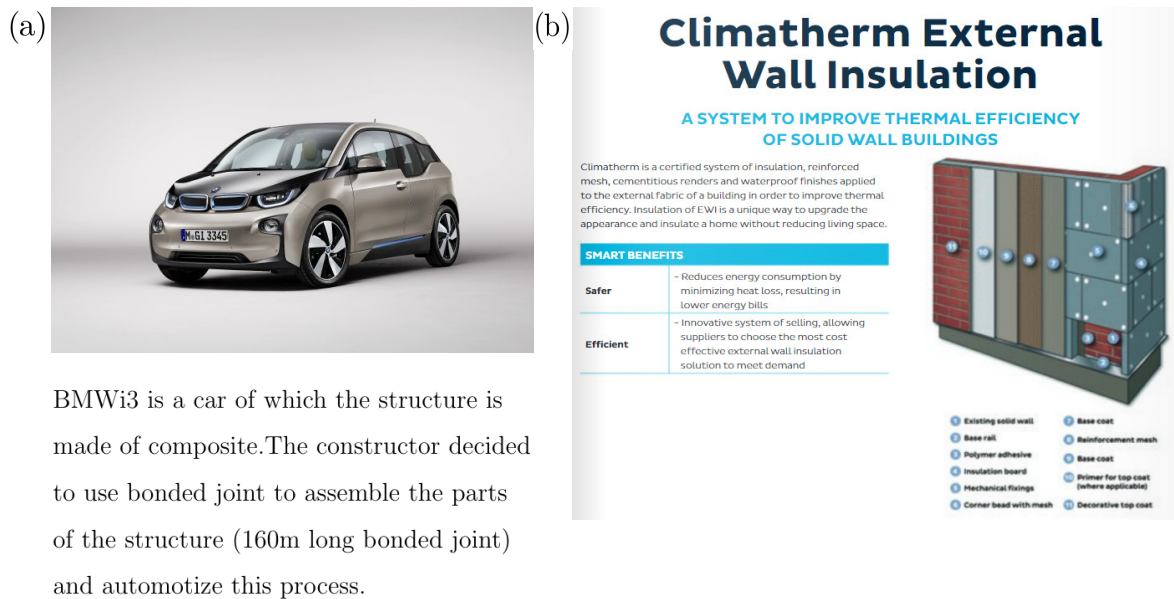


**Figure 1.1:** (a) Car BMWi3 [17]. (b) Example of use of adhesive for wall insulation from Bostik <sup>®</sup>[18].

Bonding is a known technique used since egyptian time : a sickle has been found where the teeth were bonded with tar to the wood handle. In the 19th century, first synthetic adhesive appeared : Goodyear in 1840 introduced the rubber and Dunlop in 1888 used it in the first tyre where layers of rubber were bonded together (see Fig. 1.2). In 1940, first metal to metal bondings appeared and started the era of structural bonding.

Bonding, besides assembly, has sealing properties, allows to put together structures with complicated shapes and made from dissimilar materials, can adapt to various environmental conditions. Many solutions are possible considering the variety of adhesives

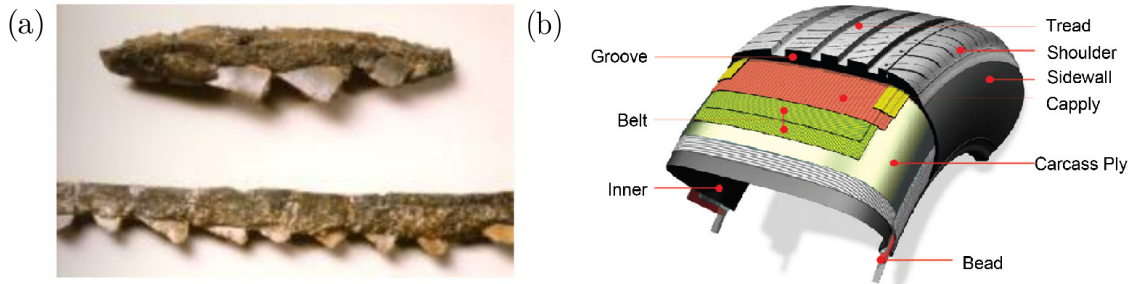


**Figure 1.2:** (a) Egyptian sickle head [19]. (b) Tyre structure view [20].

available. Moreover, loads are transferred along the whole bonded surface and not locally. However, this technology is not competitive yet for applications which require a high level of reliability due to the lack of adhesion control techniques and robust design rules. These technological issues make difficult the assessment of bonded joints sustaining long service life and which may encounter complex loading (fatigue, stationary, shock, ...) combined with aggressive physico-chemical environment (temperature, moisture, ...) that can be experienced in applications such as wind blades, tidal turbines and aeronautic structures.

Reinforcing the robustness of the failure prediction of such structures is thus necessary. This is possible with damage tolerance oriented design approaches. This requires to master the initiation and the propagation conditions of initial decohesion (also called crack) that can occur in a bonded joint. In the context of durability this problem is rather complex since several phenomena are involved in the damage process leading to a highly multiphysic and coupled problem.

This thesis took place in I2M laboratory in Bordeaux University. A part of the thesis took place in AMADE laboratory in Gerona University for knowledge sharing between the two institutions.

## 1.2 Motivation

Nowadays, most studies focus on the interlaminar fracture toughness under traction and shear loading of the resin in a composite part. If one wants to study mechanical behaviour of the adhesive layer in a structural bonded joint, peeling is the common failure mode assessed because it is the weakest failure mode. But it appears that bonded joints are generally designed to sustain shear load. Moreover, in the perspective of durability testing, the preferred test for shear loading of bonded joints is the Single Lap Joint (SLJ) test. But it suffers from many artefacts like edge effect, stress singularities and multiaxial stress conditions. Eventually, only a few testing procedures take into account the viscous behaviour and specific phenomena like the non-linear mechanisms occurring in the Fracture Process Zone (FPZ) that appears in polymeric materials when they are loaded.

The main goal of this project is to assess the mechanical behaviour of bonded joint under shear loading in severe environmental conditions (effect of the temperature). The aim for that purpose is to develop simplified procedures in a damage tolerance perspective that help understanding the crack propagation under shear loading for metal-to-metal



bonded joints.

## 1.3 Objectives

This thesis aims to define reliable test methodologies and data reduction methods to assess the mechanical behaviour of bonded joint under shear loading. Several objectives have been defined :

- Development of procedures to get the mechanical behaviour of an adhesive layer in a metal-to-metal bonded joint under shear loading. The obtained data will serve to assess durability of the bonded joint with the identification of visco-elasto-plastic parameters and crack propagation resistance with the identification of fracture toughness.
- Development of an experimental and analysis procedure to identify the bonded joint behaviour law (also called cohesive law) of the adhesive layer. This law will serve in models that predict the adhesive layer behaviour.
- Development of a model able to reproduce the adhesive layer behaviour under shear loading in a standard environment (room and humidity temperature and quasi-static loads).

## 1.4 Thesis description

Chapter 2 of this thesis presents the state of the art and address every concept approached in this study.

Chapter 3 presents one procedure to characterise the adhesive layer mechanical behaviour in a bonded joint under shear loading. This procedure performed with the Arcan test set-up allows to obtain parameters useful in a perspective of durability testing of bonded joint under shear loading.

Chapter 4 is the text of the article "Theoretical assessment of ELS test data reduction technique using virtual testing" published in 2021 [21]. A publication on the development of a semi-analytical model that predicts the bonded joint fracture behaviour under shear loading. The publication also describes a direct method to extract the behaviour law of the adhesive layer in a bonded joint.

Chapter 5 presents the experimental shear fracture test campaign conducted on metal-to-metal bonded joints. The semi-analytical model presented in chapter 3 is compared to the experimental results and validated.

Concluding remarks and perspectives are mentioned in Chapters 6.

Eventually, the list of conferences attended are presented in the appendix.

# Chapter 2

## Litterature review

### Contents

---

<b>1.1</b>	<b>Background</b> . . . . .	<b>2</b>
<b>1.2</b>	<b>Motivation</b> . . . . .	<b>3</b>
<b>1.3</b>	<b>Objectives</b> . . . . .	<b>4</b>
<b>1.4</b>	<b>Thesis description</b> . . . . .	<b>4</b>

---

This state of the art deals with the following problematic : how to analyse adhesive bonded joints behaviour under shear loading. The objective is to set the working environment to answer this problematic.

The first section presents the adhesive bonded joints at issue : how is it used from an industrial point of view and how to test it from an experimental point of view. The second section concerns the mechanical characterisation of adhesive bonded joints under shear loading : tests, experimental locks and methods. The third section is about the fracture tests available for bonded joints under mode II loading : tests, experimental locks and methods. Eventually, perspectives on durability testing of adhesive bonded joints under shear loading is addressed.

## 2.1 Adhesive bonded joints description

As seen in chapter 1, an adhesive bonded joint consists in two pieces called adherend (or substrat) linked together with a polymeric material called adhesive (see Fig. 2.1). It is a solution for assembling pieces together. Composite can be seen as material with multiple bonded joints : each layer of the resin between the fiber sheets can be seen as an adhesive layer. This is why study of bonded joints is often linked to the study of delamination in composite materials in the literature.

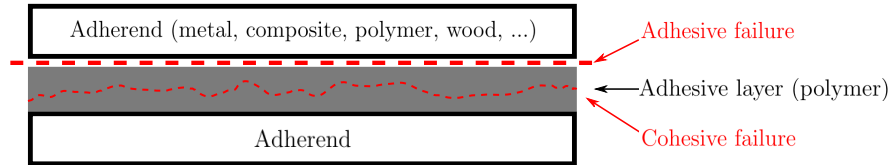


**Figure 2.1:** Adhesive bonded joint description. Representation of adhesive and cohesive failure.

Bonded joints are not only used to link pieces together but they are also used to support high levels of loads in a structure, to be reliable and durable. This thesis focuses on the use of structural adhesives for bonded joints.

The advantages of using the bonded joint technique are : weight saving, ability to assemble dissimilar materials having complex shapes, the sealing properties, the good corrosion, impact and vibration resistance and the thermal and electric insulation. Many solutions are possible considering the variety of adhesives available [1].

However, structures with bonded joints are not easy to disassemble or to recycle. Bonding two pieces together is a long and complex process : adherend surface preparation, adhesive application, adhesive layer control without destruction. Failure and damage of the adhesive layer can occur because of severe loads from quasi-static to dynamic or fatigue loads in multiple direction (tensile, shear or torsion loading). Failure and damage of the adhesive layer can also occur because of severe environmental conditions with the effect of temperature and humidity [1].

### 2.1.1 Structural bonding investigation

#### 2.1.1.1 Adhesive bonded joints test

Bonded joints are nowadays used in structural applications. Prior to that, they need to be assessed in terms of load capacity and durability under in-service conditions. This paragraph addresses the principal concepts in bonded joints testing where failure and damage have to be observed. In that way, the specimen for bonded joint mechanical test can be seen as two beams bonded together. Tests differ depending on the geometry of the beams (width, thickness, length, some specific artefact), the loading and clamping conditions in the testing machine, the data reduction method and eventually the bonded volume (the bonded area and the adhesive thickness). Nevertheless, all the specimens used in the tests mentioned in the present work have in common a parallelepiped shape which then leads to solving two-dimensioned problem for the data reduction methods. Two categories can

be distinguished. Characterisation tests allow to obtain principal material parameters of the adhesive layer like Young's modulus and strength at break as well as identifying the rheological behaviour of the adhesive layer. Fracture tests allow to analyse crack initiation and propagation in the adhesive layer. In other words, these tests allow to characterise damage evolution in the adhesive layer.

### 2.1.1.2 Failure modes

Cracked adhesive layers may sustain three different loading conditions described in Fig. 2.2. The mode I (Fig. 2.2), also called the opening or peeling mode, is produced by forces perpendicular to the crack plane. The mode II (Fig. 2.2), also called the sliding or shear mode, is produced by forces parallel to the crack plane and perpendicular to the crack line. The mode III (Fig. 2.2), also called the tearing mode, is produced by forces parallel to the crack plane and the crack front. Cracks may propagate when the bonded joint is submitted to quasi-static loads as well as creep or fatigue loadings and mechanical stresses induced by complex environmental conditions with temperature and humidity variations.

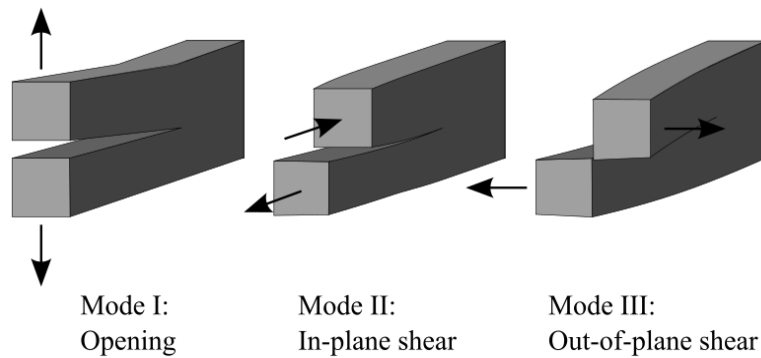


Figure 2.2: Failure modes.

It has been noticed that bonded joints show weak resistance under peel loading where lower stress levels are sustained compared to shear loading. Moreover, bonded joints are mostly used in overlap configurations [1]. This is why, in this thesis, the analysis will focus on characterisation of mode II crack propagation regime in bonded joints due to shear loading.

### 2.1.1.3 Adhesive and cohesive failures

Failure of a bonded joint can occur in two distinct ways : adhesive failure between adhesive and adherends or cohesive failure. Adhesive failure (see Fig. 2.1) deals with the capacity of the interface to create strong link between the adherends and the adhesive. Cohesive failure (see Fig. 2.1) deals with the ability of the adhesive itself to resist to mechanical loadings. Adhesive failure mainly occurs because of poor surface preparation, bad chemical link between the adherend and the adhesive layer, severe environmental conditions hence degradation of the chemical link between surfaces, bad coupling between adherend

material type and adhesive material type. Cohesive failure mainly occurs because of mechanical loads. In structural bonding for mechanical engineers, in order to evaluate the resistance of the bonded joints to crack propagation, studies focus on cohesive failure which means that the bonding step (surface preparation, adhesive application, polymerisation of the adhesive) is mastered. Cohesive failure is also a mandatory condition for bonded joints to be used in industries for structural applications.

#### 2.1.1.4 Fracture Process Zone (FPZ)

Adhesive layers are made of polymeric material which are known to exhibit viscous and time dependent behaviour. When studying a crack evolution in a bonded joint, a localized plastic deformation at the crack tip is produced because of the stress concentrations and singularities there. This partially damaged zone can still transfer stresses through aggregate interlocking and various microcracks [1, 2, 3]. This region is called the Fracture Process Zone (FPZ), it corresponds to the distance along which large stress / strain gradients are developing ahead the decohesion front [4] as shown in Fig. 2.3. The FPZ is much larger for ductile material but exist for quasi-brittle as well [3, 41]. It is also has been noticed that under shear loading, the FPZ length is more significant than under tensile loading [12, 42, 43].

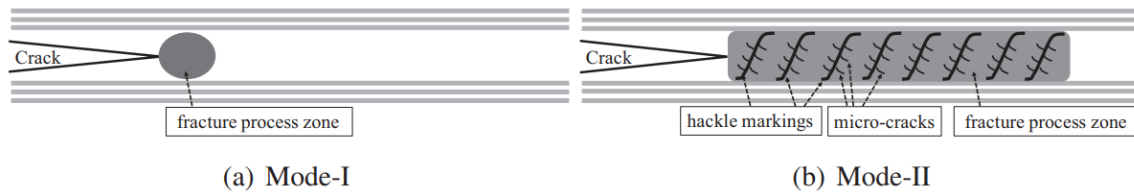


**Figure 2.3:** Fracture Process Zone (FPZ) description [22]. (a) Under mode I loading. (b) Under mode II loading.

### 2.1.2 Polymeric materials for the adhesive layer

All adhesives are polymers which are specifically formulated to develop strong interaction with adherend surfaces and achieve adequate bulk mechanical properties. In this paragraph, principal material characteristics are defined, then polymers as adhesives are described and the concept of interface and adhesion is assessed.

#### 2.1.2.1 Principal material characteristics

Polymers can be classified in four categories differentiated by their physico-chemical properties (different types of bonds between molecules and the molecular chains that compose the polymers) [24]. In order to choose the adhesive type needed for a specific application, one can rely on the bulk mechanical properties like Young's modulus, failure strength. But these properties depend on two essential parameters : the glass transition temperature  $T_g$  and the melting temperature  $T_f$  (for concerned polymers).  $T_g$  is the temperature

at which a polymer can go from relatively brittle "glassy" state into a viscous rubbery state.  $T_f$  is the temperature at which a polymer can go from solid state to liquid state. The four categories are :

- Non-crosslinked thermoplastic amorphous polymers. In these polymers, molecular chains are randomly organised. Their young's modulus is impacted by the glass transition temperature under which the polymers are in a glassy state and the young's modulus order of magnitude is 1 *GPa*. Above  $T_g$  these polymers are in a rubbery state until high temperature where the young's modulus drops significantly.  $T_g$  range is very large from negative temperature to 150 ° C.
- Semi-crystalline thermoplastic polymers. In these polymers, amorphous zones co-exist with more organized molecular chains. Their young's modulus is impacted by the glass transition temperature under which the polymers are in a glassy state and the young's modulus order of magnitude is 1 *GPa*. Above  $T_g$  and under  $T_f$  these polymers are in a smooth/elastic state and the young's modulus order of magnitude is 100 *MPa*. Above  $T_f$ , these polymers are in a rubbery state until high temperature where the young's modulus drops significantly. The young's modulus order of magnitude is then 1 *MPa*.
- Thermosetting polymers. In these polymers, the molecular chains are crosslinked. Their young's modulus is impacted by the glass transition temperature under which the polymers are in a glassy state and the young's modulus order of magnitude is 1 *GPa*. Above  $T_g$ , the young's modulus order of magnitude is 100 *MPa* and chemical degradation occurs when the temperature is too high. These polymers are usually used in a range of temperature under their  $T_g$ .
- Crosslinked elastomers. There are less crosslinking points in these polymers compared to thermosetting polymers but the evolution of the young's modulus with the temperature is similar. Above  $T_g$ , the young's modulus order of magnitude is 1 *MPa* and chemical degradation occurs when the temperature is too high. The difference with thermosetting polymers is that elastomers are typically used above their  $T_g$  (which is often low) for rubbery applications.

The glass transition temperature is a kinetic phenomenon linked with the rate at which the polymer is solicited and this concept is discussed in section 2.2.1. The melting temperature is a thermodynamic phenomenon that occurs only for amorphous polymers. Also, water molecule presence in polymers can act as a plasticizer which is linked to  $T_g$  [44]. In the case of durability assessment of bonded joint, effect of temperature and humidity on the adhesive layer mechanical behavior has to be taken into account.

### 2.1.2.2 Polymers as adhesives

For structural adhesives, synthetic polymers are used mainly. Two categories can be highlighted : reactive adhesives and physical adhesives. The reactive adhesives are thermosetting polymers and in order to create a bonded joint, their cure has to be done

trough temperature variation and chemical reaction (UV exposition, moisture, ...). The physical adhesives are thermoplastic adhesives and the cure is due to physical changes : solidification or solvent evaporation. The adhesives can be one-component products (need for external activation for polymerisation) or two-component products (resin and reactive).

The main structural adhesives available are :

- Epoxy based adhesives : they are thermosetting polymers often used in the aviation or car industry [27]. A large field of application is available because of the good adhesion on various surfaces and the good mechanical performances. Epoxy based adhesives can be either one or two component products.
- Polyurethane based adhesives are thermosetting polymers often used for their flexibility compared to epoxy adhesives. Again, these adhesives are widely used in multiple fields, one can save the nautic field because polyurethane is know for having good humidity resistance [45]. Polyurethane based adhesives can be either one or two component products.
- Acrylic based adhesives are thermoplastic polymers which need an external agent for polymerization. It can be ambient humidity. They are known for their biocompatibility [44].

Acrylic and epoxy based adhesives are more rigid than polyurethane ones. Other types of adhesives are available for more specialized applications (methacrylate based, silicone based, cyanoacrylate based, ...).

### 2.1.2.3 Interface concept

The last issue with polymers as structural adhesives is how to deal with the interface. This is the region between the adhesive layer itself and the adherends (see Fig. 2.1) where the so called "adhesive failure" presented in section 2.1.1 may occur. In structural bonding investigation, tools for description of the mechanical behaviour of bonded joints differs with the observation scale. Indeed the interface between the adhesive layer and the adherend can be seen as graded material. Rheological properties at the interface differs from the rheological properties of the adhesive layer itself. In our case, for a study with a mechanical macroscopic point of view, the connection between the adhesive layer and the adherends is supposed to be strong hence only cohesive failure is studied. Moreover, it has to be understood that even from this point a view, the mechanical behaviour of a bonded joint is controlled by the interface. There are three types of connection : mechanical anchoring (loads are transferred from the adherend to the adhesive thanks to irregularities of the adherend surfaces), physico-chemical adhesion (for polymeric adherends, the molecular chains interact with each other) and the chemical adhesion (covalent bonds are developed between the adhesive and the adherends).

### Overview

The adhesive bonded joint technique is considered as an assembly possibility for structural applications since the 20th century. It allows to fulfil multiple goals besides assembling parts together. Study of composite materials led the development of investigation procedures for bonded joints.

Bonded joints have to be challenged in order to assess the reliability of the technique for structural applications. Damage evolution can be evaluated : tools for observing crack initiation and propagation in the adhesive layer are available. However, loading conditions and fracture process zone have to be taken into account. Only metal-to-metal bonded joint will be concerned in this thesis so the focus is on the adhesive layer. The adhesive layer material in structural bonding is always polymeric. These types of materials have a large field of applications and are sensitive to multiple in-service conditions : loads, temperature, humidity.

Experimental investigation of bonded joint under shear loading is the main concern of this thesis : specimens have to relay realistic conditions but specific considerations have to be fulfilled. In what follows, mechanical characterisation tests available for bonded joints submitted to shear loading are presented with how to take into account the polymeric origin of the adhesive layer. Next, mode II fracture tests for bonded joints are presented.



## 2.2 Mechanical characterisation of bonded joints

In this section are presented the theoretical framework and modelisation of bonded joints with mechanical characterisation tests, then the principal existing mechanical characterisation tests with their drawbacks and advantages. Eventually, determination of the adhesive layer rheological properties of the adhesive layer in a bonded joint specimen is described.

### 2.2.1 Theoretical framework and modelisation of bonded joints

In order to evaluate the mechanical response of bonded joints hence to evaluate the behaviour law of the adhesive layer, various types of tests are available. Quasi-static tests allow to obtain stress-strain curves directly. Different geometries are presented in the next section with their advantages and drawbacks. These geometries can also be used for creep testing or stress relaxation tests that evidence the viscous phenomena that occur in adhesives when they are loaded. These tests allow to attest the effects of time and temperature on the adhesive layer mechanical response and determine the rheological properties of the material. Eventually, with Dynamic Mechanical Analysis (DMA), sinusoidal loading is applied and mechanical and rheological properties of the adhesives can be evaluated.

Creep testing consists in applying constant stress during a long period of time and to observe the resulting deformation. On the contrary, stress relaxation tests consist in applying constant deformation during a long period of time and to observe the resulting stress. Observing the unloading response (in both type of tests) of the adhesive also gives information on the viscous behaviour of the adhesive. Simple analytical models allow to describe the rheological behaviour of the adhesive. The base of a rheological model is to use a combination of linear elastic spring and linear viscous dash-pot (see figure 2.4 (a) and (b)). The principal parameters of these models are the stiffness  $E$ , the viscosity  $\eta$ , the characteristic relaxation times  $\tau_i$  and the yield stress  $\sigma_y$ . The most known and simplest models are the Maxwell and the Kelvin models (see figure 2.4 (c)). These models can be generalized in order to describe more precisely the behaviour of a material (see figure 2.4 (c)). In order to get models that gives better prediction, use of non-linear elements (spring, dash-pot, slider) can be required [23, 24].

It exist an other way that exhibit the viscous behaviour of polymeric material as well : sinusoidal loading. With Dynamic Mechanical Analysis (DMA) system, it is possible to conduct tests at various temperature and frequencies under sinusoidal loading. Testing at various frequencies is similar to testing at various duration (like in transitional regime) since the frequency is proportional to the inverse of time. DMA testing can be done under deformation or stress control as long as Boltzmann principle is respected and small strains occur ( $10^{-3}$  to  $10^{-2}$ ).

With sinusoidal loading, new mechanical parameters have to be defined. As an example, analysis of a shear test on a polymeric material controlled by the deformation is proposed :

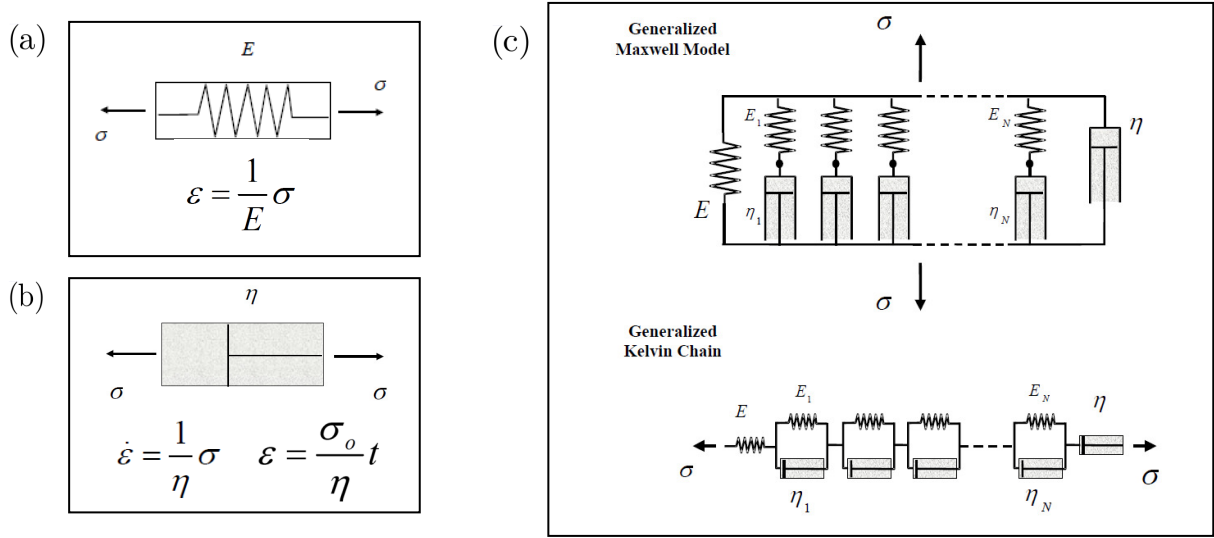


**Figure 2.4:** (a) Schematic representation of linear elastic spring with associated constitutive equation. (b) Schematic representation of linear dash-pot with associated constitutive equation and integrated constitutive equation. (c) Schematic representation of generalized visco-elastic models (Maxwell and Kelvin models) [23].

$$\gamma = \gamma_0 \sin \omega t \quad (2.1)$$

where  $\gamma$  is the shear strain,  $\gamma_0$  the initial magnitude of the signal,  $\omega$  is the angular frequency and  $t$  is the time.

The mechanical response will be :

$$\tau = \tau_0 \sin(\omega t + \delta) \quad (2.2)$$

where  $\tau$  is the shear stress,  $\tau_0$  is the magnitude of the signal and  $\delta$  is the phase lag between the strain and stress.  $\delta$  is also called loss angle and is significant of the viscosity of the tested material. From eqs. 2.1 and 2.2, storage modulus  $G'$ , loss modulus  $G''$  and phase angle  $\delta$  are defined as :

$$G' = \frac{\tau_0}{\gamma_0} \cos \delta \quad (2.3)$$

$$G'' = \frac{\tau_0}{\gamma_0} \sin \delta \quad (2.4)$$

$$\delta = \arctan \frac{G'}{G''} \quad (2.5)$$

$G'$  stands for the elastic part of the mechanical response,  $G''$  stands for the viscous part of the mechanical response.

With complex formalism, we have :

$$G^* = \frac{\tau_0}{\gamma_0} \exp(i\delta) = G' + iG'' \quad (2.6)$$

Similarly, the compliance  $J$  and young's modulus  $E$  are determined.

The tests presented just before lead to isothermal characterisation of the material. But it is known that polymeric materials are temperature dependant. Transtional testing or DMA testing can be done at various temperatures on the same material and at various durations. It exists a connection between effect of time and temperature on the mechanical response of polymers called the time-temperature superposition principle. It supposes that data collected  $D$  ( $J$ ,  $E$ ,  $G$ , creep or stress relaxation relations) at a duration  $t$  at two different temperature  $T_j$  and  $T_0$  are equal following the equation :

$$D(T_j, t) = D(T_0, a_{T_j/T_0} t) \quad (2.7)$$

where  $a_{T_j/T_0}$  is the translation factor (defined with WLF equation) that only depends on  $T_j$  and the reference temperature  $T_0$ . The time-temperature superposition principle is based on the fact that mechanical response of a polymeric material observed for short duration at high temperature is equivalent to the mechanical response observed for long duration at low temperature. This led to the development of master curves that can be used as references to predict evolution of the main data of interest at various temperatures over a larger range of time (or frequencies) than the one experimentally available. Fig. 2.5 shows typical master curve developed from typical evolution of mechanical parameters of polymeric materials.

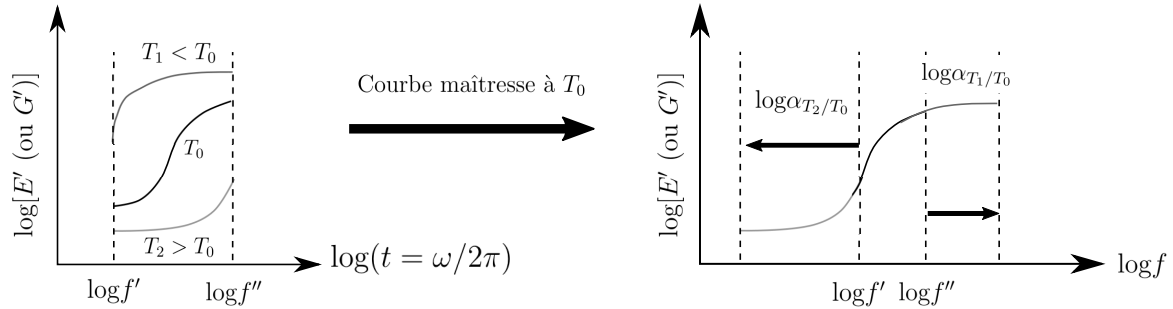


**Figure 2.5:** Master curve construction from typical evolution of mechanical parameters of polymeric material [24].

The concepts presented in this section aim to understand the mechanical response obtained with characterisation tests. In these tests, homogeneous stress state is an objectif for identification of the viscous phenomena in the adhesive layer.

## 2.2.2 Characterisation tests

Various tests exist for the characterisation of adhesive bonded joints under shear loading. Only tests where the adhesive layer is submitted to shear loading are presented here since focus is on shear behaviour of bonded joints. Moreover, the objective with these tests is to obtain pure homogeneous shear stress state in the adhesive layer. Tests consist in two slabs having rectangular cross section called adherend bonded together with an adhesive layer. Specimens are placed in a conventional tensile testing machine and each side is pulled to produce shear deformation with relative displacement between the two

adherends. Displacements are observed with extensometers or Digital Image Correlation (DIC) technique. Characterisation tests are representative of the crack onset and/or the stress-strain evolution of the adhesive bonded joints. Various geometries are proposed, they differs by the adherend thickness, the adhesive thickness, the bonded area and how the adherends are placed relatively to each other [5]. The main objective of these test set-ups is to obtain homogeneous stress state in order to identify pure shear mechanical properties for the bonded joints. The output of these tests are stress-strain curves. The advantages and drawbacks of the different test set-ups available in the literature are described in the next paragraphs. Fig. 2.6 shows the principal characterisation tests available currently.

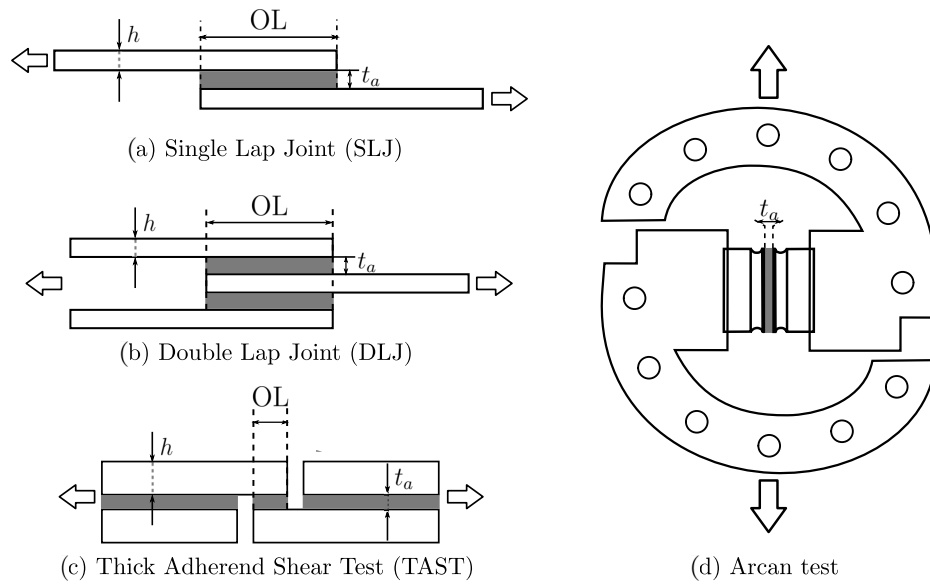


**Figure 2.6:** Shear characterisation tests for bonded joints geometries. OL is the Overlap Length.  $h$  is the adherend thickness.  $t_a$  is the adhesive thickness. (a) Single Lap Joint (SLJ) test. (b) Double Lap Joint (DLJ) test. (c) Thick Adherend Shear Test (TAST). (d) Arcan test.

### 2.2.2.1 Single Lap Joint (SLJ) test

The Single Lap Joint (SLJ) (Fig. 2.6 (a)) is the most used and oldest test because of its simple design [5]. It consists in two rectangular thin plates (adherends) bonded together [46]. The specimen geometry is defined by the thicknesses of the adhesive and the adherends so as the Overlap Length (OL, see Fig. 2.6 (a)). These parameters influence the geometry of the test which leads to more or less compliant specimen and more or less important stress singularities. Indeed, the SLJ test is submitted to a complex and heterogeneous stress distribution because of additional moment induced by the asymmetry of the geometry which deteriorates highly the homogeneity of the shear stress (see Fig. 2.7) [5, 47, 48].

The adhesive layer does not experiment pure shear loading but also peel stresses at the edges of the adhesive layer associated with both the geometrical, adhesive and adherend

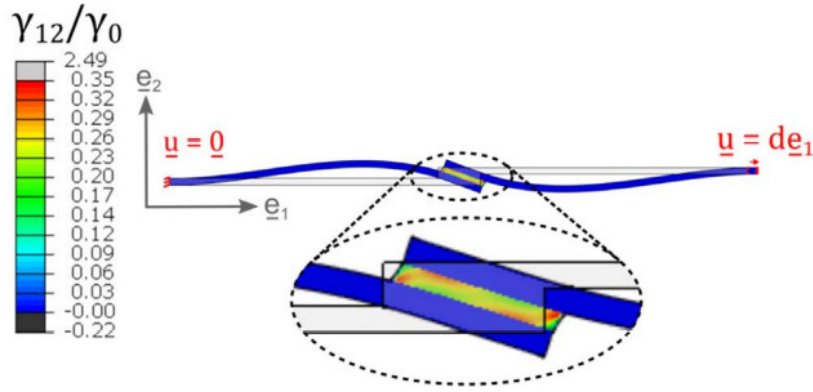


**Figure 2.7:** Deformed state of bonded joint in SLJ test configuration under load. Shear strain  $\gamma_{12} = 2\epsilon_{12}$ .  $\gamma_0$  is the macroscopic imposed shear strain [5].

material parameters (see Fig. 2.8) [25, 49]. Thicker adherends or high yield strength material for adherends could be a solution so that the stress state is less influenced [49, 50].

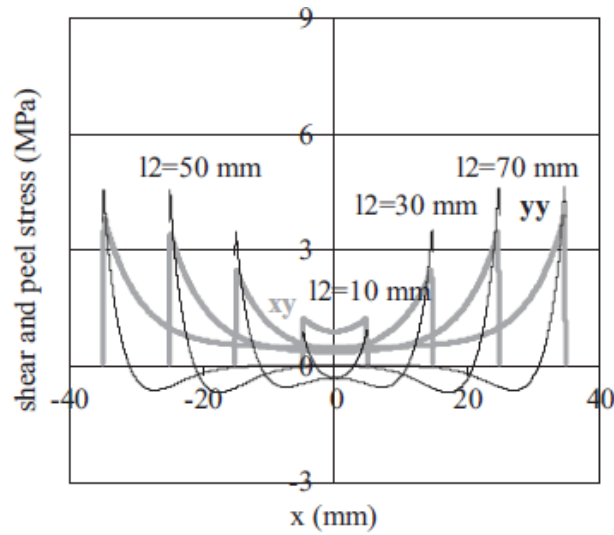


**Figure 2.8:** Shear and peel stresses in the mid-plane of the adhesive layer for an average shear stress of 1 MPa for SLJ configuration with adhesive layer shape.  $yy$  (black lines) corresponds to peel stresses.  $xy$  (grey lines) corresponds to shear stresses.  $l_2$  is the overlap length.  $x$  is the position along the adhesive layer. Adherend thickness  $h_1 = 6\text{mm}$ . Adhesive thickness  $h_2 = 0.4\text{mm}$ . [25].

### 2.2.2.2 Double Lap Joint (DLJ) test

The Double Lap Joint (DLJ) (Fig. 2.6 (b)) is an alternative version of the SLJ test. It consists in two plates bonded on both sides of one plate [51]. With this geometry, the peel stresses are redistributed and stress singularities are lower than for the SLJ test thanks to the increase of axial modulus of the adherend [26, 29]. In Fig. 2.9 (a), maximum peel and shear stress concentration at the overlap ends are reduced with the increase of the

axial modulus of the adherend. Again, pure shear in the adhesive layer is not achieved (see Fig. 2.9 (b)).

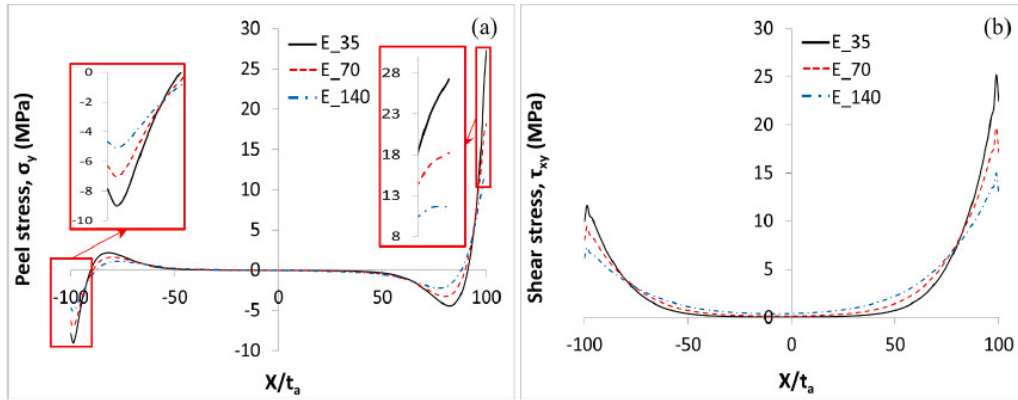


**Figure 2.9:** Effect of stiffness  $E$  variation on peel (a) and shear (b) stress distributions in the adhesive layer for DLJ test configuration. Adhesive thickness  $t_a = 0.2\text{mm}$ . Adherend thickness ratio  $t_s/t_a = 10$ . Overlap length ratio  $L_0/t_a = 200$  [26].

The overlap length is the principal geometrical value of interest and the nature of the failure depends on it. Two different failure mechanisms were distinguished : from quasi-brittle failure for short OL to ductile failure for longer OL (relatively to the specimen dimensions). More over, adhesive failure was observed for short OL whereas adherend yielding occurred for longer OL, the adhesive failure being then a secondary effect [52].

### 2.2.2.3 Thick Adherend Shear Test (TAST)

The Thick Adherend Shear Test (TAST) (Fig. 2.6 (c)) consists in four thick plates bonded together [53]. The zone of interest is the middle one, the two adherends on the outside are used to limit the rotational moment of the assembly during loading [5]. Thicker adherends are used to overcome the weaknesses of SLJ and DLJ tests : the ratio toughness/OL allows to get closer to pure homogeneous shear stress state as seen in Fig. 2.10 [5].

Shorter OL reduces significantly the peel stresses at the edge of the adhesive layer [54]. TAST can be seen as a logical extension of the SLJ test.

### 2.2.2.4 Arcan test

The Arcan test (Fig. 2.6 (d)) consists in two half disk having several holes equally spaced along the circumference [6]. No standard exists for this test set-up and numerous modified versions have been proposed following the same global scheme (one can refer to the following publications to observe different Arcan set-up geometries [5, 6, 55, 56]). The specimen is clamped to two hinges that are pinned to a tensile testing machine. This test set-up has the possibility to test the specimen under tension loading, shear loading or mixed shear-compression loading depending on the orientation of the specimen with respect to the loading direction. Bresson *et. al.* [57] used this property to evaluate the

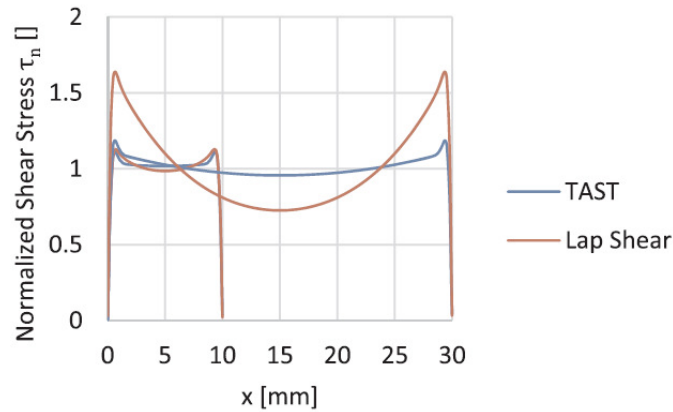


**Figure 2.10:** Shear stress repartition at joint mid-plane for the TAST and SLJ test configuration for two distinct joint overlap lengths:  $OL = 10\text{mm}$  and  $30\text{mm}$  [5].

failure envelope for epoxy adhesive. Fig. 2.11 shows stress-strain curves for two different adhesives tested under tensile and shear loading.

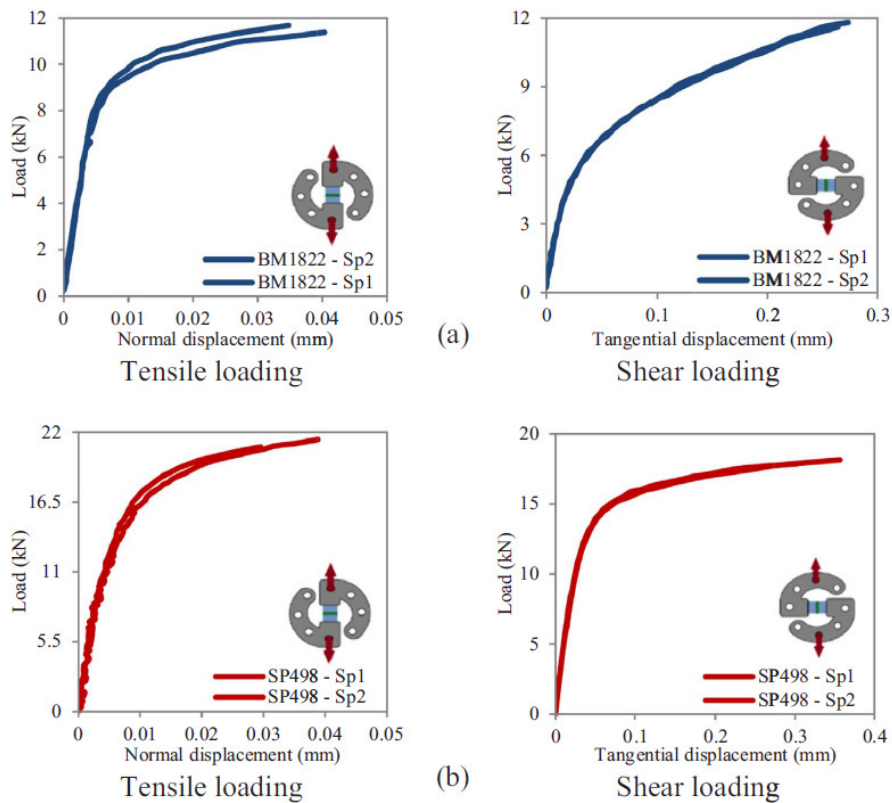


**Figure 2.11:** Load-displacement curves of epoxy based adhesive BM1822 (a) and SP498 (b). Elastic regime followed by a large non-linear regime. Evolutions are different but great deformation of the adhesive layers are always observed under shear and tension loading [27].

Arcan test has been created in 1978 by Arcan with the purpose of testing/producing uniform plane-stress state for fiber reinforced material [6]. Arcan test main goal is to

obtain controlled homogeneous stress state with specimens which have an optimized geometry (see Fig. 2.12) [5, 6, 25, 27, 55, 56, 58]. Again, the major drawback encountered with this set-up is the presence of stress singularities at the edge of the adhesive layer.

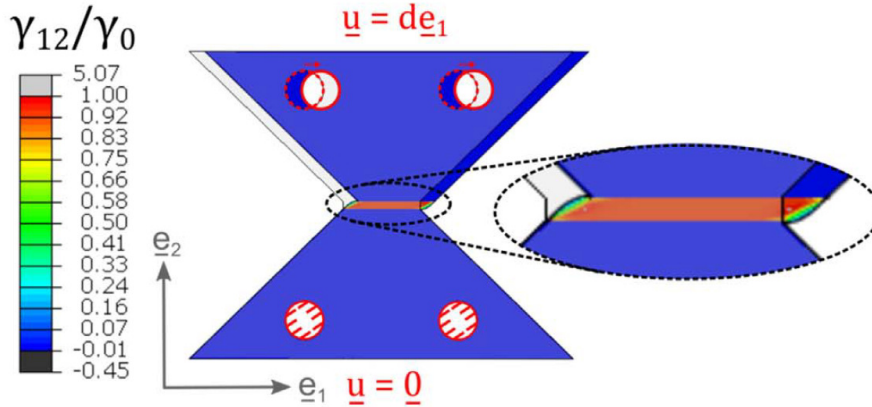


**Figure 2.12:** Deformed state of bonded joint in Arcan test configuration under load. Shear strain  $\gamma_{12} = 2\epsilon_{12}$ .  $\gamma_0$  is the macroscopic imposed shear strain  $F$ .

Numerous studies have been conducted in order to limit this phenomena : conclusions led to the necessity of beaks on the adherend as shown in Fig. 2.13 [5, 28, 47, 59]. It is also valid for other configurations like tubular butt-bonded specimen [60] or thin composite specimens [47, 61]. The adhesive thickness is also a major concern, for example it has been shown that elastic deformation in epoxy adhesive is proportional to the adhesive thickness and the failure load decrease when the adhesive thickness rises [62].

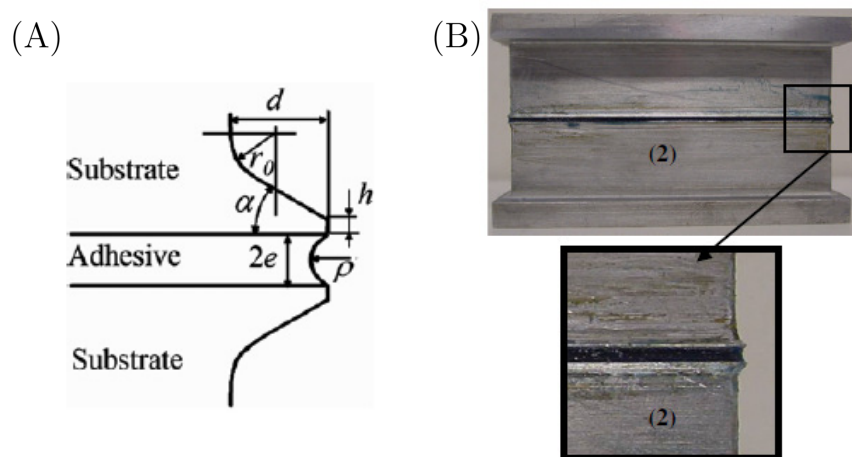


**Figure 2.13:** Geometry of Arcan test specimen : (A) drawing and (B) reality [28].

### 2.2.3 Adhesive rheological model determination

One of the major output of studies using the characterisation tests presented before is the determination of the rheological properties of the adhesive layer in a structure like specimen from simple time-strain and time-stress curves. The principal rheological properties



are the stiffness  $E$ , the viscosity  $\eta$ , the characteristic relaxation times  $\tau_i$  and the yield stress  $\sigma_y$  [24]. These properties are translated into parameters of rheological models that describe viscous material behaviour.

For example, Saeimi *et. al.* [29] studied the mechanical behaviour of a DLJ test configuration with an epoxy adhesive. Firstly, they defined a rheological model composed by linear elastic spring and linear viscous damper (see Fig. 2.14 (a)) from which they extracted a material constitutive law (see Fig. 2.14 (b)). Then they extracted the values of the material constitutive parameters through nonlinear regression of the experimental results of creep tests (strain-time curves) (see Fig. 2.14 (c)). Good agreement was found between the predicted rheological model and the experimental results, which allows to characterise the time-dependent behaviour of the material.

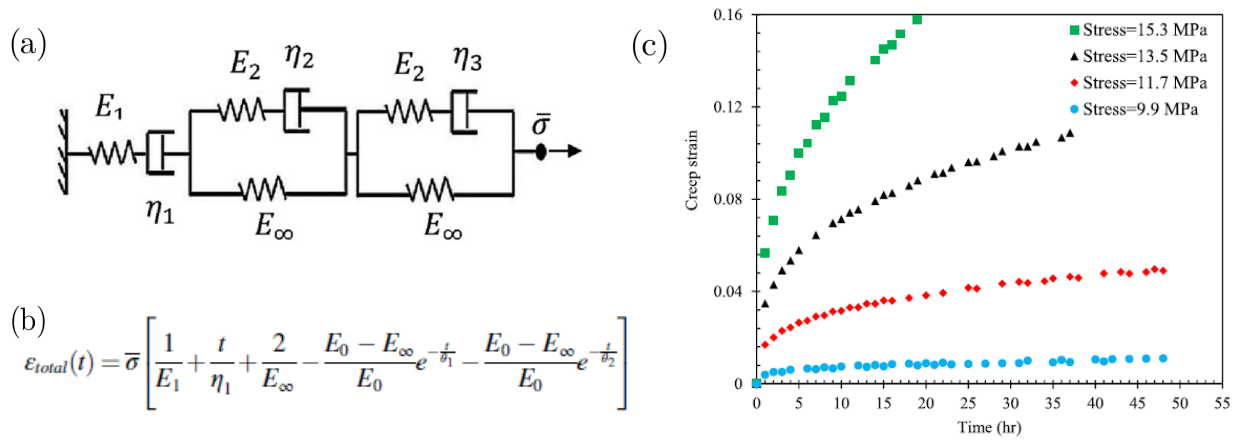


**Figure 2.14:** (a) Schematic representation of the combination of springs and damper elements (one Maxwell model and two Zener models in serie) used in the rheological model assumed in this study. (b) Model compliance expressed with strain as a function of time. Material constitutive parameters are the average stress  $\bar{\sigma}$ , stiffnesses  $E_0$ ,  $E_1$ ,  $E_2$ ,  $E_\infty$  of the spring elements, the viscosity  $\eta_1$ ,  $\eta_2$ ,  $\eta_3$  and characteristic time  $\theta_1$ ,  $\theta_2$  (defined with  $E_0$ ,  $E_\infty$ ,  $\eta_1$ ,  $\eta_2$ ). (c) Uniaxial creep test results obtained with DLJ test configuration [29].

Sometimes, use of non-linear elements (spring, dash-pot, slider) can be required [23, 24] to evidence plasticity or visco-plasticity of some materials.

The Arcan test is often used for identification of rheological properties of adhesives. Indeed, the Arcan test set-up allows to perform multiple test like creep test, quasi-static test under various loading conditions [55, 63, 64, 65, 66, 67] which enables to extract all the necessary parameters for the development of viscoelastic-viscoplastic models. Ilioni *et. al.* [64] needed two creep tests in two loading directions to identify the viscoelastic part of their model and monotonic test to identify the viscoplastic part on an epoxy based adhesive. Bidaud *et. al.* [55, 65] studied a two components polyurethane based thermoplastic adhesive that exhibited a pronounced viscous behaviour.

Characterisation of the rheological behaviour of bonded joint is important because, from a durability point of view, adhesive layers may sustain stationnary loading over a long period and other environmental conditions. With the aim of predicting behaviours

of bonded joints under severe conditions, modeling is needed to identify rheological parameters.

### Overview

Adhesives are polymeric materials and mechanical characterisation tests allow to highlight the viscous phenomena that occur when bonded joints are loaded. More over, these tests allow to obtain major parameters like young's and shear modulus at various temperatures and durations. Awareness of these quantities is a step forward to the understanding of mechanical behaviour of adhesives hence bonded joints.

Various tests exist for assessing mechanical behaviour of bonded joints under shear loading. Measuring the stress-strain curves is straightforward and experimental results of these tests allow rheological properties identification.

The major drawback of these characterisation tests is the fact that pure shear is not always achieved except for the Arcan test configuration. Moreover, these tests experience instantaneous failure (cracks propagate spontaneously). With the objective of analysing complete mechanical behaviour of bonded joint, getting only crack onset values is not enough.

Rheological properties identification is needed to complete the characterisation of adhesive layers because of their polymeric origins and their possible use in severe environmental conditions.

Understanding the stress distribution in adhesively bonded joint is necessary for reliable evaluation of the adhesive behaviour with the aim of modeling and predicting the adhesive layer mechanical behaviour. However, these mechanical characterisation tests are representative of the apparent behaviour of the bonded joint but does not evidence the damage evolution in the adhesive layer. These tests need to be completed by fracture testing and modeling where crack initiation and propagation are monitored.

## 2.3 Fracture tests of adhesive bonded joints

In contrast with mechanical characterisation tests, what can be called "fracture tests" allows to study crack initiation and propagation in an adhesive bonded joint. They also allow to get fracture toughness evaluation, which is one of the most important properties to ensure suitable levels of tolerance to damage in adhesive bonded joints [68]. This section presents the theory dealing with fracture in bonded joints, assesses the existence of mode I fracture tests and describes the geometries of mode II fracture tests.

### 2.3.1 Theoretical framework and modelisation of fracture in bonded joints

#### 2.3.1.1 Theoretical framework

This section presents the theoretical framework to understand how a crack can initiate and propagate in a bonded joint. By using Linear Elastic Fracture Mecanics (LEFM), Griffith (1920) is the first one to assume the energy balance concept for fracture tests. The principal hypotheses assumed are small deformations, elastic and linear materials, quasi static regime, straight crack propagation in a 2D model. The Griffith theory states that, for brittle materials, a crack will propagate when the reduction in potential energy that occurs due to crack growth is greater than or equal to the increase in surface energy due to the creation of new free surfaces. This theory leads to the definition of the Strain Energy Release Rate (SERR)  $G$  as :

$$G = \frac{dU_p}{dA} \quad (2.8)$$

Where  $dU_p$  is the change in potential energy resulting from the creation of the crack and  $dA = 2w.da$  is the area of the created crack surfaces (two surfaces) with  $w$  being the crack width and  $a$  the crack length.

Failure of the adhesive layer occurs when  $G$  overgoes a critical value  $G_c$ . This value is also called fracture toughness or fracture energy. It is considered as a material property by Griffith. The SERR is the principal parameter to monitor in order to evaluate damage in a bonded joint.

SERR can be evaluated with the specimen compliance. During fracture tests, applied load  $P$  and displacement  $\Delta$  of the specimen are monitored. Study of the compliance of the specimen  $C = \Delta/P$  during the fracture tests allows to get the expression of the SERR, in the hypotheses of the LEFM theory. Fig. 2.15 is a schematic representation of the compliance evolution of an elastic material after being loaded with an increment of  $dP$  resulting in an increase of  $da$  in crack length.

According to Fig. 2.15, the fracture energy  $G$  expression corresponding to the SERR is :

$$G = \frac{1}{2w} \frac{dU_p}{da} = \frac{1}{2w} \left( \frac{Pd\Delta}{da} - \frac{\Delta dP}{da} \right) \quad (2.9)$$

with  $C = \Delta/P$ ,

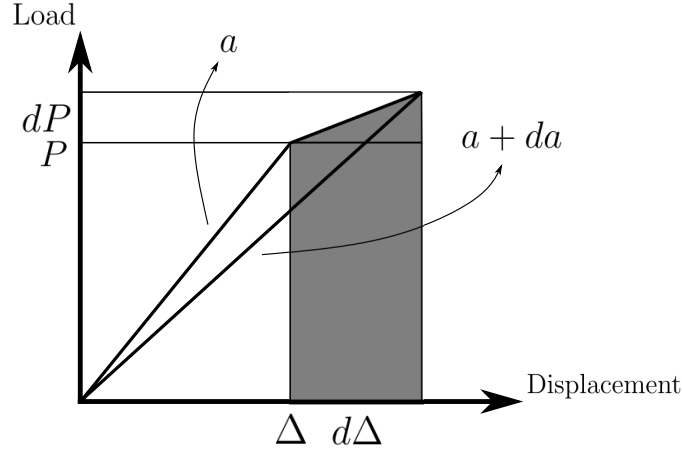


**Figure 2.15:** Schematic representation of load-displacement curve obtained during a fracture test controlled by force with an elastic material.

$$G = \frac{P^2}{2w} \frac{dC}{da} \quad (2.10)$$

Where  $w$  is the specimen width. The SERR is dependant on the compliance and its variation with respect to crack length. If :

$$\frac{dG}{da} \geq 0 \quad (2.11)$$

The compliance curve will change its "curvature" and this will be translated as a load jump meaning unstable crack propagation. This is why the following criterion need to be respected in order to have stable crack propagation and being able to monitor crack propagation :

$$\frac{dG}{da} \leq 0 \quad (2.12)$$

The SERR can be derived and estimated from the compliance expression which is often obtained using beam theory approaches. Classical formalism for mode II fracture tests are presented in section 2.3.3.

The compliance approach is based on LEFM hypotheses but adhesives are elasto-visco-plastic materials that experiment the FPZ phenomena. In fracture testing, the FPZ needs to be fully developed so that the crack can propagate in a steady state regime [3, 30, 69]. Moreover, it has been observed that large FPZs ensure stability for fracture tests [30, 69] (see Fig. 2.16) especially for tests where mode II crack propagation regime is expected. Indeed, under shear loading the FPZ can be very long [3].

The FPZ effect on the SERR has to be taken into account. The compliance approach is then not suitable unless correction terms are added in the compliance expression. This is adressed in section 2.3.3. The J-integral approach is suitable to evaluate the SERR in the case of the presence of elasto-visco-plastic phenomena at crack tip. The J-integral approach, first introduced by Rice [7], consists in evaluating the energetic balance between strain energy density at crack tip and surface traction vector along a closed path near the

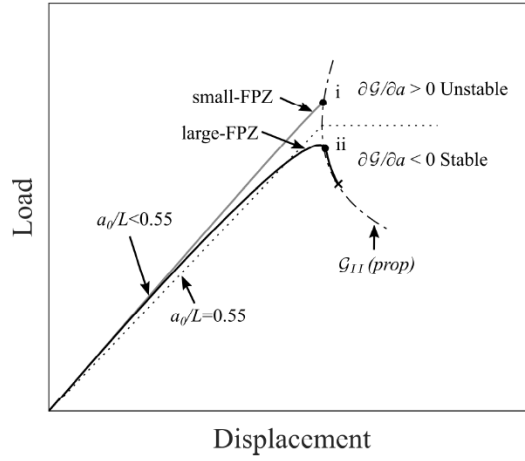


**Figure 2.16:** Classical load-displacement curve for ELS test. Crack propagates when maximum of the curve is reached.  $a_0$  is the initial crack length.  $L$  is the specimen length. Effect of the FPZ size on stability of the test [30].

crack tip.

Rice's theory shows that J-integral is equal to the strain energy release rate for a crack in a body subjected to monotonic loading if the crack extends straight ahead with respect to its original orientation. Rice also shows that the estimation of  $J$  hence the SERR is independant of the path chosen as long as it does not contour a singularity. In this way, restraining conditions of the LEFM theory like sharp crack tip are no longer an issue and SERR in elasto-plastic material can be determined [70]. Perèz *et. al.* [31] used Rice approach with mode II fracture test, the J-integral path is showed in Fig. 2.17 and the  $J$  is defined as :

$$J = \int_{\Gamma} \left[ \omega dx_2 - T_k \frac{\partial u_k}{\partial x_1} ds \right] \quad (k = 1, 2) \quad (2.13)$$

where  $\Gamma$  is a closed path enclosing the crack tip (see Fig. 2.17),  $u_k$  is the displacements vector,  $ds$  an infinitesimal arc length along  $\Gamma$ , and  $x_1$  and  $x_2$  are the horizontal and vertical coordinates, respectively.  $\omega$  is the strain energy density and  $T_k$  is the tractions vector.

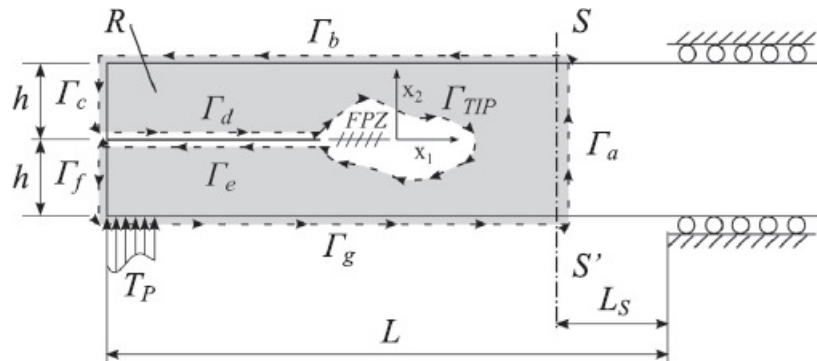


**Figure 2.17:** Schematic representation of the contour for J-integral integration for an ELS test.  $\Gamma_a, \Gamma_b, \Gamma_c, \Gamma_d, \Gamma_e, \Gamma_f, \Gamma_g$  and  $\Gamma_{TIP}$  are part of the integration path  $\Gamma$  [31].

The J-integral approach allows to extend the Griffith approach to elasto-plastic systems in terms of energetic balance and has encountered great success in a non-linear fracture mechanics framework [31, 38, 71, 72, 73].

### 2.3.1.2 Modelisation of fracture in bonded joints

For optimal specimen design and accurate predictions of the failure processes of adhesively bonded joints, the need for precise models and tools is obvious. Comparison between experimental work and simulation is a step forward the better understanding of damage propagation in an adhesive layer along a bonded joint. With simulation tools, parametrical studies can also be provided in order to save experimental time. In this section, adhesive layer behaviour law will be presented in a modeling sense (how they are implemented in fracture test modeling tools), then analytical models and eventually numerical models.

#### *Adhesive layer behaviour law*

Adhesive layer behaviour can also be called cohesive law or traction separation law. The principal parameters that describe these laws are the cohesive fracture energy and critical stresses at changes of regime [74]. It can be defined as a function of the stress at the interface  $\sigma$  versus the relative displacement  $u$  at a given point of the considered interface (adhesive layer in our case)  $x$  [70].

$$\overrightarrow{\sigma}(x) = f(\Delta\overrightarrow{u}(x)) \quad (2.14)$$

where  $\sigma$  is the stress,  $u$  is the displacement and  $x$  is the position along the adhesive layer.

Various shapes are possible for these cohesive laws : triangular, bilinear perfectly elastic plastic, bilinear elastic softening, trapezoidal, exponential, ... [68, 75]. There are described in Fig. 2.18. The area enclosed in the cohesive law is equal to the critical energy release rate above which failure occurs. The fracture process zone development is undertaken in the cohesive law when plasticity/yielding/softening is described (see plateau and decreasing part of the cohesive laws presented in Fig. 2.18). The cohesive law shows the stiffness of the adhesive and describe the FPZ development as a relationship between the stress and strain at the crack tip.

The cohesive law is dependent on the failure mode of the bonded joint [32].

Some trends have been highlighted. Bilinear elastic softening cohesive laws tends to describe better the behaviour of brittle adhesives [32, 76]. Trapezoidal, exponential or any law with plasticity and yielding aspects are more representative of ductile adhesives [32, 76]. The shape of the cohesive law is associated with the adhesive properties.

#### *Analytical and numerical models*

In order to predict the adhesive bonded joint behaviour in a fracture test, either analytical or numerical models can be used. Analytical models are first based on LEFM and Griffith energy balance concepts. Numerical models or Finite Element Analysis (FEA) are based on space-time discretisation. The approaches differ by more physic and straightforward understanding in the case of analytical model and more global understanding in the case of FEA. Every model input parameters are the geometrical parameters of the test and the adhesive layer cohesive law (from which stiffness, damage evolution and failure

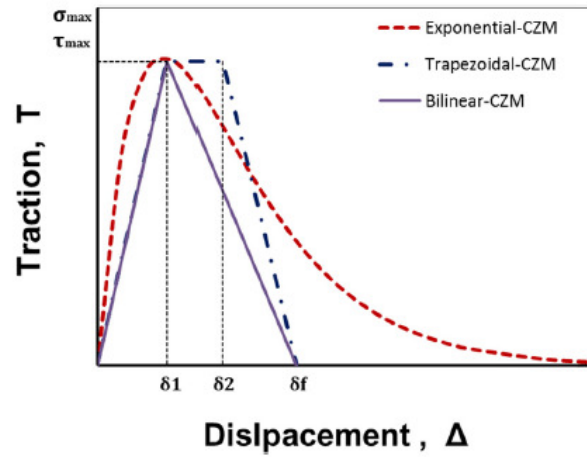


**Figure 2.18:** Schematic representation of classic cohesive law shapes that stands for failure of a bonded joint in mode I [32].

conditions are extracted). The outputs are :

- Fracture energy monitoring : evaluation of crack initiation and crack propagation.
- Displacements and carrying-load values : evaluation of stress and strains in the adhesive layer.

In case of analytical models, fracture energy is derived from the specimen compliance and displacements  $u$ ,  $v$ ,  $\varphi$  (see Fig. 2.19) of the specimen are necessary.

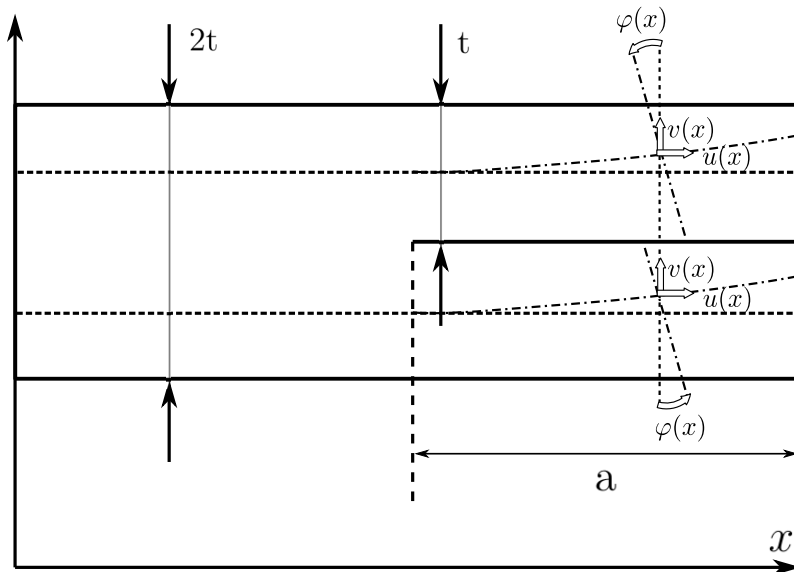


**Figure 2.19:** Classic beam representation of a fracture specimen for modelisation.  $t$  is the adherend thickness.  $a$  the crack length.  $x$  the position along the specimen length.  $u$  is the horizontal displacement.  $v$  the vertical displacement.  $\varphi$  the rotation angle.

The specimen geometry in fracture tests always corresponds to two beams in series under bending load with a  $2t$  overall thickness corresponding to the bonding part and two  $t$  thickness beams acting in parallel along the debonded part as described in Fig. 2.19. The simplest analytical models were not taking into account the adhesive layer compliance [77] hence the adhesive layer thickness  $t_a$  and its mechanical properties. Only the displacements of the adherends were analysed to predict the bonded joint fracture behaviour [78]. Nowadays, with description of the cohesive laws, the adhesive layer compliance is taken into account as well as non-linear behaviours that can occur because of adhesive layer material type. One can refer to [79] for ENF test, [30] for ELS test, [38] for the I-ELS test.

In analytical models, evaluation of the compliance is done with the Simple Beam Theory (SBT). Kinematics relation of the adherends and the adhesive layer can be expressed following Euler-Bernoulli beam theory, also called Classical Beam Theory (CBT) or Timoshenko beam theory. The latest is preferred to the CBT because the through thickness shear and normal deformations are then taken into account. Also the model can then take into account thick beams instead of thin ones which is more close to the reality [70, 80]. For the adherends, the constitutive equations are obtained using LEFM. Local potential energy density  $\delta U_p$  is calculated and integrated so compliance  $C$  is determined as a function of the crack length :

$$U_p = \frac{1}{2}C(a)P^2 \quad (2.15)$$

$C(a)$  is expressed with the geometrical parameters of the specimen, the young's and shear modulus of the adherend material.

At this step, load-displacement curve can be predicted as well as the Resistance-curve (R-curve)  $SERR = f(a)$ ,  $a$  being the crack length. Displacements (horizontal, transverse displacements and rotation of the beams) and forces (normal, transverse forces and bending moment) along the specimen length can be obtained. Factor correction for friction, clamping, large displacement effect can be added. They are determined analytically or experimentally. Griffith failure criterion is used. Fracture energy  $G$  is assumed to be constant and equal to the critical fracture energy  $G_c$  during crack propagation which means that it is stable. Crack length evolution can be monitored, and effective crack length  $a_{eff}$  can be extracted from the simulated load-displacement curve.  $a_{eff}$  analysis allows to identify effect of the correction factors when it is compared to the supposed real crack length evolution  $a$ .

As specified earlier, use of only SBT and LEFM assumptions can be obsolete. The next step is to implement in an analytical model the adhesive cohesive law. The model is called semi-analytical model then. Displacements and carrying-loads are determined in the adhesive layer hence strain and stresses. FPZ evolution can be determined. Failure criterion is still Griffith criterion, but the cohesive law allow to describe the damage evolution and the model predict more precisely what happens in the adhesive layer [32, 81].

Two types of numerical models are presented here. The one using the Virtual Crack Closure Technique (VCCT) and the one using the Cohesive Zone Model (CZM) approach. With a nodal vision of failure, VCCT states that separation at crack tip results from the



displacements of adjacent nodes behind the crack tip. The energy release rate is evaluated for a crack extension of the size of one element. Fig. 2.20 illustrates the VCCT method.

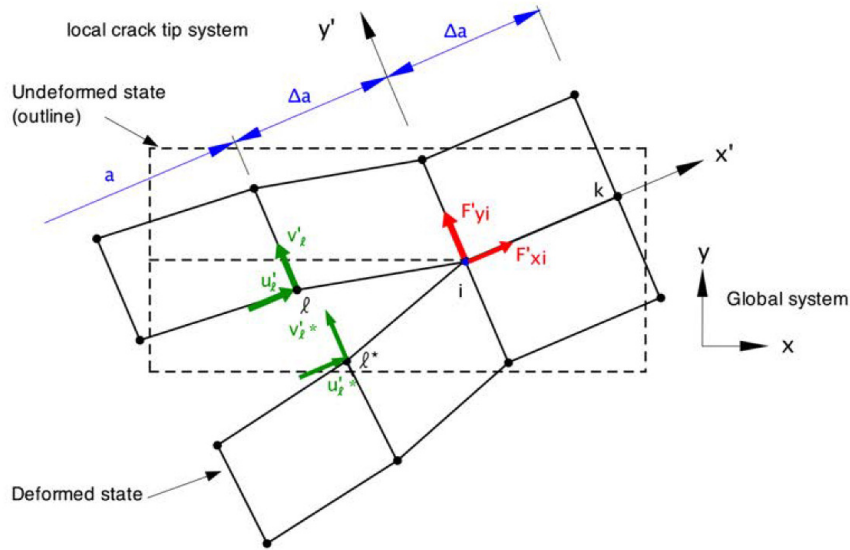


**Figure 2.20:** Undeformed and deformed representation of material with a crack [33].

The VCCT method is used when plastic dissipation at crack tip does not exist, for brittle material. Nevertheless, Jokinen *et. al.* [34, 82] used the method for ductile material and concluded that it is valid with the assumption that the plastic zone is formed and stabilised at crack tip.

The CZM approach is a combination between continuum damage and fracture mechanics [83]. With the CZM approach, the phenomena occurring near the crack tip like the ones occurring in the fracture process zone can be taken into account [84, 85] which means that plasticity also can be taken into account [86]. A CZM simulates the macroscopic damage along a crack path initially determined by using a cohesive law like the one described in Fig. 2.18. The cohesive law is then the definition of the damage criterion. Initially coincident nodes on either side of the pre-defined crack path will separate and de-bond totally. The whole failure response and crack propagation can thus be simulated.

With CZM, accurate field representations around the crack tip is required with fine meshing and special elements, where VCCT method does not need that [34]. One could refer to Fig. 2.21 to compare the two methods.

Multiple tools exist for modeling the fracture in bonded joints. In order to get precise simulation of bonded joints behaviour, some authors worked on combination of the methods [87]. VCCT and CZM are combined in [34] and analytical models can be used to validate cohesive law shape in order, for example, to put them later in more complex FEA models combined with the Cohesive Zone Model (CZM) approach [71, 81, 88].

### **Model issues**

Analytical based models have the advantages of being simpler and easier to use compare to numerical ones. But they are limited to prediction of mechanical behaviours of specimens of typical fracture tests. The most common cohesive law shapes used are idealized because of their linear behaviour at each stage of the damage evolution [88]. The

## 2.3. FRACTURE TESTS OF ADHESIVE BONDED JOINTS

Property / method	CZM	VCCT
Nucleation	Stress-concentration initiates fracture	Pre-existing singularity necessary
Damage process zone	Traction-separation law defines softening (evolution)	No softening
Fracture modality	Mode division or alternatively united deformation vector	Mode division
Material parameters	At a minimum one independent parameter in addition to fracture toughness (ERR)	Fracture toughness
Nodal release	After reaching critical energy rate or separation	After virtual closure reaches critical energy rate
Plasticity amidst crack-tip	Explicitly valid	Difficult to validate
Sensitivity	Mesh-sensitive	Minor mesh-sensitivity

**Figure 2.21:** Comparison between VCCT and CZM (advantageous features indicated with a blue color) [34].

more complex shapes like exponential cohesive laws are not easy to input in an analytical model and are therefore only used in numerical models. Simplifying hypothesis and inconsistency between the applicable failure criteria and the joint failure type (cohesive, adhesive but also ductile or brittle) are also issues that need to be addressed when analytical tool are used [89, 90]. Indeed, interpretation of the FPZ and taking into account all the possible artefacts in terms of analytical equation to solve is not straightforward and numerical approaches are thus necessary.

### 2.3.2 Mode I fracture tests

As presented in 2.1.1, there are three types of failure mode for bonded joint : peeling mode (mode I), shear mode (mode II), torsion mode (mode III).

A lot of studies have been conducted on bonded joint behaviour under mode I loading [10, 35, 91, 92, 93, 94]. The Double Cantilever Beam (DCB) test [95] has been developed by Ripling *et. al.* [96] in order to especially observe fracture in bonded joints. This test is used (see Fig. 2.22) to create opening failure because both side of the bonded joint are pulled away. Also, fracture test have been widely used for assesment of the delamination mechanism of interlaminar materials [35].

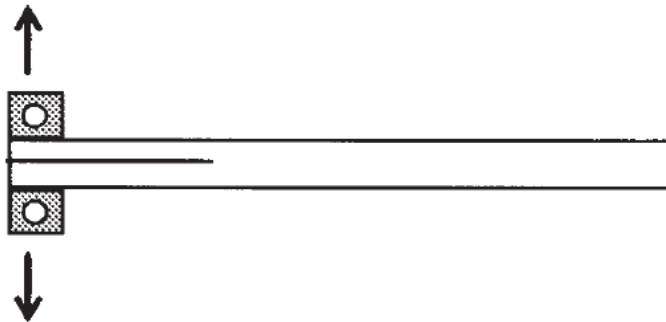


**Figure 2.22:** Double Cantilever Beam (DCB) test description [35].

But, as noticed in section 2.1.1, bonded joints have better performances under shear

loading. Mode I crack propagation scheme is avoided which means that peel and clivage loading configurations are avoided [12, 97]. Mode II and mode III are similar : shear loading is involded in both cases. But mode III loading of bonded joint in a testing context is not easy to set-up. Therefore, in this thesis, focus is on mode II fracture tests.

### 2.3.3 Mode II fracture tests

It exists various test geometries for testing bonded joints under mode II loading. These tests have in common the fact that the specimens are two beams bonded together and loaded so that shear stress is developping along the adhesive layer. The specimens have a pre-crack (an artificial starting defect) at one end of the adhesive layer to accomodate the shear deformation resulting from the bending of the cracked region [98]. The pre-crack is obtained thanks to insert (in teflon for example) placed during the manufacture of the specimen or thanks to pre-mode I or pre-mode II tests. The pre-crack tip is not perfectly microscopically sharp : in the case of teflon insert, its artificial shape can not guarantee sharp crack tip and in the case of pre-test, FPZ can appear hence the crack tip can be already disturbed by it. The stress singularity created with the pre-crack combined with bending contributes to the initiation and propagation of a crack. The specimens are put in a tensile testing machine, displacement sensors (like inclinometers [31] or Digital Image Correlation technique [88] are used to obtain data about displacements occuring during the test. The adherends are made with high strength steel grades with adherend thickness  $t = 6 - 17\text{mm}$  to avoid early adherend yielding, especially for long spans and tough adhesive. The adhesive thickness  $t_a$  common range is  $0.1 - 0.7\text{mm}$ . Fig. 2.23 shows common fracture test frames.

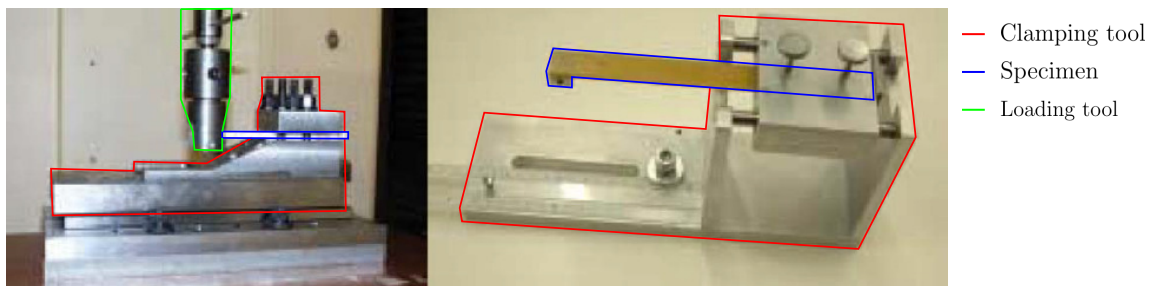


**Figure 2.23:** Photographs of two classical mode II test set-up (End loaded Split test) from two different laboratories [36].

The main goal of these tests is to observe and characterise the crack propagation thus following the SERR evolution with the R-curve. Measuring the crack length during the test is not an easy task but it can be extracted from the compliance curve  $C = \Delta/P$ . The next paragraphs describe the principal mode II fracture tests with the classical expression of  $C$  and the SERR according to Griffith theory  $G$ , their drawbacks and advantages.

Fig. 2.24 shows the principal mode II test geometries and their derivatives.

The Crack Lap Shear (CLS) test which consists in a SLJ test geometry (presented in section 2.2.2) can also be used for fracture testing of bonded joint. Indeed the bending

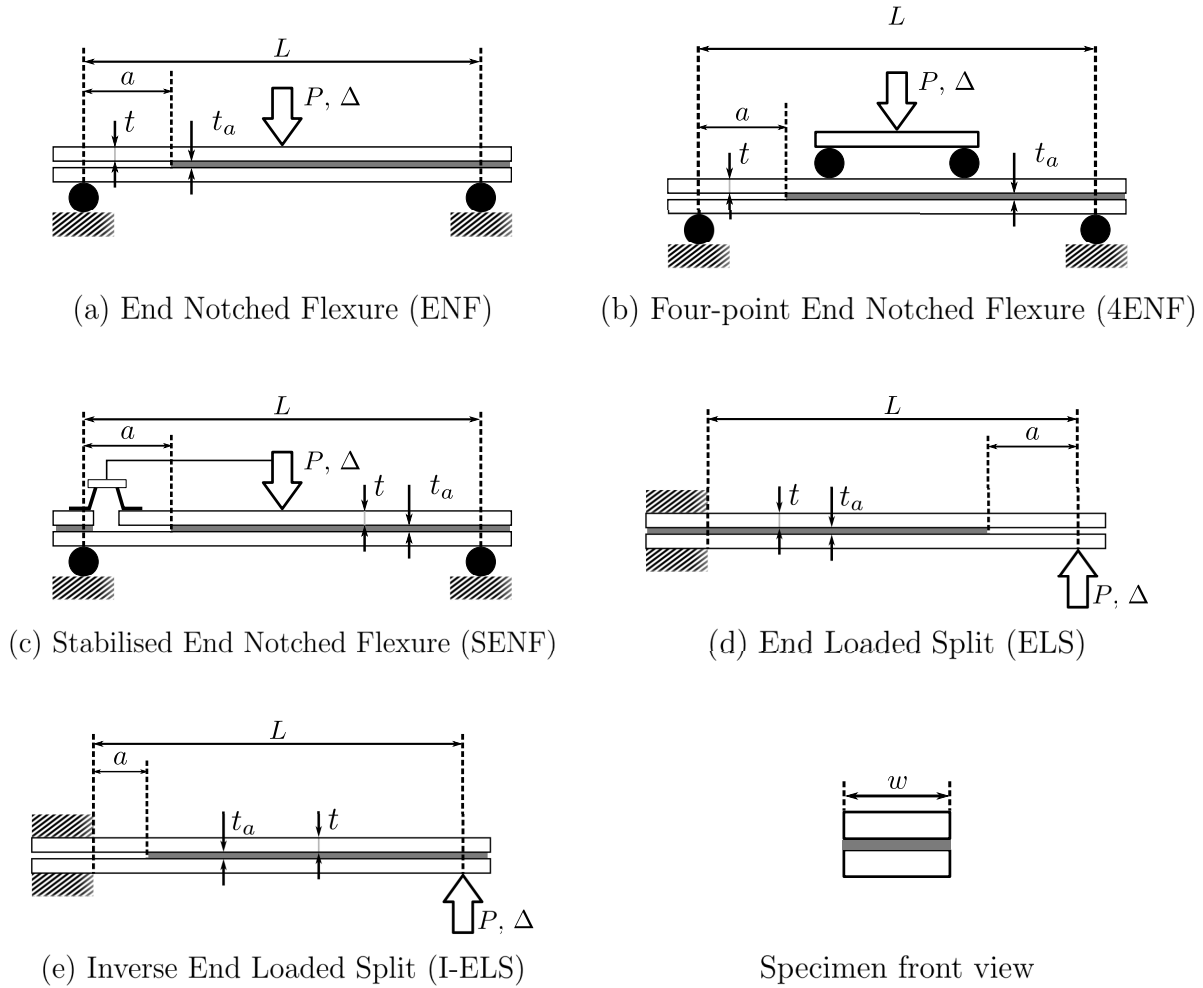


**Figure 2.24:** Fracture tests for bonded joint.  $L$  is the characteristic length of the specimen.  $a$  the initial crack length.  $t$  is the adherend thickness.  $t_a$  the adhesive thickness.  $P$  is the applied load.  $\Delta$  is the loading tool displacement.  $w$  is the specimen width. (a) End Notched Flexure (ENF) test. (b) Four-point End Notched Flexure (4ENF) test. (c) Stabilised End Notched Flexure (SENF) test. (d) End Loaded Split (ELS) test. (e) Inverse End Loaded Split (I-ELS).

moment that occurs when the sides of the specimen are pulled triggers the crack initiation and Thouless *et. al.* [99] described the data reduction scheme for SERR evaluation.

### 2.3.3.1 End Notched Flexure (ENF) test and its derivatives

The End Notched Flexure (ENF) test and its derivatives, the four-point bending ENF (4ENF) and stabilised ENF are presented in Fig. 2.24 (a), (b) and (c). The ENF test consists in a conventional fracture test specimen bent thanks to two supports with the load applied at the center of the specimen [8, 9] in a three-point bending configuration. Due to the antisymmetric loading condition, the geometry provides essentially pure mode II conditions at the crack tip. The ENF specimen was first introduced by Barrett and Foschi [100] to measure mode II critical stress intensity factor of woods and other oriented materials. The ENF specimen was first used by Chai [101] for adhesive joints. The 4ENF

test was then proposed by Martin and Davidson [102]. In this test, the loading is applied with a four-point bending set-up contrary to the classical ENF test.

According to LEFM and simple beam theory, the compliance  $C$  and SERR  $G$  expressions are for the ENF test :

$$C = \frac{\Delta}{P} = \frac{3a^3 + L^3}{8wt^3E} \quad (2.16)$$

$$G = \frac{9P^2a^2}{16w^2Et^3} \quad (2.17)$$

All dimensions are described in Fig. 2.24.  $E$  is the adherend material young's modulus.

The specimen length, initial crack length, adherend thickness, width, adhesive thickness, location of the load application point influence the ability of the test to provide reliable data from which the SERR is extracted. For tough engineering adhesive, long specimens are necessary so that the FPZ and stability of the test is ensured [103]. The adhesive thickness has an effect on the fracture toughness extracted from the ENF test : when the adhesive thickness rises, the fracture toughness rises until a limit load because of FPZ enlargement [41, 37]. Akhavansafar *et. al.* [37] studied the ENF test with a brittle adhesive. They tested different data reduction methods (SBT based, calibration based) and evidenced differences between the obtained fracture energy (see Fig. 2.25). They also showed that an increase in the loading span length (distance between the supports) reduces the obtained fracture energy which differed from its true value.

The ENF test is unstable except for very long crack lengths : when the ration  $a_0/L$  is more than 0.7 [35] the stable criterion defined in eq. 2.12 is respected. This is why the 4ENF and Stabilized-ENF (SENF) tests have been developped in which stable growth can be achieved [12, 36]. However, the 4ENF test presents more friction points than the ENF test and this can influence the toughness values obtained. Schuecker *et. al.* [104] showed that the apparent toughness value will be equal to the true toughness values in 4ENF test if a stiff fixture is employed to compensate the friction effect. The 4ENF test, however, is known for being a compliant fixture which ensure stable crack propagation. This test is also known to suffer from more complicate data reduction method needing the implementation of correction factors that allow to distinguish the adhesive layer behaviour from the adherend behaviour. More over, one can say that the analysis of the 4ENF test results allow to monitor the evolution of the quantities of interest rather than their true values [104, 105, 106, 107].

### 2.3.3.2 End Loaded Split (ELS) test and its derivatives

Fig. 2.24 (d) and (e) show the geometry of the End Loaded Split (ELS) test and its derivative. Again, all these fracture mechanic tests make use of the same specimen geometry. In the ELS case, the bending is produced by applying the load at one end of the specimen. The other end of the specimen is clamped rigidly in the vertical direction whilst being able to slide freely in the horizontal direction (so that sliding occurs between the two adherends). It is a simple bending condition compared to the ENF and 4ENF test [35]. The ELS test has been developed at Texas A & M University [10] and stan-

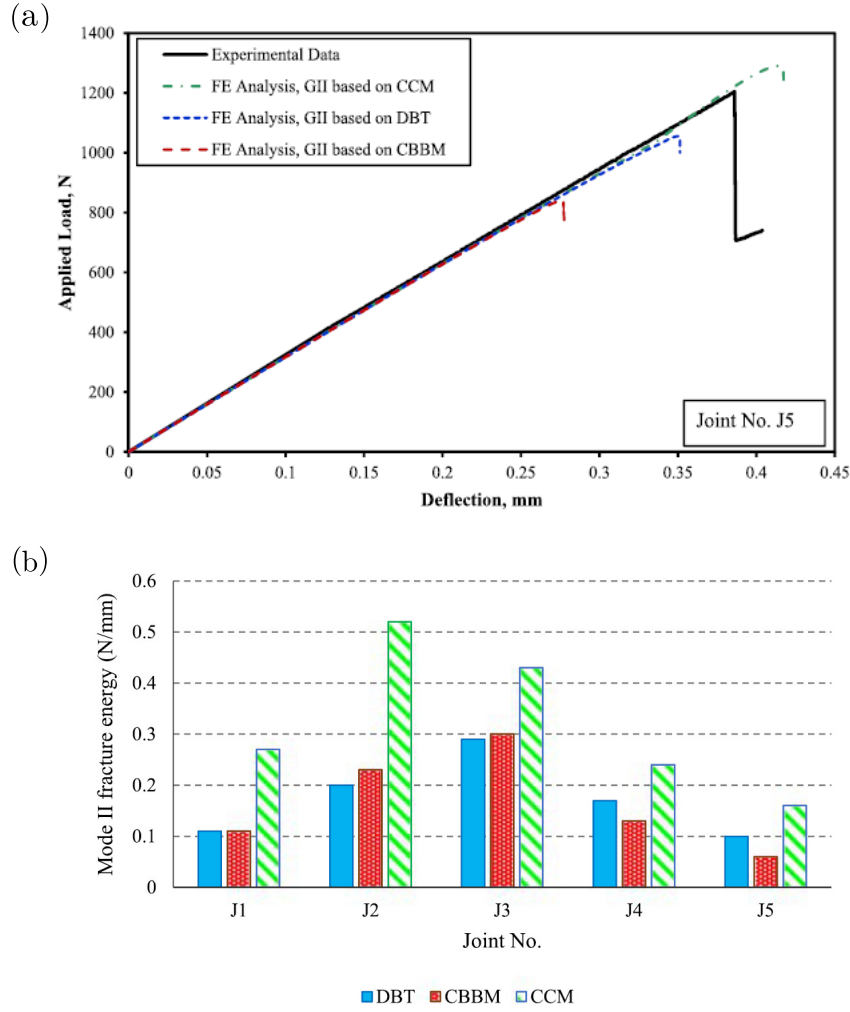


**Figure 2.25:** Data reduction method effect on result from ENF test. CCM : Compliance Calibration Method. DBT : Direct Beam Theory. Compliance Based-Beam theory. (a) Effect on compliance estimation. (b) Effect on mode II fracture energy [37].

standardized in 2014 by the International Organization for Standardization [11]. Pure mode II conditions are assessed in the adhesive layer [38].

According to LEFM and simple beam theory, the compliance  $C$  and SERR  $G$  expressions are :

$$C = \frac{\Delta}{P} = \frac{3a^3 + L^3}{2wt^3E} \quad (2.18)$$

$$G = \frac{9P^2(L-a)^2}{4w^2Et^3} \quad (2.19)$$

All dimensions are described in Fig. 2.24.

Again the specimen length, initial crack length, adherend thickness, width, adhesive thickness, location of the load application point influence the ability of the test to provide reliable data from which the SERR is extracted. Perez *et al.* studied multiple geometrical configurations and concluded that with large FPZ, stable criterion are less restrictive (FPZ

allows to be more stable) but there is a need for larger zone (longer bonded length) so that the crack can propagate. So for high toughness adhesive (so larger FPZ), longer and stronger specimen are needed [12, 30]. Also large deflection can appear with the geometry of the ELS test. It is important to contain large deflection or to take it into account with a correction factor in the data reduction method [30, 78]. Per ez *et. al.* for example took it into account in the expression of the J-integral [31]. In order to obtain stable crack growth with the ELS test, the ratio  $a_0/l$  needs to be superior to 0.55 which allows a larger zone for crack propagation and analysis from an experimental point of view [4, 35, 36, 78, 108]. Poor reproductibility is a concern for the ELS test due to the clamping configuration which increases the complexity of the data reduction method and leads to misinterpretation of the results [35, 36]. Indeed, the crack propagation is stopped when reaching the clamps because no relative displacements between the adherends are possible. Hence, the analysis of the crack evolution needs to be far from the clamps or taken into account in the data reduction method. An alternative configuration for the ELS test is the I-ELS test (see Fig. 2.24 (e)) presented by Jumel and Budzik [38, 109]. In this configuration, the crack will propagate toward lower bending moment value (see Fig. 6.2) which will ensure stable crack propagation. A longer crack propagation path is achieved. They conducted analysis on the FPZ at crack tip and concluded that results were more sensitive to the localized non-linear behaviour in the adhesive and that evaluation of the interface separation laws would be easier.

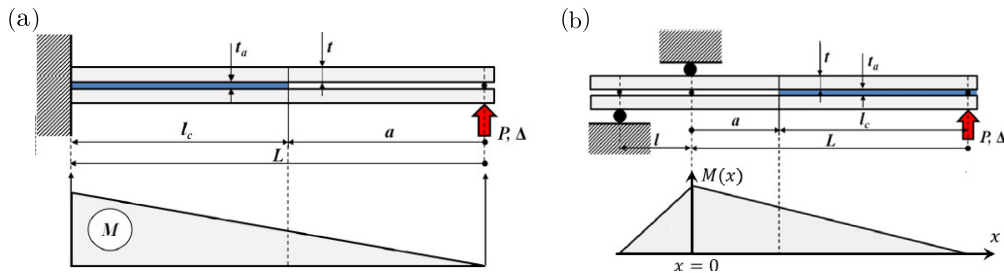


**Figure 2.26:** ELS (a) and I-ELS (b) test configurations with bending moment representations along the adhesive layer [38]. I-ELS test clamping representation is different from the one presented in Fig. 2.24 but the test principal configuration is the same.

### 2.3.3.3 Common characteristics between ENF and ELS tests

There are common issues between the ENF and ELS tests presented before.

Many authors have shown limitations to the existing data reduction methods where simple beam theory formalism is not sufficient to obtain compliance and SERR close to their true values.

Firstly, the root/clamp and friction effects have to be taken into account : the adherends actually slide with respect to each other so that shear deformation occurs but the data reduction method hypotheses are often frictionless and clamping (no displacements possible) conditions.

Secondly, for the critical SERR  $G_c$  value to be calculated with relation 2.19 for example, the crack length value should be known. It is usually done with visual inspection or

complex set-ups. Moreover, presence of a FPZ can mislead the lecture of the crack length measurement : it has to be taken into account in the overall damage length measurement. Many authors have worked on avoiding this measurement by extracting the effective crack length  $a_{eff}$  from the experimental compliance curve. They then use the effective crack length value in the SERR expression. For example, Blackman *et. al.* [12] proposed the following formalism for the ELS test :

$$C = \frac{\Delta}{P} = \frac{3(a + \Delta_{II})^3 + (L + 2\Delta_I)^3}{2wt^3E}N \quad (2.20)$$

$a + \Delta_{II}$  being the effective crack length expression for this formalism.  $\Delta_I$  and  $\Delta_{II}$  are correction factors to account for clamping conditions. They have been firstly proposed by Hashemi *et. al.* with a consequent numerical study [110]. They found that  $\Delta_{II} = 0.42\Delta_I$  and  $\Delta_I$  was obtained with experimental mode I calibration test.  $N$  is an other correction factor that accounts for the effects of applying the load to the specimen via a bonded-on end block.

This expression of the compliance  $C$  gives for the SERR  $G$  :

$$G = \frac{9P^2(a + \Delta_{II})^2}{4w^2Et^3}F \quad (2.21)$$

where  $F$  is a correction factor to account for large deflections.

For ENF crack length correction, other formalisms can be found in [97, 103]. For ELS crack length correction, other formalisms can be found in [12, 36, 97, 109]. For ENF tests friction effect, other formalisms can be found in [12, 35, 98, 111]. For ELS tests friction effect, other formalisms can be found in [77, 112]. It can be noticed that friction effects and crack length corrections are linked as well as the formalisms proposed in these articles.

In order to take into account the FPZ in fracture testing, some concepts have to be understood.

- Fracture energy is porportional to the FPZ size. Indeed the plastic zone at crack tip is rather ductile than brittle so the adhesive layer will show more resistance to instantaneous crack growth [42].
- Large FPZ implies large dimensions for the specimen which can cause large displacement effect that have to be taken into account in the data reduction method (see Fig. 2.27) [30].
- Elastic adherends are necessary [2]. If they overgoes their yield limit, the plastic deformation in the adhesive layer can be masked [89].
- The FPZ is limited by the thickness of the adhesive layer and it develops along a forced path constrained between the adherends.
- Parametric studies and trial and error procedures are needed to understand the geometrical and material needs for the FPZ to be fully developed [30, 42].



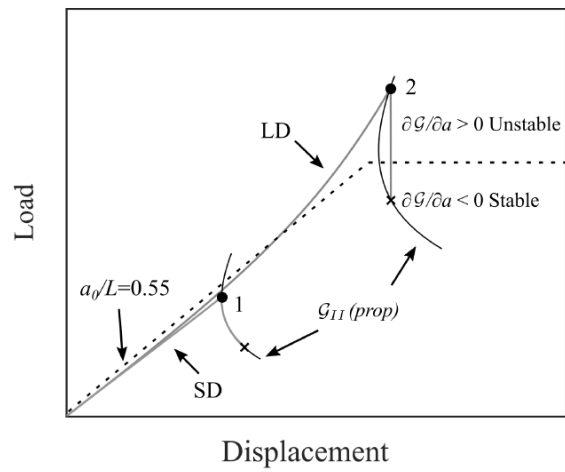


**Figure 2.27:** Classical load-displacement curve for ELS test. Crack propagates when maximum of the curve is reached.  $a_0$  is the initial crack length.  $L$  is the specimen length. Effect of large displacement (LD) on stability of the test [30].

## Overview

In this section fracture testing for damage evolution analysis in bonded joints has been described. The Griffith theory based on energy balance allowed to describe theoretically the crack initiation and propagation in an adhesive layer. The Strain Energy Release Rate (SERR) is the main parameter to obtain during fracture test and is linked to the specimen compliance.

In fracture test design, main concerns are to produce stable crack propagation meaning that the FPZ has to be fully developed and constrained. The J-integral approach is used to describe the effect of FPZ on the damage evolution in fracture testing when Griffith theory cannot without using correction factors.

It exists different types of model to predict the bonded joints behaviour. The main input of these models is the adhesive layer behaviour law. These laws evidence the presence of FPZ. The cohesive law can be determined with direct method (from the experimental data) or with an inverse method (empirical method with comparison between the model and the experiment). Analytical based models are simpler and easy to use but it exists limitations : only fracture tests are modelised, only simplified linear cohesive law shapes are implemented, simplifying assumptions can be issues when some artefacts like large displacements or adherends yielding are encountered. On the other hand, numerical models like VCCT and CZM are more difficult to developed and suffers from classical numerical issues concerning mesh, physical explanations of behaviours evidenced in the analysis. CZM model has the advantage of fully describing the nucleation and plastic flow growth near the crack tip. VCCT is an easy and effective numerical approach when the FPZ is considered fully developed and stabilised.

Mode I fracture tests are quickly described because focus is on mode II fracture tests. Two main categories are distinguished : End Notched Flexure (ENF) tests and End loaded Split (ELS) test. They vary with their loading conditions, the geometry of the specimens and the resulting set-up compliances. The ELS test and its derivatives are generally more stable than the ENF test and its derivatives, ELS test allows a larger region for crack propagation hence damage monitoring, and is easier to set-up. This test is also more recommended for tough adhesives.

A large number of contributions have been produced in order to improve the test protocol, instrumentation and data reduction method. The objective is to achieve more reliable mode II testing of adhesively bonded joints. The data reduction methods consist in assessing the compliance of the system during the test and then assessing the SERR evolution. Clamping and friction issues and crack length measurement issue can be solved using analytical correction factors.

From now on, testing of adhesive bonded joints has been described from the mechanical characterisation with identification of the rheological properties of the adhesive layer until the damage evaluation during fracture tests. These concepts need to be challenged in a durability point of view.

## 2.4 Durability testing of bonded joint

As bonded joints are used in structural application like under-water applications (boats) or aeronautic applications under various environmental conditions (temperature and humidity changes), their mechanical performances need to be assessed over a long period of time. Time, temperature, humidity (or moisture) and applied load create cumulative damage in the bonded joint which can lead to unexpected early failure. This section deals with the effect of ageing on the durability of bonded joints. First, durability of polymers used as adhesives is discussed. Then, specific testing procedures for durability testing of bonded joints are described.

### 2.4.1 Durability of polymers as adhesives

Polymeric materials are time, temperature and moisture dependent. Environmental conditions (dry, humid, hot, cold environments) and loading conditions (creep, static, fatigue loadings) deteriorate the polymeric materials. These conditions are described in this section.

#### 2.4.1.1 Loading conditions

Polymers are affected by two types of loading conditions when their durability needs to be assessed : creep loading and fatigue loading.

Creep loading corresponds to long-term exposure of the material to stationary loading conditions. Damage will grow overtime which can lead to delayed failure or residual deformations. For example, Silva and Costa *et. al.* [13, 14] studied an epoxy adhesives with a specific creep testing device (see Fig. 2.28). Silva tested the material under different stress levels for a predefined age after curing (7 days) and tested the material at the same stress level for various duration (1, 2, 3, 5 and 7 days). The aim was to identify creep effect on the studied epoxy adhesives. Some qualitative observations are given from both of these studies : the adhesive did not fail when loaded at 60% of its quasi-static failure load during 2000 hours and ageing of the adhesive causes a notorious loss of stiffness.

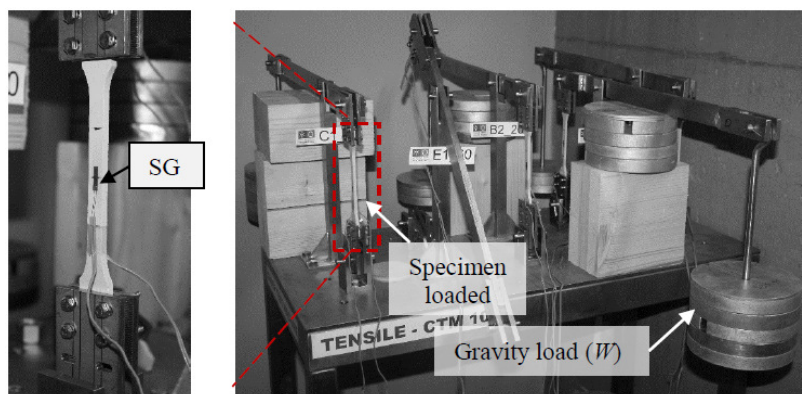


Figure 2.28: Gravity fixture for creep testing of adhesives [13].

Fatigue testing consists in applying cyclic loading conditions. Failure is caused by the progressive extension of a defect. It differs from creep testing by the rate of cycling effect, especially for polymers fatigue testing [113].

### 2.4.1.2 Environmental conditions

Temperature changes and humidity in the air affect polymeric materials.

The first point to assess is the temperature effect. The glass transition  $T_g$  and melting temperature  $T_f$  (see section 2.1.2) are the most important material parameters to take into account. Polymeric adhesives are usually used under their glass transition temperature  $T_g$ . Under  $T_g$ , Abdel-Wahab *et. al.* [39] showed the effect of rising temperature on a PMMA based adhesive (see Fig. 2.29): tensile and yield stress decrease and failure strain rises over 100 % as the temperature increases. Same conclusions have been made on epoxy based adhesives by Brewis *et. al.* [114].

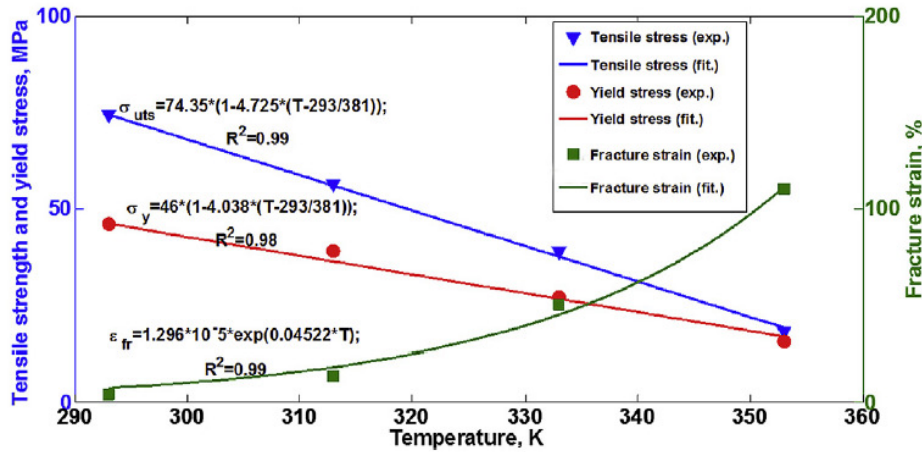


Figure 2.29: Effect of temperature on a bulk specimen made of PMMA under tensile loading [39].

It also has to be noticed that researchers use the time-temperature superposition principle to accelerate ageing of polymers [1, 24]. For example, Minahen *et. al.* [115] worked on PMMA bulk specimen and applied elevated temperature to accelerate the creep behaviour of the material. Benzarti *et. al.* did it on epoxy adhesives in order to evaluate a rheological model to predict creep behaviour of the material.

In addition to these specific temperature effects, some researcher worked on testing polymers aged under cyclic temperature. These cycles induce residual stresses in the material [1]. However, Zhang *et. al.* worked on epoxy based adhesives aged under cyclic thermal loading in 95% Relative Humidity (RH) and showed that cyclic temperature ageing does not have an effect on the residual stresses because of the presence of water that made the bond weaker.

Indeed, the second point to assess when studying polymers mechanical behaviour in various environmental conditions is the moisture or humidity effect. Studies deal with the reaction of polymers to water molecules. Water can be seen as a plasticizing agent, which make the polymer chains mobility rising, which impact the  $T_g$  [1]. This plastisization can

be reversible or can cause crack, craze or chemical reaction that are not reversible [116]. Also, water can cause material swelling which is unwanted in the case of bonded joints where the adhesive layer is constrained between two adherends [116]. Water is one of the most aggressive environment in which adhesives can be exposed and distilled water is much more damaging than salt water [116].

Also, water has an impact on the bond quality between the adhesive and the material used as an adherend. In the case of a bonded joint, the weakening of the joint is then controlled by the water diffusion within the adhesive layer [114]. Arouche *et. al.* [117] showed that, in a salt environment, water caused failure of bonded joint from cohesive to adhesive failure because of the corrosion on the steel adherend.

Polymeric materials are sensitive to various environmental conditions. Emara *et. al.* [118] studied an epoxy adhesive under creep loading with a gravity fixture in an environmental chamber under complex hygrothermal conditions. Strain gauges were used to monitor the strain evolutions. The consequences of using adhesives in these conditions are known but the behaviour of adhesives in a constrained environment (a bonded joint specimen) has to be investigated. This is adressed in the next section.

## 2.4.2 Test procedures for durability of bonded joints

Environmental conditions and mechanical loading weaken not only the bulk adhesive itself, but also the interface. Various test procedures exist for testing the durability of bonded joint specimens. They differ depending on the fixture employed, the environmental conditions applied and if they are coupled with mechanical loads and the type of mechanical loads applied (creep, quasi-static, fatigue). In this section are firstly presented the test procedures where the bonded joints are aged and then tested. Then the test procedures where the bonded joints are mechanically tested while being aged (coupling situation) are presented.

### 2.4.2.1 Post-ageing testing of bonded joint

The most common testing procedures to assess the durability of bonded joints is to aged the joint before testing it under quasi-static loading conditions. The effect of ageing is given through the analysis of the evolution of mechanical performances (as strength, stiffness, ...).

The SLJ test is often used to perform durability tests on bonded joints. For example, single lap hybrid joints (adherends in aluminium and steel) have been placed in salt-spray environment during 15 weeks before quasi-static test [119]. The adhesive layer (flexible silane based material) protected the metal interface from galvanic corrosion, and humidity did not have an effect on the shear strength. SLJ and ENF specimens were aged in deionised water at 50 °C during 2 years. Back face strain technique was used to monitor strains and a cohesive zone model with bi-linear cohesive law was used to predict the specimen behaviours. Good agreement was found. Mechanical properties degraded linearly with moisture content : residual strength decreased with increasing moisture content, thermal and swelling strain induced residual stresses at the end of the overlap for the SLJ specimen and compressive stresses at the side of the ENF specimen and tensile

in its middle [120]. Many other studies with different environmental conditions with SLJ tests have been provided in the literature : negative temperatures [121], constant temperature over different temperature levels [122, 123], immersion in water [124, 125, 126], hot wet environments [127, 128]. Other mechanical characterisation tests have been used like TAST [129] or DLJ test [130]. Some of these tests are performed on composite bonded joints, this lead to complex studies because the adherend as well as the adhesive are affected by the environmental conditions [131].

A fracture test have been developed specifically for durability assessment of bonded joint. The wedge test [15] (see Fig. 2.30) consist in a DCB specimen loaded by forcing a wedge between the beams. Adams *et. al.* [116, 132] observed reduction in strength of a bonded metal joint over time due to moisture.

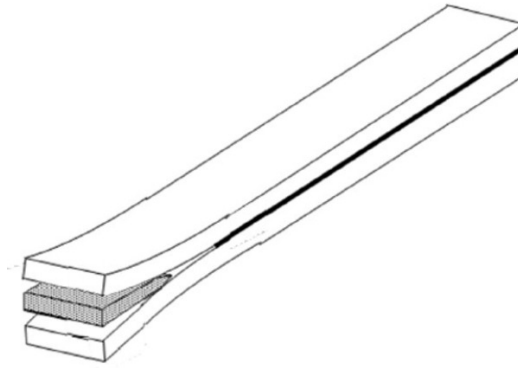


**Figure 2.30:** Wedge test for durability assessment of bonded joint [15].

Other fracture tests have been used like the Mixed Mode Bending (MMB) test [117, 133]. On composite bonded joints aged during 137 days in a salt spray chamber with 95-98 % Relative Humidity (RH) and a temperature of 35 °, Arouche *et. al.* [117] experienced both mode I and mode II failure. Fracture toughness was obtained as a function of the ageing of the specimens. The humidity caused a shift from cohesive to adhesive failure. Ameli *et. al.* [134] extracted R-curves from DCB tests on an aluminium/epoxy bonded joint under hygrothermal ageing. Fracture toughness rate  $dG/da$  rised with temperature exposure but the  $G$  initiation values remained unchanged.

All the test procedures presented in this section use a chamber to create the environmental conditions (especially the temperature changes). An other solution to test bonded joint durability under various temperature is to use electrical resistance bonded to the adherend [135].

The main conclusion from these tests after residual stresses analysis are that hygrothermal loading weaken the bond between adherend and adhesive, leading to governing interface failure. These test procedures are complex to set-up and usually takes time (over thousand hours). Next section deals with coupled mechanical and hygrothermal conditions.

### 2.4.2.2 Coupled mechanical and hygrothermal tests of bonded joints

A fewer studies deal with specimens aged in hygrothermal conditions and loaded at the same time. Two types of mechanical loading stand out : creep loading and fatigue loading.

Under creep loading, with SLJ test, Han *et. al.* [136] immersed specimens constrained in a spring-loaded jig in deionised water at 50 °C up to 3 months and tested them afterwards under quasi-static loading to evidence decrease of the residual strength. They were also measuring periodically the joint deformation caused by creep by checking the spring displacements. A bi-linear CZM was used to model the bonded joint degradation and the model was in good agreement. Others used the SLJ test in the way presented just before : with the use of strain gauges to assess continuously the joint deformations [137], under sub-zero temperature [138], under cyclic temprature loading [139]. ENF test have also been used for creep testing on epoxy/aluminium bonded joint during 30 days at room temperature and humidity [140]. Residual fracture toughness was evaluated as a function of the creep load.

Under fatigue loading, Xu *et. al.* [40, 141] worked on composite bonded joints placed in an environmental chamber attached to a tensile testing machine so that alternating load and cyclic environmental conditions were applied to the bonded joint (see Fig. 2.31). Under these conditions, damage mainly occurred in the adhesive layer and faster than for only hygrothermal conditions. Only strength was recorded (no displacements).

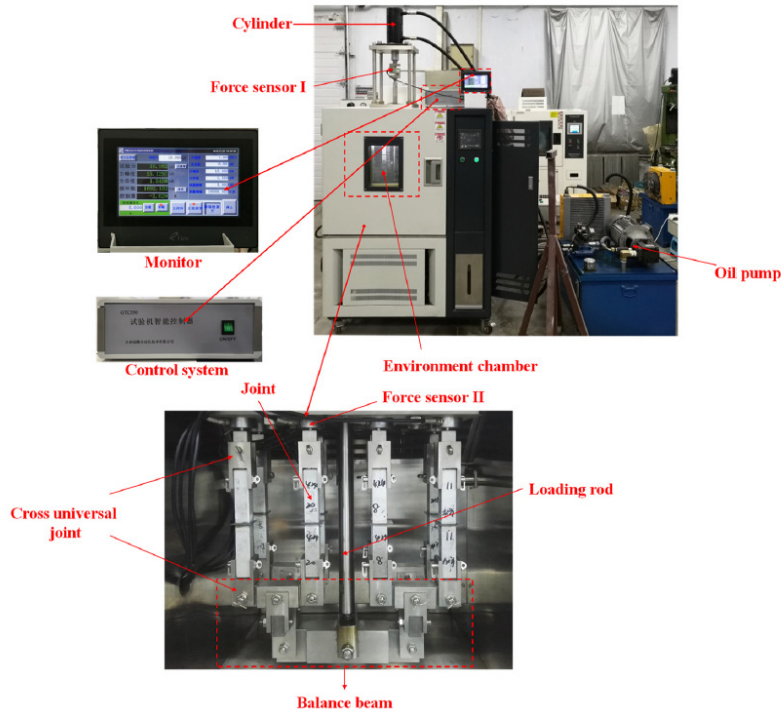


Figure 2.31: Example of environmental and alternating load coupling test device [40].

Hadavinia *et. al.* [142] obtained good prediction using Paris law on aluminium/epoxy bonded joint immersed in distilled water at 28°C. Bidaud *et. al.* [55] used the Arcan fixture and a viscoelastic-viscoplastic constitutive model to predict bonded joint life under

shear loading at room temperature and humidity.

Coupled mechanical and hygrothermal loading of bonded joint results in complex set-ups and complex data reduction schemes able to take into account the interactions between the environment and the loading effects on the mechanical behaviour of bonded joints. Saxena *et. al.* in [16] made a review on the existing time-dependent fracture mechanics (TDFM) concepts for metallic materials for high temperature components. Conclusions of the paper lead to multiple point to assess :

- Time-dependent deformation is associated with creep at crack tip. Method using J-integral approach were convincing for steady-state creep deformation at crack tip (hence secondary creep stage). For example, work in still on going for analysis of the development of creep deformations in front of a moving crack tip.
- In order to resolve the delayed crack growth problem, researchers have to break-up the problem into smaller elements and adress them one or two at a time and analytical tools and models are available to solve these elements.
- Advancements are needed in efficiently collecting crack growth data.



## Overview

Durability testing of bonded joints is a complex problem for which a lot of improvements can be brought because of the various possible test conditions and the fact that bonded joints are made of different materials. It has to be determined if failure occurs because of the adhesive layer or because of the interface between the adhesive layer and the adherends. What is the weakest part of the bonded joint under hygrothermal and mechanical loading ?

Adhesives as polymeric material are weakened by long-term cycling loading exposure, moisture and temperature. The type of coupled mechanical and hygrothermal loading depends on the application for which the joint should be designed. A lot of standards exist [143] showing the complexity of the problem.

The common way for durability testing on bonded joints is to aged the specimen before testing them under quasi-static load to evidenced decrease of the residual stresses. Common mechanical characterisation tests are used in order to do so. But it has been seen before that these tests are not suitable for damage evolution monitoring in bonded joint. However, the main conclusion of these tests is that the interface between the adhesive layer and the adherends is the weakest part of the bonded joint under hygrothermal loading.

An other point is that bonded joints for structural applications are usually used in severe environments under mechanical loads. These ageing conditions and damage mechanisms should be reproduced in an accelerate manner to validate the capability of the joint to sustain long term aggressive in-service conditions. These test configurations reproducing severe environmental conditons are difficult to set-up and only a few studies have been conducted.

Modeling and prediction of aged bonded joint are often made with FEA and cohesive zone models. No analytical models have been able to predict the behaviour of aged bonded joints.

It exist some on-going work on time-dependent fracture mechanics (TDFM) concepts for metallic materials that is possible since the last three decades thanks to the development of new tools for collecting data.

## 2.5 Conclusions

After reviewing the literature dealing with bonded joint analysis under shear loading and severe environmental conditions, many concepts have been addressed.

At first, a presentation of bonded joints have been proposed and general testing considerations have been assessed : the existence of two principal types of mechanical test for bonded joints namely mechanical characterisation tests and fracture tests, failure modes, adhesive or cohesive failure concept and the existence of the Fracture Process Zone (FPZ). Moreover, adhesive layer material has been introduced as polymeric material and described.

Secondly, the main mechanical characterisation test geometries have been described with their drawbacks and advantages from a testing point of view after the presentation of the theoretical framework. It also have been seen that these tests are useful when rheological properties need to be understood since the adhesive layers in bonded joint are polymeric materials.

Thirdly, the main fracture test geometries have been presented with their drawbacks and advantages from a testing point of view. Before that, some major concept for damage evaluation through fracture tests have been assessed : crack initiation and propagation theoretical conditions and modeling tools. Analytical models and numerical models have been assessed as well as their differences and way to use them.

Eventually, durability testing of bonded joint has been presented. Firstly from the polymeric material point of view and secondly from a testing point of view. A wide range of possibilities is open for delayed crack propagation testing and analysis.

In this thesis, the Arcan characterisation test is used under shear loading to characterise three different types of adhesive. A new data reduction method using DIC is presented in order to perform test campaign where rheological properties of the adhesives in specimen can be determined. Then a data reduction method has been developed for ELS fracture tests using the J-integral approach and a direct method for cohesive law identification is proposed. From this work, a semi-analytical model is proposed to predict behaviour of ELS test specimens. Afterwards, ELS fracture tests have been performed on specimen bonded with the three adhesives studied in the Arcan test campaign. Good agreement was found between the semi-analytical model presented before and the experimental results. Eventually, main conclusions are presented on the work presented in this thesis and a discussion about how to assess durability of bonded joints under shear loading is given.



# Chapter 3

## Mechanical characterisation of bonded joint under shear loading

### Contents

---

<b>2.1</b>	<b>Adhesive bonded joints description . . . . .</b>	<b>6</b>
2.1.1	Structural bonding investigation . . . . .	6
2.1.2	Polymeric materials for the adhesive layer . . . . .	8
<b>2.2</b>	<b>Mechanical characterisation of bonded joints . . . . .</b>	<b>12</b>
2.2.1	Theoretical framework and modelisation of bonded joints . . . . .	12
2.2.2	Characterisation tests . . . . .	14
2.2.3	Adhesive rheological model determination . . . . .	19
<b>2.3</b>	<b>Fracture tests of adhesive bonded joints . . . . .</b>	<b>22</b>
2.3.1	Theoretical framework and modelisation of fracture in bonded joints . . . . .	22
2.3.2	Mode I fracture tests . . . . .	29
2.3.3	Mode II fracture tests . . . . .	30
<b>2.4</b>	<b>Durability testing of bonded joint . . . . .</b>	<b>38</b>
2.4.1	Durability of polymers as adhesives . . . . .	38
2.4.2	Test procedures for durability of bonded joints . . . . .	40
<b>2.5</b>	<b>Conclusions . . . . .</b>	<b>45</b>

---

This work focuses on the analysis of crack initiation and propagation along bonded layers under mode II loading conditions. In this situation, the interface in laminates and multilayered systems sustains mainly shear stress. Then characterising the adhesive shear behaviour is a prerequisite. In order to do so, multiple tests are available as listed in chapter 2, all of which having both advantages and drawbacks in terms of cost / implementation, interpretation and analysis. In the following, an Arcan fixture is used to apply pure shear loading conditions to the adhesive layers which will be studied in the next chapters. To monitor the shear deformation evolution during the test of thin adhesive layer, Digital Image Correlation (DIC) is used using high magnification camera. Various testing conditions are considered to evidence the complex rheological behaviour of the adhesives tested (quasi-static test, creep test, cyclic creep-recovery test). Results are discussed from a qualitative point of view.

## 3.1 Test methods

### 3.1.1 Arcan tests

The Arcan fixture has been used extensively for characterising materials under combined tensile / shear loading conditions for years. Numerous contributions have been proposed in the adhesion / structural bonding community to make this test reliable for characterising adhesive layer mechanical behaviour under multiaxial proportional loading conditions but also to evaluate crack propagation conditions under mixed mode loading. The device (presented in Fig. 3.1) consists in two half disks having several holes equally spaced along the circumference. The specimen is clamped to these two hinges that are pinned to the tensile testing machine. The orientation of the specimen with respect to the tensile loading direction can be adjusted so as to choose the proper relative contribution of shear and tensile loading. Many designs have been proposed for the Arcan fixture depending of the nature and shape of the tested specimen. Also, the specimen geometries and manufacturing protocols have been optimized to avoid early failure due to edge effect and singular points.

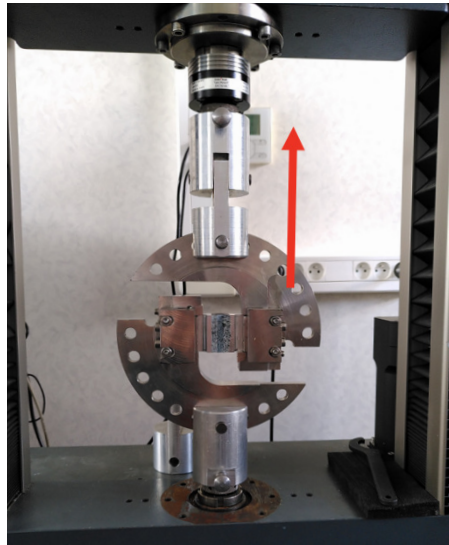


**Figure 3.1:** Presentation of the Arcan fixture mounted in shear loading configuration. The arrow shows the loading direction.

For the present contribution, the specimens are made by bonding two aluminium adherends using an alignment fixture. The aluminium adherends are made with 7075 T6 series aluminium ( $E = 72$  Gpa,  $n = 0.33$ ). The specimen geometry with beaks and main dimensions of the adherend are shown in Fig. 3.2. As suggested in chapter 2, some grooves are machined along the bonded surface contour to obtain beaks geometry which releases the local stress and limits possible stress singularities.

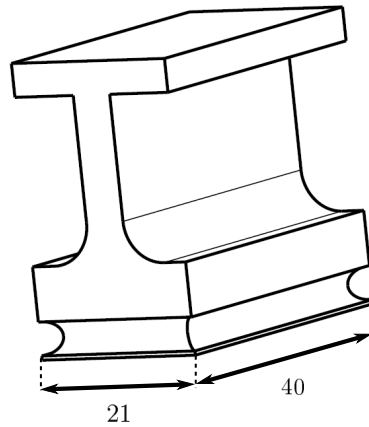


**Figure 3.2:** Arcan adherend geometry. Dimensions are in mm.

### 3.1.2 Materials

Two types of adhesives are used in this experimental study : thermoplastic and thermoset adhesives. The thermoplastic adhesive used is the SAF MIB 30 from Bostik®. It is a polymethyl methacrylate (PMMA) based flexible structural adhesive which exhibit intermediate modulus at ambient temperature condition (150-250 MPa) and large elongation at break value *c.a.* 60 %, according to manufacturer datas. The manufacturer recommends to use this adhesive within a wide range of temperature ( $-40^{\circ}\text{C}$  to  $150^{\circ}\text{C}$ ). It is also resistant to impact, vibration and humidity. The viscoelastic shear behaviour of the SAF MIB 30 adhesive has been evaluated using Dynamic Mechanical Analysis (DMA) with a specific apparatus for shear properties evaluation at room temperature and humidity (see Fig. 3.3). From the DMA measurements, the dynamic glass transition temperature of the SAF MIB 30 is found to be *c.a.*  $80^{\circ}\text{C}$ . Also, it should be noticed that the glass transition region is very large since the loss factor peak is observed in the interval *c.a.*  $[20\ 120]^{\circ}\text{C}$ . In that same interval the shear modulus varies from  $25 \cdot 10^8$  Pa to few MPa. Consequently, a pronounced viscoelastic / viscoplastic behaviour is expected in the room temperature conditions.

The thermoset adhesives used are epoxy based adhesives from 3M®: DP490 and DP760. They are sold as tough epoxy adhesives. Both are recommended by the manufacturer for high temperature uses and impact resistance. According to the product documentation, they differs from each other by the amount of modified amine which is the hardener of these two-components adhesives. DP760 is two times more viscous at  $24^{\circ}\text{C}$  in solid phase.

### 3.1.3 Specimen preparation

Various surface preparation procedures have been used depending on the nature of the adhesive used for bonding. The PMMA based adhesive SAF MIB 30 is reputed to exhibit strong adherence and large tolerance to surface preparation procedure compared to more traditional epoxy systems. Then only mechanical preparation procedure and careful cleaning was carried out following the next steps:

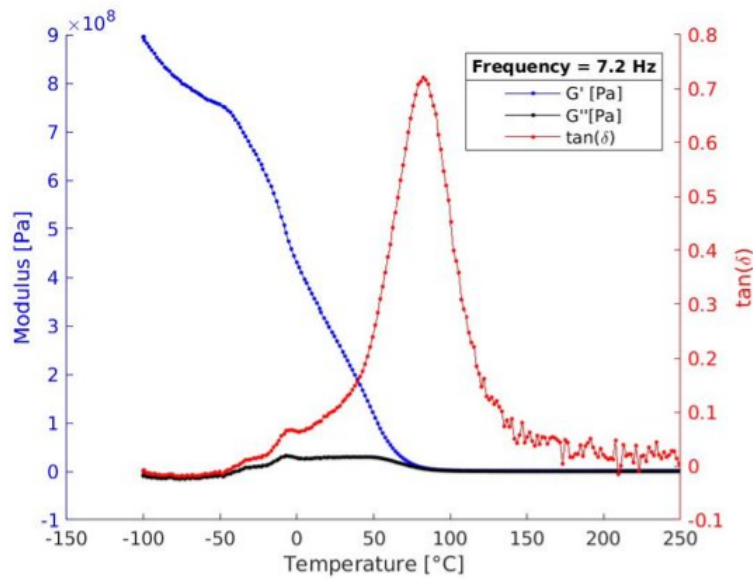


**Figure 3.3:** Dynamic mechanical Analysis of SAF MIB 30 adhesive. Storage and loss shear modulus. Evidence of glass transition temperature. Results taken at 7.2 Hz.

- Prior to bonding, adherends are sandblasted using Guyson® formula 1400 sandblasting cabinet and F 060 sized brown corundum (212 to 300  $\mu\text{m}$  diameter)
- After sandblasting, adherends are placed in an ultrasonic bath containing tap water with alkaline soap for degreasing and removing some particles
- Additionally the adherends are cleaned with nylon brush to remove additional sand particles
- Then the adherends are rinsed with tap water and distilled water to remove the soap
- After drying with hot air gun, final cleaning degreasing is carried out with polypropylene solvent.

The sole cleaning and degreasing of aluminium surface might not be sufficient prior application of epoxy based adhesives (DP490 and DP760). Alternative surface preparation procedure is used consisting in the following steps :

- First, the same cleaning process as the one described before is used on the adherends
- Then, the adherends are scoured with a caustic soda bath at 45 °C
- Then, the adherends are placed in a nitric acid bath
- Eventually, the adherends are placed in a P2 bath at 65 °C obtained by mixing sulfure acid with ferrous sulfate.



### CHAPTER 3. MECHANICAL CHARACTERISATION OF BONDED JOINT UNDER SHEAR LOADING

---

A specific alignment jig is used for bonding the two adherends together as seen in Fig. 3.4 which allows to manufacture 10 specimens at time with the same adhesive thickness. It consists in two plates on which 10 adherends each are maintained with screws. Adhesive thickness is controlled by inserting aluminium blocks between the two plates of the set-up. The adhesive is deposited to the adherend surface manually. The adhesive is supplied in 50 ml cartridges, resin and catalyzer are mixed by passing the two components through a static mixer. Excess adhesive is deposited to the surface so that adhesive squeezes out once the two plates are pressed onto one another. Joint edges are shaped by wiping manually the side of the joint with a round shape tool. Cure of the polymeric adhesives occurs during 24h at room temperature. Adhesive thickness is 1 mm.

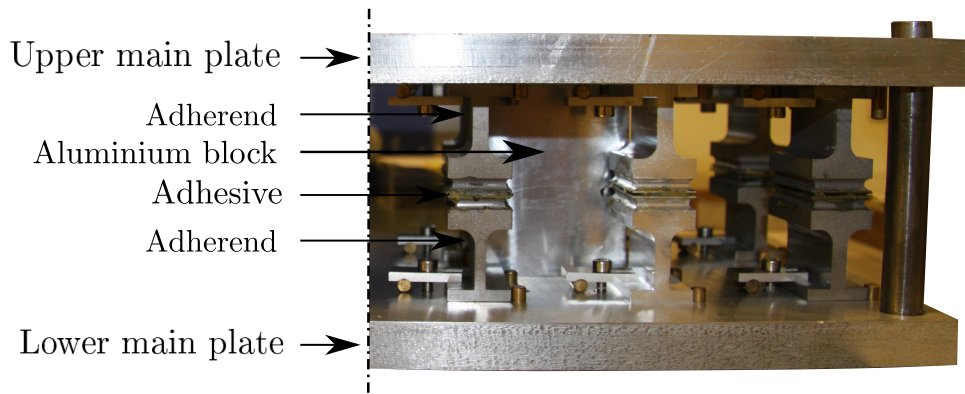


**Figure 3.4:** Presentation of the Arcan specimen manufacturing set up.

The Arcan device (bonded specimen and clamps) is then placed in a Zwick universal tensile testing machine Zwick equipped with a 10 kN load cell. In order to obtain pure shear loading, the adhesive layer is placed vertically (see Fig. 3.5).

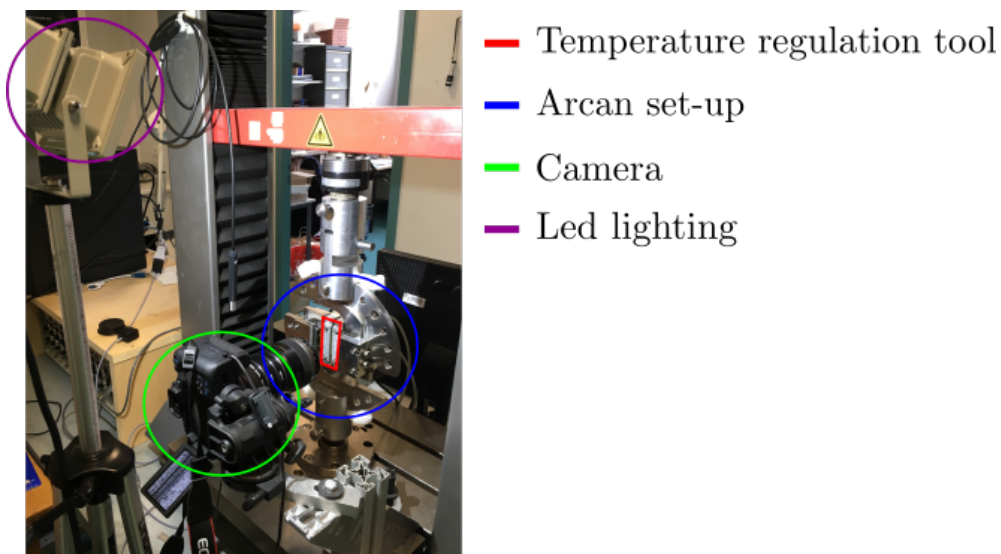


**Figure 3.5:** Presentation of the test set-up : temperature regulation tool, Arcan set-up placed in the machine, camera and led lighting.

### 3.1.4 Temperature regulation tool

The methacrylate adhesive exhibit strain rate and temperature dependence of the mechanical behaviour at near ambient temperature conditions. Then precise control of the adhesive layer temperature is necessary to ensure reproducible and reliable results. Rather than using a furnace, a precise temperature control (see Fig. 3.6) is achieved by contact heating using high power transistors powered with a feedback system. Two bipolar transistors are screwed on small aluminium parts that are clamps to the specimen after some thermal grease is deposited to ensure appropriate thermal conduction. PT100 thermocouples are inserted into each part near the transistors to measure the local temperature. A LabVIEW program using feedback control function allows to adjust the base current supplied to the transistor so as to maintain the temperature at the probe position to the desired value. *c.a.* 1mK fluctuation is observed once feedback parameters have been properly chosen.

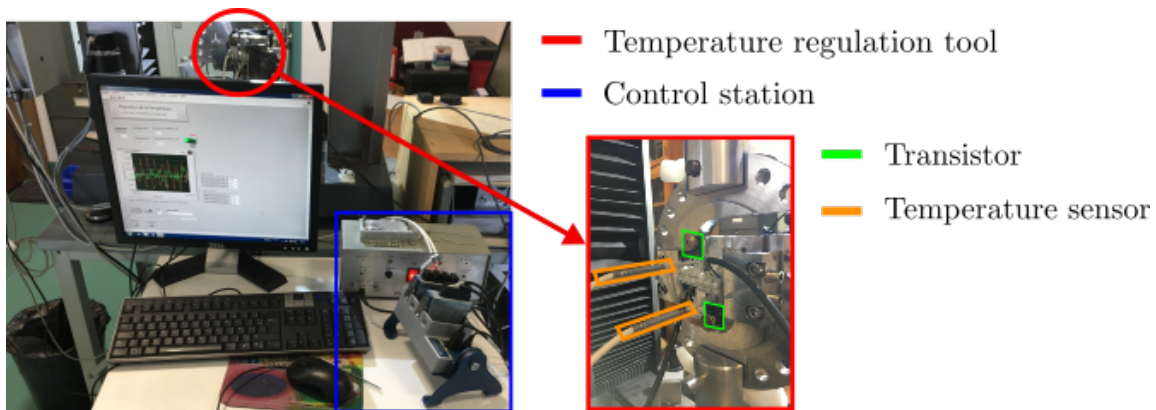


Figure 3.6: Presentation of the temperature regulation tool set-up.

### 3.1.5 Digital Image Correlation (DIC) set-up

To observe the adhesive bondline, a 750D Canon® camera equipped with a macroscopic objective EFS 60 mm from Canon® is used. The camera battery is replaced by an AC adaptor sector in order to operate the camera during a long period for creep testing. The resolution of the camera is 4000 x 6000 pixels with the chosen magnification, pixel size can be as small as 10  $\mu m$ . The image acquisition frame rate is adjusted depending of the test duration but can be also adjusted during the test depending of the observed traverse displacement rate. However, using a conventional reflex camera limits the maximum frame to 1 image every 5 seconds. The camera is installed on a tripod to tilt the camera so that the larger dimension of the image is set parallel to the bondline and so that the bondline is centered on the image. To obtain uniform lighting and avoid specimen heating, Led spot is used to enlighten the scene. For DIC displacement measurement technique to be applicable, a random pattern should be seen on the image. Then, the specimens were painted with a uniform white spray paint then small droplets of black paint were sprayed later. The small mounting plates of the temperature regulation tool were also painted

using that same protocol so that DIC algorithm could be also used to monitor their displacement on the image. When the adhesive is tested under heat control condition, the adhesive layer shear deformation will be determined from the relative displacement of the heating plates.

## 3.2 Data reduction method with Digital Image Correlation

In the following, the adhesive bondline shear deformation is evaluated from the relative motion between the two adherends of the specimen. The displacement is evaluated from the series of images of the side of specimen and using a digital image correlation (DIC) software. For DIC analysis, VIC 2D software from Correlated Solutions is used. From the digital correlation analysis, two series of data are extracted from VIC2D corresponding to the in-plane displacement field of the side of each adherend.

For each picture taken, two Zones Of Interest (ZOI) have been delimited by the edge of the plane region of the adherend. From now on, the upper adherend will be referred as adherend 1 and the lower one as adherend 2 (see Fig. 3.7).

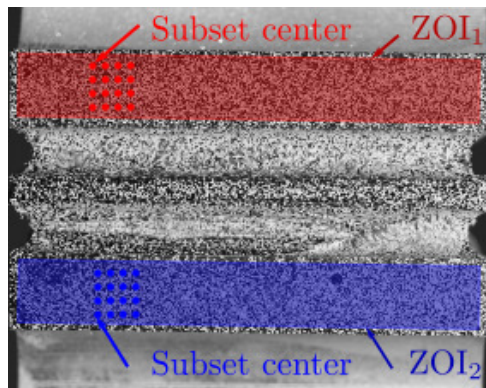
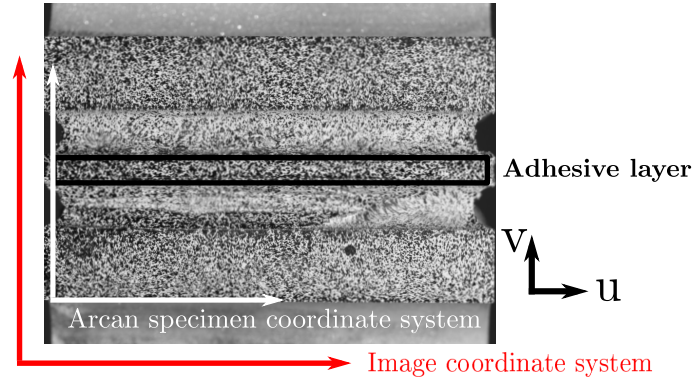


Figure 3.7: Zone Of Interest (ZOI) and subsets description.

They are composed by subsets with a unique grey intensity distribution (created by the white and black dots random pattern). The data of interest are the displacements of the centers of the subsets. In order to apply the DIC analysis, two adherends should be visible in a same image. The pattern size is defined so that every subset contains enough distinctive pattern to ensure low correlation error. The displacement field of the adherend surface is assumed to be described by a solid body motion. Three displacement vectors picked at three distinct positions are sufficient to evaluate mean displacement and adherend rotation. However, several values are obtained from the DIC analysis so that the precision is improved using mean square minimization procedure. Due to the image and subset size minimum 5 subsets normal to the bondline and 20 subsets along the bondline are generally used for displacement field evaluation. To ease the identification and assessment of the displacements of the components, the camera position is set so that

### 3.2. DATA REDUCTION METHOD WITH DIGITAL IMAGE CORRELATION

the image coordinate system is aligned with the Arcan specimen coordinate system hence the adhesive bondline see Fig. 3.8.



**Figure 3.8:** Picture and Arcan specimen coordinate systems. Description of the longitudinal displacement  $u$  and normal displacement  $v$ .

The data extracted from the DIC software are : the coordinates at reference stage of the subset centers in the image coordinate system  $(x_{1,ij}, y_{1,ij})$  and  $(x_{2,ij}, y_{2,ij})$  for adherends 1 and 2 respectively and the longitudinal and normal displacements of the subset centers at each stage  $k$  in the image coordinate system  $(u_{1,k,ij}, v_{1,k,ij})$  and  $(u_{2,k,ij}, v_{2,k,ij})$  for adherends 1 and 2 respectively. Subscripts  $ij$  refer to the position of the subset on the adherend as described in Fig. 3.9.

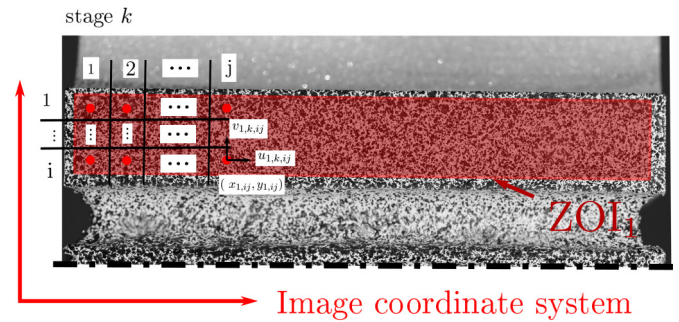


**Figure 3.9:** Description of the extracted data from the DIC software. Only half of the Arcan specimen (adherend 1) is represented.

It has been noticed that small rotation of the Arcan device occurs when it is loaded implying that the adhesive bondline is no more aligned with the horizontal direction in the image coordinate system. In Fig. 3.12, one can see the rotation of the specimen in the images. Relative displacements  $u$  and  $v$  (see Fig. 3.8) do not correspond anymore to the real longitudinal and normal displacements between each adherend. The Arcan specimen coordinate system is no longer aligned with the image coordinate system. The possible rotation of the specimen during the test can be source of inaccuracy when displacements from the DIC software are extracted. In the following, the method to take into account the rotation during the data reduction is presented. This correction is necessary to achieve precise results concerning the longitudinal relative displacement between the adherends.



Taking into account the rotation of the adherends allows also to verify the homogeneity of the normal relative displacement between the edges of the specimen in order to check if there is compression at the edges of the adhesive bondline.

$\theta_{1,k}$  and  $\theta_{2,k}$  are the rotation angles between the Arcan specimen coordinate system and the image coordinate system at stage  $k$  as defined in Fig. 3.10. The ZOIs of adherend 1 and adherend 2 are divided in vectors  $\overrightarrow{v_{1,k,n}}$  and  $\overrightarrow{v_{2,k,n}}$  respectively. These vectors are defined between two consecutive subset centers as described in Fig. 3.10. Subscripts  $n$  is used to designate the vectors during calculation.  $n$  depends on the number of subsets, which depends on the size of the random pattern.

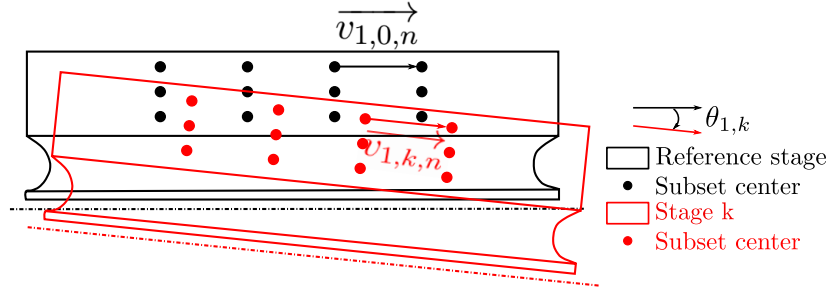


**Figure 3.10:** Rotation angle description. Only half of the Arcan specimen (adherend 1) is represented. Dimensions are overestimated.

Scalar products between vectors  $\overrightarrow{v_{1,k,n}}$  and  $\overrightarrow{v_{1,0,n}}$  (where 0 stands for initial stage) and  $\overrightarrow{v_{2,k,n}}$  and  $\overrightarrow{v_{2,0,n}}$  allow calculation of the rotation angles  $\theta_{1,k,n}$  and  $\theta_{2,k,j}$  of each vector at every stages in the image coordinate system :

$$\cos(\theta_{1,k,n}) = \frac{\overrightarrow{v_{1,k,n}} \cdot \overrightarrow{v_{1,0,n}}}{\|\overrightarrow{v_{1,k,n}}\| * \|\overrightarrow{v_{1,0,n}}\|} \quad (3.1)$$

$$\sin(\theta_{1,k,n}) = \frac{\|\overrightarrow{v_{1,k,n}} \wedge \overrightarrow{v_{1,0,n}}\|}{\|\overrightarrow{v_{1,k,n}}\| * \|\overrightarrow{v_{1,0,n}}\|} \quad (3.2)$$

Same equations are used for  $\cos(\theta_{2,k,n})$  and  $\sin(\theta_{2,k,n})$ . Since the adherends are considered as rigid bodies, the overall rotation angle of the adherends 1 and 2 is obtained with the cosinus and sinus calculated in equations 3.1 and 3.2. We have :

$$\theta_{1,k} = \cos^{-1}\left(\frac{1}{n} \sum_{i=1}^n \cos(\theta_{1,k,i})\right) \quad (3.3)$$

$\sin(\theta_{1,k,n})$  is used to obtained the sign of the rotation angle. Same procedure is used for  $\theta_{2,k}$ .

As the adherends are considered as rigid bodies, their centers of gravity are used to obtain the relative displacements between them. More precisely, the centers of gravity of each ZOI is used. Their coordinates are  $(x_{g1}, y_{g1})$  for adherend 1 and  $(x_{g2}, y_{g2})$  for adherend 2. At stage  $k$ , this coordinate system is not aligned anymore with the Arcan specimen coordinate system hence the adhesive bondline. In order to define the coordinates of the centers of gravity in the Arcan specimen coordinate system, the rotation angles  $\theta_{1,k}$  and  $\theta_{2,k}$  are used in a rotation matrix  $R$  :

$$\begin{bmatrix} x_{r1,k,ij} - x_{1,ij} \\ y_{r1,k,ij} - y_{1,ij} \end{bmatrix} = \begin{bmatrix} u_{m1,k} \\ v_{m1,k} \end{bmatrix} + \begin{bmatrix} x_{1,ij} - x_{g1} \\ y_{1,ij} - y_{g1} \end{bmatrix} R(\theta_{1,k}) \quad (3.4)$$

where  $x_{r1,k,ij}$  and  $y_{r1,k,ij}$  are the coordinates of the subset centers of adherend 1 at stage  $k$  in the Arcan specimen coordinate system. Subscripts  $ij$  refer to the position of the subset on the adherend.  $u_{m1,k}$  and  $v_{m1,k}$  are respectively the mean longitudinal and normal displacements (mean of the displacements associated to each subset center) of adherend 1 at stage  $k$ . The same calculations are done for data extracted for adherend 2. From  $x_{r1,k,ij}$  and  $y_{r1,k,ij}$ , the coordinates of the center of gravity of adherend 1 at stage  $k$  ( $x_{rg1,k}, y_{rg1,k}$ ) in the Arcan specimen coordinate system can be determined. From  $x_{r2,k,ij}$  and  $y_{r2,k,ij}$ , the coordinates of the center of gravity of adherend 2 at stage  $k$  ( $x_{rg2,k}, y_{rg2,k}$ ) in the Arcan specimen coordinate system can be determined.

Real longitudinal and normal displacements (along the adhesive layer) can now be determined. As shown in Fig. 3.11, to obtain relative displacements, gravity center, of which coordinates are ( $x_{rg1,k}, y_{rg1,k}$ ), of adherend 1 is projected on the edge of adherend 2 because adherend 2 is fixed to the base of the tensile machine.

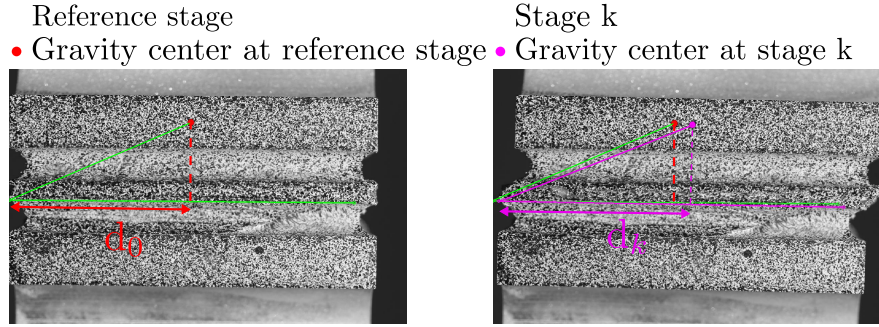


**Figure 3.11:** Relative longitudinal displacement calcul description.

$d_0$  and  $d_k$  stand for projected lengths at reference stage and stage  $k$  respectively. The transverse displacement  $\Delta_u$  is then obtained :

$$\Delta_u = d_k - d_0 \quad (3.5)$$

$\Delta_v$ , the normal displacement is computed following the same method.

Shear strain  $\gamma$  is then given by :

$$\gamma = \frac{\Delta_u}{t_a} \quad (3.6)$$

where  $t_a$  is the adhesive layer thickness.

For example, Fig. 3.12 shows classical results obtained with the data reduction method presented above. More precisely, it shows the strain field along a SAF MIB 30 adhesive tested at room temperature under quasi-static shear loading with the Arcan set-up. Picture (a) corresponds to the initial stage. Picture (b) is taken during the elastic regime, the strain field is homogeneous hence the stress state. Picture (c) is taken when the non-linear regime takes place. Here the strain field is not homogeneous anymore and one can observe localization of strain (on the left). Picture (d) is taken just before failure that occurs near the upper adherend and crosses the adhesive layer to join the lower adherend. Picture (f) shows failure surfaces of the tested specimen. The failure is assumed to be adhesive and it correlates with what it is observed with the DIC software.

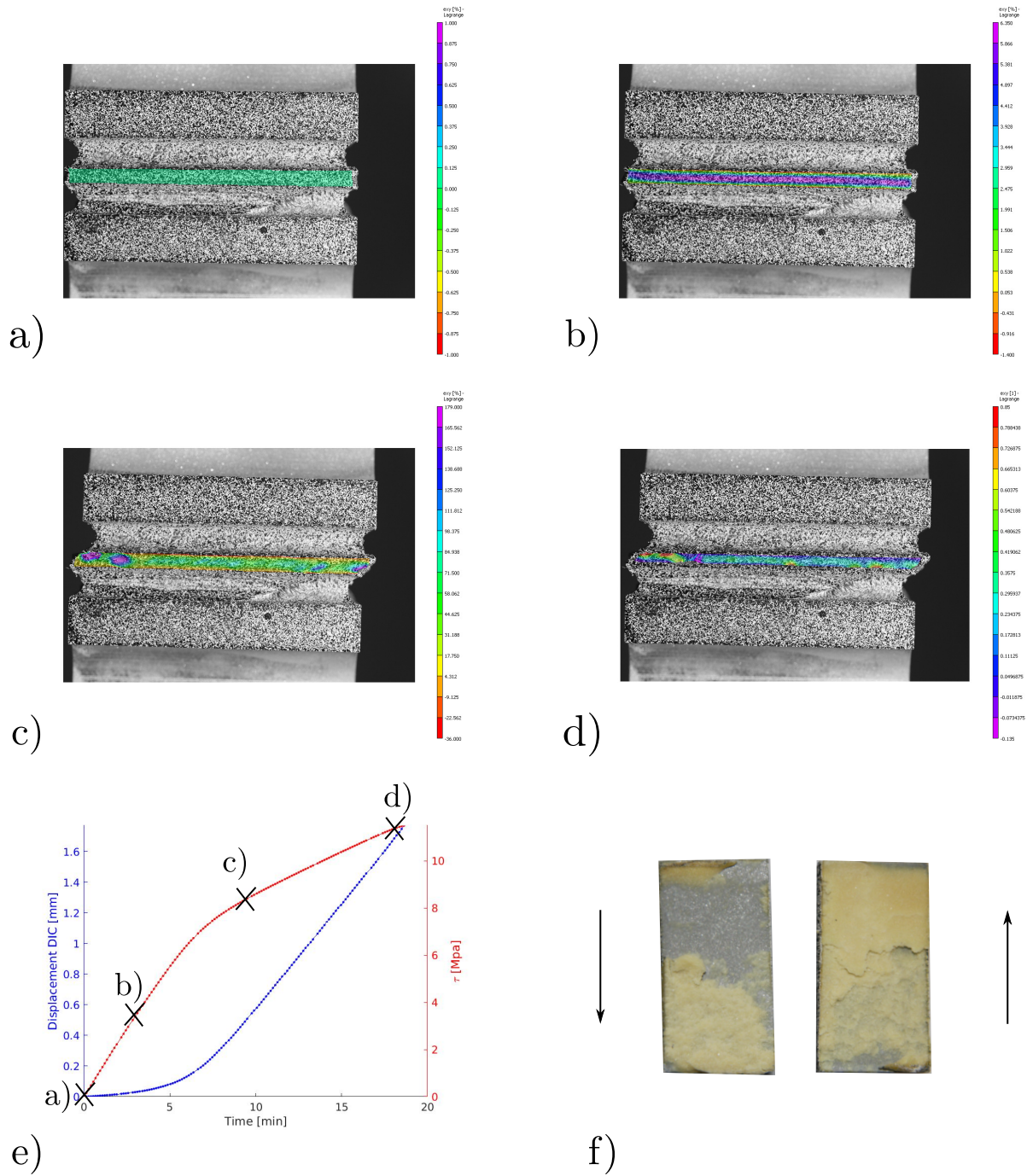


Figure 3.12: Strain field analysis.

### 3.3 Experimental results

A series of Arcan tests have been performed under various thermo-mechanical loading conditions to evaluate the mechanical behaviour of the adhesives layers on which fracture mechanics experiments will be performed later. Since focus is on mode II loading conditions only, the tests will be performed under shear loading conditions only. Quasi-static tests are first performed to determine the bondline shear modulus, yield stress and strength. Then, in order to study the viscoelastic-viscoplastic properties, isothermal creep

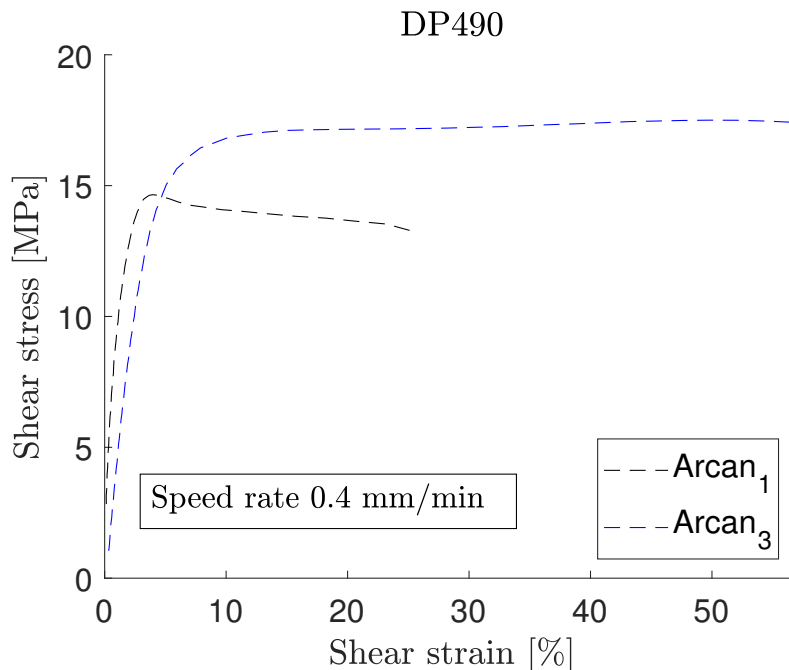


tests are conducted. The bondline deformation is evaluate from DIC measurements using the data reduction methodology detailed above.

### 3.3.1 Elastic brittle adhesive behaviour

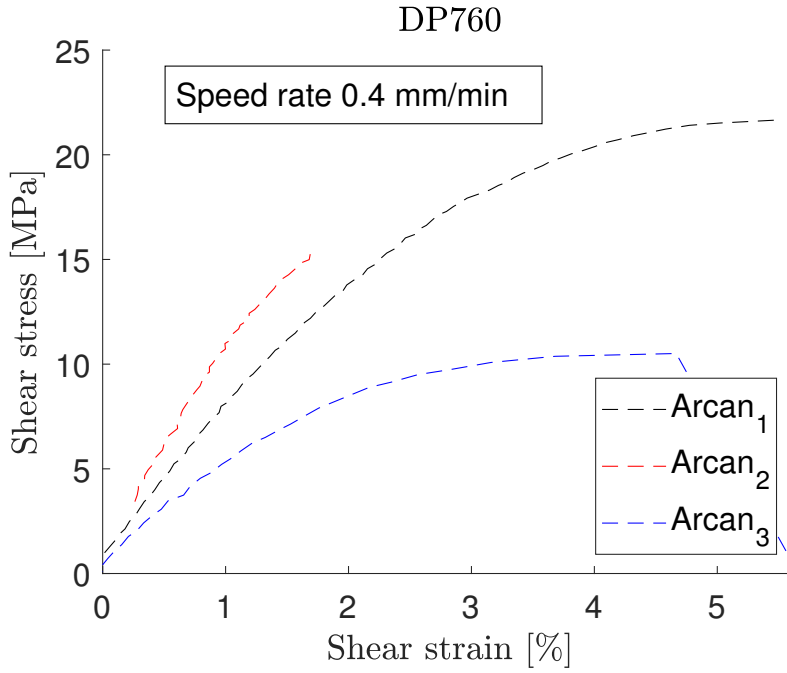
Three Arcan specimens bonded with DP490 epoxy adhesive from the same batch and three Arcan specimens bonded with DP760 epoxy adhesive were tested. Tests were conducted at room temperature under quasi-static loading. The machine crossbar speed rate was 0.4 mm/min).

Fig. 3.13 shows shear stress versus shear strain curves for DP490 adhesive obtained with DIC. Due to malfunction of the camera, images were not taken, only two tests were valid concerning DP490. Fig. 3.14 shows shear stress versus shear strain curves for DP760 adhesive obtained with DIC.



**Figure 3.13:** Shear stress vs shear strain for DP 490. DIC and machine data.

The modulus, shear stress at the peak, failure shear strain are presented in tables 3.1 and 3.2 for DP490 and DP760. Maximum shear stress for DP490 is under what is expected according to the manufacturer (30 MPa) when the adhesive is tested with single lap joint specimens. The DP490 specimens exhibit an elastic-brittle behaviour. The transition phase after the stress peak corresponds to quick damage propagation in the adhesive until failure (and no hardening or softening of the adhesive). Failure surfaces observed during these tests are presented in Fig. 3.15. Cohesive failure is assumed for DP490. According to curves 3.13 and 3.14 and tables 3.1 and 3.2, DP760 is softer than DP490, even if high variability is observed between the three DP760 specimens. The reliability of the Arcan test depends a lot on the bonding quality of the specimens. When the failure surfaces of the DP760 specimens are observed (see Fig. 3.16), one can assume



**Figure 3.14:** Shear stress vs shear strain for DP 760. DIC.

adhesive failure of the specimen and this can explain the variability of the results. In the manufacturer datasheet, the shear stress peak should be around 30 MPa. Again, the experiment shows difference with what is expected.

**Table 3.1:** DP490 properties obtained with quasi-static Arcan test in shear configuration at room temperature. DIC and machine data.

	DP490 <sub>A1</sub>	DP490 <sub>A2</sub>
Shear modulus $G$ [MPa]	548.86	406.51
Shear stress peak $\sigma_p$ [MPa]	14.65	17.02
Failure shear strain $\gamma_f$ [%]	46.6	65.44

**Table 3.2:** DP760 properties obtained with quasi-static Arcan test in shear configuration at room temperature. DIC data.

	DP760 <sub>A1</sub>	DP760 <sub>A2</sub>	DP760 <sub>A3</sub>
Shear modulus $G$ [MPa]	7.81	11.86	5.38
Shear stress peak $\sigma_p$ [MPa]	21.68	17.18	10.52
Failure shear strain $\gamma_f$ [%]	547.71	160.48	510.97

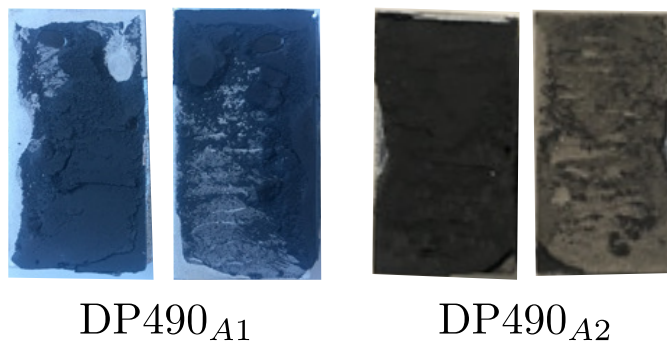


**Figure 3.15:** Failure surfaces of Arcan specimens bonded with DP490. Quasi-static test until failure.

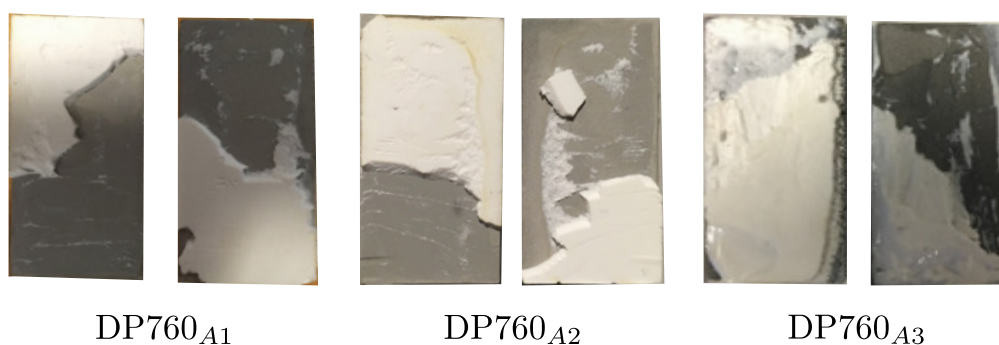


**Figure 3.16:** Failure surfaces of Arcan specimens bonded with DP760. Quasi-static test until failure.

### 3.3.2 Viscoelastic-viscoplastic ductile adhesive behaviour

A more complete set of mechanical characterisation tests have been performed on the methacrylate adhesive.

Manufacturing of these specimens is time consuming. Moreover, having multiple specimens tested generates variability in the result because of defects that appears during the production and variability of the environmental conditions in which the specimens are tested. A "rejuvenation"/post-curing procedure is used to remove internal stresses introduced in the adhesive layer by mechanical loading before a same specimen could be tested again. A preliminary step before analysing the mechanical characterisation tests is to validate the reproductibility of the test with the methacrylate based adhesive, to prove the effectiveness of the rejuvenation procedure. Also creep testing has been conducted, since these tests are time consuming, weeks can separate the tests and effect of storage have been adressed.

#### 3.3.2.1 Reproductibility of the test

Fig. 3.20 shows quasi-static test on Arcan specimen bonded with SAF MIB 30 adhesive from Bostik (®). Crossbar speed rate was 0.2 mm/min. Each specimen has been heated over  $T_g$  and cooled naturally before testing. The results presented are obtained with Digital Image Correlation (DIC). Table 3.3 presents the mean and standard deviation of

the principal parameters of interest.

**Table 3.3:** SAF MIB 30 properties obtained with quasi-static Arcan test in shear configuration at room temperature. DIC and machine data.

	DIC		Machine sensor	
	Mean	Standard deviation	Mean	Standard deviation [%]
Shear modulus $G$ [MPa]	68.37	8.32	4.82	14.9
Maximum shear stress $\sigma_p$ [MPa]	8.76	5.59	9.47	3.9
Failure shear strain $\gamma_f$ [%]	131.3	14.22	306.26	7.55

The shear stress and strain values are consistent with the values supplied by the manufacturer. The adhesive exhibit an apparent elasto-plastic behaviour with hardening. The deformation at break is high since more than 100 % value are observed for all three cases. Failure surfaces are presented in Figs. 3.17, 3.18 and 3.19. As expected for this type of adhesive, the bonding quality is more tolerant to surface preparation quality and cohesive failure is observed.



**Figure 3.17:** Failure surfaces of Arcan specimens bonded with SAF MIB 30 1. Quasi-static test until failure. Arrows designate the direction of each adherend.

The SAF MIB 30 adhesive appears to be very ductile. Much better reproducibility is observed for this adhesive than for the epoxy ones.

According to these data. The reproducibility of the test is assumed (see Fig. 3.20).

### 3.3.2.2 Rejuvenation procedure

The SAF MIB 30 adhesive is a polymethyl methacrylate based adhesive. It is an amorphous polymer which allows to use the rejuvenation procedure. Its glass transition temperature  $T_g$  is 80°C according to the manufacturer. This has been verified with Dynamic Mechanical Analysis (DMA), see Fig. 3.3. The rejuvenation procedure consists in heating the adhesive layer (which result in heating the whole arcan specimen - adherend and adhesive) over the adhesive  $T_g$  at the end of each loadings.



**Figure 3.18:** Failure surfaces of Arcan specimens bonded with SAF MIB 30 2. Quasi-static test until failure. Arrows designate the direction of each adherend.

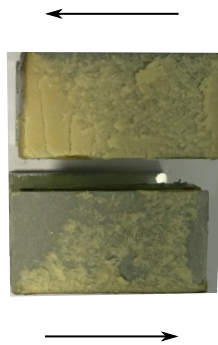


**Figure 3.19:** Failure surfaces of Arcan specimens bonded with SAF MIB 30 3. Quasi-static test until failure. Arrows designate the direction of each adherend.

For example, Fig. 3.21 shows isothermal creep tests at 3000 N (3.44 MPa) under three temperatures : 30 °C, 35 °C, 40 °C.

After the test at 30 °C, the adhesive was heated at 85 °C, over its glass transition temperature  $T_g$ . Then, it cooled naturally until room temperature. This procedure allows to get rid off internal stresses due to polymerization process and loading history. Then the specimen is heated at 35 °C for the next test. The same protocol was repeated for the test at 40 °C. The temperature was controlled with the hot plates and temperature regulation system presented in section 3.1.4. DIC strain evolution monitoring was used again but based on hot plate surface displacement measurement rather than displacement of the adherend itself.

Fig. 3.22 shows a creep test at 3000 N at room temperature for an Arcan specimen bonded with SAF MIB 30. The blue curve correspond to the specimen raw after being manufactured. The red curve correspond to the same specimen after being heated at 85°C during 30 min and cooled naturally. Data are obtained with DIC. Behaviours are similar especially in the elastic phase.

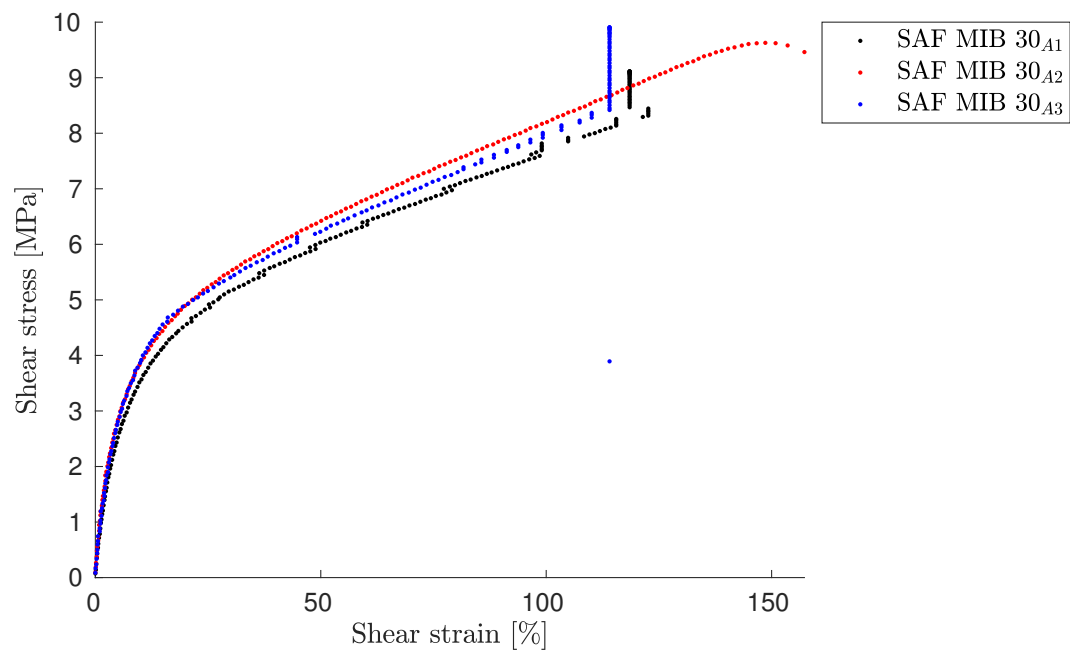


**Figure 3.20:** Shear stress versus shear strain for Arcan specimens bonded with SAF MIB 30. Quasi static test. Speed rate was 0.2 mm/min.

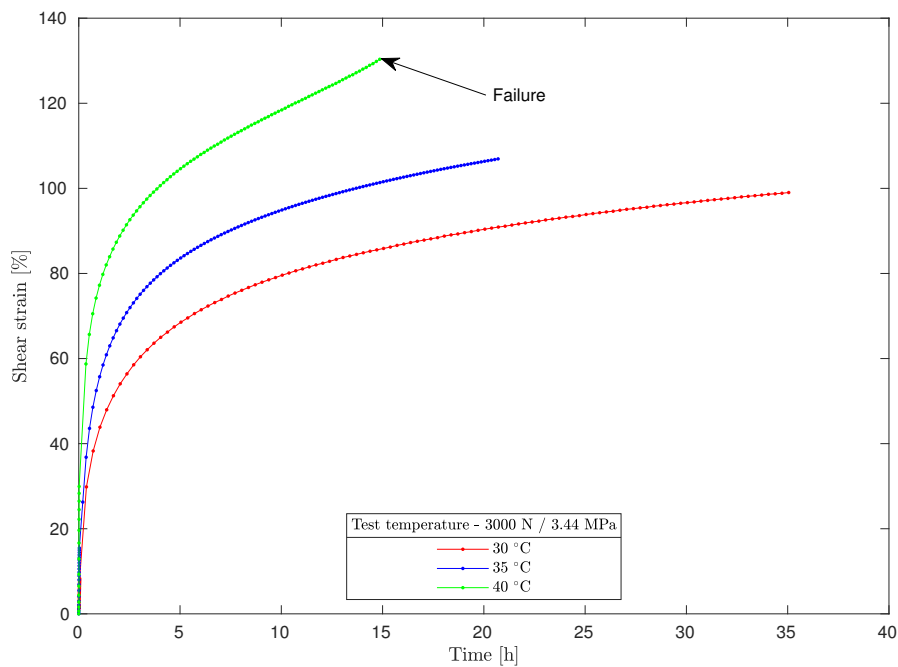


**Figure 3.21:** Creep loading test at 3000 N load - 3.44 MPa on Arcan specimen bonded with SAF MIB 30 at various temperatures. Shear strain versus time. Rejuvenated Arcan specimen. Data are obtained with the DIC.

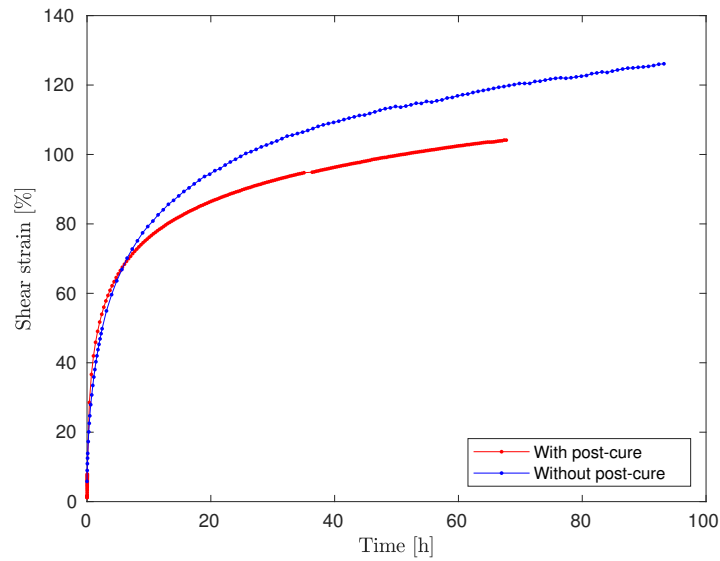


**Figure 3.22:** Creep loading test at 3000 N load on Arcan specimen bonded with SAF MIB 30. Shear strain versus time. Non-rejuvenated and rejuvenated Arcan specimen. Data are obtained with the DIC.

### 3.3.2.3 Effect of storage

An other concern is the storage of the specimens. Since the creep test are long in time. Some specimens are tested weeks after they have been manufactured. They were stored at room temperature and humidity with no light.

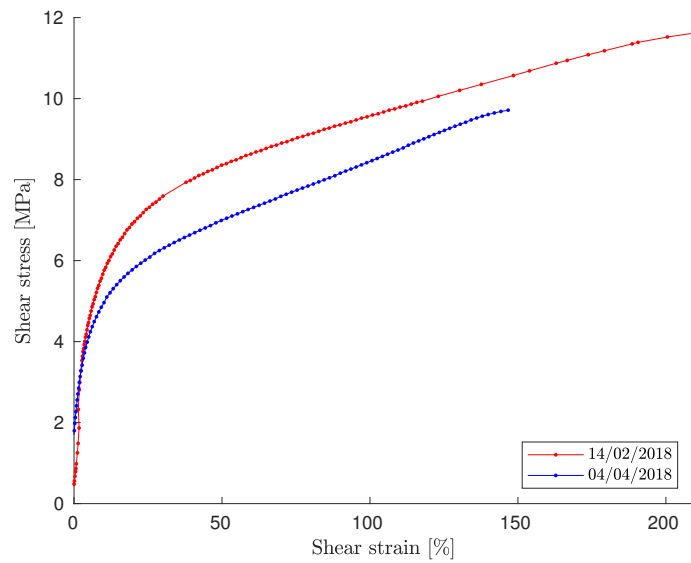
Fig. 3.23 shows creep test at 3000 N at room temperature. This specimen was not rejuvenated. The specimen has been tested two days after manufacturing and did not failed. It has later on been tested 2 months later.

According to this curve, no consistent effect of storage was assumed.

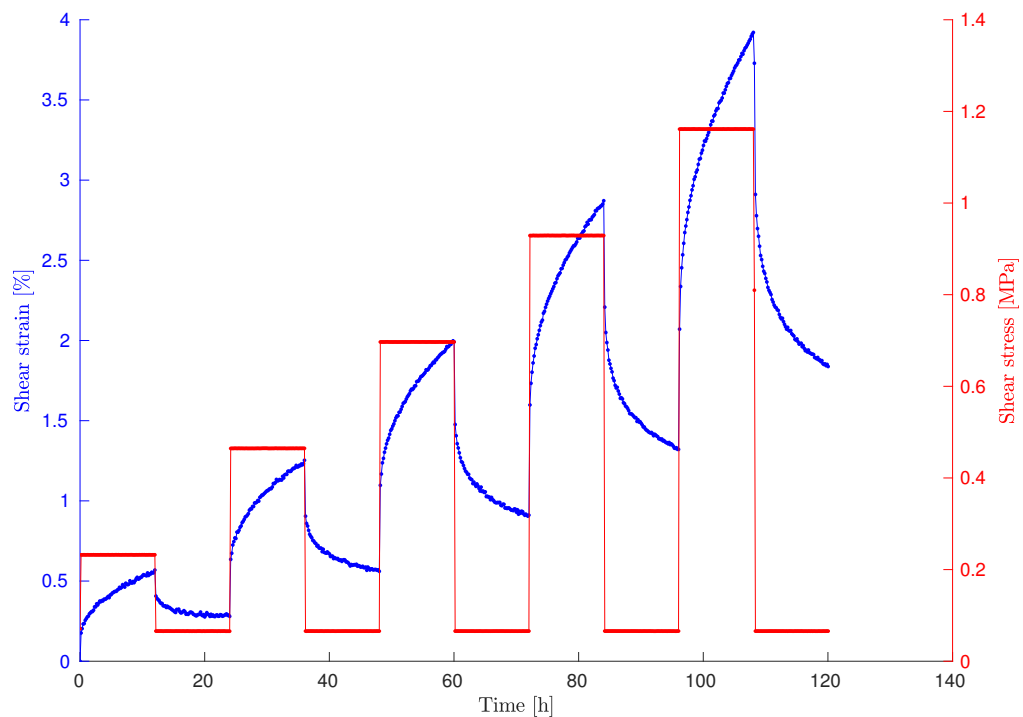
### 3.3.2.4 Cyclic creep-recovery test

Fig. 3.24 shows strain versus time evolution and the corresponding shear stress. This cyclic creep-recovery test is a classic test procedure to evaluate the non-linear viscous behaviour of an adhesive.

Long term creep experiments have been performed at room temperature (*c.a.* 23°C) trying to capture the transition between viscoelastic / viscoplastic regime. Loading and recovery period duration are 12 h. The initial loading value is 0.2 MPa. For each sequence, the load is increase by 0.2 MPa for 5 cycles. For the test conditions used here, no viscoelastic regime is observed since residual strain is observed after the first cycle. This result is unexpected since the stress level range is [0.23 1.16] MPa. It corresponds to linear part of the monotonic curves of the adhesive (Fig. 3.20). The residual strain rises linearly at each cycle (see Fig. 3.25). The adhesive presents high viscoplasticity.



**Figure 3.23:** Creep loading test at 3000 N load on Arcan specimen bonded with SAF MIB 30. Shear strain versus time. Non-rejuvenated Arcan specimen. Data are obtained with the DIC.



**Figure 3.24:** Cyclic creep-recovery test on Arcan specimen bonded with SAF MIB 30 adhesive. Shear strain versus time and applied stress. Data are obtained with the DIC.



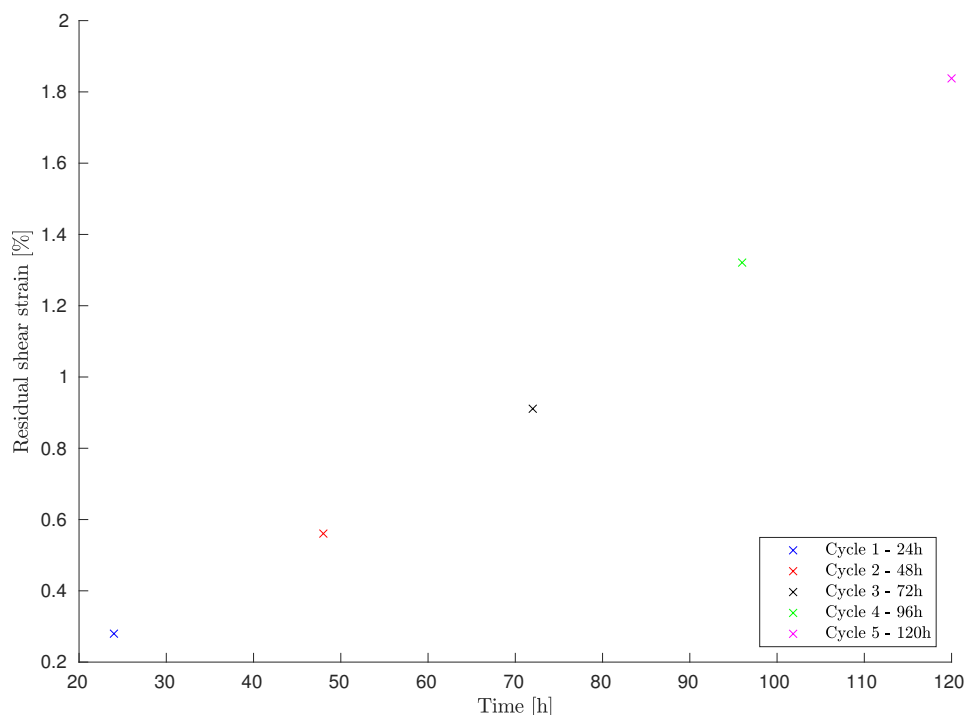


**Figure 3.25:** Cyclic creep-recovery test on Arcan specimen bonded with SAF MIB 30 adhesive. Residual shear strain at the end of each cycle versus time. Data are obtained with the DIC.

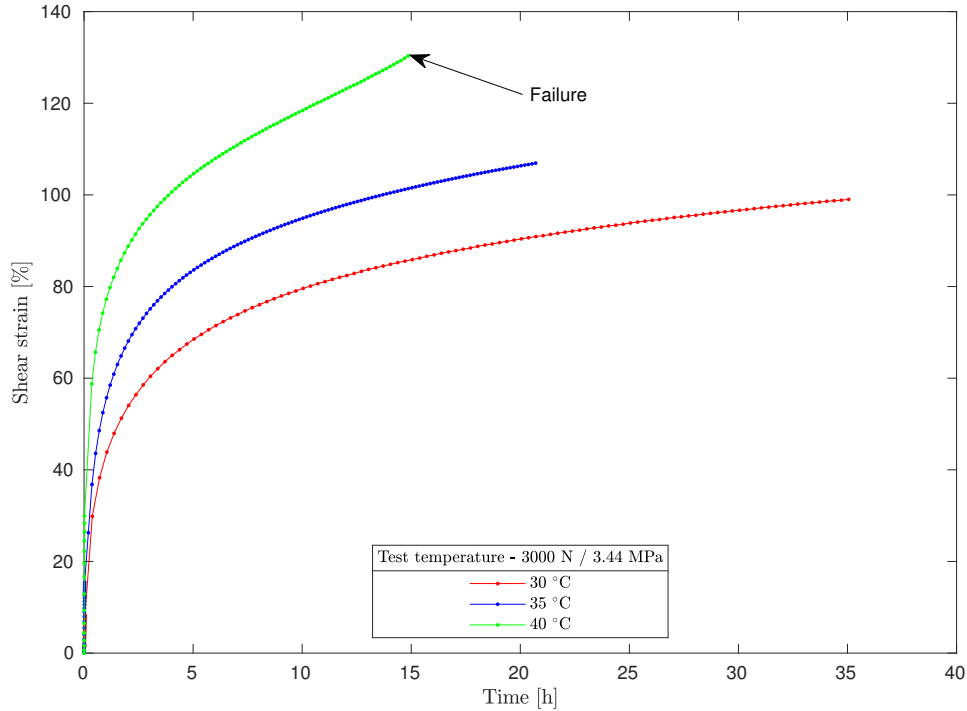
### 3.3.2.5 Isothermal creep tests

Fig. 3.26 (same curve as Fig. 3.21), it has been added here for an easier reading) shows isothermal creep tests at 3000 N (3.44 MPa) under three temperatures : 30 °C, 35 °C, 40 °C. Only one specimen was used to conduct these three tests thanks to the rejuvenation procedure. Under such loading conditions, irreversible creep deformation regime is reached since specimen failure is finally observed. Then supplementary tests have been performed under much lower applied stress.

Fig. 3.27 shows creep tests at 400 N (0.41 MPa) under nine temperatures : 30 °C, 35 °C, 40 °C, 45 °C, 50 °C, 55 °C, 60 °C, 65 °C, 70 °C. The same rejuvenation protocol has been used, hence only one specimen has been tested. The displacements data are obtained with the DIC. The minimum applied load is chosen so as to obtain reliable applied force measurement within the range of the load cell thus expecting viscoelastic regime this time.

Next, creep tests at room temperature at various load level have been conducted : from 200 N to 7000 N (see Fig. 3.28). Again the rejuvenation procedure has been used so that all measurement are performed on a unique specimen for loadings performed in the interval [200 - 5000] N until failure of this specimen. Then an other specimen has been used for the 7000 N test.

Fig. 3.26 shows that at 30 °C under 3000 N/3.44 MPa, the adhesive shear strain



**Figure 3.26:** Creep loading test at 3000 N load - 3.44 MPa on Arcan specimen bonded with SAF MIB 30 at various temperatures. Shear strain versus time. Rejuvenated Arcan specimen. Data are obtained with the DIC.

reached secondary creep stage and similar behaviour is observed at 35 °C. However, at 40 °C, the adhesive failed cohesively after 15h of test after reaching the classical tertiary stage of creep testing.

According to Fig. 3.27, when the temperature rises, the strain plateau is reached faster, proof of a viscous flow activated by the temperature. No failure was observed during these tests. Fig. 3.29 (a) shows strain level at 1h, 5h, 10h, 20h, 30h and 40h of the 400 N creep test versus the applied temperature. As the temperature gets closer to the glass transition temperature, the gap evidenced in Fig. 3.29) (b) between the levels of strain is reduced and tends to a non-linear evolution.

In Fig. 3.28, shear strain versus time is plotted. When the applied load varies between 200 N and 1000 N, the curves tend to a plateau. The recovery was not recorded during these tests but according to Fig. 3.20, there should be already residual strain hence plasticity. At 3000 N, in concordance with quasi-static test (see Fig. 3.20), shear strain takes longer to reach the plateau. At 5000 N and 7000 N, the creep rate rises significantly and culminates in failure.

These creep tests evidence the fact that this adhesive exhibit viscosity. Combined with the cyclic creep-recovery test, one can assume that this adhesive has an viscoelastic-viscoplastic behaviour. These types of tests are in line with similar ones that are useful when rheological properties of the adhesive layer are assessed.

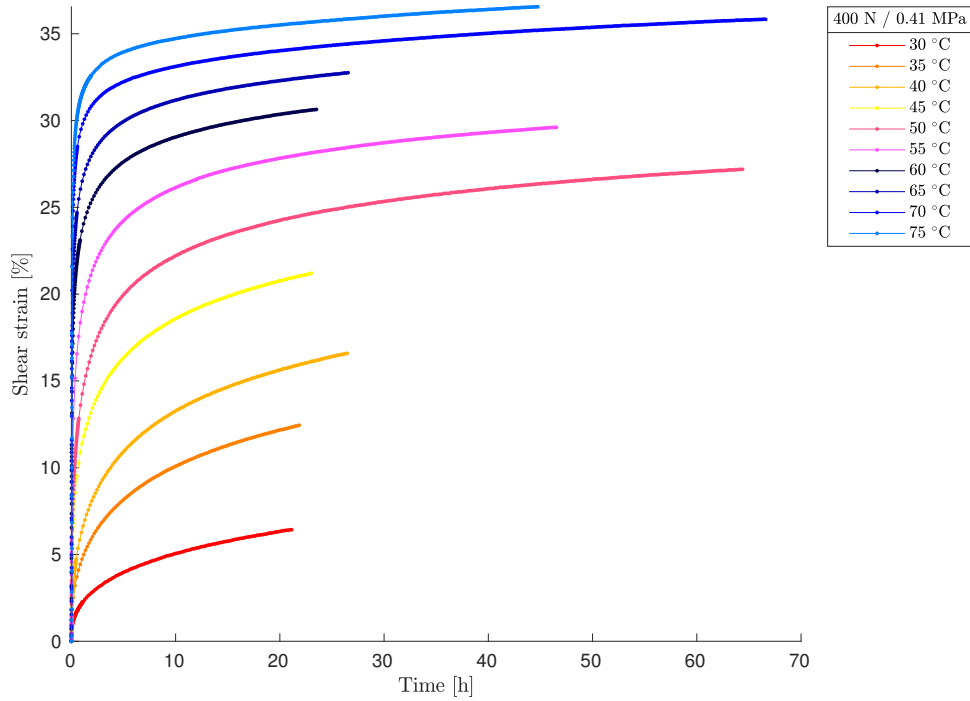


**Figure 3.27:** Creep loading test at 400 N load - 0.41 MPa on Arcan specimen bonded with SAF MIB 30 at various temperatures. Shear strain versus time. Rejuvenated Arcan specimen. Data are obtained with the DIC.

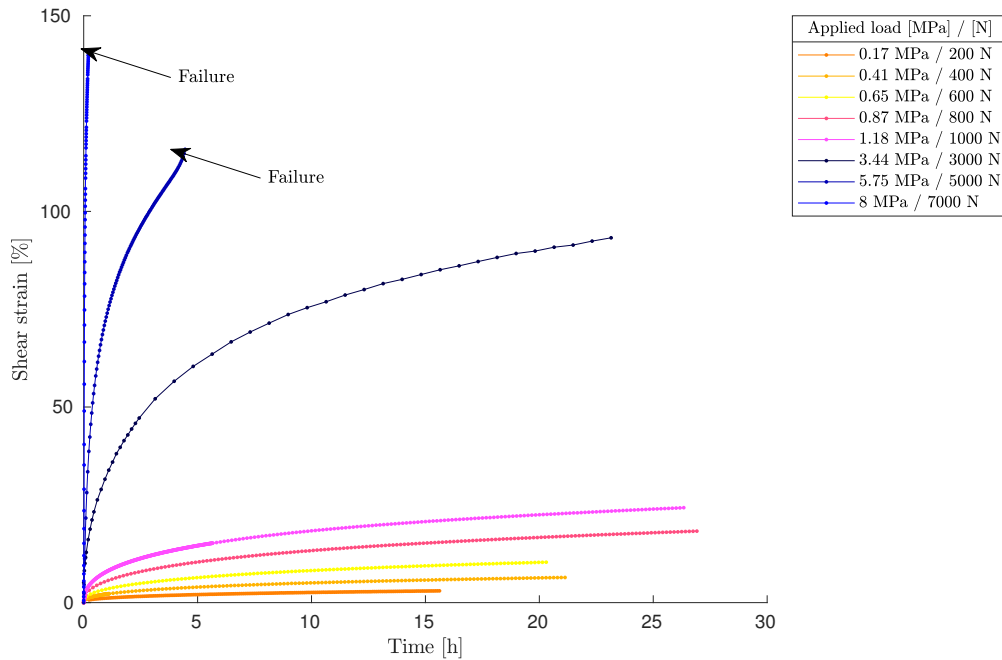


**Figure 3.28:** Creep loading test at various load level on Arcan specimen bonded with SAF MIB 30 at room temperature. Rejuvenated Arcan specimens. Data are obtained with the DIC.

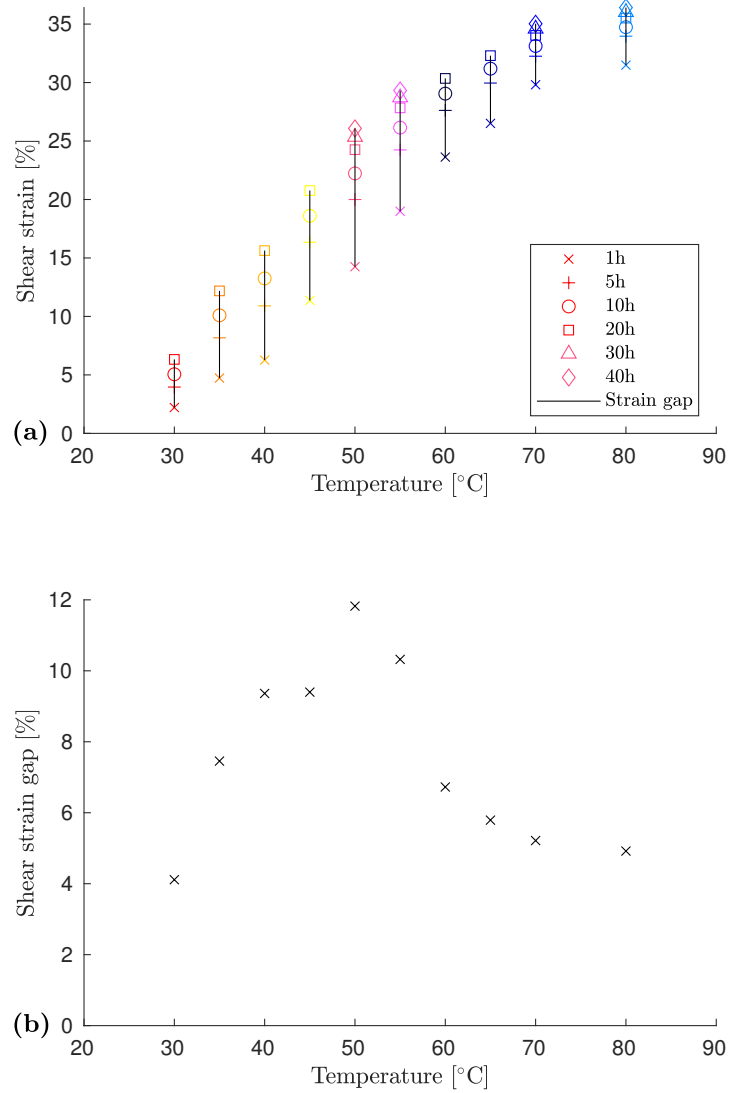


**Figure 3.29:** Creep loading test at 400 N load - 0.41 MPa on Arcan specimen bonded with SAF MIB 30 at various temperatures. (a) Shear strain at 1h, 5h, 10h, 20h, 30h, 40h versus temperature. (b) Shear strain gap versus temperature. Rejuvenated Arcan specimen. Data are obtained with the DIC.

### 3.4 Conclusions

The shear behaviour of three different structural adhesives have been studied qualitatively using Arcan test protocol combined with DIC monitoring of the bondline deformation. Measurement of the strains were not perturbed by the thermal regulation tool. It is possible to predict the failure path tendency prior to failure.

In particular, the thermo-mechanical behaviour of methacrylate adhesive (SAF MIB 30®) that exhibit pronounced viscous behaviour has been studied under creep loading condition using a thermal regulation control tool. These measurements allowed to evidence viscoelastic / viscoplastic transition so as temperature activation of the viscous processes. On the contrary epoxy adhesives (DP490® and DP760®) does not show pronounced viscous behaviour in the near room temperature condition but quasi-brittle behaviour. All the necessary tests to developed rheological models are available as well as investigation of crack onset in elastic-brittle material. This could be used in mechanical fracture studies as pre-testing before going on fracture test with adhesive joint specimen with pre-cracks.

Failure surfaces showed both adhesive and cohesive failure. It highlights the variability of the results obtained with Arcan tests.

SAF MIB 30® seems to be an appropriate candidate to evaluate time-dependent strain rate dependent effect in the mode II crack initiation and propagation conditions in bonded specimens. Epoxy DP490® and DP760® seem to be appropriate candidates to monitor crack initiation and propagation mechanisms in bonded joint in quasi-static tests.

# Chapter 4

## Theoretical assessment of ELS test data reduction technique using virtual testing

### Contents

---

<b>3.1</b>	<b>Test methods</b>	<b>49</b>
3.1.1	Arcan tests	49
3.1.2	Materials	50
3.1.3	Specimen preparation	50
3.1.4	Temperature regulation tool	53
3.1.5	Digital Image Correlation (DIC) set-up	53
<b>3.2</b>	<b>Data reduction method with Digital Image Correlation</b>	<b>54</b>
<b>3.3</b>	<b>Experimental results</b>	<b>59</b>
3.3.1	Elastic brittle adhesive behaviour	60
3.3.2	Viscoelastic-viscoplastic ductile adhesive behaviour	62
<b>3.4</b>	<b>Conclusions</b>	<b>72</b>

---

This chapter is the reproduction of an article published in 2021 in International Journal Of Fracture.

After describing, in the previous chapter, the methodology to obtain rheological model with the Arcan test and the use of digital image correlation, we are interested in this chapter in providing the theoretical environment for the ELS fracture test.

More precisely, the ELS test is described and a semi-analytical model of this test is provided. A virtual testing campaign is performed to analyse the sensitivity of the load-displacement curves and R-curves to the adhesive layer behaviour law. From this analysis, a direct method to identify the adhesive layer shear behaviour from the experimental results is described.

## Abstract

In this paper a theoretical analysis of crack initiation and propagation conditions in a bonded specimen loaded under pure mode II condition is proposed. The End-Loaded-Split (ELS) test response is evaluated using a semi-analytical model where the adherends are modeled as two deformable Timoshenko beams and considering non-linear behaviour of the adhesive. Bi-linear elastic-plastic, elastic-softening and trapezoidal Adhesive Layer Shear Behaviours (ALSBs) have been implemented and studied. From the results we observed that the load-displacement curve does not permit accurate evaluation of the adhesive layer shear behaviour. An alternative procedure consisting of analyzing the strain energy release rate versus shear displacement at the crack tip is proposed for data reduction of ELS test results.

## 4.1 Introduction

Thanks to their high technical and economical performances, adhesive joining technique has become the preferred methodology for manufacturing structural assemblies in many applications. In transportation industries (car, train, naval, aerospace) or other critical applications, high reliability is needed so that not only the product and process can be robust but also the design methodologies. In this context, a damage tolerance approach is recommended. Controlling possible crack extension leads to a more secured design than a safe live approach, where joint design is based on crack onset conditions.

Bonded joints are generally designed so that the adhesive sustains shear load and peel stresses are minimized. Therefore mode II crack propagation regimes are expected [97, 12]. Multiple test configurations are available for mode II testing of laminates and bonded joints. Most of the time, the specimen is bent so that shear stresses develop along the adhesive layer. In the End Notched Flexure (ENF) tests, 3 or 4 point bending conditions are applied to the specimen, while in the End Loaded Split (ELS) test simple bending [35] condition is applied. These tests are reputed to suffer from unstable crack propagation [30], poor reproductibility [36, 35] due to friction [112] effects and crack length measurement issues [103, 109, 36, 97, 12], small region for crack propagation. Recently, a large number of contributions have been presented aiming at improving the test protocols, instrumentation and data reduction techniques to achieve more reliable mode II testing of bonded adhesive layers. Also, new standards have been under development for mode II testing.

Amongst, the various existing test configurations, the ELS seems to be more effective than the others because of pure shear loading achievement in all the adhesive layer [103], an easy set-up and a larger region for crack propagation. Precisely, stable crack propagation occurs when the crack length to specimen length ratio  $a_0/L \geq 0.55$  for an ELS test controlled by displacement and under Linear Elastic Fracture Mechanics (LEFM) assumptions, whereas this ratio is 0.7 for ENF tests [4].

An important point of consideration in those fracture mechanics tests is the extend of the Fracture Process Zone (FPZ) corresponding to the distance along which large stress / strain gradients develop ahead of the decohesion front [4]. During crack nucleation and

propagation regimes the adhesive layer exhibits visco-elasto-plastic behaviour equivalent to a non-linear behaviour but can still transfer stresses. In mode II testing the extent of the FPZ is generally much larger than the one observed during mode I testing on a same system (substrate / adhesive layer). The effect of non linearity is then more pronounced which may render conventional data reduction method based on LEFM concepts obsolete. Indeed, LEFM addresses the only crack propagation conditions of joints experiencing mainly linear behavior, while more recent Non Linear Fracture Mechanics (NLFM) approaches, such as those based on Rice's contour integral (J-integral) [7, 31, 71, 72] or cohesive zone modeling [88, 32, 81], consider both crack nucleation and propagation regimes trying to describe the development of the FPZ ahead the crack front. However, for robust implementation of these new techniques and reliable prediction of joint failure, adhesive layer behaviour should be determined accurately. Indeed, improper Adhesive Layer Shear Behaviour (ALSB) evaluation may lead to large errors on joint strength prediction. Cricri *et. al.* for example showed a precise inverse method using FE simulations for adhesive layers subject to shear load [70].

In the present contribution, a virtual testing approach is proposed to investigate the application of ELS testing procedures to bonded adhesive layers exhibiting large process zones. Such a condition is now frequently encountered due to the use of more deformable adhesives for structural applications. A semi-analytical model of the ELS test applicable for bonded joint having identical adherends is derived. Adherend deformations are described using shear deformable Timoshenko beam model. The non-linear adhesive layer behaviour under shear loading conditions is described with a four-parameter-bilinear or with a trilinear (trapezoidal) law. With this model, all measurable quantity evolutions during the ELS test are simulated taking into account various experimental conditions and parameters. Using this virtual approach, one can evaluate how sensitive are these evolutions to the adhesive layer behaviour. Then the relative merits of various applicable data reduction methods for the evaluation of these parameters could be compared.

## 4.2 ELS test description

The ELS test is a simple bending test performed on a cantilever specimen which is symmetric with respect to the tested adhesive layer. In the following, bonded joints made with two isotropic homogeneous slabs (thickness :  $t = 5$  mm, width :  $w = 25$  mm, length :  $L = 150$  mm, Young's modulus :  $E = 70$  GPa, Poisson's ratio :  $\nu = 0.3$ ) are considered. The analysis is limited to elastically deforming adherends. The two adherends are partially bonded together over a distance  $l_c = 65$  mm with a thin adhesive layer (thickness :  $t_a = 0.5$  mm, Young's modulus :  $E_a$ , Poisson's ratio :  $\nu_a$ ). An initial crack  $a_0 = L - l_c$  is generally artificially introduced by leaving an end of the specimen free of adhesive or placing some PTFE insert during the bonding procedure. Due to the specimen symmetry and loading condition, the adhesive layer sustains a uniform shear stress except near the crack tip where severe stress gradients are expected thus leading to crack onset and propagation after the ultimate load is reached. Since the adhesive layer is loaded under only shear, mode II crack propagation condition is achieved. All the quantities are presented



in Fig. 4.1.

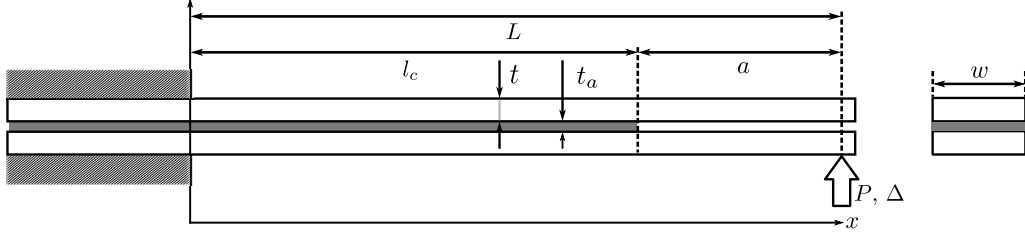


Figure 4.1: End Loaded Split (ELS) test configuration description.

Crack onset and propagation conditions can be determined using classical LEFM approach  $\mu = \mu_c$ ,  $\mu$  being the Strain Energy Release Rate (SERR) and  $\mu_c$  its critical value.  $\mu$  is obtained using the classical Irwin-Kies equation :

$$\mu = \frac{1}{2w} \frac{\partial C(a)}{\partial a} P^2 \quad (4.1)$$

With,  $C(a)$  being the specimen compliance and P the applied load.  $C$  can be evaluated with the simple beam theory, assuming the adhesive layer compliance is negligible and the adherend deformation can be described with classical beam models leading to (description in A - 1):

$$C(a) = \frac{L}{2\kappa GS} + \frac{1}{2EI} \left( \frac{a^3}{4} + \frac{L^3}{12} \right) \quad (4.2)$$

$$\mu = \frac{3a^2 P^2}{16wEI} = \frac{9a^2 P^2}{4w^2 t^3 E} \quad (4.3)$$

Crack length correction factors are generally used to take into account the possible influence of the adhesive layer compliance. Amongst the many drawbacks of the test, the intrinsic unstable nature of crack propagation may be the most troublesome [36].

Load-displacement curve is the main output of ELS tests. Fig. 4.2 shows  $P(\Delta)$  curves obtained with the semi-analytical model presented in section 4.3 for a specimen with an elastic-softening adhesive behaviour (see SOFT1 in table 4.1 for the ALSB description) and for two different initial crack length values :  $a_0 = 85$  mm and  $a_0 = 60$  mm. These crack values correspond to  $a_0/L$  ratios respectively higher and lower to 0.55 which respectively leads to stable and unstable crack propagation. Indeed, a snap back behaviour is observed when  $a_0 = 60$  mm (dashed curve). For both situation, the FPZ is fully developed when the crack propagation onset occurs.

This snap back behaviour can easily be exhibited using the theoretical load-displacement relation considering  $\mu = \mu_c$  during crack propagation phase :

$$C = \frac{\Delta}{P} = \frac{L}{2\kappa GS} + \frac{L}{2EI} \left( \frac{1}{4} \left( \frac{2wt^{3/2} E^{1/2} \mu_c^{1/2}}{3P} \right)^3 + \frac{L^3}{12} \right) \quad (4.4)$$

Where  $C$  is the specimen compliance. Also, this allows the use of a semi-analytical model.

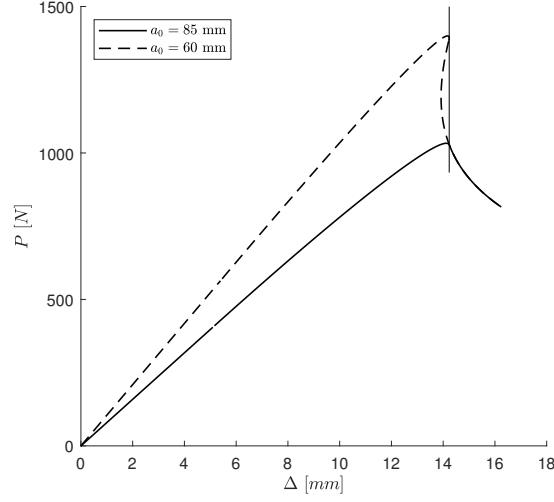


**Figure 4.2:** Load-displacement curve for elastic-softening (SOFT1) configuration with two different initial crack lengths. Unstability of the ELS test description.

Indeed, according to SBT theory, the compliance can also be expressed as a function of the crack length (see A - 1):

$$C(a) = \frac{\Delta_{SBT}}{P} = \frac{L}{2\kappa GS} + \frac{1}{2EI} \left( \frac{a^3}{4} + \frac{L^3}{12} \right) \quad (4.5)$$

Fig. 4.3 shows  $P(\Delta)$  curves for a purely elastic adhesive layer with the SBT (eq. 4.5) and the semi-analytical model (presented in section 4.3) that takes into account the adhesive layer compliance. The effect of the adhesive layer compliance is clearly evidenced. It can be included in relation 4.5. Usually, the influence of interface compliance is introduced by using crack length correction additive value [12, 110, 75]. These correction terms are determined either experimentally or using analytical expressions obtained with appropriate modeling of specimen deformation following Kaninen's approach [144]. In the present analysis, similar method is used to determine root rotation values taking into account the effect of transverse shear and specimen deformation near the crack tip and clamping position (see A - 3):

$$\varphi_r = \frac{P}{2EI} \frac{St^2}{St^2 + 4I} \left[ \frac{1}{\lambda_\tau^2} + \frac{a}{\lambda_\tau} \right] \simeq \frac{P}{2EI} \frac{St^2}{St^2 + 4I} \frac{a}{\lambda_\tau} \quad (4.6)$$

$$v_r = \frac{P}{2EI} \frac{St^2}{St^2 + 4I} \left[ \frac{l_e}{\lambda_\tau^2} - \frac{1}{\lambda_\tau^3} + \frac{a}{\lambda_\tau^3} \right] \quad (4.7)$$

An approximate expression of the specimen compliance can then be determined in which the root rotation and deflection coefficient are taken into account to be compared to equation 4.5:

$$C(a) = \frac{\Delta_{app}}{P} = \frac{\Delta_{SBT}}{P} + \frac{\varphi_r a}{P} + \frac{v_r}{P} \quad (4.8)$$

The root rotation coefficient  $\varphi_r$  is affected by both adhesive layer compliance in the

near crack tip region but also near the clamped edge of the specimen. Influence of the clamped edge might be strongly influenced by fixture design and stiffness while it is not the case near the crack tip region. The relative contribution of attachment to crack tip effect according to relation 4.6 is equal to  $a/\lambda_\tau$ . This ratio is small compared to other dimensions meaning that the influence of the process zone in the near crack tip region is much larger than the one in clamping region. The root deflection coefficient is so small that its influence can be neglected. The simplified expression of the root rotation coefficient can be used when the ELS with linear elastic adhesive behaviour problem needs to be solved or when plastic zone extend is very small. In the case of non-linear behaviour of the adhesive layer (plasticity for example), there is no such analytical expressions to describe the kinematic of the specimen as well as the shear strain and stress evolution. An iterative approach is considered and described in the next section.

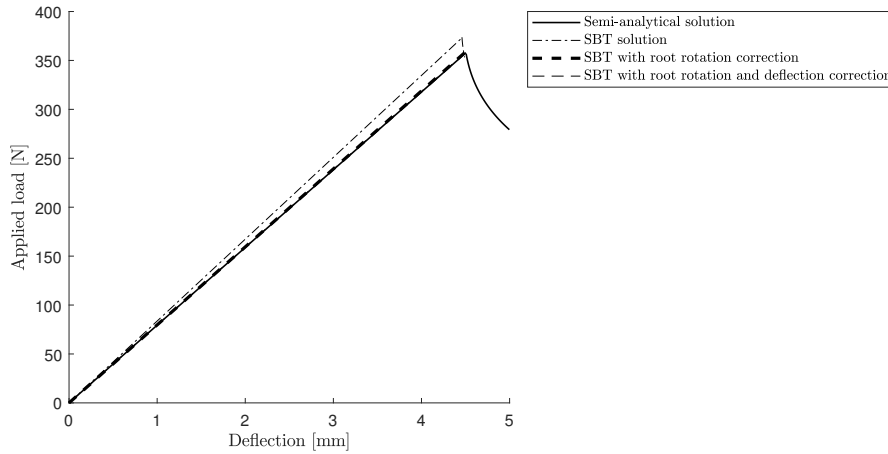


**Figure 4.3:** Load-displacement curve for purely elastic configuration. Effect of adhesive layer compliance.

### 4.3 Influence of adhesive layer compliance/nonlinear behaviour in an ELS test

For thick and/or very flexible adhesive layer, the Simple Beam Theory (SBT) is not applicable and the adhesive layer behaviour should be introduced in order to have more reliable description of the crack initiation and propagation. In the following symmetric bonded specimens are considered. The two identical adherends (same elastic properties and dimensions) are represented with shear deformable Timoshenko beams. The adhesive layer is represented with a continuous shear spring distribution having nonlinear behaviour. The specimen static and kinematic configurations along the bonded length are given by the evolution of internal forces (normal :  $N(x)$ , Shear :  $T(x)$ , Bending moment :  $M(x)$ ) and beam cross section displacement (longitudinal :  $u(x)$ , deflection :  $v(x)$ , rotation :  $\varphi(x)$ ) functions (see Fig. 4.4).

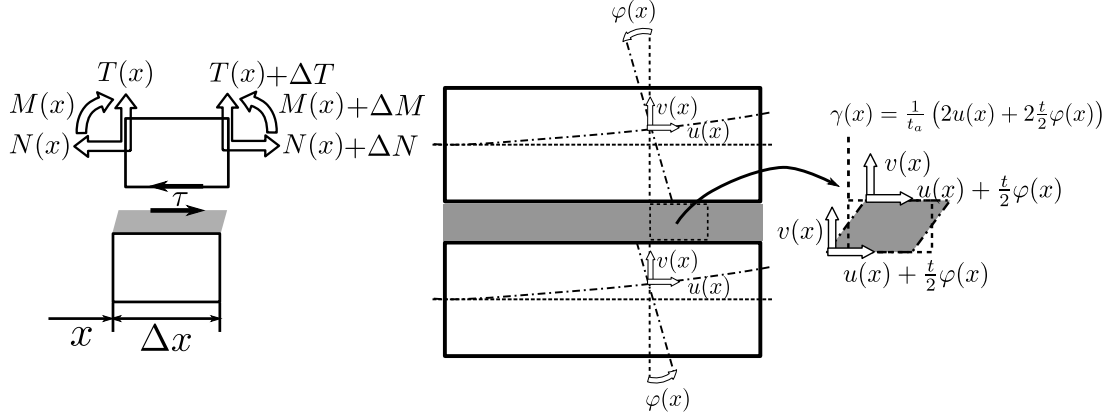


**Figure 4.4:** Kinematic and static quantities definition.

The constitutive equations to be solved and their derivation are given in A - 2. For the elastic regime, from :

$$\tau(x) = \frac{G_a}{t_a} \left[ 2u(x) + 2\frac{t}{2}\varphi(x) \right] = G_a \gamma \quad (4.9)$$

we get a third order differential equation is found controlling the shear stress distribution along the adhesive layer:

$$\frac{d^3\tau}{dx} - \frac{2wG_a}{t_a} \left[ \frac{1}{EI} \left( \frac{t}{2} \right)^2 + \frac{1}{ES} \right] \frac{d\tau}{dx} = 0 \quad (4.10)$$

with  $S = wt$  being the adherend cross section area,  $I = wt^3/12$  its second moment of inertia and  $G_a$  the adhesive shear modulus. The solution of the characteristic equation in  $\tau(x)$  is :

$$\tau(x) = Ae^{\lambda_\tau X} + Be^{-\lambda_\tau(X+l_e)} + \tau_m \quad (4.11)$$

with

$$\lambda_\tau = \sqrt{2\frac{G_a}{t_a}w \left[ \frac{1}{EI} \left( \frac{t}{2} \right)^2 + \frac{1}{ES} \right]} \quad (4.12)$$

$l_e$  is the length of the elastically deforming zone,  $X$  varies in the interval  $[-l_e; 0]$ .  $\lambda_\tau$  is an important parameter since it controls the extent of the elastic large gradient region ahead the crack tip but also near the specimen clamping. For thick and/or flexible bonded joint,  $\lambda_\tau$  values may be very large and close to the specimen dimensions so that interaction between process zone and specimen edge may occur. In such conditions, the crack propagation is not self-similar anymore, LEFM hypothesis is not valid anymore and ELS data reduction scheme should be revisited. Also, for ductile adhesives, large FPZs develop ahead the crack tip that exhibit nonlinear ALSB. For such a situation, Non Linear Fracture Mechanics (NLFM) concepts or Cohesive Zone Models (CZM) should be used to analyse crack initiation and propagation conditions. ALSBs are mainly phenomenological

and many shapes have been proposed for describing adhesive layers mechanical behaviour. Many of them represent the stress versus relative displacement evolution as a series of connected linear segments:

$$\tau(\gamma) = G_t^i \gamma + \tau_0^i \quad \text{for} \quad \gamma^{i-1} \leq \gamma \leq \gamma^i \quad (4.13)$$

with  $G_t^i$  being the local tangent modulus. In the following three types of ALSB will be considered, bilinear elastic-plastic, bilinear elastic-softening (also designated as triangular) and trapezoidal ALSB (see Fig. 4.5).

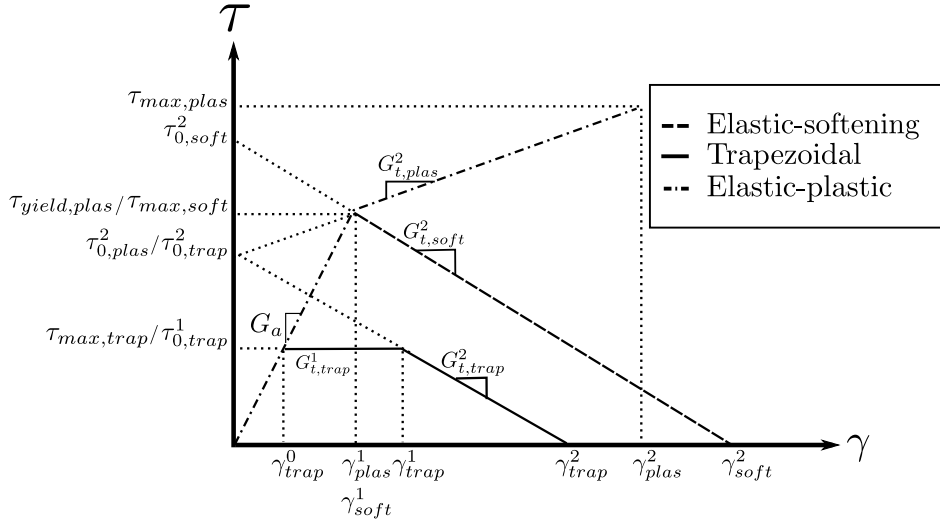


**Figure 4.5:** Different types of Adhesive Layer Shear Behaviour (ALSB).

Using relation (4.13) with the beam equilibrium and constitutive equations leads to the same characteristic equation, as Eq. (4.11), but replacing the adhesive Coulomb modulus with the local tangent shear modulus. The local shear stress evolution is again given by:

$$\tau_i(x) = A_i e^{\lambda_\tau^i X} + B_i e^{-\lambda_\tau^i (X+l_i)} + \tau_{mi} \quad (4.14)$$

with

$$\lambda_\tau^i = \sqrt{2 \frac{G_t^i}{t_a} w \left[ \frac{1}{EI} \left( \frac{t}{2} \right)^2 + \frac{1}{ES} \right]} \quad (4.15)$$

For positive secant modulus and hardening behaviour,  $\lambda_\tau^i$  is real and positive, while for softening behaviour and negative secant modulus,  $\lambda_\tau^i$  is imaginary leading to trigonometric  $\tau(x)$  evolution. A special condition is observed when  $G_t = 0$ , where second order polynomial evolution of the shear stress is found.

The problem in the most complex situation to be solved is represented in Fig. 4.6 which is a fully developed process zone with trapezoidal ALSB. The determination of specimen deformation and stress distribution results in a non linear least square minimisation procedure to determine the length,  $l_i$ , of each segments to verify all continuity and boundary conditions in between regions associated with each local tangent behaviour



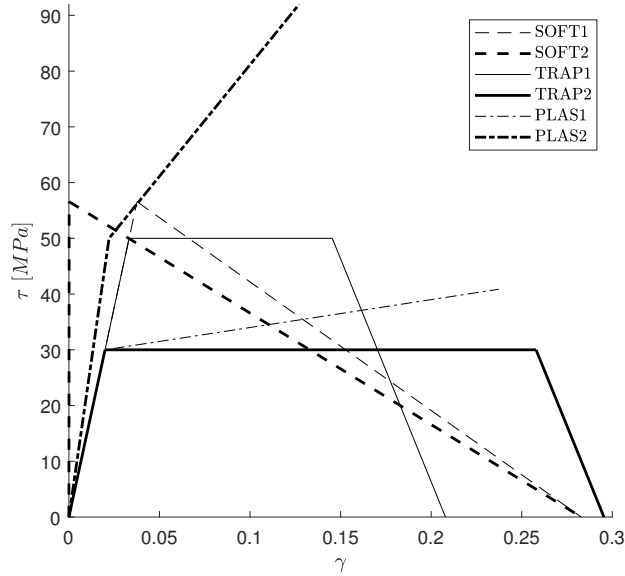
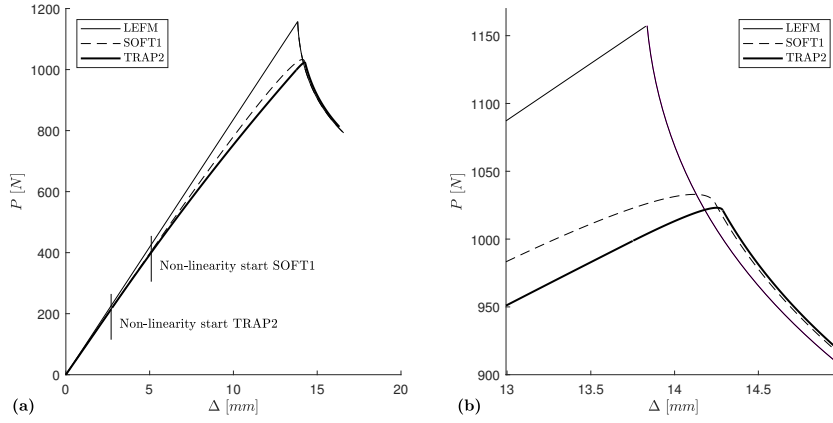


Figure 4.7: Stress-strains curves of the ALSB configurations.

Table 4.1: Adhesive layer properties for various ALSB configurations

ALSB	Shear modulus $G_a$ [GPa]	Maximum shear stress $\tau_{max}$ [MPa]	Tangent shear modulus $G_t^i$ [GPa]	Damage shear strain $\gamma_y^i$ [-]	Fracture energy $\mu_{IIc}$ [kJ/m <sup>2</sup> ]
SOFT1	1.5	56.57	-2.3067e-1	...	4
SOFT2	3.75e2	56.57	-2.001e-1	...	4
TRAP1	1.5	50	-8e-1	0.1454	4
TRAP2	1.5	30	-8e-1	0.2579	4
PLAS1	1.5	40.867	5e-2	...	4
PLAS2	2.25	91.965	4e-1	...	4

forces, shear stress and strain are easy to access. Investigation of these quantities shown in Fig. 4.9 allows for a better identification of the non-linear behaviour of the specimen response caused by the presence of the adhesive layer. In Figs. 4.9, 4.10 and 4.11, for each graph, evolutions are plotted for 2 applied load values : at the end of the reversible regime and at the end of the FPZ development stage. The grey patch and vertical lines describe the extent of the process zone once it is fully developed (bold lines). Crack tip position is easily evidenced with these curves. Non-linearity of the specimen behaviour is also visible on all curves. However behaviours between the two inputted ALSBs at the end of the FPZ development stage are once again very similar. Study of shear strain and stress can provide more information on some parameters of the ALSB as shown in Fig. 4.11. Displacements and local forces are linked to the cohesive stress and strain with a third order differential equation meaning that an inverse method could be used to identify ALSB from the study of these quantities. Instantaneous specimen configurations can be reproduced with a simple beam with elastic adhesive layer model replacing the exact non



**Figure 4.8:** Load-displacement curves for elastic-softening (SOFT1) and trapezoidal (TRAP2) configurations. (a) Overview. (b) Close up.

linear adhesive layer behaviour with an effective adhesive layer rigidity. Measurement of shear stress, normal force and bending moment can not be done directly. Non contact measuring techniques like Digital Image Correlation (DIC) could provide access to all beam displacements and thus strains and local forces. Indeed, using relation 4.9 which defines the shear strain  $\gamma$  as a function of beam rotation  $\varphi$  and transverse displacement  $u$ , study of beam displacements through DIC method could give access to the shear strain  $\gamma$ .

In order to identify the adhesive ALSB, R-curve analysis is more efficient than  $P(\Delta)$  curve analysis and straightforward to carry out experimentally. To estimate the SERR  $\mu$ , the Corrected Beam theory with Effective crack length (CBTE) and J-integral approaches are discussed.

The major difficulty encountered when measuring  $\mu$  is accessing the real crack length value. With the CBTE approach based on Griffith's energy balance method [145] (see appendix A - 1), the real geometrical crack length  $a$  is replaced by an effective crack length  $a_{eff}$  calculated from the compliance expression (see Eq. (4.2)) :

$$a_{eff} = \sqrt[3]{8EI \left( C(a) - \frac{L^3}{24EI} - \frac{L}{2\kappa GS} \right)} \quad (4.16)$$

$a_{eff}$  is independent of the measured crack length and can be determined from the  $P(\Delta)$  curve. However, as seen previously, the SBT approximation is not sufficient to describe specimen compliance. According to Eq. (4.8), a new effective crack length taking into account artefacts that disturb specimen compliance (root effect, FPZ, operating fault, ...) could be calculated by using Eq. (4.8).

In the R-curve analysis, the effective crack length is used to determined the effect of the FPZ on the energy released before crack propagation (because it is increasing without any real geometrical crack propagation). Fig. 4.12 shows the evolution of  $(a + 1/\lambda_\tau)/a_{eff}$  and  $(a + l_{FPZ} + 1/\lambda_\tau)/a_{eff}$  (bold lines) ratios as a function of  $a_{eff}$  for the two ALSBs configurations considered. Crack propagation corresponds to the line breaks. Obvious



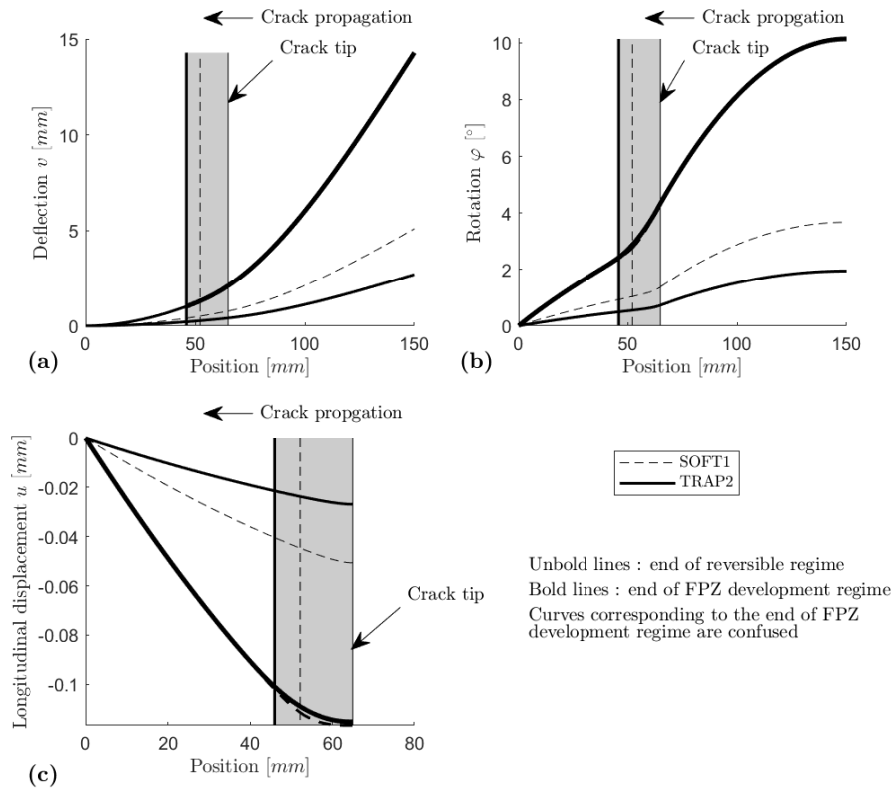


**Figure 4.9:** Displacement evolutions versus position along the specimen length for elastic-softening (SOFT1) and trapezoidal (TRAP2) configurations. (a) Beam deflection. (b) Beam rotation. (c) Beam longitudinal displacement. Refer to Fig. 4.7 for ALSB identification.

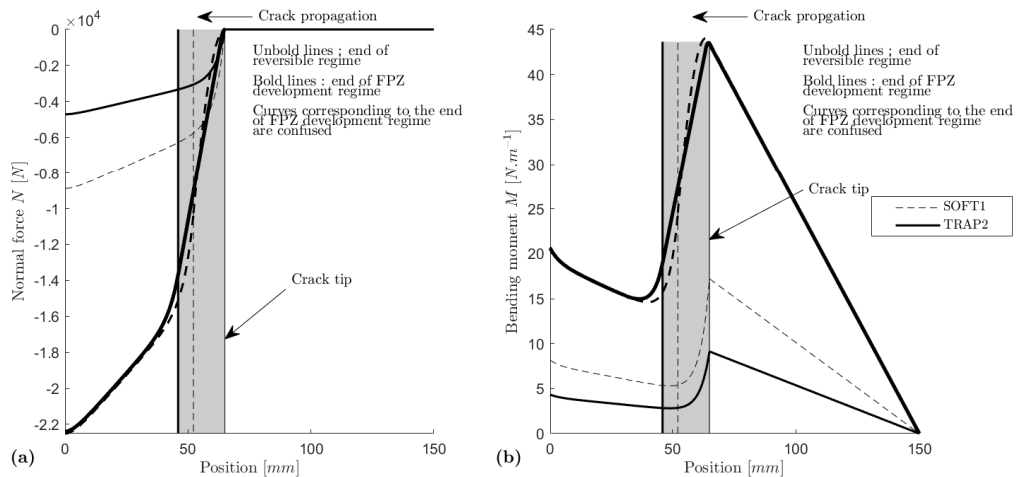


**Figure 4.10:** Normal force (a) and bending moment (b) evolutions along the specimen length for elastic-softening (SOFT1) and trapezoidal (TRAP2) configurations. Refer to Fig. 4.7 for ALSB identification.

difference is seen between no correction on the real crack length and corrected crack

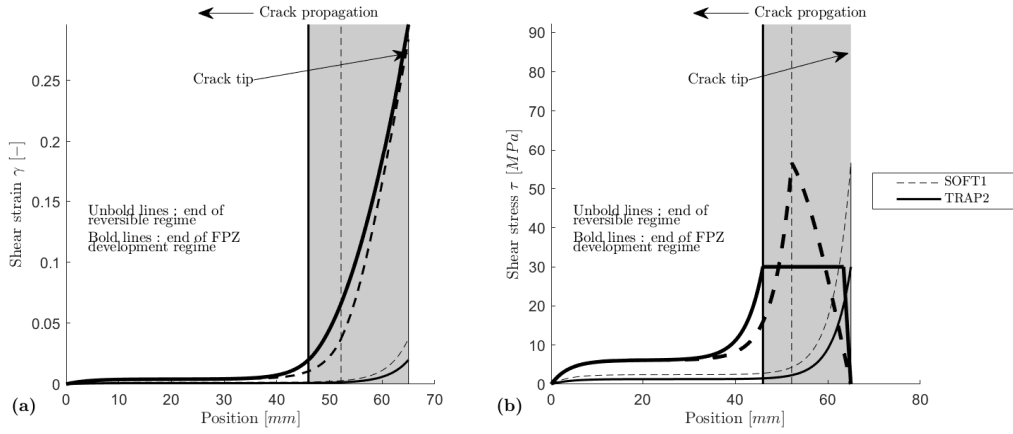


**Figure 4.11:** Shear strain (a) and stress (b) evolutions along the specimen length for elastic-softening (SOFT1) and trapezoidal (TRAP2) configurations. Refer to Fig. 4.7 for ALSB identification.

length with the damaged zone size  $l_{FPZ}$  and the parameters that control the extent of the elastic region. First, in elastic regime (dotted line in figure 4.12), the apparent crack length is corrected by the term  $1/\lambda_\tau$ . Then, the need for correction term is obvious and it appears to be less than the FPZ size. During the crack propagation phase, in self-similar regime, the length of the fracture process zone for the SOFT1 ALSB is 25 % of the bonded length ( $l_c$ , see figure 4.6) and for the TRAP2 ALSB, the length of the FPZ represents 35 % of the bonded length  $l_c$ . In the case of a purely elastic behaviour of the adhesive, the  $a_{eff}$  is increased by a constant correction factor  $1/\lambda_\tau$  which depends on the geometry of the specimen, initial stiffness of the adhesive layer and adherends elastic mechanical properties. Clearly, when the FPZ is developing, monitoring the specimen compliance evolution and using the elastic correction is not sufficient to track the crack tip position. Another terms should be proposed that should be calibrated experimentally since it depends on the ALSB and then on the nature of the adhesive layer.

The CBTE theory uses Griffith's expression :

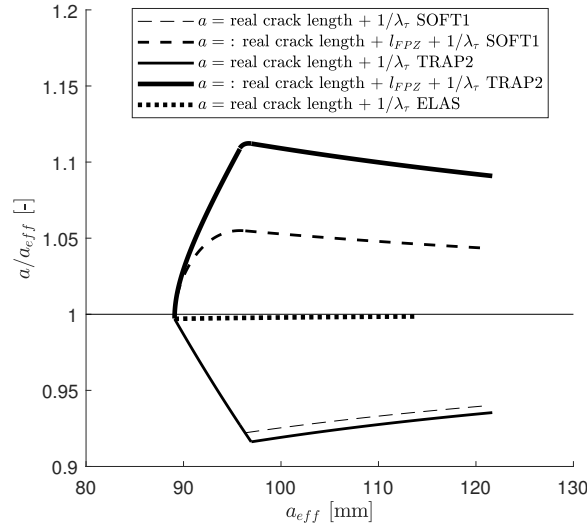
$$\mu = \frac{1}{2w} \frac{\partial C(a)}{\partial a} P^2 \quad (4.17)$$

The J-integral approach also known as the contour integral based on Rice's work uses the following expression developed by Pérez [31] *et. al.* :

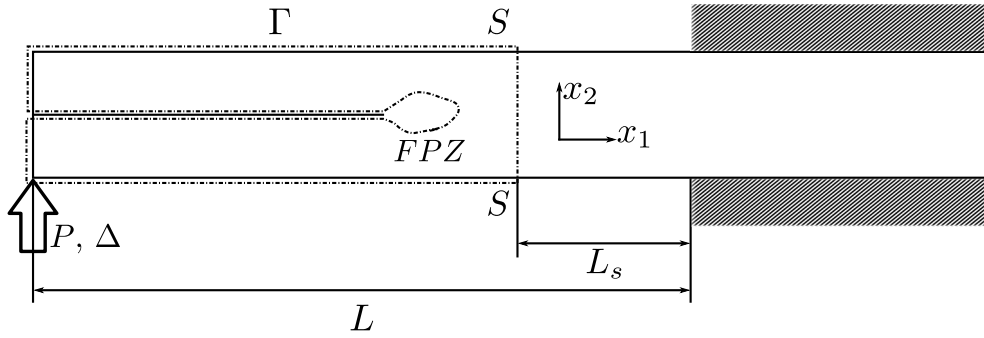
$$J = \frac{3}{5} \frac{P^2}{Gw^2t} + \frac{P}{w} (\tan \theta_P - \tan \theta_S) - \frac{Et}{3} \left( \frac{3}{2} \frac{P(L - L_s)}{Ewt^2} \right)^2 \quad (4.18)$$

where  $\theta_P$  and  $\theta_S$  correspond to rotation angles of the cross section of one adherend at load point and section  $S$  respectively (see Fig. 4.13). This expression allows for calculation of SERR independently of the boundary conditions and real geometrical crack length.

Fig. 4.14 shows the SERR according to the CBTE theory and the J-integral theory against the effective crack length  $a_{eff}$  for the two considered configurations. Evolutions between CBTE theory and J-integral theory are similar. After a rising part, the crack



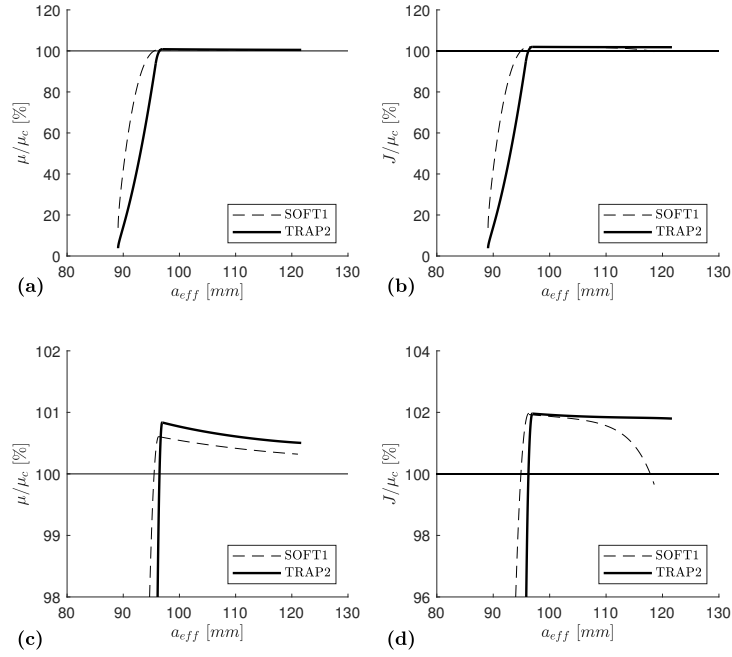
**Figure 4.12:** Crack length ratio evolutions for elastic-softening (SOFT1), trapezoidal (TRAP2) and purely elastic (ELAS) configurations.



**Figure 4.13:** Integration path, section definition of the ELS test for derivation of J-integral equation.

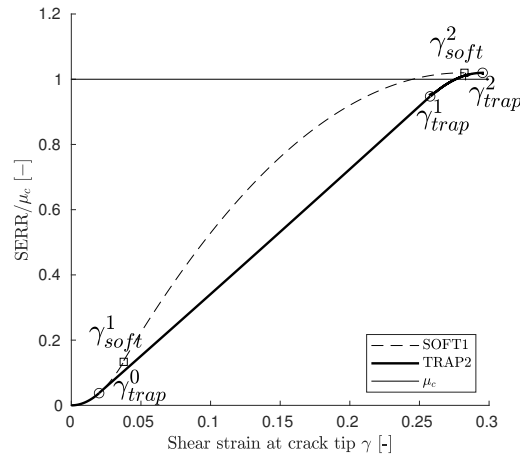
growth resistance is quasi-constant (it decreases slightly) and close to the critical SERR of the adhesive  $\mu_c$ . Both of the two theories overestimate the critical SERR : 0.66 % on average for the CBTE approach and 2.11 % on average for the J-integral approach. When using  $a_{eff}$ , R-curve evolutions during FPZ development phase (before the plateau) are different depending on the ALSB implemented in the semi-analytical model (see Fig. 4.14). However, variation of  $a_{eff}$  during FPZ development is very small (about 5 %) which is not a range large enough to distinguish behaviours especially when experimental work is going on. Therefore, a new procedure consisting in plotting shear strain  $\gamma$  versus SERR  $\mu$  calculated with J-integral is presented here.

Fig. 4.15 shows SERR according to J-integral theory versus shear strain  $\gamma$  for the two configurations considered. Squares and circles highlight the points  $\gamma_{soft}^1, \gamma_{soft}^2, \gamma_{trap}^0, \gamma_{trap}^1, \gamma_{trap}^2$  on the curve. These points corresponds to changes of the curvature of the  $J(\gamma)$  curve hence changes of regime. In this cases, variation of  $\gamma$  is about 85 %. More over as described before,  $\gamma$  is experimentally accessible with DIC. Analysis of the curves in



**Figure 4.14:** SERR normalized by the critical strain energy release rate  $\mu_c$  vs effective crack length for elastic-softening (SOFT1) and trapezoidal (TRAP2) configurations according to CBTE theory (a) and J-integral theory (b). (c) and (d) are close ups of respectively (a) and (b).

Fig. 4.15 shows that when ALSB exhibit plasticity, a linear evolution is seen on the  $J(\gamma)$  curve. Maximum shear strain is accessible as well as shear strain range of the plateau (in the case of the trapezoidal law). When ALSB exhibit softening behaviour, the  $J(\gamma)$  curve exhibit a convex curvature.



**Figure 4.15:** SERR normalized by the critical strain energy release rate  $\mu_c$  vs shear strain at crack tip for elastic-softening (SOFT1) and trapezoidal (TRAP2) configurations (with key-points identification).

Fig. 4.16 is a comparison between the implemented ALSB and simulated ALSB obtained with the first derivatives of the  $J(\gamma)$  curves for SOFT1 and TRAP2. The derivation of the  $J(\gamma)$  is made with a simple rate of change. By using :

$$\tau = \frac{1}{t_a} \frac{dJ}{d\gamma} \quad (4.19)$$

The shape of the ALSB is thus obtained. Figure 4.18 shows the implemented ALSBs and the simulated ALSBs as if they were experimentally obtained with noise. The level of noise is 1 % of the mean value of the strain energy release rate of each ALSB (SOFT1 and TRAP2). It is obtained thanks to a function “*rand*” in Matlab that creates an uniform array of numbers in the interval [0, 1]. A close up is shown in figure 4.17. Again, relation 4.19 is used to evaluate the ALSB from the noisy data.

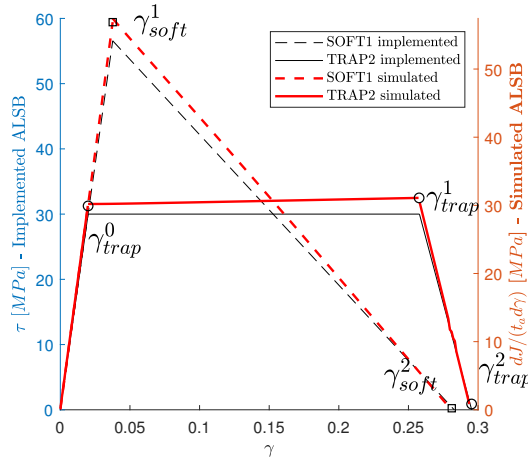


**Figure 4.16:** First derivate of  $J(\gamma)$  curve versus shear strain at crack tip for SOFT1 and TRAP2 ALSB configurations.

In Fig. 4.19 the  $J(\gamma)$  curves corresponding to the ALSBs presented in Fig. 4.7 are shown. Effect of value of the plateau, effect of softening or hardening and size of irreversible domain are evidenced on these curves. More over, when applying the procedure described before (derivation of  $J(\gamma)$  curves), the ALSBs implemented in the first place are found as seen in Fig. 4.20.

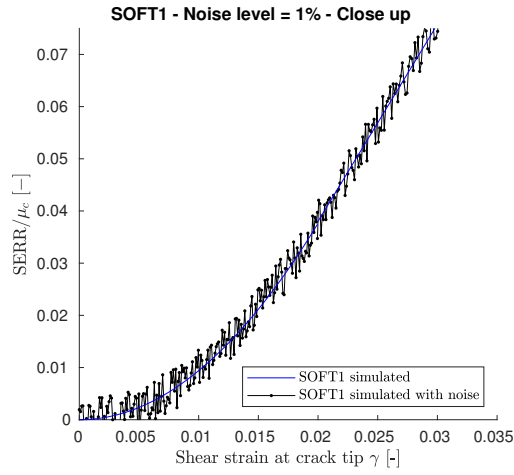


**Figure 4.17:** Close ups on SERR normalized by the critical strain energy release rate  $\mu_c$  vs shear strain at crack tip for elastic-softening (SOFT1) and trapezoidal (TRAP2) configurations with virtual 1 % noise.

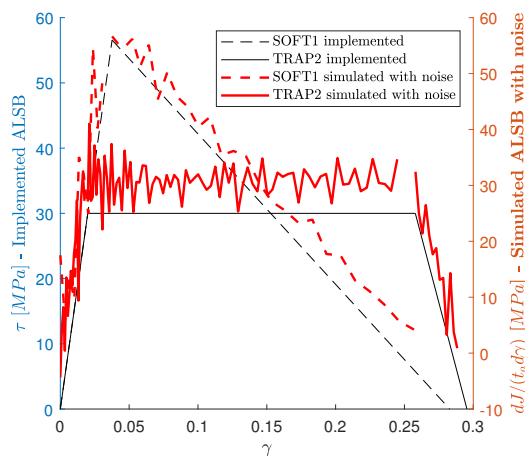


**Figure 4.18:** First derivate of  $J(\gamma)$  curve versus shear strain at crack tip for SOFT1 and TRAP2 ALSB configurations with virtual noise.

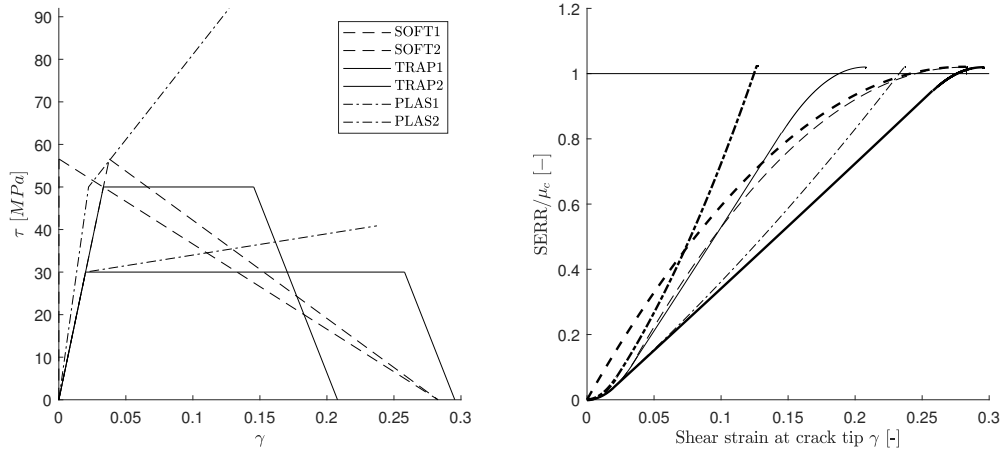


**Figure 4.19:** SERR vs shear strain at crack tip for all configurations. Refer to Fig. 4.7 for ALSB identification.

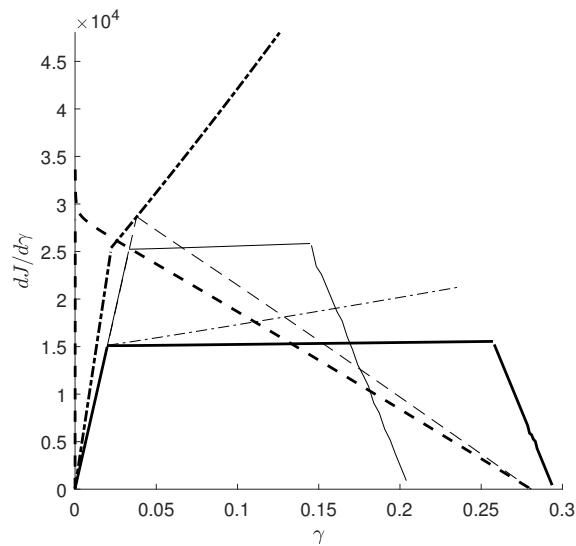


**Figure 4.20:** First derivatives of SERR vs shear strain at crack tip for all configurations. Refer to Fig. 4.7 for ALSB identification.

## 4.5 Conclusions

A new semi-analytical model has been proposed using Timoshenko beam theory for the ELS test. This model takes into account the adhesive layer behaviour. The adhesive layer behaviour is described as a succession of segment and multiple shapes can be implemented. In this article, bilinear elastic-plastic and elastic-softening ALSB and trapezoidal ALSB have been implemented in the semi-analytical model and quantity evolutions such as shear strain along the adhesive joint, adherend cross sectional displacements were obtained. The major output of the ELS test is load displacement curve. It has been shown that the measure of these curves can not give enough precision when ALSB shape identification and thus the effect of plasticity or softening behaviour is required.

ELS test main purpose is to obtain critical strain energy release rate. Two approaches are used to get to it : CBTE and J-integral. With simulated results, analysis of these approaches showed that the use of the J-integral approach gets rid off experimental artefact that perturbs analysis when CBTE approach is used. Presence of FPZ characterized by plastic or soft behaviour or both in the ALSB shape has a visible impact on  $J(\gamma)$  curves, more than on other quantities evolutions. The use of the new procedure that analyses energy versus shear strain evolution identifies ALSB shape when an ELS test is used. By differentiating the  $J(\gamma)$  curve, the shape of the ALSB law can be obtained. If the ALSBs are categorised in two main categories : bi-linear and trapezoidal, a simple calculation can give stress values to completely identify the ALSB. Further work can be conducted in the future where ALSB will not be categorised in only two categories. However, the derivation of the  $J(\gamma)$  curves is a functioning inverse method.

With new experimental methods like DIC [146, 55, 147], quantities needed in the new procedure using  $J(\gamma)$  analysis can be recorded precisely.



## A Appendix

### A - 1 Compliance assessment

The classical beam theory does not take into account the adhesive layer compliance. The specimen is seen as Timoshenko beams under flexure caused by applied load  $P$ . Specimen dimensions are seen in Fig. 4.1.

The Griffith's energy balance gives the Strain Energy Release Rate  $\mu$  (SERR) as :

$$\mu = \frac{1}{2w} \frac{\partial C(a)}{\partial a} P^2 \quad (4.20)$$

To obtain the compliance  $C(a)$ , the whole specimen potential energy  $W_e$  is integrated :

$$W_e = \frac{1}{2} C(a) P^2 \quad (4.21)$$

$$\delta W_e = \frac{1}{2} \frac{T^2}{\kappa G S_{eff}} + \frac{1}{2} \frac{M^2}{EI_{eff}} \quad (4.22)$$

$T$  is the transverse force and  $M$  the bending moment.  $S_{eff}$  and  $I_{eff}$  are respectively effective area and effective quadratic bending moment of the part of the specimen concerned.  $\kappa$  is the beam shear correction factor  $\kappa = 5/6$ ,  $E$  and  $G$  are respectively Young's and Coulomb's modulus of the adherends. Considering the specimen as a  $2t$  thickness beam along the bonded length  $l_c$  connected to two  $t$  thickness beams in parallel along the crack length  $a$  (all beams width is  $w$ ), we have :

$$T(x) = P \quad \text{for } 0 \leq x \leq L \quad (4.23)$$

$$M(x) = P(L - x) \quad \text{for } 0 \leq x \leq L \quad (4.24)$$

$$S_{eff} = 2S = 2wt \quad (4.25)$$

$$I_{eff} = 8I \quad \text{for } 0 < x < L - a, \quad I_{eff} = 2I \quad \text{for } L - a < x < L, \quad I = \frac{wt^3}{12} \quad (4.26)$$

We then find the whole specimen compliance as a function of the crack length  $a$  and the expression for the SERR :

$$C(a) = \frac{L}{2\kappa GS} + \frac{1}{2EI} \left( \frac{a^3}{4} + \frac{L^3}{12} \right) \quad (4.27)$$

$$\mu = \frac{3a^2 P^2}{16wEI} = \frac{9a^2 P^2}{4w^2 t^3 E} \quad (4.28)$$

## A - 2 Full derivation of constitutive equations

According to Timoshenko beam theory, the constitutive equations linking local forces to the displacements are :

$$M(x) = EI \frac{d\varphi(x)}{dx} \quad (4.29)$$

$$T(x) = \kappa GS \left[ \frac{dv(x)}{dx} - \varphi(x) \right] \quad (4.30)$$

$$N(x) = ES \frac{du(x)}{dx} \quad (4.31)$$

Where  $I = wt^3/12$  is the quadratic bending moment of one adherend cross section,  $\kappa$  is the beam shear correction factor  $\kappa = 5/6$ ,  $G$  is the shear modulus of the adherends,  $S = wt$  is the area of one adherend cross section. The local static equilibrium (see Fig. 4.4) is described with the following equations :

$$\frac{dM(x)}{dx} + T(x) - w \frac{t}{2} \tau(x) = 0 \quad (4.32)$$

$$\frac{dT(x)}{dx} = 0 \quad (4.33)$$

$$\frac{dN(x)}{dx} - w \tau(x) = 0 \quad (4.34)$$

Where  $\tau(x)$  is the shear stress along the adhesive. The shear strain  $\gamma$  is (see Fig. 4.4):

$$\gamma(x) = \frac{1}{t_a} \left( 2u(x) + 2 \frac{t}{2} \varphi(x) \right) \quad (4.35)$$

We obtain the shear stress distribution from Eqs. (4.29) to (4.35) depending on the Adhesive Layer Shear Behaviour (ALSB).

Shear stress for the elastic regime can be defined as :

$$\tau(x) = \frac{G_a}{t_a} \left[ 2u(x) + 2 \frac{t}{2} \varphi(x) \right] \quad (4.36)$$

Combining Eqs. (4.29) to (4.36) leads to a third order differential equation :

$$\frac{d^3\tau}{dx^3} - \frac{2wG_a}{t_a} \left[ \frac{1}{EI} \left( \frac{t}{2} \right)^2 + \frac{1}{ES} \right] \frac{d\tau}{dx} = 0 \quad (4.37)$$

The solution to this equation in  $\tau(x)$  is :

$$\tau(x) = Ae^{\lambda_\tau X} + Be^{-\lambda_\tau(X+l_e+l_1+l_2)} + \tau_m \quad (4.38)$$

with

$$\lambda_\tau = \sqrt{2 \frac{G_a}{t_a} w \left[ \frac{1}{EI} \left( \frac{t}{2} \right)^2 + \frac{1}{ES} \right]} \quad (4.39)$$

Where  $X$  varies in the interval  $[-l_e; -(l_1 + l_2)]$ .  $X$ ,  $l_1$ ,  $l_2$  are defined in Fig. 4.6.  $\tau_m$  is the mean shear stress. To obtain general expression for the local forces  $N(x)$ ,  $T(x)$ ,  $M(x)$  and the displacements  $u(x)$ ,  $v(x)$  and the rotation  $\varphi(x)$ ,  $\tau(x)$  is replaced by its expression in Eqs. (4.29) to (4.34) finding :

$$N(x) = w\tau_m X + A \frac{w}{\lambda_\tau} e^{\lambda_\tau X} - B \frac{w}{\lambda_\tau} e^{-\lambda_\tau(X+l_e+l_1+l_2)} + N_0 \quad (4.40)$$

$$M(x) = -\frac{P}{2}X + \frac{wt}{2} \left[ w\tau_m X + \frac{A}{\lambda_\tau} e^{\lambda_\tau X} - \frac{B}{\lambda_\tau} e^{-\lambda_\tau(X+l_e+l_1+l_2)} \right] + M_0 \quad (4.41)$$

$$T(x) = -\frac{P}{2} \quad (4.42)$$

$$u(x) = \frac{1}{ES} \left[ w\tau_m \frac{X^2}{2} + \frac{Aw}{\lambda_\tau^2} e^{\lambda_\tau X} + \frac{Bw}{\lambda_\tau^2} e^{-\lambda_\tau(X+l_e+l_1+l_2)} + N_0 X \right] + u_0 \quad (4.43)$$

$$\varphi(x) = \frac{1}{EI} \left[ -\frac{P}{2} \frac{X^2}{2} + \frac{wt}{2} \left[ \frac{\tau_m}{2} X^2 + \frac{A}{\lambda_\tau^2} e^{\lambda_\tau X} + \frac{B}{\lambda_\tau^2} e^{-\lambda_\tau(X+l_e+l_1+l_2)} \right] + M_0 X \right] + \varphi_0 \quad (4.44)$$

$$v(x) = \frac{1}{\kappa GS} \frac{P}{2} X + \frac{1}{EI} \left[ -\frac{P}{4} \frac{X^3}{3} + \frac{wt}{2} \left[ \frac{\tau_m}{2} \frac{X^3}{3} + \frac{A}{\lambda_\tau^3} e^{\lambda_\tau X} - \frac{B}{\lambda_\tau^3} e^{-\lambda_\tau(X+l_e+l_1+l_2)} \right] + \frac{M_0}{2} X^2 \right] + \varphi_0 X + v_0 \quad (4.45)$$

Where  $N_0$ ,  $M_0$ ,  $u_0$ ,  $\varphi_0$  and  $v_0$  are integration constants. In the case of softening or hardening behaviour, shape of the ALSB is defined by a local tangent modulus  $G_t^2 \neq 0$ . A similar third order differential equation is obtained :

$$\frac{d^3 \tau_2}{dx} - \frac{2wG_t^2}{t_a} \left[ \frac{1}{EI} \left( \frac{t}{2} \right)^2 + \frac{1}{ES} \right] \frac{d\tau_2}{dx} = 0 \quad (4.46)$$

Leading to a similar stress distribution :

$$\tau_2(x) = A_1 e^{\lambda_\tau^2 X} + B_1 e^{-\lambda_\tau^2(X+l_2)} + \tau_{m2} \quad (4.47)$$

with

$$\lambda_\tau^2 = \sqrt{2 \frac{G_t^2}{t_a} w \left[ \frac{1}{EI} \left( \frac{t}{2} \right)^2 + \frac{1}{ES} \right]} \quad (4.48)$$

Where  $X$  varies in the interval  $[-l_2; 0]$ .  $l_2$  being the length of the damaged zone as described in Fig. 4.6.  $X = 0$  corresponds to the crack tip position.  $\lambda_\tau^2$  is the characteristic wave number that controls the extent of the process zone.  $\tau_2$  is the shear stress along the damaged region of the adhesive developed during the softening or hardening stage. As for the elastic stage,  $\tau_2$  is replaced by its expression in Eqs. (4.29) to (4.34) which gives similar expressions to Eqs. (4.40) to (4.45).

In the case of a trapezoidal ALSB, a perfectly plastic behaviour is considered where the local tangent modulus is equal to 0. Shear stress for this regime can be defined as :

$$\tau_1 = \tau_{max} \quad (4.49)$$

After solving a second order differential equation, local forces and displacements can therefore be described as :

$$N_1(x) = w\tau_{max}X + N_{01} \quad (4.50)$$

$$M_1(x) = -\frac{P}{2}X + \frac{wt}{2}\tau_{max}X + M_{01} \quad (4.51)$$

$$u_1(x) = \frac{1}{ES} \left( w\tau_{max} \frac{X^2}{2} + N_{01}X \right) + u_{01} \quad (4.52)$$

$$\varphi_1(x) = \frac{1}{EI} \left( -\frac{P}{2} \frac{X^2}{2} + \frac{wt}{2}\tau_{max} \frac{X^2}{2} + M_{01}X \right) + \varphi_{01} \quad (4.53)$$

$$v_1(x) = \frac{1}{\kappa GS} \frac{P}{2}X + \frac{1}{EI} \left( -\frac{P}{4} \frac{X^3}{3} + \frac{wt}{4}\tau_{max} \frac{X^3}{3} + M_{01} \frac{X^2}{2} \right) + \varphi_{01}X + v_{01} \quad (4.54)$$

Where, in this trapezoidal case,  $X$  varies in the interval  $[-(l_1 + l_2); -l_2]$ .

A simple optimisation procedure is used to simulate the mechanical response of an ELS specimen. Indeed, the whole specimen is represented with segments connected together where shear stress distribution are given by relations (4.38) and (4.47). Considering displacements and cohesive forces along the adherend, the parameters to be identified are the lengths of each segment ( $l_e, l_1, l_2$ ). This procedure is illustrated in algorithms 1 in the case of a bilinear ALSB with the following boundary conditions (see Fig. 4.6) :

- Boundary condition considering the specimen clamped at its left end :  $u(0) = 0$ ,  $v(0) = 0$  and  $\varphi(0) = 0$ .
- At crack tip,  $N_2(l_e + l_2) = 0$  and  $M_2(l_e + l_2) = Pa/2$  since there is no loaded adhesive. The specimen behaves like a simple beam under flexure.

- Continuity conditions between elastic region and damaged region (see Fig. 4.6) :  
 $u(l_e) = u_2(l_e)$ ,  $v(l_e) = v_2(l_e)$ ,  $\varphi(l_e) = \varphi_2(l_e)$ ,  $N(l_e) = N_2(l_e)$ ,  $M(l_e) = M_2(l_e)$ .
- Fully developed FPZ condition :  $\tau_2(l_e) = \tau_{max}$ .
- Shear stress condition :  $\tau = \tau_{max}$ .
- Compatibility conditions :  $u(x)$  and  $\varphi(x)$  are replaced by their expression (Eqs. 4.43 and 4.44) in Eq. 4.36. Then identification between shear stress distribution (see Eq. 4.38) and shear stress as a function of shear strain (see Eq. 4.36) gives :

$$\tau_m = cste \quad (4.55)$$

$$\tau_m = 2\frac{G_a}{t_a} \left[ \left( \frac{1}{ES} \left[ w\tau_m \frac{X^2}{2} + N_0X \right] + u_0 \right) + \frac{t}{2} \left( \frac{1}{EI} \left[ -\frac{PX^2}{2} + \tau_m \frac{tw}{2} \frac{X^2}{2} + M_0X \right] + \varphi_0 \right) \right] \quad (4.56)$$

Polynomial terms in Eq. 4.56 must be equal to zero because  $\tau_m = cste$ , so we obtain :

$$\tau_m = \frac{P}{wt} \frac{St^2}{4I + St^2} \quad (4.57)$$

$$M_0 = -\frac{2I}{tS} N_0 \quad (4.58)$$

$$\tau_m = 2\frac{G_a}{t_a} \left[ u_0 + \frac{t}{2}\varphi_0 \right] \quad (4.59)$$

Algorithm 1 describes how local forces and displacement are obtained for the elastic, FPZ development and crack propagation regimes for a bilinear ALSB. More over, it describes how the maximum length for the process zone is obtained : multiple lengths are tested until shear strain goes over maximum shear strain ( $\gamma_2$ ). For each length of process zone, local forces and displacements are obtained. Similarly, during crack propagation regime, for each crack length  $a$  tested, quantities are calculated, especially shear strain. If shear strain is included in an interval  $[\gamma_{max} - \varepsilon, \gamma_{max} + \varepsilon]$ , crack propagates (crack length  $a$  rises).  $\varepsilon$  is the precision expected with respect to the ALSB parameters. More over it permits the semi-analytical model to converge to a solution. If shear strain is not in the interval, size of the FPZ  $l_{FPZ}$  has to be adjusted. In the case of bi-linear ALSB,  $l_{FPZ} = l_2$ . In the case of trapezoidal ALSB,  $l_{FPZ} = l_1 + l_2$ .

Getting the local forces and displacements describes crack propagation along the adhesive layer as a function of the applied load. Shear stress and strain are obtained and can be correlated with the adhesive layer shear behaviour. These quantities depends on

the geometrical and ALSB parameters.

---

**Algorithm 1** Virtual ELS test - Fracture Process Zone development

---

**Input:** Geometrical parameters, Adhesive Layer Shear Behaviour

**Output:** Load-Displacement curve ( $P-\Delta$ ), local forces ( $N(x)$ ,  $M(x)$ ), displacements ( $u(x)$ ,  $v(x)$ ,  $\varphi(x)$ ), shear strain and shear stress at crack tip ( $\gamma_{ct}$ ,  $\tau_{ct}$ ) in the cross section of specimen along the adhesive layer. **Return ultimate FPZ length.**

- 1: Calculate all the quantities :  $P$ ,  $\Delta$ ,  $N(x)$ ,  $M(x)$ ,  $u(x)$ ,  $v(x)$ ,  $\varphi(x)$ ,  $\gamma_{ct}$ ,  $\tau_{ct}$  at the FPZ development treshold for elastic region sized  $L - a_0$
  - 2: **while**  $\gamma_{ct} \leq \gamma_2$  **do**
  - 3:   Calculate all the quantities for elastic region sized  $L - a_0 - l_2$  and damaged region sized  $l_2$
  - 4:   Increase  $l_2$  :  $l_2 = l_2 + \Delta_{l_2}$
  - 5: **end while**
  - 6: **while**  $a \leq a_f$  ( $a_f$  is the final crack length) **do**
  - 7:   **if**  $\gamma_2 - \varepsilon \leq \gamma_{ct} \leq \gamma_2 + \varepsilon$  **then**
  - 8:     Calculate all the quantities for elastic region sized  $L - a - l_2$  and for the FPZ region sized  $l_2$
  - 9:     Increase  $a$  :  $a = a + \Delta_a$
  - 10:   **else**
  - 11:     **if**  $\gamma_{ct} \geq \gamma_2 + \varepsilon$  **then**
  - 12:       Reduce  $l_2$  :  $l_2 = l_2 - \Delta_{l_2}$
  - 13:       Calculate all the quantities
  - 14:     **else**
  - 15:       **if**  $\gamma_{ct} \leq \gamma_2 - \varepsilon$  **then**
  - 16:         Increase  $l_2$  :  $l_2 = l_2 + \Delta_{l_2}$
  - 17:         Calculate all the quantities
  - 18:       **end if**
  - 19:     **end if**
  - 20:   **end if**
  - 21: **end while**
- 

### A - 3 Approximate solution

The shear stress distribution is :

$$\tau(x) = \tau_m + Ae^{\lambda_\tau X} + Be^{-\lambda_\tau(X+l_e+l_1+l_2)} \quad (4.60)$$

$\tau_m$  is the mean shear stress.  $X$ ,  $l_e$ ,  $l_1$ ,  $l_2$  are described in Fig. 4.6. Assuming non interacting large gradient regions at both bondline edge, the boundary condition at the crack tip edge  $X = 0$  reduced to :

$$N(X = 0) = 0 = \frac{Aw}{\lambda_\tau} + N_0 \quad (4.61)$$

$$M(X = 0) = 0 = \frac{wt}{2} \frac{A}{\lambda_\tau} + M_0 \quad (4.62)$$

$N_0, M_0$  are integration constants. With compatibility conditions obtained with the method described in A - 2 :

$$M_0 = -\frac{2I}{St}N_0 \quad (4.63)$$

$$\tau_m = \frac{P}{wt} \frac{St^2}{St^2 + 4I} \quad (4.64)$$

We obtain :

$$A = \frac{\lambda_\tau}{w} \frac{St}{St^2 + 4I} Pa \quad (4.65)$$

$$N_0 = -\frac{St}{St^2 + 4I} Pa \quad (4.66)$$

$$M_0 = \frac{2I}{St^2 + 4I} Pa \quad (4.67)$$

So near crack tip region ( $B = 0$ ) :

$$\tau(x) = \frac{P}{wt} \frac{St^2}{St^2 + 4I} [1 + \lambda_\tau a e^{\lambda_\tau X}] \quad (4.68)$$

and near clamping region with  $\tau(X = -l_e) = 0$

$$\tau(x) = \frac{P}{wt} \frac{St^2}{St^2 + 4I} [1 - e^{-\lambda_\tau(X+l_e+l_1+l_2)}] \quad (4.69)$$

Replacing Eq. (4.69) in classical constitutive equations, we obtain :

$$\varphi(x) = \frac{1}{EI} \left[ -\frac{PX^2}{4} + \frac{wt}{2} \tau_m \left[ \frac{X^2}{2} + \frac{4I}{St^2} aX - \frac{1}{\lambda_\tau^2} e^{-\lambda_\tau(X+l_e+l_1+l_2)} \right] \right] + \varphi_0 \quad (4.70)$$

with  $\varphi(X = -l_e) = 0$

$$\varphi_0 = -\frac{1}{EI} \left[ -\frac{Pl_e^2}{4} + \frac{wt}{2} \tau_m \left[ \frac{l_e^2}{2} - \frac{4I}{St^2} al_e - \frac{1}{\lambda_\tau^2} \right] \right] \quad (4.71)$$

near crack tip

$$\varphi(x) = \frac{1}{EI} \frac{wt}{2} \frac{A}{\lambda_\tau^2} + \varphi_0 \quad (4.72)$$

$$\varphi(X = 0) = \frac{P}{EI} \frac{4I}{St^2 + 4I} \left[ \frac{l_e^2}{2} + al_e \right] + \frac{P}{EI} \frac{St^2}{St^2 + 4I} \left[ \frac{1}{\lambda_\tau^2} + \frac{a}{\lambda_\tau} \right] \quad (4.73)$$

$$\varphi_r = \frac{P}{EI} \frac{St^2}{St^2 + 4I} \left[ \frac{1}{\lambda_\tau^2} + \frac{a}{\lambda_\tau} \right] \simeq \frac{P}{EI} \frac{St^2}{St^2 + 4I} \frac{a}{\lambda_\tau} \quad (4.74)$$

$\varphi_r$  is the root rotation coefficient.

The same procedure is applied to determine the root deflection coefficient  $v_r$  :

$$v(x) = \frac{P}{2\kappa GS} + \frac{1}{EI} \left[ -\frac{PX^3}{12} + \frac{wt}{2} \tau_m \left[ \frac{X^3}{6} + \frac{4I}{St^2} a \frac{X^2}{2} + \frac{1}{\lambda_\tau^3} e^{-\lambda_\tau(X+l_e+l_1+l_2)} \right] \right] + \varphi_0 X + v_0 \quad (4.75)$$

with  $v(X = -l_e) = 0$

$$v_0 = \frac{Pl_e}{\kappa GS} + \frac{P}{2EI} \frac{4I}{St^2 + 4I} \left[ \frac{l_e^3}{3} + \frac{3}{4} a l_e^2 \right] - \frac{P}{2EI} \frac{St^2}{St^2 + 4I} \left[ \frac{1}{\lambda_\tau^3} - \frac{l_e}{\lambda_\tau^2} \right] \quad (4.76)$$

near crack tip

$$v(x) = \frac{wt}{2EI} \frac{B}{\lambda_\tau^3} + v_0 \quad (4.77)$$

$$v(X = 0) = \frac{Pl_e}{\kappa GS} + \frac{P}{2EI} \frac{4I}{St^2 + 4I} \left[ \frac{l_e^3}{3} + \frac{3}{4} a l_e^2 \right] + \frac{P}{2EI} \frac{St^2}{St^2 + 4I} \left[ \frac{l_e}{\lambda_\tau^2} - \frac{1}{\lambda_\tau^3} + \frac{a}{\lambda_\tau^3} \right] \quad (4.78)$$

$$v_r = \frac{P}{2EI} \frac{St^2}{St^2 + 4I} \left[ \frac{l_e}{\lambda_\tau^2} - \frac{1}{\lambda_\tau^3} + \frac{a}{\lambda_\tau^3} \right] \quad (4.79)$$





# Chapter 5

## Use of Digital Image Correlation in mode II testing : ELS test

### Contents

---

<b>4.1</b>	<b>Introduction</b>	<b>74</b>
<b>4.2</b>	<b>ELS test description</b>	<b>75</b>
<b>4.3</b>	<b>Influence of adhesive layer compliance/nonlinear behaviour in an ELS test</b>	<b>78</b>
<b>4.4</b>	<b>Virtual testing results</b>	<b>81</b>
<b>4.5</b>	<b>Conclusions</b>	<b>91</b>
<b>A</b>	<b>Appendix</b>	<b>92</b>
A - 1	Compliance assessment	92
A - 2	Full derivation of constitutive equations	93
A - 3	Approximate solution	97

---

In this chapter, End Loaded Split (ELS) tests have been performed on various specimens with various geometrical configurations (different sizes of initial crack length, adherend and adhesive thicknesses). Digital Image Correlation (DIC) is used to obtain the kinematics of the specimen and thus the new type of resistance curve  $J(\gamma)$  presented in chapter 4. Comparison between the experimental results and the virtual test results from the semi-analytical model presented in chapter 4 shows good agreement. The objective is to investigate further the ELS test for the analysis of bonded joint behaviours under shear loading.

## 5.1 Test method

### 5.1.1 Materials

Adherends are made with 7075 T6 series aluminium ( $E = 72$  Gpa,  $\nu = 0.33$ ,  $G = 26$  GPa, tensile yield strength  $\sigma_y = 500$  MPa). Two polymethyl-metacrylate (PMMA) based adhesives are tested in this study : SAF MIB 30 (from Bostik) and Araldite 2021 (from Araldite). The properties of these adhesives are described in table 5.1.

**Table 5.1:** Adhesives mechanical properties. Data are extracted from the manufacturer data sheet and the study presented in chapter 3.

	Shear modulus $G_a$ [GPa]	Failure shear stress $\sigma_{fa}$ [MPa]	Failure shear strain $\gamma_{fa}$ [%]
SAF MIB 30	82	0.65	128
Araldite 2021	96	0.61	-

The SAF MIB 30 adhesive have been tested in an other study by means of the Arcan test set up (see chapter 3) and it has been concluded that it is a very compliant adhesive. The Araldite 2021 is an adhesive known for its strength under shear and peel loading.

For both of the adhesives, the same manufacturing protocol has been used : after sand-blasting, the adherends were placed in an ultrasonic bath for cleaning and isopropylene solvent was applied.

The adhesive was deposited to one adherend surface manually. The adhesive is supplied in 50 ml cartridges. Excess adhesive was deposited to the surface so that adhesive squeezes out once the second adherend is placed on top of the first one. Adhesive thickness is controlled by teflon insert placed on both side of the first adherend (no adhesive is applied on these locations). Joint edges are shaped by wiping manually the side of the joint with a round shaped tool. Cure of the polymeric adhesives occurs during 24h at room temperature.

### 5.1.2 ELS test description

The End Loaded Split (ELS) test geometry is presented in Fig. 5.1.  $t$  is the adherend thickness,  $w$  the specimen width,  $L$  is the working length between the load application point and the clamp,  $l_c$  is the bonded length,  $t_a$  is the adhesive thickness,  $a_0$  is the initial crack length.

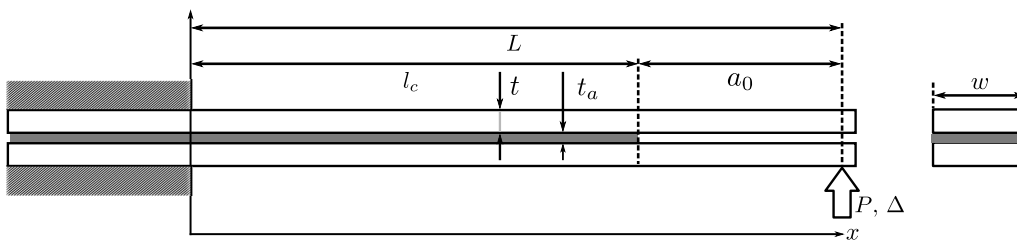


**Figure 5.1:** End Loaded Split (ELS) test configuration description.

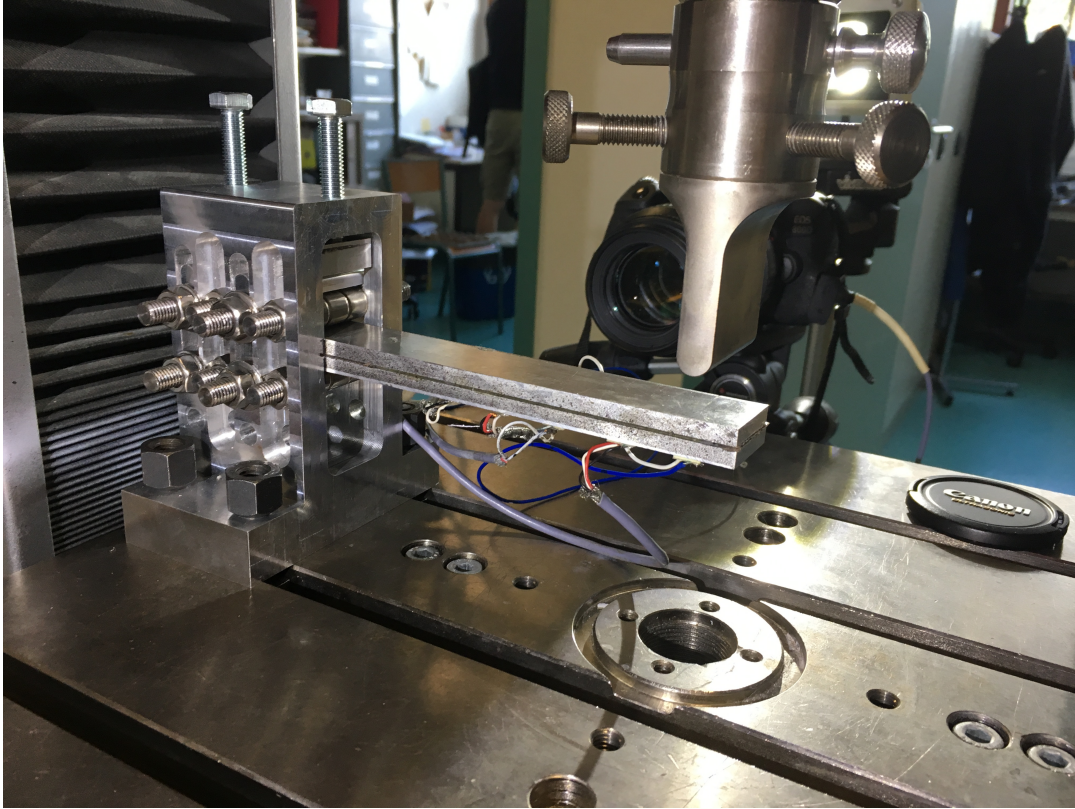


Figure 5.2: I2M laboratory ELS test set-up.

The ELS test is known to exhibit unstable crack propagation unless the initial crack length is larger than 55 % of the specimen length ( $a_0/L \geq 0.55$ ) [11].

Tests on the SAF MIB 30 adhesive has been conducted in the I2M laboratory in Bordeaux, France. In Fig. 5.2 a clamping fixture using three rollers is used to attach the specimen to the machine and not constraining the horizontal relative displacement between the adherends. The machine used was an Instron equipped with a 10 kN load cell.

Tests on the Araldite 2021 has been conducted in the AMADE laboratory in Girona, Spain. For clamping the specimen, the set-up presented in Fig. 5.3 has been used. It differs from the previous one because the specimen is clamped between two plates. This set (specimen and the two plates) can slide so the applied load location point is always at the same position. The machine used was a MTS Insight equipped with a 100 kN load cell.

### 5.1.3 DIC set-up

For the first set-up described in section 5.1.2, a 750D Canon® camera is used equipped with a macroscopic objective EFS 60 mm from Canon®. The camera battery is replaced by an AC adaptor sector in order to operate the camera during all the test duration. The resolution of the camera is 4000 x 6000 pixels with the chosen magnification, pixel size can be as small as 10  $\mu m$ . The image acquisition frame rate is adjusted depending of the test duration but can be also adjusted during the test depending of the observed traverse displacement rate. However, using a conventional reflex camera limits the maximum frame

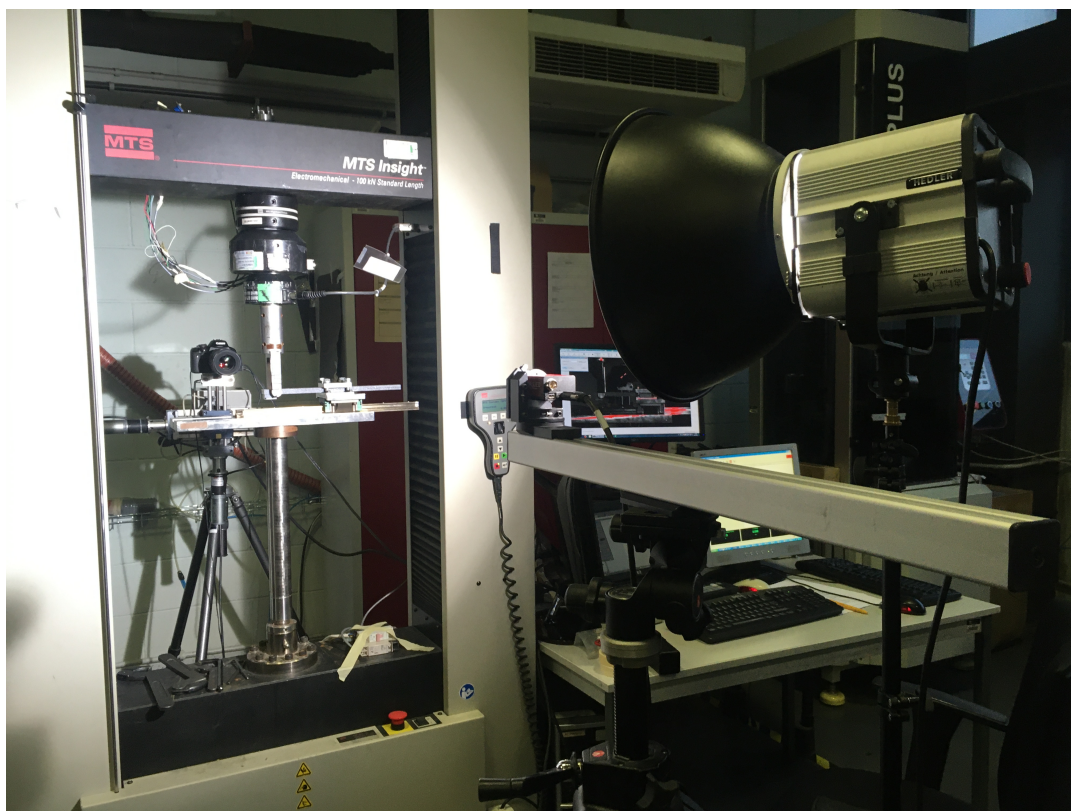


Figure 5.3: AMADE laboratory ELS test set-up.

to 1 image every 5 seconds. The camera is installed on a tripod to tilt the camera so that the larger dimension of the image is set parallel to the bondline and so that the bondline is centered on the image. To obtain uniform lighting and avoid specimen heating, Led spot is used to enlighten the scene.

For the second set-up described in section 5.1.2, a CCD camera from a 3D set-up has been used alone. During the tests frame rate acquisition was set to 1 picture every 5 seconds. The camera is mounted on a tripod which is set manually by the operator. Classic light far from the set-up has been used.

In both cases, for DIC displacement measurement technique to be applicable, a random pattern should be seen on the image : specimens were painted with white spray paint then small droplets of black paint were sprayed later.

## 5.2 Data reduction method with Digital Image Correlation

The software used for analysis in a 2D space is VIC 2D from Correlated Solutions. Data extracted from VIC2D are then computed into a matlab code specific for the ELS test analysis. In our case, the interest in using DIC is to obtain with macroscopic and "easy to use" tools, the kinematics of the ELS specimen and the shear deformation in the adhesive layer. This is why the analysis is conducted in a 2D space rather than in a 3D space which



## 5.2. DATA REDUCTION METHOD WITH DIGITAL IMAGE CORRELATION

is more expensive in terms of work to set-up the tools and in terms of computational work on the pictures.

For each picture taken, two Zones Of Interest (ZOI) that correspond to each adherend are determined (see Fig. 5.4).

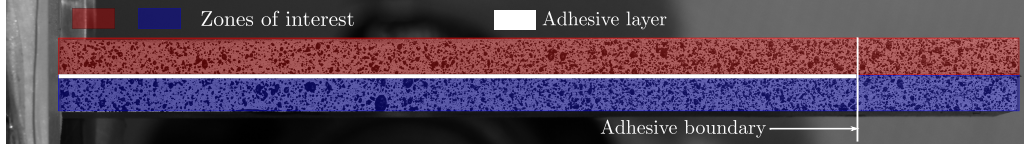


**Figure 5.4:** Description of the two zones of interest (ZOIs) on ELS test specimen.

The objective is to assess longitudinal and normal displacements and rotation angle along the adherends and thus the shear strain in the adhesive. With the following procedure, the data reduction method takes into account the adhesive thickness and the large displacements involved during the test. More over, the use of least square method allows to minimize noise and error from the analysis of the DIC software data.

The two ZOIs are composed by subsets for which horizontal and vertical displacements of their centers are extracted for every picture (see Fig. 5.5). The confidence interval of each subset (from the DIC software) is also extracted for every picture.

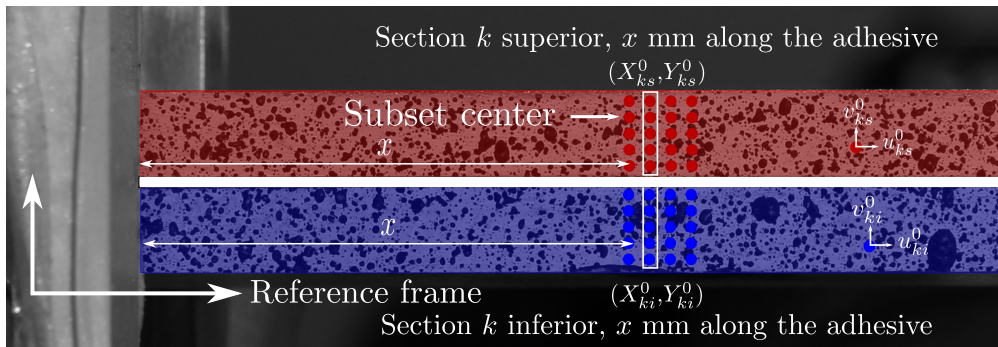


**Figure 5.5:** Description of the two zones of interest (ZOIs) on ELS test specimen. Description of the sections and their coordinates and reference frame, displacements of the centers of the subsets, position along the adhesive layer.

The procedure to assess shear strain of the adhesive layer is divided into three steps (see Fig. 5.6) : firstly, cutting each ZOI into sections and find their center of gravity. Secondly, extracting the displacements (horizontal, vertical and rotation angle) of these sections by referring to the center of gravity. Finally, doing a projection of the center of gravity of each section on sides of the adhesive to obtain shear strain along the adhesive.

Adherends are supposed to be rigid bodies. Pictures are supposed to be well aligned with the horizontal. Alignment means that sections are initially vertical so that in picture  $i$ :

$$X_k^j = -\tan(\varphi_k)Y_k^j + \delta_k \quad (5.1)$$

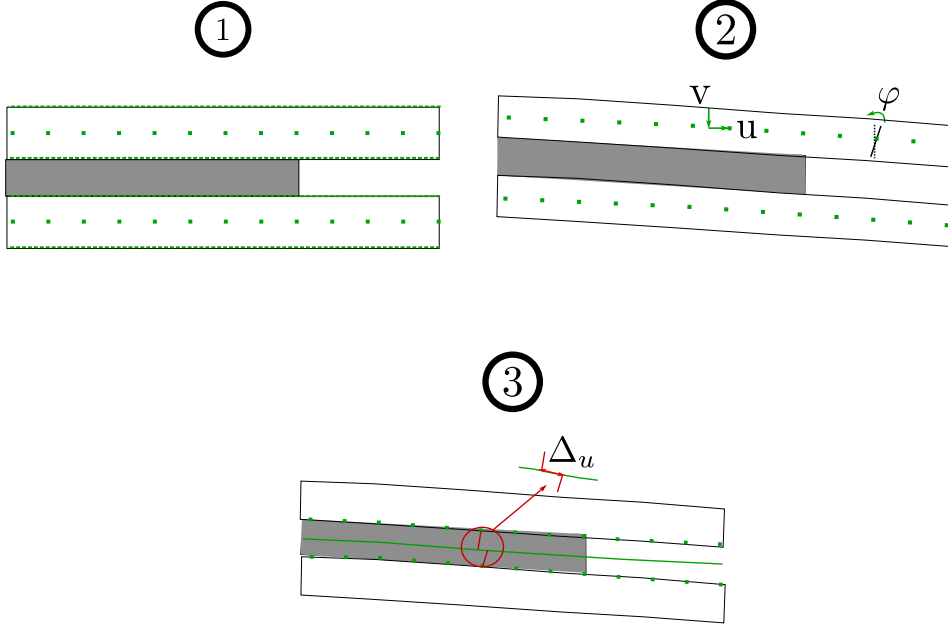


**Figure 5.6:** Description of the three principal steps for the DIC data reduction method.

Where  $(X_k^j, Y_k^j)$  are the coordinates of a section  $k$  of an adherend composed by  $N$  points as seen in Fig. 5.5.  $\varphi_k$  is the rotation angle of the section against the center of gravity.  $\delta_k$  is the intercept of the line along the section and the vertical axe corresponding to the initial position of the section.

The DIC software gives a confidence interval  $\sigma_k^j$ . It corresponds to the standard deviation on displacement between the reference image and deformed image. In order to find the angle of rotation and take into account  $\sigma_k^j$ , the least squared method is used :

$$\chi^2 = \sum_{j=1}^N \left( \frac{X_k^j + \tan(\varphi_k)Y_k^j - \delta_k}{\sigma_k^j} \right)^2 \quad (5.2)$$

$$\frac{\partial \chi^2}{\partial \tan(\varphi_k)} = 2 \sum_{j=1}^N \left( \frac{X_k^j Y_k^j + \tan(\varphi_k)Y_k^{j2} - \delta_k Y_k^j}{\sigma_k^{j2}} \right) = 0 \quad (5.3)$$

$$\frac{\partial \chi^2}{\partial \delta_k} = 2 \sum_{j=1}^N \left( \frac{-X_k^j - \tan(\varphi_k)Y_k^j + \delta_k}{\sigma_k^{j2}} \right) = 0 \quad (5.4)$$

By inverting the matrix deduced from the equation system formed by eq. 5.2, 5.3 and 5.4, we can find the rotation angle  $\varphi_k$  of each section (of both the lower and upper adherend) for every picture  $i$  :

$$\begin{bmatrix} \sum_{j=1}^N \frac{X_k^j Y_k^j}{\sigma_k^{j2}} \\ \sum_{j=1}^N \frac{X_k^j}{\sigma_k^{j2}} \end{bmatrix} = \begin{bmatrix} -\sum_{j=1}^N \frac{Y_k^{j2}}{\sigma_k^{j2}} & \sum_{j=1}^N \frac{Y_k^j}{\sigma_k^{j2}} \\ -\sum_{j=1}^N \frac{Y_k^j}{\sigma_k^{j2}} & \sum_{j=1}^N \frac{1}{\sigma_k^{j2}} \end{bmatrix} \begin{bmatrix} \tan(\varphi_k) \\ \delta_k \end{bmatrix} \quad (5.5)$$

Once the rotation angles are determined, the coordinates  $(X_{g,k}, Y_{g,k})$  of the centers of gravity of each section from the lower and upper adherend are recomputed with a rotation

matrice :

$$\begin{bmatrix} X_{rot,k} - X_{g,k} \\ Y_{rot,k} - Y_{g,k} \end{bmatrix} = \begin{bmatrix} \cos(\varphi_k) & -\sin(\varphi_k) \\ \sin(\varphi_k) & \cos(\varphi_k) \end{bmatrix} \begin{bmatrix} X_k^0 - X_{g,k} \\ Y_k^0 - Y_{g,k} \end{bmatrix} \quad (5.6)$$

Where  $(X_{rot,k}, Y_{rot,k})$  are the obtained coordinates. The mean displacement vector that corresponds to the displacement of the center of gravity is :

$$\begin{bmatrix} U_k \\ V_k \end{bmatrix} = \begin{bmatrix} X_k^j - X_{rot,k} \\ Y_k^j - Y_{rot,k} \end{bmatrix} \quad (5.7)$$

Again the least square method is used to overcome noise and errors :

$$\chi^2 = \sum_{j=1}^N \left( \frac{X_k^j - X_{rot,k} - U_k}{\sigma_k^j} \right)^2 \quad (5.8)$$

$$\chi^2 = \sum_{j=1}^N \left( \frac{Y_k^j - Y_{rot,k} - V_k}{\sigma_k^j} \right)^2 \quad (5.9)$$

When derivating we have :

$$U_k = \frac{1}{\sum_{j=1}^N \frac{1}{\sigma_k^j}} \sum_{j=1}^N \left( \frac{X_k^j - X_{rot,k}}{\sigma_k^j} \right)^2 \quad (5.10)$$

$$V_k = \frac{1}{\sum_{j=1}^N \frac{1}{\sigma_k^j}} \sum_{j=1}^N \left( \frac{Y_k^j - Y_{rot,k}}{\sigma_k^j} \right)^2 \quad (5.11)$$

In order to obtain the longitudinal et normal displacements of sections of the adhesive layer, the center of gravity of sections of the adherend are projected on sides of the adhesive layer :

$$\begin{bmatrix} \Delta_{u,k} \\ \Delta_{v,k} \end{bmatrix} = \begin{bmatrix} \cos(\varphi_{m,k}) & \sin(\varphi_{m,k}) \\ -\sin(\varphi_{m,k}) & \cos(\varphi_{m,k}) \end{bmatrix} \begin{bmatrix} X_{p,l} - X_{p,s} \\ Y_{p,l} - Y_{p,s} \end{bmatrix} \quad (5.12)$$

Then the shear strain is obtained by divided the longitudinal displacement by the adhesive thickness.

$$\gamma = \frac{\Delta_{u,k}}{t_a} \quad (5.13)$$

With DIC, the tool displacement is obtained without having to take into account the machine compliance. Moreover, with this method, deflection and rotation along the lower and upper adherends are obtained. The relative displacement between the adherends is also obtained which allows to obtain shear strain in the adhesive layer. The classical output is shown for shear strain and rotation angle in Fig. 5.7.

In chapter 4, a semi-analytical model of the ELS test with a new procedure for mode II investigation is presented. The  $J(\gamma)$  curve procedure allows to get the Adhesive Layer Shear Behaviour (ALSB) from the contour integral  $J$  and the shear strain at crack tip. The



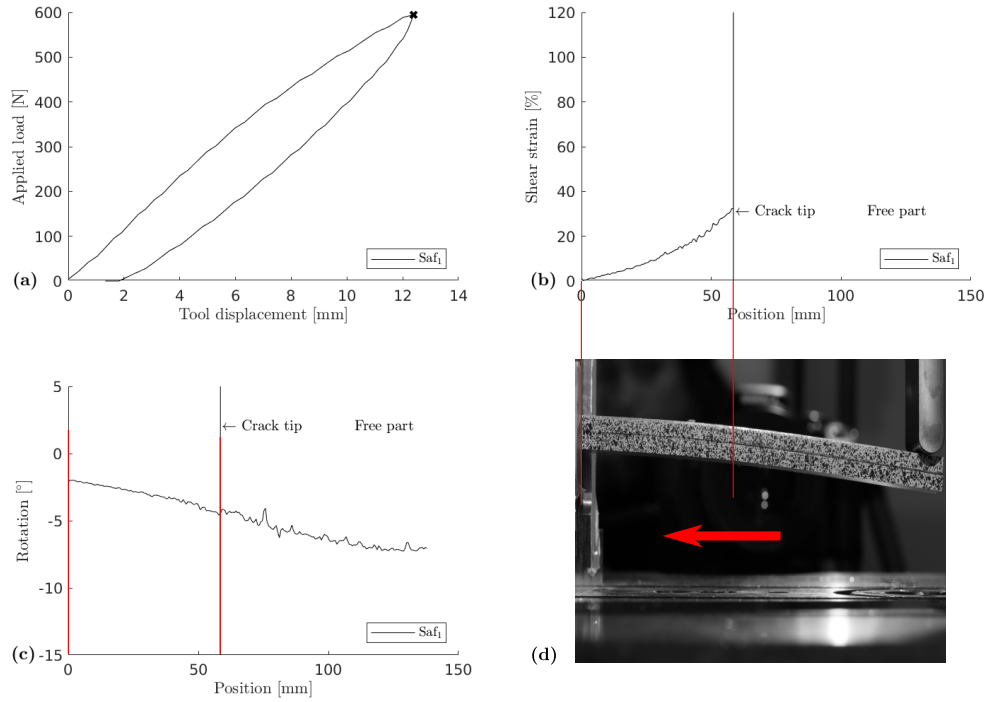


**Figure 5.7:** Exemple of quasi-static test on ELS specimen bonded with SAF MIB 30 adhesive. Load displacement curve (a). Shear strain versus position along the adhesive layer at maximum load (b). Rotation angle versus position along the superior adherend at maximum load (c). Picture of the specimen bent at maximum load and localisation of the adhesive layer (d). The arrow shows the crack propagation direction.

ALSB is the shear stress versus shear strain curve that describe the adhesive behaviour in mode II. This is what is used in Cohesive Zone Modeling to implement the adhesive behaviour in a FEA model. The contour integral  $J$  is :

$$J = \frac{3}{5} \frac{P^2}{Gw^2t} + \frac{P}{w} (\tan \theta_P - \tan \theta_S) - \frac{Et}{3} \left( \frac{3P(L - L_s)}{2Ewt^2} \right)^2 \quad (5.14)$$

Where  $P$  is the applied load,  $G$  the shear modulus of the adherends,  $w$  the adherend width,  $t$  is the adherend thickness,  $E$  is the adherend young's modulus,  $L$  is the working length.  $\theta_p$  is the rotation angle of the section of the adherend located at the load application point.  $\theta_s$  is the rotation angle of a section far from the crack tip and not too close to the clamp.  $L_s$  is the distance between the clamp and the section  $s$ . In this case,  $L_s = 10$  mm.  $\theta_p$  and  $\theta_s$  are obtained thanks to the DIC. We have :

$$\tau = \frac{1}{t_a} \frac{dJ}{d\gamma} \quad (5.15)$$

Where  $\tau$  is the adhesive shear stress,  $J$  the contour integral,  $t_a$  the adhesive thickness,  $\gamma$  the adhesive shear strain at crack tip. In order to obtain the ALSB from the  $J(\gamma)$  curve, a variation rate is calculated every 2 points. The precision of the resulting ALSB depends

on the number of point of the experimental  $J(\gamma)$  curve, so it depends on the camera frame rate and the duration of the test.

### 5.3 ELS test experimental results

Various adhesives have been tested as well as various geometric configurations for ELS specimens. First, the results for specimens bonded with the SAF MIB 30 adhesive are presented, and then the results for specimens bonded with the Araldite 2021 adhesive. The objective of all these different configurations is to perform in-depth analysis on the ELS test and its experimental implementation.

#### 5.3.1 Fracture tests with ductile material (SAF MIB 30)

Three ELS specimens bonded with SAF MIB 30 adhesive have been tested under quasi-static loading at 0.5 mm/min at room temperature. In this configuration the working length  $L$  is 140 mm, the adherend thickness  $t$  is 5 mm, the specimen width  $w$  is 25 mm. Specific specimen characteristics are presented in table 5.2.

**Table 5.2:** ELS Specimen bonded with SAF MIB 30 adhesive : geometrical characteristics

	Initial crack length $a_0$ [mm]	Adhesive thickness $t_a$ [mm]
SAF <sub>1</sub>	82	0.65
SAF <sub>2</sub>	82	0.72
SAF <sub>3</sub>	96	0.61

Fig. 5.8 shows the load displacement curves and shear strain at maximum load versus the position along the adhesive layer (as described in Fig. 5.7 (a) and (b)).

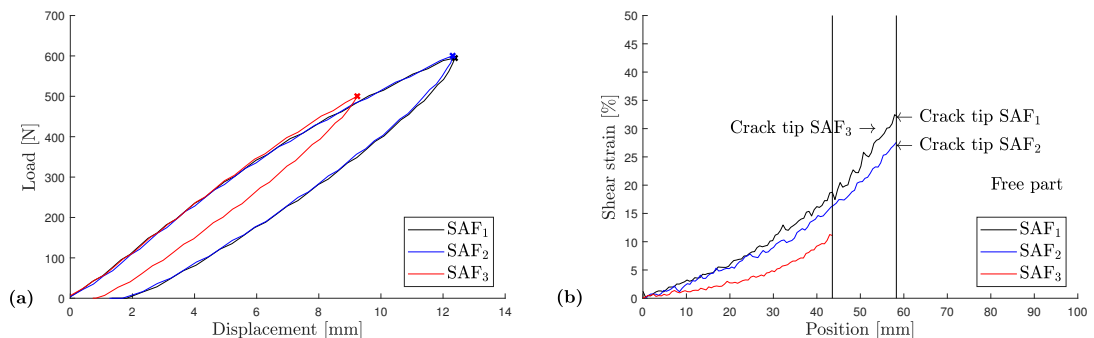


**Figure 5.8:** Experimental results for specimen bonded with SAF MIB 30 adhesive. Quasi-static tests at room temperature at 0.5 mm/min. (a) Load versus displacement curves. (b) Maximum shear strain versus position along the adhesive layer. Each curve corresponds to the load level evidenced with a cross on Fig. (a).

According to Fig. 5.8 (a), the test is assumed to be reproducible. On Fig. 5.8 (b), intersections of the vertical lines and the curves show the shear strain at crack tip : there

**Table 5.3:** Shear strain value at crack tip for specimen bonded with SAF MIB 30 adhesive.

	Maximum load level [N]	Shear strain at crack tip [%]
SAF <sub>1</sub>	600	31
SAF <sub>2</sub>	600	28
SAF <sub>3</sub>	500	23

is no crack propagation for these tests and it is confirmed by the value highlighted by these intersections and reported in table 5.3.

According to the previous study (see chapter 3), crack onset for the SAF MIB 30 is around 128 % where, in the case of these tests, maximum shear strain value reached is 31 %. Residual displacement is observed when loading is over 500 N.

Theoretically, the sizing of this ELS test is done with the hypothesis of elastically behaved adherends. The specimen is modeled as a beam composed by two bonded adherends under bending with  $2t$  thickness. Applied load  $P$  is assumed to be equally distributed between the two adherends as described in Fig. 5.9.

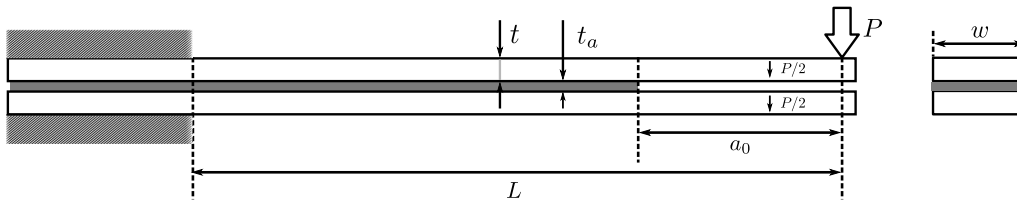


**Figure 5.9:** Initial geometry for the ELS test dimensioning.

Yield load was calculated as follow, from simple beam theory :

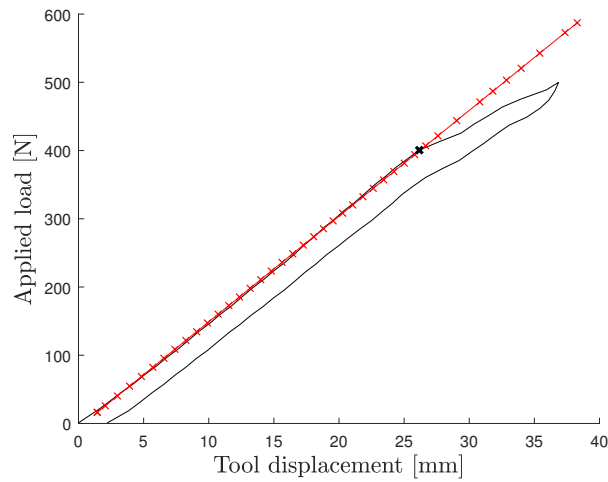
$$P_y = \frac{\sigma_y w t^2}{6L} = 1487 \text{ N} \quad (5.16)$$

Where  $P_y$  is the yield load at which the specimen should yield,  $\sigma_y$  is yield stress of aluminium 7075 T6,  $w$  is the width of the specimen,  $T = 2t = 10 \text{ mm}$  is the specimen thickness,  $L$  is the working length. Yield load is supposed to be 1487 N.

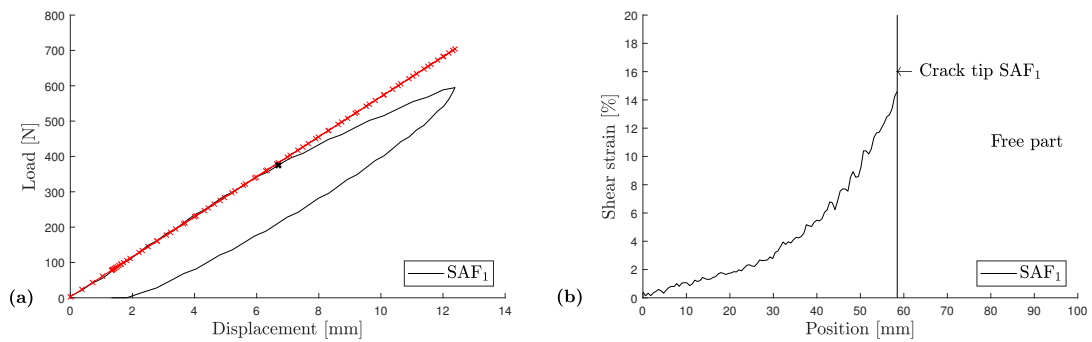
Fig. 5.10 shows the load displacement curve of a single adherend with 5 mm thickness  $t$ , 25 mm width  $w$ , 130 mm working length  $L$ . It was tested under quasi-static load at 0.5 mm/min. Yield occured at 400.5 N.

Fig. 5.11 shows load-displacement curve and shear strain along the adhesive layer at 375 N for the SAF<sub>1</sub> specimen.

The non-linearity of the curve is evidenced with the linear regression plotted in a crossed red line. The onset of non-linearity is at 375 N. Non-linearity of the load-displacement curve was not expected at this low level but at the yield level calculated with equation 5.16. It is explained by the presence of the adhesive layer. It has been noticed after the three tests conducted that the adherends yielded near the clamp. The adhesive layer with SAF MIB 30 adhesive is so compliant that the load is not equally distributed between the two adherends during the test : the adherends yield as if they were not part of a two adherends bonded beam but a unique adherend loaded under  $P$ .



**Figure 5.10:** Quasi-static tests at room temperature at 0.5 mm/min for aluminium 7075 T6 beam. Crossed red line is a linear regression. Black cross is yield onset.



**Figure 5.11:** Experimental results for specimen SAF<sub>1</sub> bonded with SAF MIB 30 adhesive. Quasi-static test at room temperature at 0.5 mm/min. (a) Load versus displacement curves. Red crossed line is a linear regression. (b) Shear strain at load level marked with a cross on (a) versus position along the adhesive layer.

The shear strain level at crack tip is 15 %, which is far from shear strain level needed for crack onset.

In this case, since there is no crack initiation in the adhesive and yielding of the adherends, the  $J(\gamma)$  procedure is not applied. Indeed, there is not enough informations on the behaviour of the adhesive (elastic behaviour, fracture process zone development) to fully apply this procedure.

The yielding of the adherends is an issue for the ELS test because the theoretical environment is set with the major hypothesis of elastically behaved adherends. No crack propagation is possible with this geometry. A solution could be the modification of the adherend thickness or the adherend material.

### 5.3.2 Fracture test with Araldite 2021 adhesive

Five ELS specimens bonded with Araldite 2021 have been tested under quasi-static load at 0.5 mm/min at room temperature. Various geometries have been tested. They are presented in table 5.4.

**Table 5.4:** Description of Araldite specimens geometry.  $L$  is the working length.  $a_0$  is the initial crack length.  $a_0/L$  the ELS ratio.  $t$  the adherend thickness.  $t_a$  the adhesive thickness.

	$L$ [mm]	$a_0$ [mm]	$a_0/L$ [-]	$t$ [mm]	$t_a$ [mm]
Araldite <sub>49</sub>	165.85	100	0.7	8	0.37
Araldite <sub>52</sub>	95	34	0.35	5	0.34
Araldite <sub>53</sub>	95	68	0.7	5	0.43
Araldite <sub>54</sub>	144	58	0.4	5	0.46
Araldite <sub>56</sub>	95	68	0.7	5	0.5

Fig. 5.12 shows the load-displacement curves and  $J(\gamma)$  curves for each test.

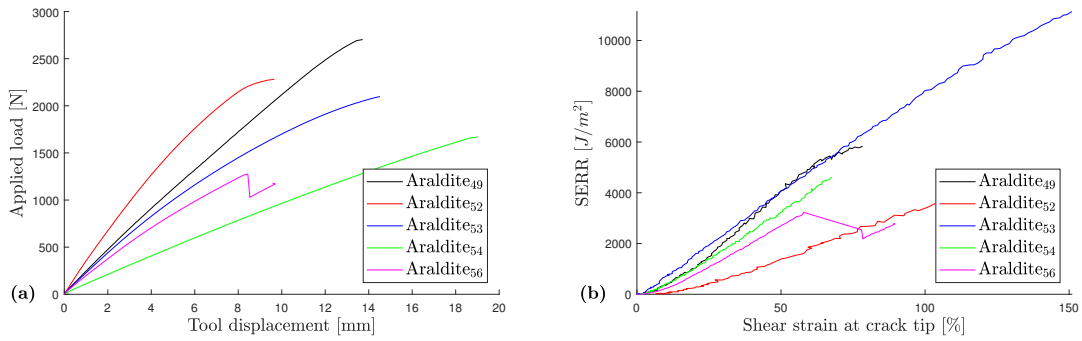


**Figure 5.12:** Load-displacement curve for all Araldite specimen (a).  $J(\gamma)$  curves for all Araldite Specimen (b).

Specimen Araldite<sub>49</sub> failed almost cohesively along  $\approx 57$  mm as seen in Fig. 5.13. It is the most representative test that have been conducted because  $a_0/L$  ratio is 0.7 and failure occurred.

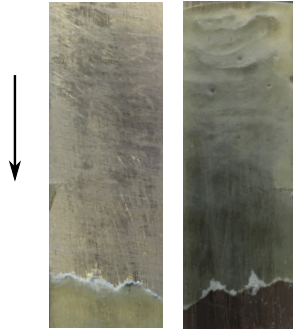
Specimen Araldite<sub>52</sub> failed almost cohesively as seen in Fig. 5.14. The  $a_0/L$  ratio was in this case 0.35. The shear failure did not occurred over a long distance (around  $\approx 22.5$  mm), however the crack propagation was stable even with the ratio  $a_0/L = 0.35$ .

Specimen Araldite<sub>53</sub> failed adhesively as seen in Fig. 5.15. This could be explained by bad adherend surface preparation.

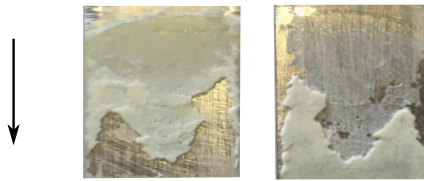
Specimen Araldite<sub>54</sub> failed adhesively as seen in Fig. 5.16. This can be explained by the presence of a defect that appeared during the manufacturing process.

Specimen Araldite<sub>56</sub> failed cohesively along around  $\approx 13.8$  mm. The crack was unstable which does not correspond to what is predicted by the standard [11].

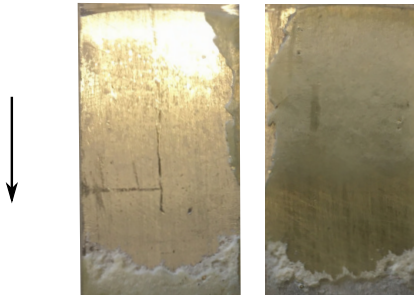
The differences between the load-displacement curves are explained because of the initial geometry of the tests : ratios  $a_0/L$  were different. Also, the thickness of the adherend is not always the same. According to Fig. 5.12 and the informations on the



**Figure 5.13:** Failure surface of specimen Araldite<sub>49</sub>. Arrow shows the crack propagation direction.



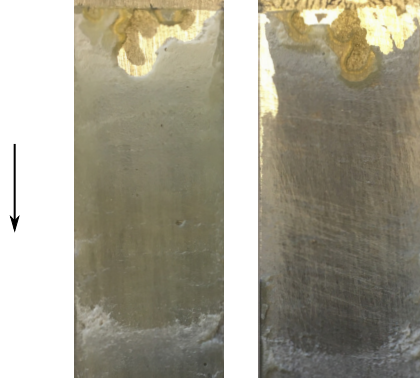
**Figure 5.14:** Failure surface of specimen Araldite<sub>52</sub>. Arrow shows the crack propagation direction.



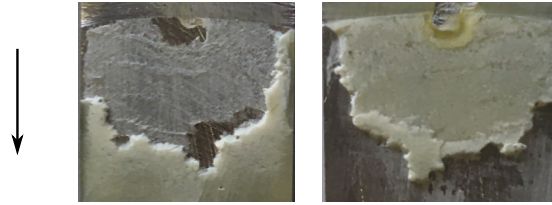
**Figure 5.15:** Failure surface of specimen Araldite<sub>53</sub>. Arrow shows the crack propagation direction.

failure of the specimen, the best geometry is the one of the Araldite<sub>49</sub> specimen. Which correspond to classic recommendations presented in the standard. Specimen Araldite<sub>56</sub> failed cohesively but crack propagation is unstable even though the ELS ratio  $a_0/L$  is 0.7. Specimen Araldite<sub>52</sub> also failed cohesively which still gives informations on the adhesive layer behaviour even if the specimen geometry does not fulfill all the standard recommendations.

Fig. 5.18 shows shear stress versus shear strain  $\tau(\gamma)$  curves for each specimens. The noisy curves were obtained with a variation rate applied on the  $J(\gamma)$  curve. The extracted ALSB curves correspond to the simplified version of the  $\tau(\gamma)$  by means of linear segments. They are assumed trapezoidal because of the convex  $J(\gamma)$  evolution in the beginning, then the linear evolution and eventually concave evolution. The ALSB curves have dissimilar behaviour even though they should correspond to the same adhesive and be an intrasec property.



**Figure 5.16:** Failure surface of specimen Araldite<sub>54</sub>. Arrow shows the crack propagation direction.



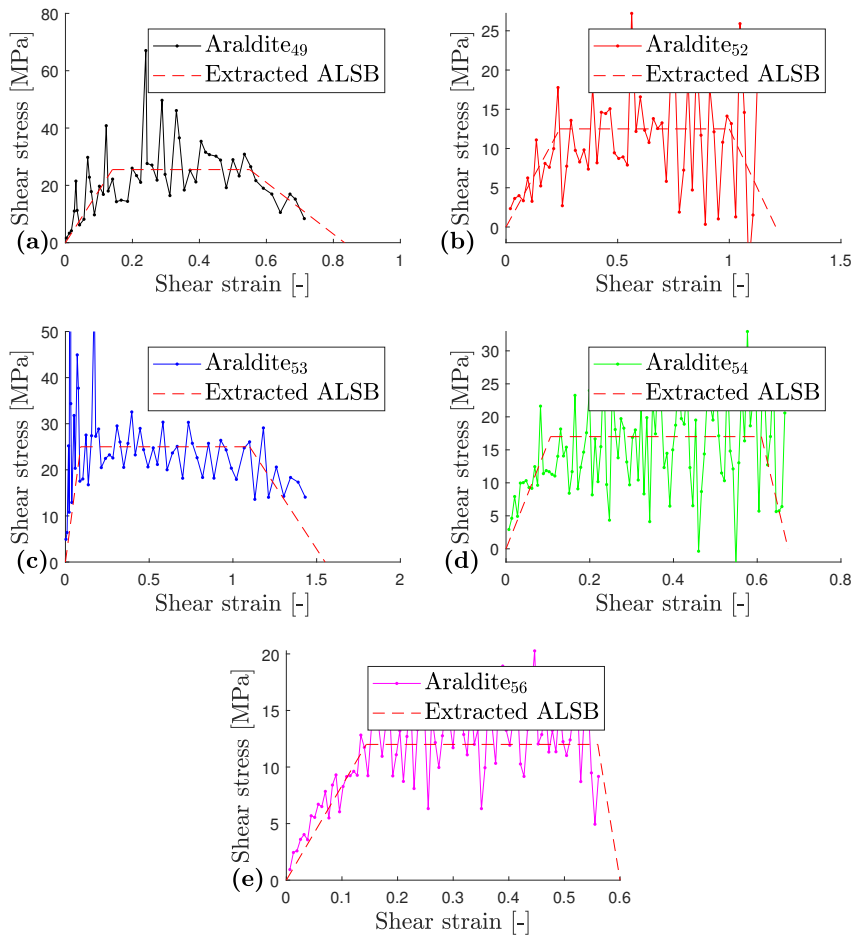
**Figure 5.17:** Failure surface of specimen Araldite<sub>56</sub>. Arrow shows the crack propagation direction.

Fig. 5.19 shows the shear stress versus shear strain  $\tau(\gamma)$  extracted from the experimental data of specimens Araldite<sub>49</sub>, Araldite<sub>52</sub> and Araldite<sub>56</sub>.

Table 5.5 presents the principal values of interest used to describe the ALSB when it is implemented in the semi-analytical model. The discrepancies between these values can be explained by the manufacturing process and its resulting flaws and the geometry of the specimens. Indeed, the working length  $L$  and adherend thickness  $t$  of the specimen Araldite<sub>56</sub> are lower than the ones of specimen Araldite<sub>49</sub> which explain the instability and short failure length. Even if the ELS ratio constraint is respected, the geometry of specimen Araldite<sub>56</sub> does not allow to obtain appropriate results on crack propagation under mode II loading in a likewise bonded joint structure.

**Table 5.5:** Description of extracted ALSB for specimens Araldite<sub>49</sub>, Araldite<sub>52</sub>, Araldite<sub>56</sub>.  $G_a$  is the extracted adhesive shear modulus.  $\tau_{max}$  is the maximum shear stress.  $\gamma_2$  is the shear strain at which softening behaviour begins.  $\gamma_{max}$  is the maximum shear strain.  $t_a$  the adhesive thickness.

	$G_a$ [MPa]	$\tau_{max}$ [MPa]	$\gamma_2$ [-]	$\gamma_{max}$ [-]
Araldite <sub>49</sub>	182	25.5	0.55	0.83
Araldite <sub>52</sub>	52	12.5	1	1.2
Araldite <sub>56</sub>	85	12	0.56	0.6



**Figure 5.18:** Shear stress versus shear strain curves and extracted ALSB for all Araldite specimens.

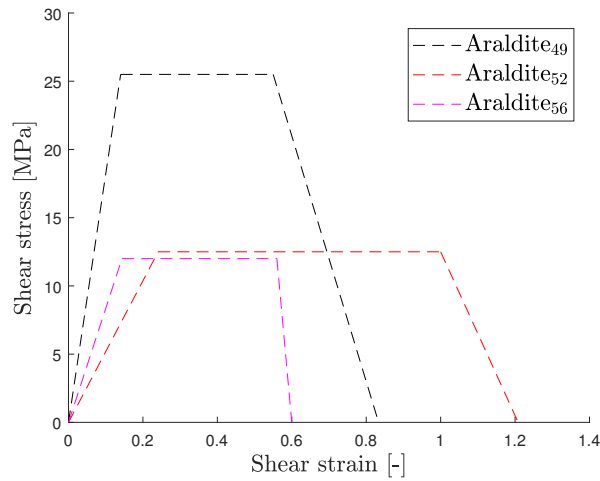


**Figure 5.19:** ALSB for specimens Araldite<sub>49</sub>, Araldite<sub>52</sub>, Araldite<sub>56</sub>.



## 5.4 Inverse identification of the Adhesive Layer Shear Behaviour

Specimen Araldite<sub>49</sub> is the most representative test of the batch of Araldite specimens. Fig. 5.20 shows comparison between experimental data and simulated data with the semi-analytical model presented in chapter 4 and the extracted ALSB that has been implemented (Fig. 5.20 (a)).

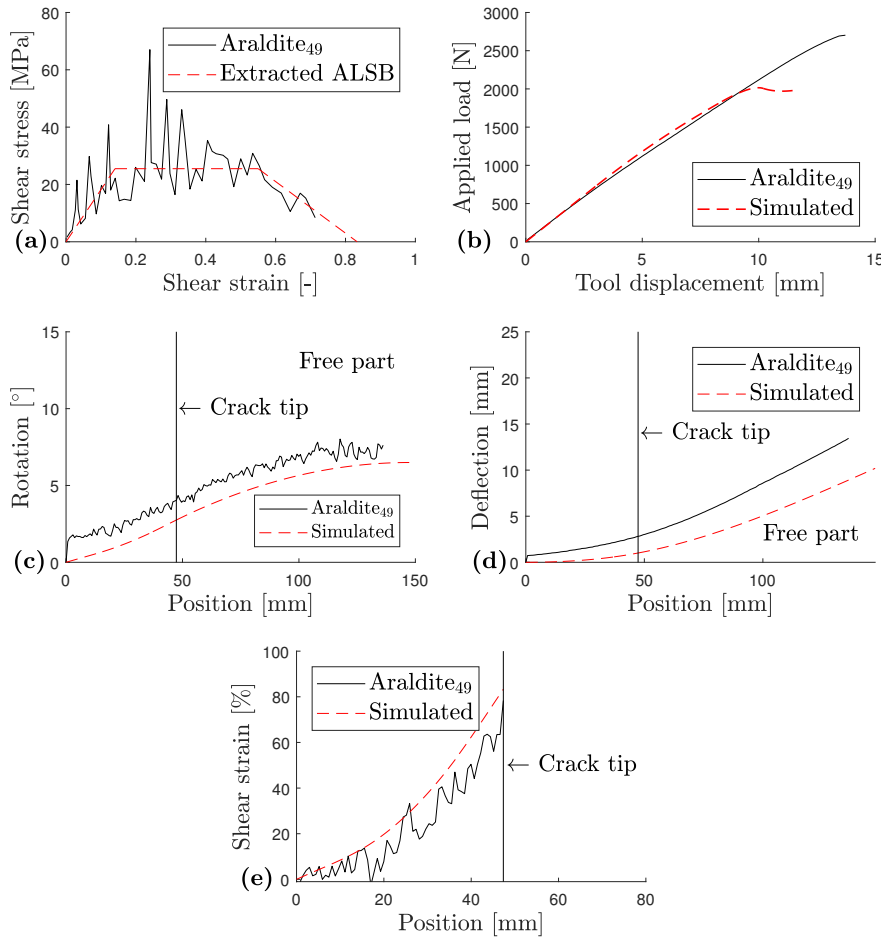


**Figure 5.20:** Comparison between experimental data and simulated data of Araldite<sub>49</sub> specimen. Shear stress versus shear strain curve - ALSB (a). Load-displacement curves (b). Rotation angle versus position along the adherend (c). Deflection versus position along the adherend (d). Shear strain versus position along the adhesive layer (e).

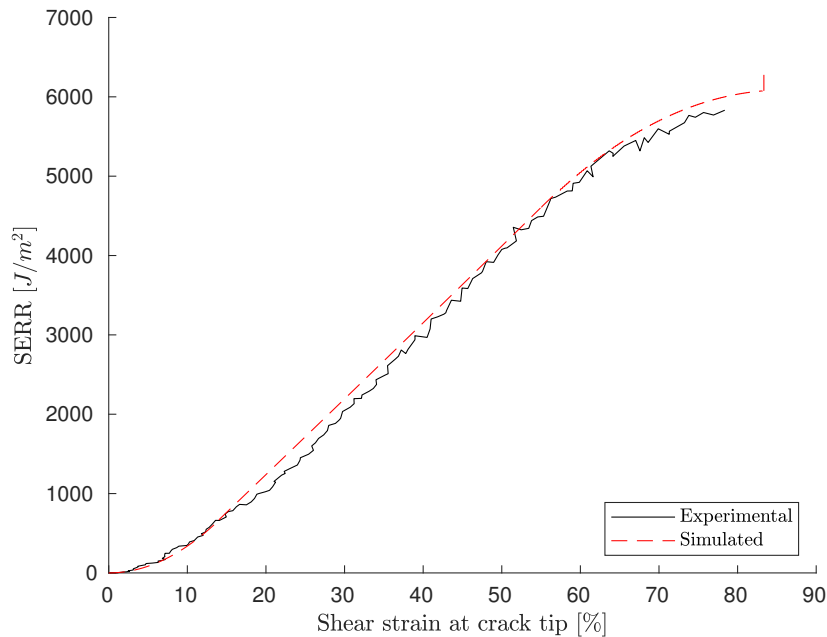
Fig. 5.20 (b) shows the comparison between the load displacement curves obtained experimentally and with the semi-analytical model. Compliance of the whole specimen is well assessed by the semi-analytical model. However, the failure load is under-estimated with the semi-analytical model.

Fig. 5.20 (c) shows the rotation angle of the section of the upper adherend versus the position along the adherend at the failure load. The experimental and simulated results are compared. The behaviour of these curves are similar. The experimental curve shows an offset compared to the simulated one that can be explained by the initial condition taken into account when the semi-analytical model was developed. Indeed, in the semi-analytical model the boundary conditions assume a fully clamp situation.

Fig. 5.20 (d) shows the deflection of the upper adherend versus the position along the adherend at the failure load. The experimental and simulated results are compared. Again the evolutions are similar and an offset exists because of the boundary conditions definition.

Fig. 5.20 (e) shows the shear strain of the adhesive along the adherend at failure load. The experimental and simulated results are compared. Prediction of the shear strain by the semi-analytical model is good.

Fig. 5.21 shows the  $J(\gamma)$  curves of both the experimental and simulated test. From the extracted ALSB implemented in the semi-analytical model, the prediction of the model fit well the experimental data.



**Figure 5.21:**  $J(\gamma)$  curves obtained with the experimentation for the specimen Araldite<sub>49</sub> (full line) and with the semi-analytical model (dotted line).

## 5.5 Discussion and conclusion

A new experimental methodology for mode II investigation of adhesive layer behaviour in bonded joint has been presented. The use of DIC allows to get free of the set-up compliance and to access kinematic data like deflection, rotation of the specimen all along the specimen length. DIC also allows to get shear strain along the adhesive layer and

especially at crack tip by computing the longitudinal displacement between the adherends. With these informations, the  $J(\gamma)$  curve method can be applied to extract the ALSB of the adhesive.

Tests have been conducted on two different adhesives. The SAF MIB 30 appears to be really ductile and modifications have to be done on the geometry of the specimen if investigation of crack propagation in this adhesive under mode II loading is needed. The Araldite 2021 is brittle enough to experiment crack propagation with the geometries tested in this study. Cohesive failure has been obtained as well as adhesive failure over the same batch of specimens. ELS ratio  $a_0/L$  under 0.55 have been tested and crack propagated with stability over short distance. Manufacturing process is proven to have large effect on the behaviour of the specimen and the Araldite 2021 adhesive requires specific adherend surface treatment than the one applied for this study.

The semi-analytical model has been validated. Experimental evolution of the kinematics of the specimen as well as shear strain of the adhesive evolution and  $J(\gamma)$  evolution fit with the evolutions predicted by the semi-analytical model. The input was the ALSB extracted from the experimental data and outputs correspond to what is expected experimentally. The semi-analytical model presented in chapter 4 can be used as a prediction tool when the ALSB is known. It also can be used as a verification tool in view of extracting the ALSB in order to implement it in a numerical cohesive zone model.

# Chapter 6

## Conclusions and future work

### Contents

---

<b>5.1</b>	<b>Test method</b>	<b>102</b>
5.1.1	Materials	102
5.1.2	ELS test description	102
5.1.3	DIC set-up	103
<b>5.2</b>	<b>Data reduction method with Digital Image Correlation</b>	<b>104</b>
<b>5.3</b>	<b>ELS test experimental results</b>	<b>109</b>
5.3.1	Fracture tests with ductile material (SAF MIB 30)	109
5.3.2	Fracture test with Araldite 2021 adhesive	112
<b>5.4</b>	<b>Inverse identification of the Adhesive Layer Shear Behaviour</b>	<b>116</b>
<b>5.5</b>	<b>Discussion and conclusion</b>	<b>117</b>

---

## 6.1 Concluding remarks

This thesis deals with analysis of mode II failure of bonded joints under severe environmental conditions. The aim is to develop simplified procedures in a damage tolerance perspective that help understanding the crack propagation under shear loading in the adhesive layer for metal-to-metal structural bonded joints.

Firstly, Arcan tests have been performed on three different types of adhesives : two thermoset adhesives (epoxy based) and one thermoplastic adhesive (methacrylate based) (see chapter 3). Arcan set-up was configured in order to submit the bonded joint to shear loading. Quasi-static and creep tests under various temperature levels have been performed. Temperature was applied with a specific thermal regulation tool. A digital image correlation set-up was used to identify deformations in the adhesive layer and the procedure to extract the adhesive layer strains was described. Viscous behaviours of the three adhesives were qualitatively identified.

- The DIC method allows to monitor with an easy set-up the bondline deformation. Measurements of strains were not pertubated by the use of the thermal regulation tool that heated the adherends and thus the adhesive layer.
- The DIC method allows to measure true strains in the adhesive layer and to identify strain localisation. This leads to being able to identify the failure path in the adhesive layer.
- The thermoplastic adhesive exhibit pronounced viscous behaviour even at room temperature and the viscoelastic / viscoplastic transition is activated with rising temperatures.
- The thermoset adhesives show quasi-brittle behaviour at room temperature rather than viscous behaviour.
- Cohesive and adhesive failures occur. This evidences the variability of Arcan tests due to bad surface preparation of the adherend before bonding.

With the Arcan test set-up, experimental test campaigns on various types of adhesives can be conducted in order to develop rheological models and investigate crack onset in elastic-brittle materials. Such an experiemental test campaign is a prerequisite to fracture studies were focus is on damage monitoring. The tests conducted in this thesis lead to the conclusion that the thermoplastic adhesive seems appropriate to evaluate mode II crack initiation and propagation in bonded joint under severe environmental conditions were viscous effect are important to take into account. As for the thermoset adhesives, they seem to be appropriate candidates for monitoring crack initiation and propagation mechanisms in the bonded joints tested with fracture tests under quasi-static loading.

Secondly, a theoretical analysis of crack initiation and propagation conditions in a bonded joint loaded under pure mode II condition have been proposed (see chapter 4). An ELS test specimen has been virtually tested with a semi-analytical model that takes into account the adhesive layer shear behaviour. In the semi-analytical model, the adherend are defined as two identical timoshenko beams. As for the adhesive layer, it is

described with a non-linear succession of segments. Multiple shapes are implemented : bi-linear elastic-plastic, bi-linear elastic-softening and trapezoidal. Adherend displacements/adherend cross sectional displacements and shear strain in the adhesive layer are simulated and their sensitivity to the ALSB shapes is evaluated. Furthermore, a direct method to extract the ALSB from the experiment is described thanks to the evaluation of applicable data reduction methods (mainly Griffith approach and J-integral approach) for the ELS test.

- The adhesive layer shear behaviour is taken into account in the semi-analytical model. These laws allow to describe the damage evolution at crack tip in the adhesive layer hence to describe the FPZ evolution. Moreover, the elastic modulus, maximum shear stress admissible, shear strain at failure are described with ALSB laws.
- The major output of the ELS test is load-displacement curves and R-curves. From the virtual testing campaign results, it has been observed that load-displacement curves do not permit accurate evaluation of the adhesive layer shear behaviour. Because of experimental artefacts like root rotation and deflection and poor sensitivity to the ALSB shape. Root rotation and deflection effects have been corrected with analytically determined factors in the virtual data reduction method. Poor sensitivity to the ALSB shape has been corrected by analysing strain energy release rate ( $G$  or  $J$ ) versus shear displacement ( $\gamma$ ) curves rather than load-displacement curves or R-curves.
- Griffith and J-integral approaches have been evaluated to study the SERR evolution. Analyses show that J-integral approach gets rid off experimental artefacts that perturb analysis when Griffith approach is used.
- The direct method to extract the ALSB from the ELS test consists in differentiating the  $J(\gamma)$  curve.
- The presence of FPZ characterised by plastic or softening behaviour in the ALSB law has a visible impact the  $J(\gamma)$  curve. Before SERR stabilisation : a linear evolution means that the ALSB has a plateau, a concave evolution means that the ALSB has a pronounced softening part, a convex evolution means that the ALSB has a pronounced plastic part.

The semi-analytical model allows to predict ELS test specimen behaviour under quasi-static loading. From this model, a new direct method has been evaluated to extract ALSB of the adhesive layer from the experimental results using the J-integral approach. With new experimental methods like DIC, quantities evolution needed in the J-integral expression can be recorded precisely.

Thirdly, ELS tests have been conducted on two thermoplastic adhesives : a very compliant adhesive already tested with the Arcan test campaign and a new adhesive with a quasi-brittle behaviour (see chapter 5). The last adhesive is recommended to observe crack initiation and propagation evolution in fracture tests under quasi-static loading.

Various geometrical configurations (changes in span length  $L$ , initial crack length  $a_0$ , adherend thickness  $t$ ) have been tested. DIC is used to get the kinematics of the specimen needed for the application of the direct method with  $J(\gamma)$  curve presented in chapter 4. The application of the DIC method in the case of shear strain at crack tip evaluation is fully described. Experimental results and simulation obtained with the semi-analytical model show good agreement.

- The use of DIC allows to get free of the set-up compliance and to access all kinematic data and the shear strain in the adhesive layer. With these data, the  $J(\gamma)$  curve method can be applied to extract the ALSB of the adhesive.
- Experimental results show that adherend yielding occurred with the compliant adhesive. This implies modification on the specimen geometry and in the data reduction method to take into account the large deflection involved.
- Crack initiation and propagation were observed for the quasi-brittle adhesive. Cohesive and adhesive failures have been observed. The specimen geometry with classic parameter values (ratio  $a_0/L$  under 0.55) showed crack propagation over short distance.
- The semi-analytical model as well as the direct method to extract ALSB with  $J(\gamma)$  curve analysis have been validated. A trapezoidal (segmented) ALSB has been extracted from the experimental tests and then implemented in the semi-analytical model. The simulated and experimental results show good agreement.

The ELS test appears to be a good candidate for mode II fracture testing of bonded joints. With quasi-brittle adhesives, crack initiation and propagation can be observed. In order to develop mode II fracture testing procedures, a good combination between test and material have been found. However, manufacturing process is proven to have big effect on the behaviour of the specimens (cohesive or adhesive failure mainly). Moreover, the data reduction method has been validated and the direct identification method of the ALSB shape have been validated by comparison of experimental results and simulated ones. The semi-analytical model can be used as a prediction tool for mode II ELS fracture test or a verification tool for checking if an ALSB is representative of the material used for the adhesive layer in a bonded joint.

## Overview

This thesis aimed to define reliable test methodologies and data reduction methods to assess the mechanical behaviour of bonded joint under shear loading and severe environmental conditions.

First, two testing procedures using digital image correlation have been developed to assess the mechanical behaviour of an adhesive layer in a metal-to-metal bonded joint under shear loading. These procedures are :

- The Arcan test with the use of DIC. Rheological model of the adhesive can be determined with this test methodology. Identifying the adhesive elasto-viscoplastic behaviour is important in durability testing since long-time exposure loadings and temperature and humidity variations are expected.
- The ELS test with the use of DIC. Crack initiation and propagation can be monitored with this test methodology. Following damage evolution under quasi-static loading is a first step in the comprehension of what can a bonded joint sustain over its utilisation.

Next, an experimental method has been described that allow to identify the adhesive layer shear behaviour directly. This law is the first input in simulation tool (analytical or numerical) that predict the bonded joints mechanical behaviour.

Eventually, a semi-analytical model has been developed and is able to predict the bonded joint behaviour (kinematics of the adherend, shear strain and stress in the adhesive layer) under shear loading in a standard environment (room and humidity temperature and quasi-static loads).

## 6.2 Perspectives and future work

The state of the art section, in the beginning of the manuscript, showed concepts assessed in this thesis : mechanical characterisation and fracture testing of bonded joints, modelisation of the behaviour of bonded joints and ageing effects on durability of bonded joints. These concepts combined with the work done in this thesis should serve to assess crack propagation resistance (by identification of fracture toughness) and durability of bonded joints (by identification of visco-elasto-plastic parameters).

### 6.2.1 Mechanical characterisation

It has been seen that mechanical characterisation tests allow to identify principal material parameters (Young's and shear modulus, yield stress and strain, strength and elongation at break), crack onset conditions and rheological properties. The Arcan test set-up appeared to be the best candidate to evaluate these properties. In this thesis, the Arcan test set-up has been used with DIC and proved its usefulness. Viscous and plastic phenomena have



been identified. Unfortunately, a complete rheological investigation have not been done. Other creep tests at various temperature and strain rate have to be conducted in order to produce a complete rheological model for the different adhesive types tested (ductile, quasi-brittle). However the method with DIC is valid and fully described for such studies.

### 6.2.2 Fracture testing

Fracture testing is an other major concept of this thesis. ELS test has been chosen to monitor damage propagation in a bonded joint. The data reduction method has been validated and improved with the use of DIC thanks to the application of a new direct method using the J-integral approach.

In this thesis, only thermoplastic adhesives with different behaviours (ductile or quasi-brittle) have been tested with the ELS test. And the direct method has only been applied on the quasi-brittle adhesive, crack propagation never occurred for the ductile adhesive. A further investigation on specimen geometry and testing conditions has to be led to being able to observe crack propagation in such adhesive.

Only the ELS test have been used but the ENF and I-ELS tests are also good candidates for mode II fracture testing and a comparison between these methods (ELS, I-ELS and ENF tests) could allow a better identification of the contributions in the results of the artefacts from the test set-up (friction, clamping conditions) and the true adhesive layer behaviour.

### 6.2.3 Modelisation

A semi-analytical model for the ELS fracture test has been proposed.

It is easy to use, it takes into account the adhesive layer compliance and some artefact like the root rotation and deflection effect. Good predictions have been found between the model and experimental results and it is possible to get shear strain in the adhesive layer as well as kinematic displacements of the specimen. However, artefacts like friction effect inside the specimen or friction effect of the load application tool or clamping set-up have not been analysed and should be added in the model.

The major input in this model is the ALSB and it has limitations. Indeed, only three adhesive layer shear behaviour shapes have been virtually tested, all described with linear segments. Multiple shapes could be imagined. For example, multi-linear ALSB with double plastic plateau which could be implemented in the actual semi-analytical model. But more complex shapes like exponential is much more complicated since the semi-analytical imposes ALSB shapes that can be discretised.

The semi-analytical model stands only for quasi-static loading. Time-dependent ALSB linked to rheological model have been implemented yet in analytical models. This consideration leads to durability of bonded joint questioning.

### 6.2.4 Durability

It has been seen in the state of the art of this thesis that multiple solutions exist for evaluation of ageing on durability of bonded joint. Two main approaches stand out :

post-ageing testing of bonded joints (where residual stresses are evaluated after ageing) and coupled mechanical and hygrothermal testing of bonded joints.

With rheological modelling of adhesives layer, time-dependant behaviour of the bonded joint can be determined. Moreover, temperature and moisture effects can be predicted. With semi-analytical model or FEA combined with CZM and the ALSB, damage evolution in bonded joint can be predicted. These two modelling concepts, rheological approach or cohesive law approach, are intrinsically linked since they both describe the adhesive layer behaviour but with a different understanding, time-dependent or behaviour at crack tip respectively. A perspective on this work is to link rheological properties to crack propagation studies and being able to, with one general cohesive model taking into account ageing effect and defect (presence of a crack) effect, predict bonded joint behaviour under shear loading and severe environmental conditions.

First of all, effect of coupled mechanical loading and hygrothermal conditions have to be experimented. In this case, focus is on creep load application (rather than fatigue load application) on fracture tests. Fracture energy must change when creep takes place in the adhesive layer. For example, Carneiro *et. al.* [140] tested epoxy/aluminium bonded joints with the ENF test. Specimens were placed in a testing machine for 30 days (720 hours). Fracture energy was evaluated with the compliance-based method. The endurance load limit (time without crack propagation) is investigated and results are creep curves (load application tool displacement versus time) and residual fracture energy after 30 days at 70 %, 75 % and 80 % of the quasi-static maximum load (initially determined) as a function of the creep load. Their main conclusion is that maximum shear creep fracture energy value, meaning the maximum amount of the energy that the cracked joint can absorb without rupture, is obtained when the bonded joint is submitted to 70 % of the maximum load.

For durability characterisation of bonded joints, the interesting output is the energy dissipation during crack growth. Constant strain energy release rate when crack propagates is needed [148] so that crack propagation conditions are insured. A new test device insuring pure bending to a classical fracture specimen (two bonded beams with initial defect at one end) is proposed and shown in Fig. 6.1. It consists in applying an offset load on a lever arm clamped to the specimen with the initial crack located at the arm clamping position.

LEFM and SBT give for this test geometry :

$$G_{II} = \frac{9P^2a^2}{4w^2t^3E} = \frac{9M^2}{4w^2t^3E} \quad (6.1)$$

Where  $P$  is the applied load,  $a$  is the crack length,  $w$  is the specimen width,  $t$  is the adherend thickness,  $E$  is the adherend Young's modulus and  $M$  the applied moment. This test set-up configuration induce a constant applied moment to the specimen (see Fig. 6.2) and thus, with reference to eq. 6.1, constant strain energy release rate.

This test set-up can then be placed in an environmental chamber where specimen will be submitted to coupled mechanical and hygrothermal loading. With DIC method, crack propagation can be tracked and durability R-curves can be plotted.

Ageing of bonded joint is a complex problem. With this thesis, damage evolution

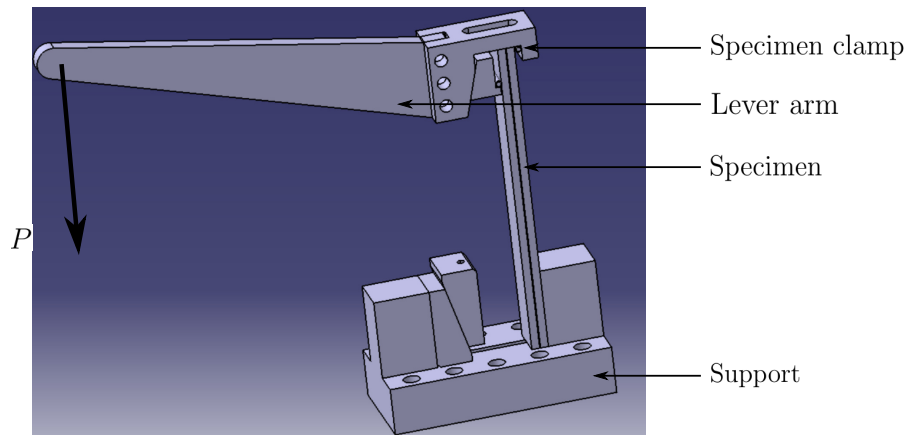


Figure 6.1: Pure Bending Test (PBT) for bonded joint.

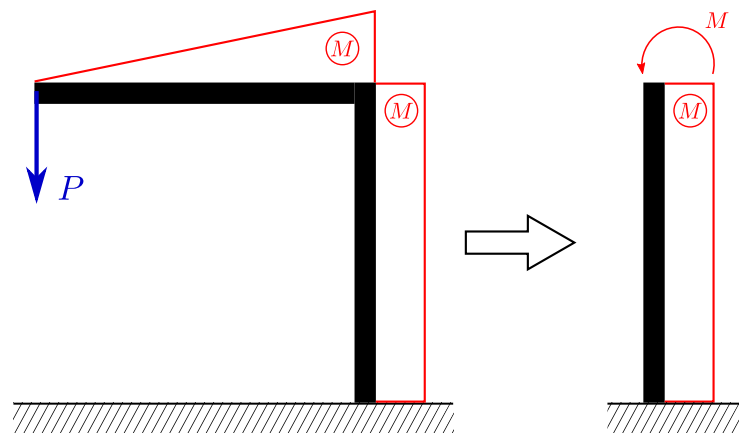


Figure 6.2: Schematic representation of the moments in PBT.

in the adhesive layer has been evaluated with a simple procedure using DIC. With the semi-analytical model, failure prediction in bonded joint under quasi-static shear loading is possible. Moreover, it has been shown that rheological behaviour of the adhesive layer in a bonded joint can be assessed with simple procedure using, again, DIC. All of these developments will be useful for progressing on the ageing problem by monitoring the damage evolution in a bonded joint under shear loading and severe environmental conditions.

# Appendix A

## List of attended conferences

- Aussois 2019 - Rupture des Matériaux et des Structures - Mécanismes et modélisations face aux applications industrielles. Poster presentation. See Fig. A.1.
- JADH 2019 - Journées d'Étude sur l'Adhésion. Poster presentation and training courses on adhesion and mechanical behaviour of bonded joints. See Fig. A.2.
- 7th ECCOMAS Thematic Conference on The Mechanical Response of Composites. Conference in Girona (Spain).

INSTITUT DE  
MECANIQUE  
ET D'INGENIERIE

université  
de  
BORDEAUX

Institut de mécanique et d'ingénierie  
**Bordeaux**

AMADE  
Universitat de Girona

ARTS  
ET METIERS  
ParisTech

COMPORTEMENT MÉCANIQUE DES JOINTS COLLÉS  
SOUS SOLLICITATION DE CISAILEMENT

**Justine BERTRAND**<sup>[1]</sup>  
 Julien JUMEL<sup>[1]</sup>, Jordi RENART<sup>[2]</sup>, Jean-Benoît KOPP<sup>[3]</sup>

<sup>[1]</sup> I2M, Université de Bordeaux, CNRS UMR 5295, 33405 Talence ; <sup>[2]</sup> AMADE Research Group, Gérone, Espagne ; <sup>[3]</sup> I2M, Arts et Métiers ParisTech, CNRS UMR 5395, 33405 Talence

### Contexte & Objectifs

**Assemblage collé** : technique **ef cace** et **performante** pour des structures sous sollicitation de **cisaillement**  
 → Étude de l'**amorçage** et de la **propagation de f ssure** au sein d'un assemblage collé  
 → **Simulation** analytique du comportement de la structure

Décrire le processus de rupture des assemblages collés en mode II

### Matériaux et Moyens expérimentaux

**Matériaux**

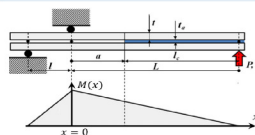
- SAF 30 MIB (à base de PMMA)
- Adhésif caractérisé en laboratoire (Arcan)
- $Y_{max} = 128 \%$
- Aluminium 7075
- Substrats

**Méthode**

- Deux appareils photo (vue locale et vue globale)
- Machine de traction universelle Zwick, cellule de charge 10 kN

### L'essai I-ELS : Propagation de f ssure stable en mode II

**Inverse End-Loaded Split - I-ELS**  
 → La f ssure se propage vers le point d'application de la charge



[1] Jumel et. al (2018)

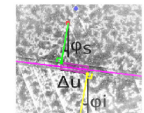
**Corrélation d'images :**  
 → Analyse à l'aide de données macroscopiques  
 → Analyses distinctes des trois composants (deux substrats, un adhésif sous forme de joint)

Détermination déplacement transversal :

$$\begin{bmatrix} \Delta u \\ \Delta v \end{bmatrix} = \begin{bmatrix} \cos(\varphi_{mk}^i) & \sin(\varphi_{mk}^i) \\ -\sin(\varphi_{mk}^i) & \cos(\varphi_{mk}^i) \end{bmatrix} \begin{bmatrix} Xp_{mk}^i - Xps_k^i \\ Yp_{mk}^i - Yps_k^i \end{bmatrix}$$

Détermination angle de rotation d'un substrat :  $X_k^i = \tan(\varphi_k^i) * Y_k^i + \delta_k^i$

Détermination angle de rotation moyen :  $\varphi_{mk}^i = \frac{\varphi_{mk}^i + \varphi_{mk}^i}{2}$

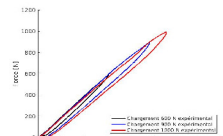


$\gamma = \frac{\Delta u}{t_a}$

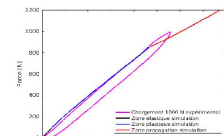
### Résultats

**Modélisation analytique**  
 → Théorie des poutres avec hypothèse de **Timoshenko**  
 → **Loi bi-linéaire** décrivant l'interface collé  
 → Prise en compte de la **zone de propagation de f ssure**

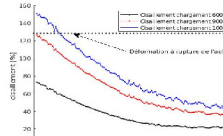
**Essais quasi-statiques :**  
 → Analyse de la **charge** et de la **décharge**  
 → Identif cation des **déformations résiduelles**




→ Chargement à la limite de l'amorçage de f ssure et plastification des substrats



→ Amorçage de f ssure



→ Amorçage de f ssure



### Conclusions & Perspectives

- Essai de **f ssuration stable** pour un assemblage collé avec un adhésif à base de **polyméthacrylate de méthyl**
- Simulation analytique de l'essai en prenant en compte le **comportement elasto-visco-plastique de l'interface**
- Évaluation de la **durabilité d'un assemblage collé** sous sollicitation de cisaillement

[1] J. Jumel & M. K. Budzik. Inverse end-loaded-split test analysis of ect of small scale yielding. *Theoretical and Applied Fracture Mechanics*, 96 :775-789, August 2018

**Aussois 2019**  
Rupture des Matériaux et des Structures

@i2m\_dumas  
Justine.bertrand@u-bordeaux.fr

Figure A.1: Aussois poster. "Comportement mécanique des joints sous sollicitation de cisaillement"

## Modèle analytique de l'essai ELS pour l'étude des joints collés sous sollicitation de cisaillement

**Justine BERTRAND<sup>[1]</sup>**

Julien JUMEL<sup>[1]</sup>, Jordi RENART<sup>[2]</sup>, Jean-Benoît KOPP<sup>[3]</sup>

<sup>[1]</sup> I2M, Université de Bordeaux, CNRS UMR 5295, 33405 Talence ; <sup>[2]</sup> AMADE Research Group, Gérone, Espagne ; <sup>[3]</sup> I2M, Arts et Métiers ParisTech, CNRS UMR 5395, 33405 Talence

### Contexte & Objectifs

- Assemblage collé** : moyen **ef cace** et **performant** pour des structures sous sollicitation de **cisaillement**
- Étude de l'**amorçage** et de la **propagation de f ssure** au sein d'un assemblage collé
  - **Simulation** analytique du comportement de la structure
  - Étude de dif érentes lois cohésives décrivant le comportement de l'adhésif

Description du mécanisme de rupture des assemblages collés en mode II – Ef et de la plasticité de l'adhésif sur ce mécanisme

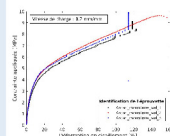
### Experimental : Essais Arcan et ELS

**Epreuve Arcan** :

- Adhésif : SAF 30 MIB (PMMA)
- Substrats : Aluminium 7075

**Méthode** :

- Essais quasi-statiques
- Corrélation d'image pour obtenir les déformations



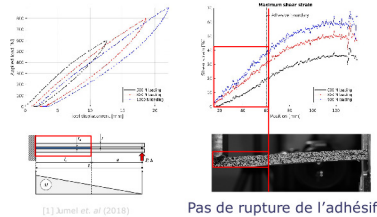
#### Comportement plastique observé

**Essai ELS**

- Assemblage collé avec pré-f ssure
- Sollicitation en cisaillement de l'adhésif par flexion de l'éprouvette

**Corrélation d'images** :

- Analyse à l'aide de données macroscopiques
- Analyses distinctes des trois composants (deux substrats, un adhésif sous forme de joint)
- Prise en compte rotation des substrats et des grands déplacements



[1] Jumel et al (2018)

Pas de rupture de l'adhésif

Identification lois cohésives, observation du mécanisme de rupture des assemblages collés sous sollicitations de cisaillement

### Conclusions & Perspective

- **Plastification** de l'adhésif : dif culté à évaluer l'évolution de la **longueur de f ssure** et à évaluer le **taux de restitution d'énergie**
- Simulation analytique de l'essai : caractérisation de la zone de progrès de f ssure : inf uence de la plasticité et évolution.
- Prédiction du comportement de l'éprouvette par test virtuel pour étude de la durabilité des assemblages collés
- Évaluation de la **durabilité d'un assemblage collé** sous sollicitation de cisaillement

[1] J. Jumel & M. K. Budzik. Inverse end-loaded-split test analysis of ect of small scale yielding. *Theoretical and Applied Fracture Mechanics*, 96 :775-789, August 2018

### Analytique : Test virtuel essais ELS

**Modélisation analytique**

- Théorie des poutres avec hypothèse de **Timoshenko**
- Conditions limites : éprouvette encastree
- Prise en compte de la **plasticité et de l'adoucissement**

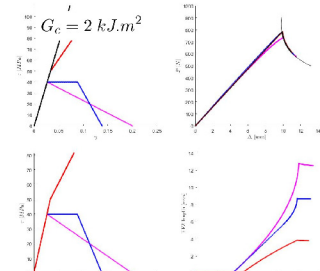
**Mise en évidence de la zone de progrès de f ssure**

$$\begin{aligned}
 N(x) &= ES \frac{du(x)}{dx} & M(x) &= EI \frac{d^2u(x)}{dx^2} \\
 T(x) &= \kappa GS \left[ \frac{dv(x)}{dx} - \varphi(x) \right] & \tau(x) &= G_a \gamma(x)
 \end{aligned}$$

$$\frac{d^3 \tau}{dx^3} - \frac{2\omega G_a}{t_a} \left[ \frac{1}{EI} \left( \frac{t}{2} \right)^2 - \frac{1}{ES} \right] \frac{d\tau}{dx} = 0$$

$$\tau(x) = A e^{\lambda x} + B e^{-\lambda x} + C + \tau_m$$

$$\lambda = \sqrt{\frac{2\omega G_a}{t_a} \left[ \frac{1}{EI} \left( \frac{t}{2} \right)^2 - \frac{1}{ES} \right]}$$



La forme de la loi cohésive n'a pas d'ef et sur la courbe Force-Déplacement bien que la zone de progrès de f ssure soit fortement impactée

Figure A.2: JADH poster. "Modèle analytique de l'essai ELS pour l'étude des joints collés sous sollicitation de cisaillement"

APPENDIX A. LIST OF ATTENDED CONFERENCES

---

# Bibliography

- [1] Cognard Jacques. *Science et technologie du collage / Jacques Cognard*. Presses polytechniques et universitaires romandes, réimpression corrigée edition. → pages viii, 6, 7, 8, 39
- [2] Meyers Marc André. *Mechanical behavior of materials / Marc André Meyers, ... Krishan Kumar Chawla, ...* Cambridge University Press, 2nd ed. edition. → pages viii, 8, 35
- [3] H. Chai. Shear fracture. 37(2):137–159. → pages viii, 8, 23
- [4] A. B. de Morais and M. F. S. F. de Moura. Evaluation of initiation criteria used in interlaminar fracture tests. 73(16):2264–2276. → pages viii, 8, 34, 74
- [5] Alexandre Jouan and Andrei Constantinescu. A critical comparison of shear tests for adhesive joints. 84:63–79. → pages ix, xxvii, xxviii, 15, 16, 17, 18, 19
- [6] M. Arcan, Z. Hashin, and A. Voloshin. A method to produce uniform plane-stress states with applications to fiber-reinforced materials. 18(4):141–146. → pages ix, 17, 18, 19
- [7] J. R. Rice. A path independent integral and the approximate analysis of strain concentration by notches and cracks. 35(2):379–386. → pages x, 23, 75
- [8] A.J. Russell and K.N. Street. FACTORS AFFECTING THE INTERLAMINAR FRACTURE ENERGY OF GRAPHITE/EPOXY LAMINATES. volume 1, pages 279–228. → pages x, 31
- [9] ASTM d7905/d7905m-19e1 : Standard test method for determination of the mode II interlaminar fracture toughness of unidirectional fiber-reinforced polymer matrix composites. → pages x, 31
- [10] P.S. Vanderkley. Mode i-mode II delamination fracture toughness of a unidirectional graphite/epoxy composite. → pages x, 29, 32
- [11] ISO 15114:2014 : Fibre-reinforced plastic composites — determination of the mode II fracture resistance for unidirectionally reinforced materials using the calibrated end-loaded split (c-ELS) test and an effective crack length approach. → pages x, 33, 103, 112



- [12] B.R.K. Blackman, A.J. Kinloch, and M. Paraschi. The determination of the mode II adhesive fracture resistance, GIIC, of structural adhesive joints: An effective crack length approach. 72(6):877–897. → pages x, 8, 30, 32, 34, 35, 74, 77
- [13] Patrícia Moreira Silva, José Sena-Cruz, Miguel Azenha, and Gonçalo Gomes Escusa. Experimental investigation on creep behaviour of an epoxy adhesive. → pages xi, xxix, 38
- [14] Inês Costa and Joaquim Barros. Tensile creep of a structural epoxy adhesive: Experimental and analytical characterization. 59:115–124. ISBN: 0143-7496 Publisher: Elsevier. → pages xi, 38
- [15] ASTM d3762-03(2010) : Standard test method for adhesive-bonded surface durability of aluminum (wedge test) (withdrawn 2019). → pages xi, xxix, 41
- [16] Ashok Saxena. Creep and creep–fatigue crack growth. 191(1):31–51. → pages xi, 43
- [17] BMW Press. Press media : Lancement de la BMW i3. → pages xviii, xxvii, 2
- [18] Brochure bostik - doing more than sticking things together. → pages xviii, xxvii, 2
- [19] Le collage : un moyen ancestral, moderne et durable d’assemblage. → pages xviii, xxvii, 3
- [20] Sang Lee, K. Jeong, Kee-Woon Kim, and Jang Kim. Numerical estimation of the uneven wear of passenger car tires. 06:780–793. → pages xviii, xxvii, 3
- [21] J. Bertrand, J. Jumel, J. Renart, and J.-B. Kopp. Theoretical assessment of ELS test data reduction technique using virtual testing. 229(2):195–213. → pages xx, 4
- [22] Dong Quan, Josu Labarga Urdániz, and Alojz Ivanković. Enhancing mode-I and mode-II fracture toughness of epoxy and carbon fibre reinforced epoxy composites using multi-walled carbon nanotubes. 143:81–92. → pages xxvii, 8
- [23] Piaras Kelly. Solid mechanics part i: An introduction to solid mechanics. 94042. → pages xxvii, 12, 13, 20
- [24] Jean-Louis Halary and Françoise Lauprêtre. *Mécanique des matériaux polymères*. Humensis. Google-Books-ID: 5hKWDgAAQBAJ. → pages xxvii, 8, 12, 14, 20, 39
- [25] J. Y. Cognard, R. Créac’hcadec, and J. Maurice. Numerical analysis of the stress distribution in single-lap shear tests under elastic assumption—application to the optimisation of the mechanical behaviour. 31(7):715–724. → pages xxviii, 16, 19
- [26] Nawres J. Al-Ramahi, Roberts Joffe, and Janis Varna. Numerical analysis of stresses in double-lap adhesive joint under thermo-mechanical load. 233:111863. → pages xxviii, 16, 17
- [27] L. Alfonso, C. Badulescu, and N. Carrere. Use of the modified arcan fixture to study the strength of bonded assemblies for automotive applications. 80:104–114. → pages xxviii, 10, 18, 19

- 
- [28] Jean Yves Cognard. Numerical analysis of edge effects in adhesively-bonded assemblies application to the determination of the adhesive behaviour. 86(17):1704–1717. → pages xxviii, 19
- [29] M. A. Saeimi Sadigh, B. Paygozar, L. F. M. da Silva, and E. Martínez-Pañeda. Creep behaviour and tensile response of adhesively bonded polyethylene joints: Single-lap and double-strap. 102:102666. → pages xxviii, 16, 20
- [30] M. Pérez-Galmés, J. Renart, C. Sarrado, and J. Costa. Suitable specimen dimensions for the determination of mode II fracture toughness of bonded joints by means of the ELS test. 202:350–362. → pages xxviii, xxix, 23, 24, 27, 34, 35, 36, 74, 81
- [31] M. Pérez-Galmés, J. Renart, C. Sarrado, A. Rodríguez-Bellido, and J. Costa. A data reduction method based on the j-integral to obtain the interlaminar fracture toughness in a mode II end-loaded split (ELS) test. 90:670–677. → pages xxviii, 24, 25, 30, 34, 75, 85
- [32] J. Zhang, J. Wang, Z. Yuan, and H. Jia. Effect of the cohesive law shape on the modelling of adhesive joints bonded with brittle and ductile adhesives. 85:37–43. → pages xxviii, 25, 26, 27, 75
- [33] Ronald Krueger, Kunigal Shivakumar, and Ivatury Raju. *Fracture Mechanics Analyses for Interface Crack Problems - A Review*. Journal Abbreviation: 54th AIAA/ASME/ASCE/AHS/ASC Structures, Structural Dynamics, and Materials Conference Publication Title: 54th AIAA/ASME/ASCE/AHS/ASC Structures, Structural Dynamics, and Materials Conference. → pages xxviii, 28
- [34] Jarno Jokinen, Mikko Kanerva, Markus Wallin, and Olli Saarela. The simulation of a double cantilever beam test using the virtual crack closure technique with the cohesive zone modelling. 88:50–58. → pages xxviii, 28, 29
- [35] P. Davies, B. R. K. Blackman, and A. J. Brunner. Standard test methods for delamination resistance of composite materials: Current status. 5(6):345–364. → pages xxviii, 29, 32, 34, 35, 74
- [36] B. R. K. Blackman, A. J. Brunner, and J. G. Williams. Mode II fracture testing of composites: a new look at an old problem. 73(16):2443–2455. → pages xxix, 30, 32, 34, 35, 74, 76
- [37] Alireza Akhavan-Safar, Mazaher Salamat-talab, Arsalan Ajdani, Majid R. Aya-tollahi, and Lucas F. M. da Silva. Mode II fracture energy characterization of brittle adhesives using compliance calibration method. 43(9):1928–1937. → pages xxix, 32, 33
- [38] J. Jumel and M. K. Budzik. Inverse end-loaded-split test analysis effect of small scale yielding. 96:775–789. → pages xxix, 25, 27, 33, 34

- [39] A.A. Abdel-Wahab, S. Ataya, and V.V. Silberschmidt. Temperature-dependent mechanical behaviour of PMMA: Experimental analysis and modelling. 58:86–95. → pages xxix, 39
- [40] Qianhui Xu, Feng Li, Wenlong Mu, Jingxin Na, Wei Tan, and Guangbin Wang. Effect of hygrothermal and alternating load coupled aging on CFRP/al bonded joints. 109:102912. → pages xxix, 42
- [41] J. C. P. Figueiredo, R. D. S. G. Campilho, E. A. S. Marques, J. J. M. Machado, and L. F. M. da Silva. Adhesive thickness influence on the shear fracture toughness measurements of adhesive joints. 83:15–23. → pages 8, 32
- [42] Jiawen Xie, Anthony M. Waas, and Mostafa Rassaian. Estimating the process zone length of fracture tests used in characterizing composites. 100-101:111–126. → pages 8, 35
- [43] J. Li Högberg, Bent F. Sørensen, and Ulf Stigh. Constitutive behaviour of mixed mode loaded adhesive layer. 44(25):8335–8354. ISBN: 0020-7683 Publisher: Elsevier. → page 8
- [44] K. Chen and R. Hsu. Evaluation of environmental effects on mechanical properties and characterization of creep behavior of PMMA. 30(2):267–274. → pages 9, 10
- [45] I. Lubowiecka, M. Rodríguez, E. Rodríguez, and D. Martínez. Experimentation, material modelling and simulation of bonded joints with a flexible adhesive. 37:56–64. → page 10
- [46] ISO 9664:1993 : Adhesives — test methods for fatigue properties of structural adhesives in tensile shear. → page 15
- [47] J.Y. Cognard, L. Sohier, and P. Davies. A modified arcan test to analyze the behavior of composites and their assemblies under out-of-plane loadings. 42(1):111–121. → pages 15, 19
- [48] Rouhollah H. Goudarzi and Mohammad Reza Khedmati. An experimental and numerical investigation of adhesive bond strength in al-GFRP single lap and double butt lap joints due to applied longitudinal loads. 15(4):403–416. → page 15
- [49] L.F.M. Silva, J Ramos, Miguel de Figueiredo, and Telmo Strohaecker. Influence of the adhesive, the adherend and the overlap on the single lap shear strength. 7. → page 16
- [50] P.A.M.G.P. Bamberg, U. Reisgen, A. Schiebahn, J.D.V. Barbosa, B. Marx, and R.S. Coelho. Digital image correlation analysis of the effects of the overlap length, adhesive thickness and adherends yield strength over similar and dissimilar joints of high strength steel and aluminum alloys. 83:69–75. → page 16
- [51] ASTM d3528-96(2016) : Standard test method for strength properties of double lap shear adhesive joints by tension loading. → page 16

- 
- [52] Marta Kałuza, Jacek Hulimka, Jan Kubica, and Marcin Tekieli. The methacrylate adhesive to double-lap shear joints made of high-strength steel—experimental study. 12(1):120. → page 17
- [53] ISO 11003-2:2019 : Adhesives — determination of shear behaviour of structural adhesives — part 2: Tensile test method using thick adherends. → page 17
- [54] J.-Y. Cognard, L. Sohier, P. Davies, and B. Gineste. Analysis of the non-linear behaviour of an adhesive in an assembly. 7(3):265–276. → page 17
- [55] P. Bidaud, R. Créac’hcadec, D. Thévenet, J.-Y. Cognard, and P. Jousset. A prediction method of the behavior of adhesively bonded structures under cyclic shear loading based on a characterization of the viscous aspects of the adhesive in an assembly. 91(9):701–724. → pages 17, 19, 20, 42, 91
- [56] Claudiu Badulescu, Celia Germain, Jean-Yves Cognard, and Nicolas Carrere. Characterization and modelling of the viscous behaviour of adhesives using the modified arcan device. 29(5):443–461. → pages 17, 19
- [57] Grégory Bresson, Julien Jumel, Martin E. R. Shanahan, and Pierre Serin. Strength of adhesively bonded joints under mixed axial and shear loading. 35:27–35. → page 17
- [58] Demetrio Jackson dos Santos and Gilmar Ferreira Batalha. Failure criterion for adhesively bonded joints using arcan’s experimental method. 24(4):441–445. → page 19
- [59] J. Yves Cognard, R. Créac’Hcadec, and L. Sohier. Strategies for the analysis of the behavior of an adhesive in bonded assemblies. 133(3). → page 19
- [60] A. Spaggiari, D. Castagnetti, and E. Dragoni. A design oriented multiaxial stress-based criterion for the strength assessment of adhesive layers. 157:66–75. → page 19
- [61] L. Sohier, J. Y. Cognard, and P. Davies. Analysis of the mechanical behaviour of adhesively bonded assemblies of composites under tensile–shear out-of-plane loads. 53:65–74. → page 19
- [62] J. Y. Cognard, P. Davies, L. Sohier, and R. Créac’hcadec. A study of the non-linear behaviour of adhesively-bonded composite assemblies. 76(1):34–46. → page 19
- [63] G. Stamoulis, N. Carrere, J.-Y. Cognard, P. Davies, and C. Badulescu. Investigating the fracture behavior of adhesively bonded metallic joints using the arcan fixture. 66:147–159. → page 20
- [64] A. Ilioni, C. Badulescu, N. Carrere, P. Davies, and D. Thévenet. A viscoelastic-viscoplastic model to describe creep and strain rate effects on the mechanical behaviour of adhesively-bonded assemblies. 82:184–195. → page 20

- [65] P. Bidaud, R. Créachcadec, P. Jousset, and D. Thévenet. A fatigue life prediction method of adhesively bonded joints based on visco-elastic and visco-plastic behavior: Application under cyclic shear loading. 30(15):1641–1661. → page 20
- [66] C. Badulescu, J. Y. Cognard, R. Créac'hcadec, and P. Vedrine. Analysis of the low temperature-dependent behaviour of a ductile adhesive under monotonic tensile/compression–shear loads. 36:56–64. → page 20
- [67] L. Dufour, B. Bourel, F. Lauro, G. Haugou, and N. Leconte. A viscoelastic-viscoplastic model with non associative plasticity for the modelling of bonded joints at high strain rates. 70:304–314. → page 20
- [68] A. B. de Morais. Elastic-plastic analysis of the adhesively bonded end-notched flexure specimen. 188:80–92. → pages 22, 25
- [69] M. F. S. F. De MOURA, N. DOURADO, J. J. L. MORAIS, and F. A. M. PEREIRA. Numerical analysis of the ENF and ELS tests applied to mode II fracture characterization of cortical bone tissue. 34(3):149–158. Publisher: John Wiley & Sons, Ltd. → page 23
- [70] Gabriele Cricri. Cohesive law identification of adhesive layers subject to shear load – an exact inverse solution. 158:150–164. → pages 24, 25, 27, 75
- [71] C. Wu, R. Huang, and K.M. Liechti. Simultaneous extraction of tensile and shear interactions at interfaces. 125:225–254. → pages 25, 28, 75
- [72] K. Leffler, K. S. Alfredsson, and U. Stigh. Shear behaviour of adhesive layers. 44(2):530–545. → pages 25, 75
- [73] M.R. Molteno and T.H. Becker. Mode i-III decomposition of the j-integral from DIC displacement data. 51(6):492–503. → page 25
- [74] A. J. Kinloch, C. F. Korenberg, K. T. Tan, and J. F. Watts. Crack growth in structural adhesive joints in aqueous environments. 42(15):6353–6370. → page 25
- [75] H. Khoramishad, M. Hamzenejad, and R. S. Ashofteh. Characterizing cohesive zone model using a mixed-mode direct method. 153:175–189. → pages 25, 77
- [76] U. T. F. Carvalho and R. D. S. G. Campilho. Validation of pure tensile and shear cohesive laws obtained by the direct method with single-lap joints. 77:41–50. → page 25
- [77] Y. Wang and J. G. Williams. Corrections for mode II fracture toughness specimens of composites materials. 43(3):251–256. → pages 27, 35
- [78] H. Wang, T. Vu-Khanh, and V. N. Le. Effects of large deflection on mode II fracture test of composite materials. 29(6):833–849. → pages 27, 34
- [79] A. B. de Morais. Analysis of the fracture process zone and effective crack length in the adhesively bonded end-notched flexure specimen. 0(0):1–26. → page 27

- 
- [80] Y. Y. Su and X. L. Gao. Analytical model for adhesively bonded composite panel-flange joints based on the timoshenko beam theory. 107:112–118. → page 27
- [81] C.D.M. Liljedahl, A.D. Crocombe, M.A. Wahab, and I.A. Ashcroft. Damage modelling of adhesively bonded joints. 141(1):147–161. → pages 27, 28, 75
- [82] Jarno Jokinen, Markus Wallin, and Olli Saarela. Applicability of VCCT in mode I loading of yielding adhesively bonded joints—a case study. 62:85–91. → page 28
- [83] Lucas F. M. da Silva and Raul D. S. G. Campilho. Advances in numerical modelling of adhesive joints. In Lucas Filipe Martins da Silva and Raul D. S. G. Campilho, editors, *Advances in Numerical Modeling of Adhesive Joints*, pages 1–93. Springer Berlin Heidelberg. → page 28
- [84] G.I Barenblatt. The formation of equilibrium cracks during brittle fracture. general ideas and hypotheses. axially-symmetric cracks. 23(3):622–636. → page 28
- [85] G. I. Barenblatt. The mathematical theory of equilibrium cracks in brittle fracture. In H. L. Dryden, Th. von Kármán, G. Kuerti, F. H. van den Dungen, and L. Howarth, editors, *Advances in Applied Mechanics*, volume 7, pages 55–129. Elsevier. → page 28
- [86] Donald Stephen Dugdale. Yielding of steel sheets containing slits. 8:100–104. → page 28
- [87] M.Z. Sadeghi, A. Gabener, J. Zimmermann, K. Saravana, J. Weiland, U. Reisgen, and K.U. Schroeder. Failure load prediction of adhesively bonded single lap joints by using various FEM techniques. 97:102493. → page 28
- [88] B.F. Sorensen and T.K. Jacobsen. Determination of cohesive laws by the j integral approach. 70(14):1841–1858. → pages 28, 30, 75
- [89] P.C. Mohapatra and L.V. Smith. Adhesive hardening and plasticity in bonded joints. 106. → pages 29, 35
- [90] F.A.L. Viana, R.D.S.G. Campilho, and R.J.B. Rocha. Fracture modelling of adhesively-bonded joints by an inverse method. 13(48):286–303. → page 29
- [91] D. Álvarez, B.R.K. Blackman, F.J. Guild, and A.J. Kinloch. Mode I fracture in adhesively-bonded joints: A mesh-size independent modelling approach using cohesive elements. 115:73–95. → page 29
- [92] Alirio Villamil, Juan Rodriguez, Alicia Porras, and Maribel Barrera. Mode I crack propagation experimental analysis of adhesive bonded joints comprising glass fibre composite material under impact and constant amplitude fatigue loading. 14:4380. → page 29
- [93] S. Mall and G. Ramamurthy. Effect of bond thickness on fracture and fatigue strength of adhesively bonded composite joints. 9(1):33–37. → page 29

- [94] M. D. Banea, L. F. M. da Silva, and R. D. S. G. Campilho. The effect of adhesive thickness on the mechanical behavior of a structural polyurethane adhesive. 91(5):331–346. Publisher: Taylor & Francis. → page 29
- [95] ASTM d5528-13 : Standard test method for mode I interlaminar fracture toughness of unidirectional fiber-reinforced polymer matrix composites. → page 29
- [96] S. Mostovoy, E. J. Ripling, and C. F. Bersch. Fracture toughness of adhesive joints. 3(2):125–144. Publisher: Taylor & Francis. → page 29
- [97] George F. Hardy. A review of: “ADHESION AND ADHESIVES: SCIENCE AND TECHNOLOGY, by a. j. kinloch, chapman and hall, london and new york, 1987, 441 pp. 28(2):199–200. → pages 30, 35, 74
- [98] L. A. Carlsson, J. R. J. W. Gillespie, and R. B. Pipes. On the analysis and design of the end notched flexure (ENF) specimen for mode II testing:. → pages 30, 35
- [99] M.S. Kafkalidis and M.D. Thouless. The effects of geometry and material properties on the fracture of single lap-shear joints. 39(17):4367–4383. → page 31
- [100] J. D. Barrett and R. O. Foschi. Mode II stress-intensity factors for cracked wood beams. 9(2):371–378. → page 31
- [101] H. Chai and S. Mall. Design aspects of the end-notch adhesive joint specimen. 36(1):R3–R8. → page 31
- [102] R.H. Martin and B.D. Davidson. Mode II fracture toughness evaluation using four point bend, end notched flexure test. 28(8):401–406. → page 32
- [103] K.S. Alfredsson. On the instantaneous energy release rate of the end-notch flexure adhesive joint specimen. 41(16):4787–4807. → pages 32, 35, 74
- [104] C. Schuecker and B.D. Davidson. Effect of friction on the perceived mode II delamination toughness from three- and four-point bend end-notched flexure tests. (1383):334–344. → page 32
- [105] Barry D. Davidson, Xuekun Sun, and Anthony J. Vinciguerra. Influences of friction, geometric nonlinearities, and fixture compliance on experimentally observed toughnesses from three and four-point bend end-notched flexure tests. 41(10):1177–1196. → page 32
- [106] B.D. Davidson and X. Sun. Effects of friction, geometry, and fixture compliance on the perceived toughness from three- and four-point bend end-notched flexure tests. 24(15):1611–1628. → page 32
- [107] X. Sun and B.D. Davidson. Numerical evaluation of the effects of friction and geometric nonlinearities on the energy release rate in three- and four-point bend end-notched flexure tests. 73(10):1343–1361. → page 32

- 
- [108] H. Wang and T. Vu-Khanh. Use of end-loaded-split (ELS) test to study stable fracture behaviour of composites under mode II loading. 36(1):71–79. → page 34
- [109] M.K. Budzik and J. Jumel. Inverse end loaded split test configuration for stable mode II crack propagation in bonded joint: macroscopic analysis—effective crack length approach. 207(1):27–39. → pages 34, 35, 74
- [110] S. Hashemi, A. J. Kinloch, and J. G. Williams. The analysis of interlaminar fracture in uniaxial fibre-polymer composites. 427(1872):173–199. → pages 35, 77
- [111] Chengye Fan, P. Y. Ben Jar, and J. J. Roger Cheng. A unified approach to quantify the role of friction in beam-type specimens for the measurement of mode II delamination resistance of fibre-reinforced polymers. 67(6):989–995. → page 35
- [112] T. Ben Zineb, A. Sedrakian, and J.L. Billoet. An original pure bending device with large displacements and rotations for static and fatigue tests of composite structures. 34(5):447–458. → pages 35, 74
- [113] Kim C. Dao and Dennis J. Dicken. Fatigue failure mechanisms in polymers. 27(4):271–276. ISBN: 0032-3888 Publisher: Wiley Online Library. → page 39
- [114] D.M. Brewis, J. Comyn, and R.J.A. Shalash. The effect of moisture and temperature on the properties of an epoxide-polyamide adhesive in relation to its performance in single lap joints. 2(4):215–222. → pages 39, 40
- [115] Timothy M. Minahen and Wolfgang G. Knauss. Creep buckling of viscoelastic structures. 30(8):1075–1092. ISBN: 0020-7683 Publisher: Elsevier. → page 39
- [116] R.D. Adams, J.W. Cowap, G. Farquharson, G.M. Margary, and D. Vaughn. The relative merits of the boeing wedge test and the double cantilever beam test for assessing the durability of adhesively bonded joints, with particular reference to the use of fracture mechanics. 29(6):609–620. → pages 40, 41
- [117] Marcio Arouche, Mohamed Nasr Saleh, Sofia Teixeira de Freitas, and Silvio de Barros. Effect of salt spray ageing on the fracture of composite-to-metal bonded joints. 108. → pages 40, 41
- [118] M. Emar, L. Torres, M. Baena, C. Barris, and M. Moawad. Effect of sustained loading and environmental conditions on the creep behavior of an epoxy adhesive for concrete structures strengthened with CFRP laminates. 129:88–96. → page 40
- [119] L. Calabrese, G. Galtieri, C. Borsellino, G. Di Bella, and E. Proverbio. Durability of hybrid clinch-bonded steel/aluminum joints in salt spray environment. 87(9):3137–3147. ISBN: 1433-3015 Publisher: Springer. → page 40
- [120] S. Sugiman, A. D. Crocombe, and I. A. Aschroft. Experimental and numerical investigation of the static response of environmentally aged adhesively bonded joints. 40:224–237. ISBN: 0143-7496 Publisher: Elsevier. → page 41



- [121] A. Rudawska, J.W. Sikora, M. Müller, and P. Valášek. The effect of environmental ageing at lower and sub-zero temperatures on the adhesive joint strength. 97:102487. → page 41
- [122] Fan Zhang, Xin Yang, Hui-Ping Wang, Xiaowei Zhang, Yong Xia, and Qing Zhou. Durability of adhesively-bonded single lap-shear joints in accelerated hygrothermal exposure for automotive applications. 44:130–137. → page 41
- [123] Fan Zhang, Xin Yang, Yong Xia, Qing Zhou, Hui-Ping Wang, and T. Yu. Experimental study of strain rate effects on the strength of adhesively bonded joints after hygrothermal exposure. → page 41
- [124] C. D. M. Liljedahl, A. D. Crocombe, M. A. Wahab, and I. A. Ashcroft. Modelling the environmental degradation of adhesively bonded aluminium and composite joints using a CZM approach. 27(6):505–518. ISBN: 0143-7496 Publisher: Elsevier. → page 41
- [125] A.D. Crocombe. Durability modelling concepts and tools for the cohesive environmental degradation of bonded structures. 17(3):229–238. → page 41
- [126] Jingru Ni, Junying Min, Hailang Wan, Jianping Lin, Shuang Wang, and Qingmian Wan. Effect of adhesive type on mechanical properties of galvanized steel/SMC adhesive-bonded joints. 97:102482. → page 41
- [127] Richard Court, Michael Sutcliffe, and Seyyed Tavakoli. Ageing of adhesively bonded joints - fracture and failure analysis using video imaging techniques. 21:455–463. → page 41
- [128] J. W. Wylde and J. K. Spelt. Measurement of adhesive joint fracture properties as a function of environmental degradation. 18(4):237–246. ISBN: 0143-7496 Publisher: Elsevier. → page 41
- [129] E.M Knox and M.J Cowling. Durability aspects of adhesively bonded thick adherend lap shear joints. 20(4):323–331. → page 41
- [130] Hartmut Pasternak and Samer Sahellie. Conversion factors of the temperature effect on the shear strength of adhesively-bonded steel joints. 22:666–672. → page 41
- [131] Hafiz Iqbal, Shantanu Bhowmik, and R. Benedictus. Durability of PBI adhesive bonded joints under various environmental conditions. 89. → page 41
- [132] Daniel O. Adams, K. L. DeVries, and Clint Child. Durability of adhesively bonded joints for aircraft structures. 22. → page 41
- [133] W. K. Loh, A. D. Crocombe, MM Abdel Wahab, and I. A. Ashcroft. Environmental degradation of the interfacial fracture energy in an adhesively bonded joint. 69(18):2113–2128. ISBN: 0013-7944 Publisher: Elsevier. → page 41

- 
- [134] Amir Ameli, M. Papini, and J. Spelt. Fracture r-curve of a toughened epoxy adhesive as a function of irreversible degradation. 527:5105–5114. → page 41
- [135] Michael Johlitz, Stefan Diebels, and Wulff Possart. Investigation of the thermoviscoelastic material behaviour of adhesive bonds close to the glass transition temperature. 82. → page 41
- [136] X. Han, A.D. Crocombe, S.N.R. Anwar, and P. Hu. The strength prediction of adhesive single lap joints exposed to long term loading in a hostile environment. 55:1–11. → page 42
- [137] Chantal de Zeeuw, Sofia Teixeira de Freitas, Dimitrios Zarouchas, Markus Schilling, Romina Lopes Fernandes, Pedro Portella, and Ute Niebergall. Creep behaviour of steel bonded joints under hygrothermal conditions. 91. → page 42
- [138] Jian Li, Li Yi-bo, Yanhong Xiang, Qing Pan, Chao Chen, Jinsong Liu, and Xiang Hu. Effect of hygrothermal-mechanical exposure on the residual strength of adhesively bonded joints. 100:102616. → page 42
- [139] S. Fevery, S.K. Latré, D. Vandepitte, S. Debruyne, and H. Hallez. Combination and interaction of ageing parameters on single lap shear adhesive joints. 111:102978. → page 42
- [140] R.M. Carneiro Neto, A. Akhavan-Safar, E.M. Sampaio, J.T. Assis, and L.F.M. da Silva. Assessment of the creep life of adhesively bonded joints using the end notched flexure samples. 133:105969. → pages 42, 125
- [141] Wenlong Mu, Jingxin Na, Wei Tan, Guangbin Wang, Hao Shen, and Xiaoying Li. Durability of adhesively bonded CFRP-aluminum alloy joints subjected to coupled temperature and alternating load. 99:102583. → page 42
- [142] H. Hadavinia, A.J. Kinloch, M.S.G. Little, and A.C. Taylor. The prediction of crack growth in bonded joints under cyclic-fatigue loading II. analytical and finite element studies. 23(6):463–471. → page 42
- [143] R. P. Brown, D. Kockott, P. Trubiroha, W. Ketola, and J. Shorthouse. A review of accelerated durability tests. → page 44
- [144] M.F. Kanninen. A dynamic analysis of unstable crack propagation and arrest in the DCB test specimen. 10(3):415–430. → page 77
- [145] Griffith A. A. The phenomena of rupture and flow in solids. In *Encyclopedia of Tribology*, pages 1570–1573. Springer US. → page 83
- [146] B. Blaysat, J.P.M. Hoefnagels, G. Lubineau, M. Alfano, and M.G.D. Geers. Interface debonding characterization by image correlation integrated with double cantilever beam kinematics. 55:79–91. → page 91

- [147] J.M. Gorman and M.D. Thouless. The use of digital-image correlation to investigate the cohesive zone in a double-cantilever beam, with comparisons to numerical and analytical models. 123:315–331. → page 91
- [148] D. Plausinis and J.K. Spelt. Application of a new constant g load-jig to creep crack growth in adhesive joints. 15(4):225–232. → page 125

## Durabilité des assemblages collés sous sollicitation de cisaillement

**Résumé :** Cette thèse porte sur la durabilité des assemblages collés sous sollicitation de cisaillement. Cette méthode d'assemblage, en concurrence avec les méthodes de rivetage, soudage ou encore de pliage, permet d'obtenir des liaisons étanches, d'assembler des pièces/structures aux formes compliquées et aux matériaux dissimilaires et de s'adapter à diverses conditions environnementales. Les joints collés sont généralement conçus pour supporter une charge de cisaillement. Cependant, cette technologie n'est pas encore compétitive pour les applications qui exigent un haut niveau de fiabilité : chargement complexe (fluage, stationnaire, choc, ...) couplé à un environnement physico-chimique agressif (température, humidité, ...).

L'objectif principal de cette thèse est d'évaluer le comportement mécanique des joints collés sous sollicitation de cisaillement afin de renforcer la robustesse des méthodes de prédiction du comportement des joints collés. Pour répondre à cette problématique, deux procédures d'essai utilisant la corrélation d'images numériques ont été développées pour évaluer le comportement mécanique des joints collés : l'essai Arcan permettant d'identifier le comportement rhéologique de la couche adhésive et l'essai End Loaded Split (ELS) permettant d'observer l'endommagement dans la couche adhésive. Ensuite, une méthode expérimentale a été décrite permettant d'identifier directement le comportement en cisaillement de la couche adhésive (loi cohésive). Cette loi est la première entrée dans un outil de simulation (analytique ou numérique) qui prédit le comportement mécanique des joints collés. Finalement, un modèle semi-analytique a été développé et est capable de prédire le comportement du joint collé (déplacements des substrats, déformation et contrainte de cisaillement dans la couche adhésive) sous une sollicitation de cisaillement dans un environnement standard (température et humidité ambiantes et chargement quasi-statique).

**Mots-clés :** Assemblage collé, Cisaillement, Durabilité, Polymères, Rupture, Modèle analytique

---

## Ageing of bonded joint under shear loading

**Abstract:** This thesis deals with ageing of bonded joints under shear loading. The bonded joint technique competing with riveting, welding or folding methods, has sealing properties, allow to put together structures with complicated shapes and made with dissimilar materials and can be adapted for various environmental conditions. Bonded joints are generally designed to withstand shear loads. However, this technology is not competitive yet for applications which require a high level of reliability : complex loading (creep, quasi-static, impact, ...) coupled with an aggressive physico-chemical environment (temperature, humidity, ...).

The main objective of this thesis is to evaluate the mechanical behaviour of bonded joints under shear loading in order to enhance the robustness of the methods for predicting the behaviour of bonded joints. To address this issue, two test procedures using Digital Image Correlation (DIC) were developed to assess the mechanical behaviour of bonded joints: the Arcan test was used to identify the rheological behaviour of the adhesive layer and the End Loaded Split (ELS) test was used to observe damage evolution in the adhesive layer. Then, an experimental method was described to directly identify the shear behaviour of the adhesive layer (cohesive law). This law is the first input in simulation tools (analytical or numerical) that can predict the mechanical behaviour of bonded joints. Eventually, a semi-analytical model was developed which is able to predict the behaviour of the bonded joint (adherent displacements, shear strain and stress in the adhesive layer) under shear loading in a standard environment (ambient temperature and humidity and quasi-static loading).

**Keywords:** Bonded joint, Shear, Ageing, Polymers, Failure, Analytical model

---

Unité de recherche

Institut de Mécanique et d'Ingénierie UMR 5295, 33400 Talence, France.

